SEMICONDUCTOR RING LASERS FOR HIGH SPEED COMMUNICATIONS

A Research Carried out at the

Department of Electronics and Electrical Engineering,

University of Glasgow.

Submitted to the University of Glasgow for the Degree of Doctor of Philosophy

To my wife

For our tenth anniversary

Acknowledgement

During the three unforgettable years many people have in various ways contributed to the research leading to this Ph.D. thesis. It is my wish to express my most sincerely gratitude to all those people, among whom the following are particularly important.

I owe my biggest thanks to my supervisor Prof. Peter J. R. Laybourn. He has supervised the research with a great scholar's foresight. In all ways he is the perfect teacher who never losses his understanding of the student's situation and only needs very gentle tugs to put them on the correct bearings.

Dr. Thomas F. Krauss, who broke new grounds in the research of semiconductor ring lasers, selflessly devoted great amount of time and effort to passing on his rich experience and insight in the topic. Without his countless discussion sessions into the smallest details, the research could never have gone this far. He must also be thanked for introducing me to the basic skills of cleanroom work, which proves to be invaluable both in the course of this research and in my future career.

Prof. Chris D. W. Wilkinson kindly authorised the access to the dry-etch facilities, which has been essential to the fabrication of devices. Dr. Simon Hicks, Dr. Saad Murad and the dry-etch team provided the training and knowledge necessary for good dry-etching to be carried out. Dr. A. C. Bryce kindly authorised the use of the rapid thermal annealer (RTA) and provided necessary training. Mrs. Lois Hobbs and the cleanroom team in the Department of Electronics and Electrical Engineering have provided superb technical support in terms of sample preparation and photolithography.

Dr. Brigette Vogele and the MBE group have been very important in supplying good quality III-V QW materials. Dr. B. S. Ooi and Dr. P. Cusumano have been very helpful for their discussions about the IFVD techniques. Dr. Karen McIlvaney offered her help on anti-reflective coating of devices.

I must Thank the Sino-Bristish Friendship Scholarship Scheme (SBFSS) for funding my study at Glasgow. I feel enormously indebted to my motherland China and her people who raised and educated me.

Finally, I give my special thanks to my wife Ligang for all she has sacrificed to support my study. She has shouldered all hardship without the slightest complaint and regret. She has given me the greatest encouragement and spiritual strength. Also not to be forgotten is our daughter Haiyue who has always been with us and has always been wonderful.

Table of Contents

Abstract I

1 Introduction-Aim of This Work 1

1-1 OTDM-Concept and Structure
1-2 Devices Involved in OTDM
1-3 Approach Pursued in This Work

2 Materials and Fabrication Techniques 8
2-1 Material Considerations
2-2 III-V QW materials and Their Characterisation
2-3 Standard Processes for Definition of Waveguide Devices
2-4 Self-aligned Process for Second-level Lithography
2-5 Quantum-well Intermixing

3 Multi-mode Interference (MMI) Couplers 34

3-1 Theory and Modelling of MMI couplers
3-2 Results
3-3 Discussion

4 Light Source I-Semiconductor Ring Lasers (SRLs) and Its Improvement 45

4-1 Review
4-2 External Efficiency
4-3 Extended Cavity Semiconductor Ring Lasers
4-4 Linearity of L-I Characteristics and Spectral Properties.
4-5 Summary

5 Light Source II-Mode-locked Operation of Semiconductor Ring Lasers 70

5-1 Theory and Computer Modelling of Passively Mode-locked Semiconductor Ring Lasers.
5-2 Experimental Devices
5-3 Experimental Results
5-4 Summary

6 Electro-absorptive (EA) Modulators 105

6-1 The Operational Principle of EA Modulators
6-2 Design and Fabrication of the Device
6-3 Characterisation Results
6-4 Integration Considerations
6-5 Summary

7 Conclusion and Future Work 121

Abstract

The work described in this thesis is aimed at exploring the possibility of optically integrating an OTDM transmitter system operating at 4X10Gb/s on an appropriate substrate. It has been shown that such an OTDM transmitter system could be integrated on III-V semiconductor quantum well (QW) substrates if the design of the substrate, the choice of fabrication techniques and the design of the devices are carefully considered. Suitable device structures for the three main kinds of devices involved in OTDM transmitters, namely light source, optical multiplexers (couplers) and optical modulators, have been discussed. Significant progress regarding these aspects, both theoretical and experimental, has been achieved.

Light source

Semiconductor ring lasers (SRLs) have been studied because of their potential for forming integrated short light pulse sources without employing either facet mirrors or precision gratings and therefore are simple to fabricate.

1) Large SRLs with cavity circumferences up to several millimetres have been successfully operated in both pulse pumped and CW mode. Such large SRLs are needed for producing mode-locked pulse trains with frequencies in the order of tens of gigahertz.

2) The low external efficiency associated with SRLs, due to both its long cavity length and large feedback ratio, has been dealt with. The external efficiency of semiconductor ring lasers has been improved over the value of ~16% of previous devices employing a single 0.5/0.5 2x2 MMI coupler. By using the asymmetric 2x2 MMI coupler, 3x3 MMI coupler and two 2x2 MMI couplers as the SRLs' output mechanism, its external efficiency has been increased by factors of 1.2, 1.4 and 1.7, respectively. The dual 2x2 MMI coupler device was AR coated to get η_{ex} values as high as 33%. This value is reasonably good for a device in a PIC where the consecutive devices are connected by low loss waveguides. The performance of the dual MMI coupler SRL has been improved significantly in terms of external efficiency.

3) Multiple (up to 4) outputs have been produced from these devices, which enables them to be used in an OTDM system as the light source without incorporating additional power splitters.

4) The mechanisms causing non-linearity in SRLs L-I characteristics have been studied and the linearity shown to be improved by several means including AR coating, deeper waveguide profile and passive output coupler.

5) Passive waveguides and extended cavity SRLs with very long cavity length (up to 7.5mm) have been fabricated by employing the IFVD technique and successfully operated. The L-I characteristics of the extended cavity SRLs show a linearity similar to that of F-P lasers.

6) The mode-locking properties of semiconductor ring lasers has been studied theoretically. By means of computer simulations based on both the lumped element model and the travelling wave model, an in-depth understanding of the passive mode-locking process in SRLs has been achieved. The mode-locking properties of several cavity configurations, namely the symmetric configuration, the asymmetric configuration and the dual absorber configuration, have been compared. It is shown that in terms of wider mode-locked region and shorter pulse width, the dual absorber configuration is superior to the others. Moreover, the dual MMI, dual absorber configuration is more suitable for OTDM application not only because it generates four outputs and therefore eliminates the need to use addition power splitters, but also because the pulse timing from these outputs is such that only T/4 delay lines are needed to produce the correct timing difference between the 4 channels.

The theoretical study enables the prediction of operational modes of an SRL with intra-cavity saturable absorber under certain gain section injection and absorber reverse bias voltage, provided sufficient information concerning the semiconductor QW material.

7) Experimentally, mode-locked SRLs with both asymmetric and dual absorber, dual MMI coupler configurations have been successfully fabricated and operated.

The asymmetric configuration shows operation properties very similar to that predicted by the computer simulation. A mode-locked spectrum as wide as 200GHz (HMFW) with very small chirp has observed, corresponding to a pulse width of about 2.4ps.

The pulse width of the dual absorber configuration has been measured to be about 9ps with a time-band width product of 0.45. The wider pulse width can be attributed to the band-width limiting effect caused by facet feedback. Mode-locking mixed with self-pulsation and pure self-pulsation have also been observed in injection and reverse bias conditions agree with that predicted by simulation. The designing, fabrication, and CW and mode-locked operation of large ridge waveguide SRLs are reported here for the first time.

As a result of the continued research on semiconductor ring lasers at Glasgow, it can now be firmly established that this kind of device is a very suitable and *practical* light source for PIC applications that require either CW or short pulse outputs.

Waveguide Coupler

Multi-mode interference (MMI) couplers have been studied in this project. They were chosen because of both their good tolerance to errors in fabrication and their outstanding feature of allowing multiple access, a major requirement for multiplexers and demultiplexers. MMI couplers play two roles in the proposed integrated OTDM transmitter. They will be used as the output couplers of the semiconductor ring lasers (which actually take the place of the power splitter if the dual 2x2 MMI coupler device or 3x3 MMI coupler device is used) as well as the multiplexer.

1) MMI couplers have been modelled using an effective index (EI) slab waveguide approximation. The parameters of the MMI couplers have been calculated and optimised by charting the mode excitation,

propagation and interference processes in the input, multi-mode and output waveguides. The tolerance to various waveguide geometric parameters has been calculated.

2) Experimentally, besides 2x2 MMI couplers used in SRLs, 3x3 and 4x4 MMI couplers with strip-loaded waveguide profile have also been fabricated and tested. The 3x3 MMI couplers shows a homogeneity of 1.3 dB among the outputs while for 4x4 MMI couplers the best homogeneity achieved is about 3dB.

Electroabsorption (EA) modulators

For semiconductor QW substrates, electroabsorption (EA) is certainly the most attractive modulation mechanism to explore. EA modulators have been experimentally studied in this project from several aspects.

1) The junction capacitance of the QW materials has been measured and compared to the theoretically calculated value by solving the Poisson equation across the p-i-n junction.

2) A modulator structure intended to reduce the parasitic capacitance between the p- and n-contacts by using deep etched waveguide and thick insulation layer (<2μm) has been designed and fabricated on two different double QW materials.

3) Their DC modulation characteristic has been studied. Despite the substrate material having only two QWs because of threshold considerations of the light source, a modulation index of 8.8dB/V has been achieved with a maximum available modulation depth of 23dB.

4) The high frequency characteristics of the modulators have been analysed experimentally. S parameter measurements up to 26GHz have been carried out. An equivalent circuit model has been derived from the measured data. The model allows the bandwidth of the modulator to be determined. It also highlights the need to reduce both the junction capacitance and device series resistance in order to increase the bandwidth of the modulator.

Integration

In this work, it has been intended to investigate all the devices from the integration point of view. This has been reflected in many aspects in the device design and fabrication process. Integration has always been a very important factor to consider in the determination of substrate material structure, device configuration, waveguide structure and fabrication techniques. As a result, the devices developed in this project are suitable for the proposed purpose of an integrated OTDM transmitter system.

Investigation into integration techniques has also been carried out. The most important was to introduce bandgap difference on a semiconductor QW material. IFVD technique is studied and produced some encouraging results such as the extended cavity SRL, which integrates an active section with a passive MMI coupler. Vertically coupled waveguide structures have also been investigated in an attempt to produce extended cavity lasers. The design considerations of extended cavity lasers employing this waveguide structure have been discussed.

1 Introduction-Aim of This work

Over the years, the demand for telecommunication capacity has been growing in a explosive manner. Although the use of optical fibre systems enabled the transmission of multi-gigabaud data flow, the push for even higher data rates has never seemed to be stronger in both local-area network (LAN) and long-haul context. While single mode optical fibre can provide bandwidth in the order of 10THz, this bandwidth is far from being fully explored. The major limitations to the conventional intensity modulation direct detection (IM-DD) optical fibre transmission system have been 1) the speed of the electronic devices required to handle (i.e., to construct and to process) a data flow rate in excess of 10Gb/s and 2) the modulation bandwidth of semiconductor lasers.

Major efforts have been made on both issues. As summarised by Bowers [1], progress in heterojunction bipolar transistor (HBT) technology has enabled the multiplexing of digital signal up to the rate of 27Gb/s. Higher speed driver, receiver and demultiplexer have also been demonstrated. The 3dB bandwidth of semiconductor lasers has come close to 30GHz by minimising carrier transport effects in the GaInAs/GaAs quantum well system. This progress should enable an IM-DD system to operate in a data rate up to near 30Gb/s.

Such efforts, however great their progress has been, will be getting more and more difficult, and the two above mentioned limitations will finally stop any further effort from being worthwhile because of both technical and economical considerations.

There are other ways to get around the difficulties associated with these speed limits so that transmission of even higher data rates in an optical fibre channel can be facilitated. Instead of constructing a data flow electronically, recent research work has provided schemes for doing so optically. Therefore the problems of speed of electronics and modulation bandwidth of lasers are largely eliminated. These schemes mainly fall into the categories of Wavelength Division Multiplexing (WDM) and Optical Time-Division Multiplexing (OTDM).

WDM employs light sources of slightly different wavelengths (typically spaced 10nm from each other) for different signal channels to be transmitted in the same optical fibre. Thus in one transmission window (e.g., at the λ=1.55μm low attenuation window) it is possible to transmit up to 100 channels in one fibre. In WDM there has to be no relation of any kind between the signal channels other than the specified channel spacing. Therefore they could be of very different nature and at very different data rate, such as computer data and TV signal. Access is thus very flexible. However, in application in long-haul systems such as transcontinental or transoceanic systems, such incoherence of signals makes WDM a very unsuitable candidate because the transmission distance of the scheme will suffer from dispersion limitation of the fibre as in any conventional IM-DD system. WDM therefore is a more promising scheme for LAN where diversity and flexibility of service is strongly sought after.

---

[1] Bowers, J., 'Ultrafast Optoelectronics', Plenary paper, OFC'1993.

In an OTDM system [1, 2] high bit-rate data flow is constructed by *optically* interleaving lower bit-rate *optical* data flows, instead of doing so electronically. Therefore strict timing or phase relation has to be maintained throughout the system. However, it does not necessarily require more than one light source for different signal channels and it is obviously possible to utilise soliton transmission technology to overcome the dispersion limitation and to greatly enhance the transmission distance. On the other hand, OTDM requires short optical pulses of low duty cycle to be generated in order for more channels to be multiplexed together to form a higher bit-rate data flow as well as for soliton transmission to be carried out. Experimental systems based on discrete semiconductor laser pulse sources and fibre-optic components have been demonstrated . Tucker et al [2] gave a comprehensive discussion on the considerations of OTDM system design and demonstrated some experimental results. More recent transmission experiments were carried out at BT [3,4,5] Unrepeatered transmission of 4x5Gbit/s OTDM signal over 137km was achieved [3]. Er-doped fibre amplifiers were used to extend the transmission distance to 205km [4,5]. Higher bit-rate soliton transmission at 32Gbit/s over 90km was also realised [6] and 64Gbit/s multiplexing and demultiplexing experiments [7] were demonstrated.

In many ways OTDM and WDM are complementary in the sense that each seem to have their own advantages which overcome the other's disadvantage. Encouraged by the above mentioned publisher's work and based on many successive research projects carried out in the Optoelectronics Research Group, the aim of this work and the works to follow is to explore the possibility of optically integrating an OTDM transmitter system operating at a high bit-rate on an appropriate substrate. In order to work on such a system, it is worthwhile examining the OTDM scheme in more detail, which is done in the following sections.

---

[1] Bowers, J., 'Ultrafast Optoelectronics', Plenary paper, OFC'1993.

[2] Tucker, R. S. et al, 'Optical time-division multiplexing for very high bit-rate trnsmission', J. Lightwave Technology, 1988, VOL.11, pp1737-1749.

[3] Wickens, G. E., *et al*, 'Nonlinear transmission of 20Gbit/s optical time-division multiplexed data, over 205km of dispersion shifted fibre', Electron. Lett., 1992,2, pp.117-118.

[4] Wickens, G. E., *et al*, '20Gbit/s, 205km optical time-division multiplexed transmission system', Electron. Lett., 1991, 11, pp973-974.

[5] Spirit, D. M., et al, '137km, 4X5Gbit/s optical time-division multiplexed unrepeatered system with distributed erbium fibre preamplifier', Electron. Lett., 1992, 13, pp.1218-1220

[6] Anderekson, P. A., *et al*, '32Gb/s optical soliton transmission over 90km', IEEE Photonics Technology Letters, 1992, 1, pp.76-79.

[7] Anderekson, P. A., *et al*, '64Gb/s all-optical demultiplexing with the nonlinear optical-loop mirror', IEEE Photonics Technology Letters , 1992, 6, pp.644-647.

1-1 OTDM-Concept and Structure

The diagram of an OTDM transmitter is shown in Fig. 1-1[1]. The optical short pulse generated from the source is split into N identical pulse streams. (Several individual pulse sources can be used instead, but they are unlikely to have the same time domain and spectral properties so splitting pulse stream from one pulse source is probably the better choice). These pulse streams are modulated by incoming electronic data flows and delayed by appropriate amounts so that there is a T/N timing delay between adjacent pulse streams, then multiplexed into one pulse stream which is N times the frequency of the original pulse source.

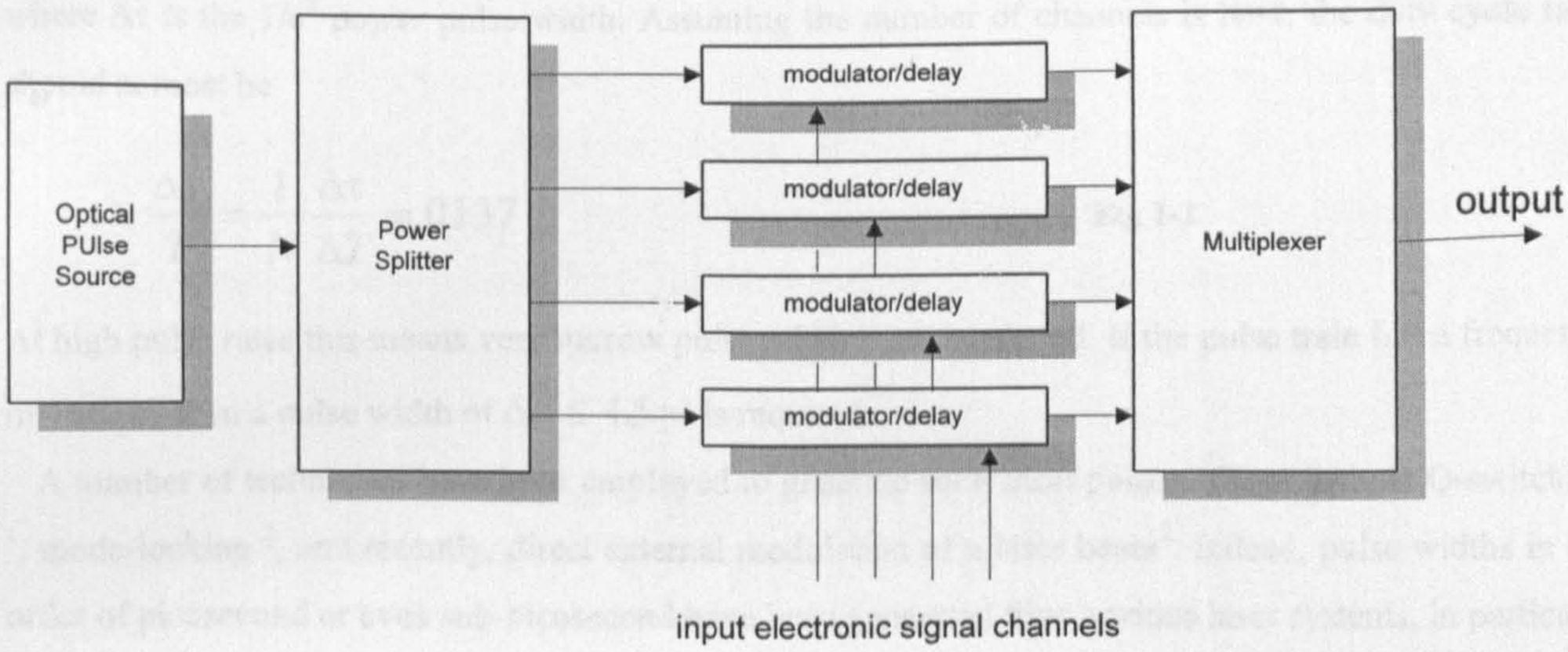

Fig. 1-1 Diagram of OTDM transmitter system

As an upgrading for electronic multiplexing, the data bit-rate of each channel in an OTDM system should be chosen to be at a speed which electronic multiplexing can reach without great difficulty. 10Gbit/s was quoted [1] as the next commercially available transmission speed after 2.4Gbit/s and beyond this point electronic multiplexing will be difficulty despite above mentioned progress in HBT technology. On the other hand, too low a speed would result in inconvenience in OTDM since the size of the laser light source, the length of the delay lines, etc., would be large. Therefore, at present, 10Gbit/s is believed to be an appropriate dividing point between electronic multiplexing and OTDM.

1-2 Devices Involved in OTDM

In this section, the availability and principal requirement for each device involved in the OTDM transmitter will be briefly reviewed and discussed in a context of system performance. Detailed analysis will left to respective chapters dealing with each of them. A brief discussion is also given on the possibility of integration.

---

1 Bowers, J., 'Ultrafast Optoelectronics', Plenary paper, OFC'1993.

1-2-1 The Light Source

The light source should be able to produce an optical pulse train of very small duty cycle ratio (i.e., the ratio of pulse width $\Delta\tau$ to the pulse repetition period T) in order to leave enough room between pulses so that other channels can be inserted. For example, for Gaussian pulses, if the crosstalk between two adjacent channels is to be less than -26dB as is required by a resultant error rate of 10^{-9} and considering that there are pulses on both side of one particular pulse, which doubles the penalty, the time spacing between the two channels should at least be

$$\Delta T = 1.827\Delta\tau \qquad \textbf{Eq. 1-1}$$

where $\Delta\tau$ is the $1/e^2$ power pulse width. Assuming the number of channels is N=4, the duty cycle ratio should at most be

$$\frac{\Delta\tau}{T} = \frac{1}{N}\frac{\Delta\tau}{\Delta T} = 0.137 \qquad \textbf{Eq. 1-2}$$

At high pulse rates this means very narrow pulse width must produced. If the pulse train has a frequency of 10GHz, then a pulse width of $\Delta\tau \leq 4.5$ ps is required.

A number of techniques have been employed to generate such short pulses. These include Q-switching [1], mode-locking [2], and recently, direct external modulation of a laser beam[3]. Indeed, pulse widths in the order of picosecond or even sub-picosecond have been generated from various laser systems, in particular semiconductor lasers. Detailed comparison of these schemes will be carried out in **Chapter 5**.

1-2-2 Couplers-power splitter and multiplexer

As shown in the diagram, once the short pulse train is generated, it must be equally split into N identical pulse trains, and these pulses will have to be multiplexed or combined into one pulse train after modulation and delay. Splitting and combining have been readily achieved by optical fibre couplers in previous work. For systems based on planar substrates, a number of coupler structures such as directional couplers [4] and multimode interference couplers [5] are also available.

---

[1] Vasil'ev, P. P., *et al*, 'High-power, low jitter encoded picosecond pulse generation using an RF-locked self-Q-switched multicontact GaAs/GaAlAs diode laser', Electron. Lett., 1993, 18, pp.1593-1594.

[2] Derickson, D. J., et al, "Short pulse generation using multisegment mode-locked semiconductor lasers," IEEE J-QE, VOL.28, NO. 10, Oct. 1992, pp.2186-2202.

[3] Suzuki, M., et al, 'Transform limited optical pulse generation up to 20 GHz repetition rate by a sinusoidally driven InGaAsP electroabsorption modulator', J. of Lightwave Technology, 1993, No.3, pp.468-473.

[4] Snyder, A. W. and Love, J. D., 'Optical waveguide theory', London : Chapman & Hall, 1983.

[5] Soldano, L. B., *et al*, 'Planar monomode optical couplers based on multimode interference effects', Journal of Lightwave Technology, VOL.12, 1992, pp.1843-1849.

It is worth noting that the use of the above mentioned couplers as multiplexers, which are based on the linear propagation properties of light and are thus reciprocal, will introduce a substantial power loss because only 1/N of the input power of each channel will enter the output waveguide. Couplers based on optical non-linear effects would be able to overcome this drawback. But up to date they still need a rather high input optical pulse power to be operational [1] and their performance is far from practical use. On the other hand, the power loss may be compensated by introducing optical amplifiers. However, amplifiers could result in pulse broadening.

1-2-3 Modulators and delay lines

For each channel, some modulation mechanism is needed to impart data on to the pulse train carrier . This can be performed by optical waveguide external modulators. There are various kinds of modulators which suits the purpose, e.g., electro-optical (EO) modulators made on $LiNbO_3$ substrates, electroabsorptive (EA) modulators based on Franz-Keldish Effect (FKE) in bulk semiconductor and based on Quantum Confined Stark Effect (QCSE) in semiconductor quantum-wells [2,3].

The basic characteristic of the modulator is its speed or switch on-off time. It is obviously essential that the modulator should be switched on or off in a time no longer than the pulse repetition period T so that each pulse can represent 1 bit data. According to Nyquist's Law, this requires the modulator's bandwidth is at least half the data bit-rate or

$$\Delta f = \frac{1}{2T} \qquad \text{Eq. 1-3}$$

To reach such a speed means that the modulator should have very small parasitic RF parameters. The modulator is also expected to have a large modulation index (i.e., the change in output optical power per unit input electric signal magnitude), to cause minimum optical power loss and to be able to cope with large input optical power. How to achieve these often conflicting requirements will be discussed in Chapter 6.

Delay lines are simply waveguides of low optical loss. Their length should be different from each other by an amount

$$\Delta L = v_g \frac{T}{N} \approx \frac{c}{n_{eff}} \frac{T}{N} \qquad \text{Eq. 1-4}$$

---

[1]Davis, M. K and Digonnet, M. J. F., 'Switching power reduction using a pumped nonlinear directional coupler', IEEE Photonics Technology Letters, 1996, Vol.8, No.10, pp.1328-1330.
[2] Wood, H. T., 'Multiple quantum well waveguide modulators', Journal of Lightwave Technology, VOL. 6, No.6, 1988, pp.742-757.
[3]Smit-Rink, S., *et al,* 'Linear and non-linear optical properties of semiconductor quantum wells', Advances in Physics, 1989, VOL.12, No.2, pp.89-188.

where v_g is the propagation constant of the waveguides, c is the velocity of light in free space and n_{eff} is effective refractive index of the waveguides which is very close to the refractive index n of the waveguide material.

1-2-4 Photonic Integrated Circuit (PIC)

The possibility of optical integration of such an OTDM transmitting system depends on whether these devices are compatible in several aspects.

1)Substrate material. It is essential that all the devices are able to be fabricated on the same substrate. Frequently used substrates for PICs include glass or molten quartz, non-linear crystals such as quartz and $LiNbO_3$, and III-V compound semiconductors. Waveguides and (optically) linear couplers can be fabricated on all, modulators can be fabricated on non-linear crystal and semiconductor substrates, and light sources may be fabricated on semiconductor and rare-earth doped glass substrates [1]. It is believed that III-V semiconductor is the best choice not only because the three kinds of devices involved here are compatible with this substrate and semiconductor lasers have been extremely successful and are practically the only light source to use in optical fibre communication systems, but also because its property of high refractive index n (typically 3.5 in contrast to 1.5 of glass). A large n means the geometric size of devices would be smaller when their optical length is often determined by other factors, particularly by the data bit-rate in OTDM (Eq.1-4).

2)Substrate structure. It is important that the devices involved require only similar substrate structure, e.g., the cutting direction of the crystal, the layer structure if a multilayer substrate is to be used. Otherwise the integration would be very difficult. It is notable that in the proposed OTDM PIC, the laser, the modulator and the couplers have almost identical waveguide layer structure if III-V semiconductor substrate is to be used.

3)Fabrication techniques. For different devices different fabrication techniques would have to be employed. If one certain technique used will severely impair the performance of other devices, then integration is prohibited. While the devices in the OTDM can be fabricated using largely the same semiconductor processing techniques, there are certain problems concerning the bandgap of the semiconductor substrate. These will be discussed in Chapter 2.

In general, the above discussion has established that an OTDM transmitter system could be integrated on III-V semiconductor substrate provided care be taken in the design of the substrate, the choice of fabrication techniques and the design of the devices.

1-3 Approach Pursued in This Work

Bearing in mind the ultimate long-term aim, there are two categories of problems to be solved in order to facilitate its achievement.

---

[1] Vossler, G. L., Brooks, C. J. and Winik, K. A., 'Planar Er-Yb glass ion-exchanged wave-guide laser', Electronics Letters, 1995, Vol.31, No.14, pp.1162-1163.

1)Develop suitable devices for use in this PIC based on existing devices by adapting their structure to the need and to operate them in the correct mode of operation so that they meet the performance requirement proposed in Devices Involved in OTDM.

Most semiconductor lasers rely on a Fabry-Perot (F-P) cavity formed by two cleaved facets. This, however, is not practical in an PIC. Instead, a F-P cavity can be formed by dry etching [1]. But etched facets will introduce loss between the laser and subsequent devices in an PIC. There will also be unwanted optical feedback from the front facet of the device next to the laser. Other mechanisms can be used to form a laser cavity, such as gratings in distributed feedback (DFB) and distributed Bragg reflector (DBR) lasers. These produce lasers of very good performance but are rather difficult to fabricate because of the sub-micron resolution required by the gratings.

An alternative way of forming a laser cavity is to use a self-looped waveguide resonator, resulting in semiconductor ring lasers (SRLs). SRLs combine many features that recommend their use in photonic integrated circuits (PICs). They are easily defined by photolithography and can be arbitrarily positioned, because they do not need accurate gratings or cleaved facets for feedback. Their circular geometry also makes them very suitable for mode-locked operation because colliding-pulse mode-locking naturally takes place.

SRLs have been intensively investigated in the group and other groups world-wide. While past work mainly focused on smaller devices (diameter~100μm), the purpose of this work requires rather large devices to be operational(see Chapter 2). Methods of improving the performance and configuration of large SRLs are first described in Chapter 4. Attempts to operate the device mode-locked at the proposed frequency are then described in Chapter 5.

The performance of the SRL is directly related to the output coupler it uses. Consequently, it is necessary to look into the problems and resolutions involving the couplers and this is dealt with in Chapter 3. The effort is focused on the multimode interference (MMI) couplers for a number of reasons.

The investigations on modulators are described in Chapter 6, focusing on the electro-absorptive (EA) modulators. The DC modulation characteristics, wavelength dependence and the high frequency equivalent circuit model are studied.

2)Develop suitable techniques for fabrication of the devices as well as the integration.

Before setting out to study the devices, a large part of Chapter 2 is devoted to the fabrication techniques that all the devices will depend on. Not all these techniques are existing, standard processes. It is also appropriate there to describe the substrates used in the whole work, and the principles of how the devices are designed.

---

[1] Behfar-Rad, A., Wong, S. S., Ballantyne, J. M., Soltz, B. A., and Harding, C. M., Applied Phys. Lett. Vol.54, 1989 pp.493-495.

2 Materials and Fabrication Techniques

2-1 Material Considerations

III-V compound semiconductors have been intensely studied and well established in applications concerning optoelectronic devices, particularly semiconductor lasers and light detectors. They are also very attractive substrates for integrated optics not only because that they offer excellent compatibility with most optical and optoelectronic devices, but also because they provide the further possibility of integrating these devices together with semiconductor electronic devices such as transistors. This will obviously be extremely desirable.

2-1-1 Semiconductor Bulk and Quantum-well Materials

Bulk material was used in earlier III-V semiconductor optoelectronic devices. It is still being used in many occasions. But with the introduction of quantum-well (QW) structures, the band structure of the semiconductors and the carrier transportation processes in them can be modified to give superior performance [1]. QW semiconductor lasers can have much lower threshold current than those made of bulk material. They can also have much wider modulation bandwidth. QW structures also give rise to a number of new effects such as the Quantum Confined Stark Effect (QCSE) [2], or greatly enhance some effects difficult to observe in bulk material such as the exciton absorption and related carrier dynamics [3]. These are of practical importance here. For example, QCSE, coupled with exciton resonant absorption, increases the modulation index of an EA absorptive modulator significantly over those employing Franz-Keldish Effect (FKE) in bulk semiconductors [2].

2-1-2 Considerations Regarding Quantum-well Material

When choosing semiconductor QW material as the substrate on which the proposed PIC will be built, there are many important aspects to be considered when designing the layer structure.

1) Material system. Although at the most useful wavelengths (λ=1.3 or 1.55μm) material structures are mostly based on InGaAsP/InP quaternary alloy system, the material growth and fabrication techniques are far easier and more reliable for the AlGaAS/GaAs material system. Throughout the development history of semiconductor optoelectronic devices it has often been the case that new or prototypical devices were first realised on AlGaAs/GaAs material and transferred to other material systems later.

---

[1] Zory, P. Jr., edit, 'Quantum-well laser', London : Academic Press, c1993.

[2] Schmitt-Rink, S., Chemla, D. S., and Miller D. A. B., , 'Linear and non-linear optical properties of semiconductor quantum wells', Advances in Physics, 1989, VOL.12, No.2, pp.89-188.

[3] Weisbuch, C. and Vinter, B., 'Quantum semiconductor structures:fundamentals and Applications', San Diago: Academic Press, c1991.

2) Number of wells. The number of quantum-well to be incorporated in a QW structure depends on several factors, the most important being the type of devices to be fabricated on the substrate and their structural parameters. Therefore the optimal wafer structure for different devices could be very different. When an PIC involving several kinds of devices is to be built using a single QW material, it is often necessary to make concessions between devices so that an overall optimisation is reached.

As an laser medium, the gain-injection relationship of a QW structure is greatly affected by the number of QWs as is plotted in Fig. 2-1 [1]. In general there is a optimal number of QWs given by

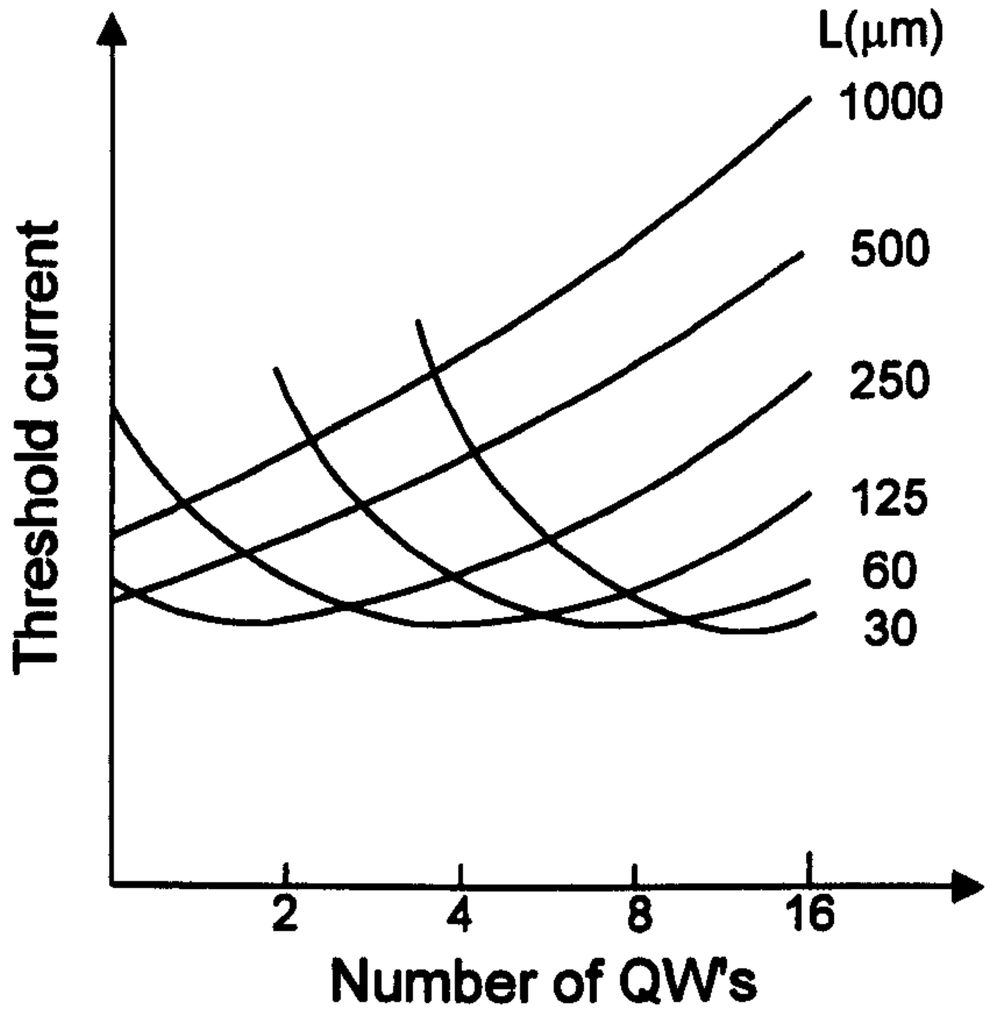

Fig. 2-1 Threshold current versus number of QWs for various cavity lengths

$$n_{qw} = Int(g_{th} / g_0) \qquad \text{Eq. 2-1}$$

wnere g_{th} is the threshold gain coefficient and g_0 the saturation parameter defined by McIlroy [2]. Because g_{th} is determined by the laser threshold condition

$$g_{th} = \frac{1}{\Gamma_{qw}}\left[\alpha_i + \frac{1}{L}\ln(\frac{1}{R})\right] \qquad \text{Eq. 2-2}$$

and decreases with increasing laser cavity length L (Γ_{qw} being the lateral optical mode confinement factor of each QW), longer lasers would require a material with fewer QWs. In the case of this work, a mode-locked semiconductor laser would have to be used, whose cavity length will be determined by the pulse repetition period T and the refractive index n of the material

$$L = (\frac{1}{2}) \cdot \frac{Tc}{n} \qquad \text{Eq. 2-3}$$

---

[1] Zory, P. Jr., edit, 'Quantum-well laser', London : Academic Press, c1993. Chapter 3.

[2] McIlroy, P. W. A., *et al*, 'Analysis and application of theoretical gain curves to the design of multi-quantum-well lasers', IEEE J. Quantum Electronics, VOL.21, 1985, pp.1958-1963.

and would be in the order of several millimetres. In such a laser the loss term caused by the output is small compared to the material loss α_i. This would favour a single quantum-well structure when the material is of good quality (α_i is small) if low threshold current were to be achieved.

On the other hand, the EA modulator would favour more quantum-wells. Suppose, when subject to unity external modulation voltage, the change of absorption coefficient $\Delta\alpha$ of each quantum-well is a fixed quantity, then the modulation index of the device will be related to the number of wells n_{qw} by [1]

$$m = \exp(n_{qw}\Gamma_{qw} \cdot \Delta\alpha L) \qquad \textbf{Eq. 2-4}$$

where L is the length of the modulator. In other words, to achieve a certain m the length of the modulator can be shortened if more QWs are used, which benefits the performance by reducing the device capacitance.

So a value of n_{qw}=2 or may be a good choice for the purpose of the work. In the light source, the actual waveguide loss coefficient α_i may be increased over that of the material itself due to losses introduced in the fabrication process. This may justify an increased n_{qw}. Also an increase of n_{qw} just over 1 cuts the modulator length the most (by 50% and 66% for n_{qw}=2 and 3, respectively), while further increase is less significant. Throughout this project n_{qw}=2 (DQW-Double Quantum-well) structure is used.

2-1-3 Bandgap

When considering integration of different kinds of devices on a single III-V semiconductor substrate, the different bandgap energy values required by each kind of device is a very important and very frustrating issue. Take the proposed PIC as an example. Three kinds of devices are involved here, the laser source, the coupler and delay line waveguides, and the modulators. It is essential that, at the wavelength or photon energy of the light source, the couplers and delay lines are expected to have low loss. This could be achieved by making the bandgap energy at where these devices are fabricated much larger than that of the laser source so the light is not absorbed via stimulated absorption. Meanwhile, the modulator should also have low loss when no modulating signal is applied and its absorption should be increased to a very substantial value when the signal is applied. This would ask for a local bandgap energy moderately larger then that of the laser, but can be brought by the modulating signal to be equal to, or even smaller than that of the laser source. Therefore three different bandgap values are expected on the same substrate as illustrated in Fig. 2-2.

This task of making different bandgap values on the same substrate has not been an easy one to fulfil. Here QW structures again surpass bulk material because the effective bandgap (i.e., the difference between the lowest quantised state energies in the conduction band and the valence band) is determined

---

* The factor $\frac{1}{2}$ is for Fabry-Perot cavity lasers. For ring cavity lasers this should be unity. If a mode-locking freqguency of 10 GHz and n=3.5 is used, then the cavity length should be 4.3mm for the former and 8.6mm for the latter.

[1] Wood, T. H., 'Multiple quantum well waveguide modulators', J. of Lightwave Technology, VOL. 6, No.6, 1988, pp.742-757.

by *both* the material composition (in $Al_xGa_{1-x}As/GaAs$ system, the percentage concentration x of aluminium) *and* the geometrical parameters (shape and thickness) of the QWs, while that of the bulk material is only determined by the former. Several ways of obtaining such a substrate are:

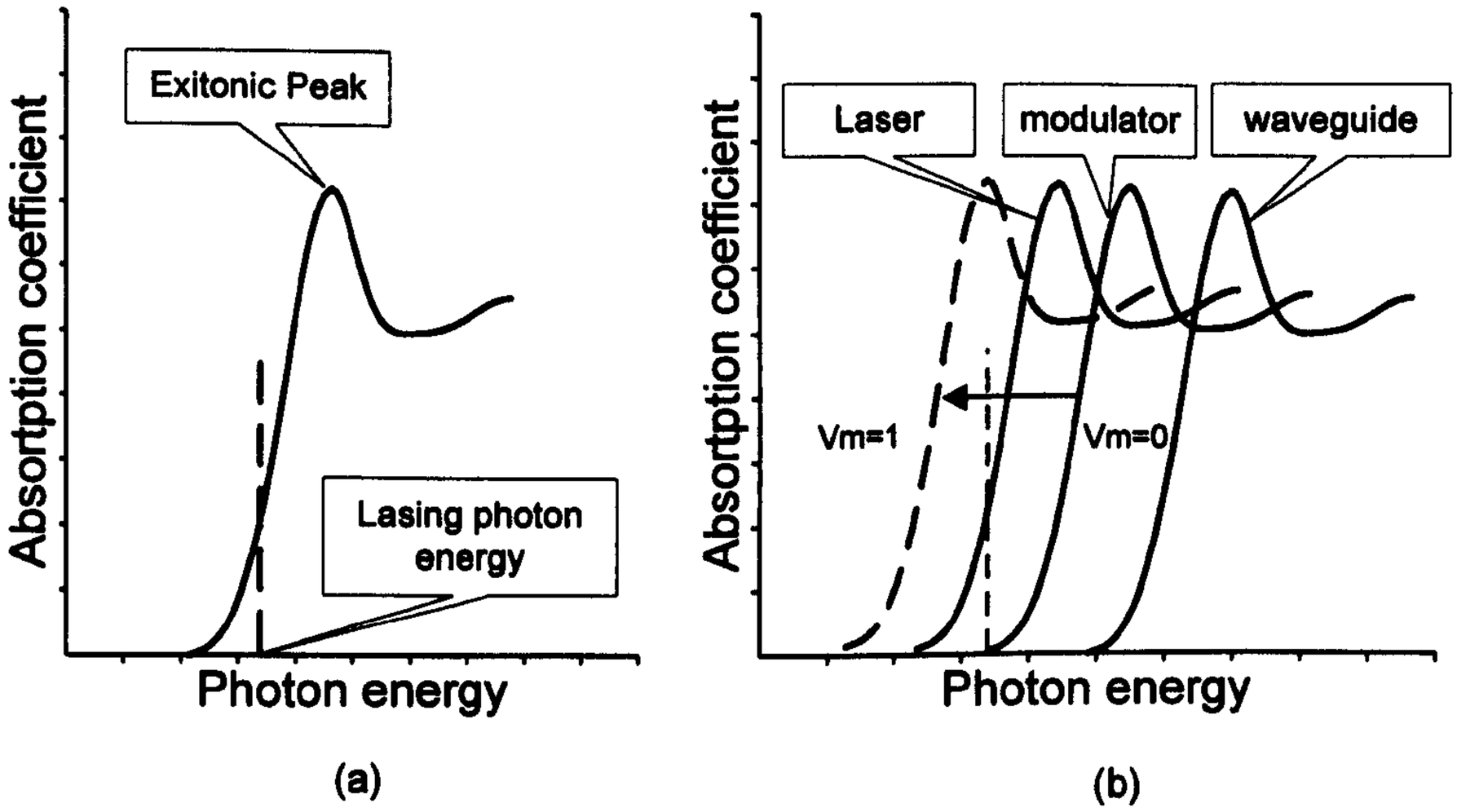

Fig. 2-2 (a) Absorption near band edge in semiconductor QW structure.(b)Relative band edge difference proposed for the integration. The absorption peak of the modulator is expected to shift to the lasing photon energy when signal is applied.

1) Regrowth. The substrate is first grown with an waveguide layer of bandgap E_{g1}, then this layer is etched in selected areas and another waveguide layer of bandgap E_{g2} is grown. The resulting structure is shown in Fig. 2-3(**a**). The problem with such a scheme is that the two waveguide layers can be misaligned, causing a coupling loss at the interface. It also needs two epitaxial processes which will be expensive and time consuming.

2) Patterned substrate epitaxy [1](Fig. 2-3 (b)). The substrate is patterned prior to the growth process so that narrow ridges are formed. During the growth the composites over ridges of different width will experience different lateral diffuse process, resulting in different composition and layer thickness locally. This method applies particularly well to the QW structure because a small thickness change would result in significant bandgap change, so a wider bandgap is obtained over the narrow ridges.

3)Vertically coupled waveguide structure(Fig. 2-3 (**c**)). This structure uses two waveguide layers-one over the other. Their material composition is different so they have different bandgap energy values. These waveguides are optically coupled to each other so that light can transfer from one to the other. The upper layer, for example, can be made thc lasing medium and the lower layer the low loss waveguide.

---

[1]Koyama, F., *et al*, 'GaInAs/GaInAsP strained quantum well monolithic electroabsorption modulator/amplifier by lateral bandgap control with nonplanar substrates', Elec. Lett., VOL.29, No.24, 1993, pp.2104-2106.

During fabrication the upper layer is removed except where the light source is located so that low loss waveguide is realised elsewhere. This scheme can work quite well if the devices are designed properly.

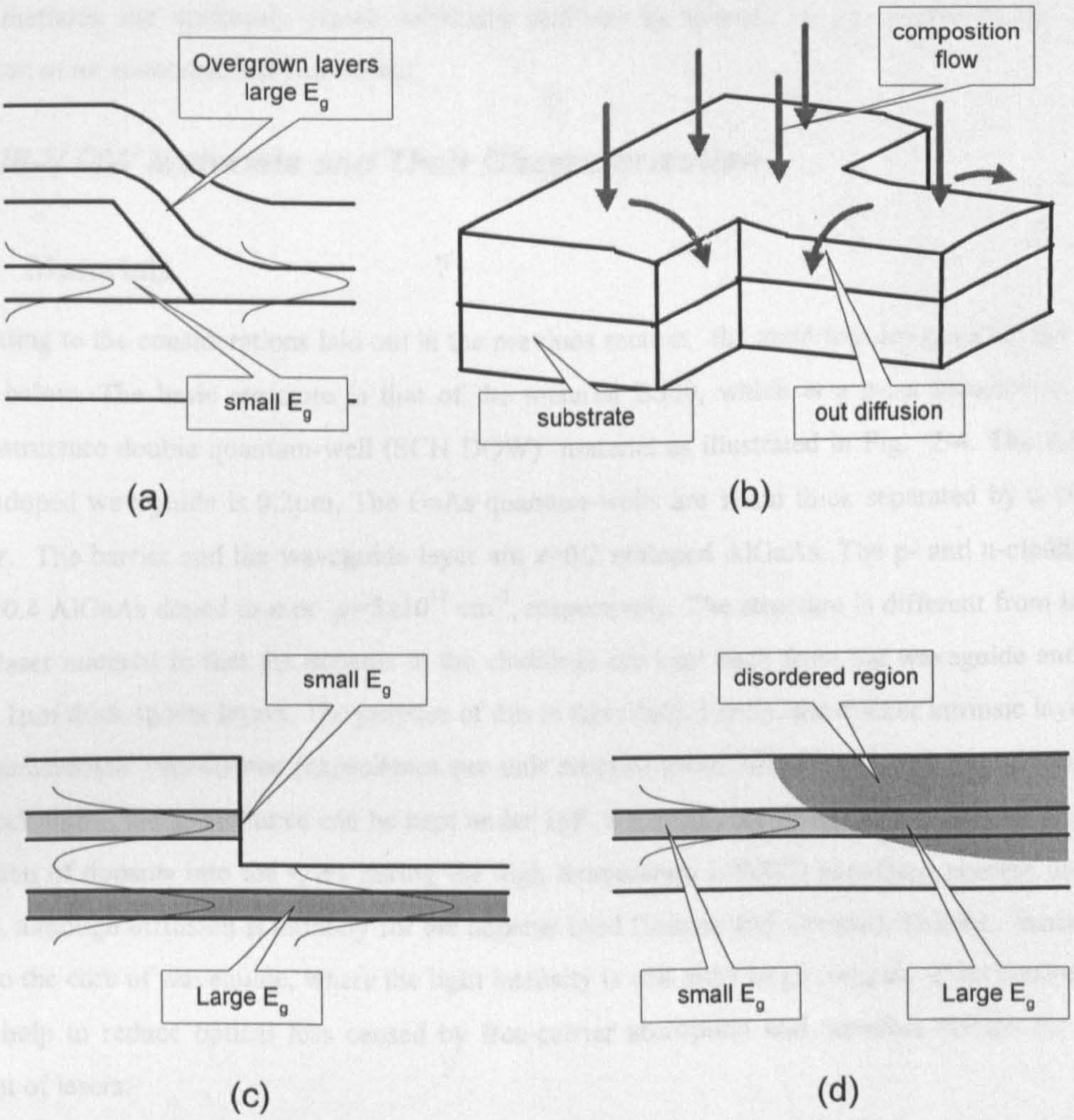

Fig. 2-3 Different approach of producing bandgap difference on the same substrate. (a)regrowth, (b) patterned substrate growth, (c)vertically coupled waveguides and (d)disordering.

4)Disordering (Fig. 2-3**(d)**)[1]. Disordering in semiconductors is a disturbance to the lattice of the semiconductor crystal by the introduction of foreign 'particles' such as impurities, excessive native elements and/or vacancies. This disturbance will then change the energy band structure of the semiconductors and therefore their bandgap energy. In a QW structure, this effect works mainly through changing the profile of the QWs by intermixing the previously well-defined interface between the well and the barriers, causing the quantised state energies and thus the effective bandgap to change.

In this work the latter two methods are explored with the emphasis on the QW intermixing caused by impurity-free vacancy-induced disordering (IFVD) mainly due to their flexibility. In the other two

---

[1] Marsh, J., "Quantum-well intermixing", Semiconductor Sci. & Tech., 1993, 8, pp.1136-1155.

methods the substrate must be patterned prior or in some stage of epitaxial growth. This only apply to a certain circuit layout and the resultant structure is of little use for other purposes. In the contrary, the latter methods use uniformly grown substrates and can be tailored to any circuit layout. They are therefore more economic and convenient.

2-2 III-V QW Materials and Their Characterisation

2-2-1 Materials

According to the considerations laid out in the previous section, the materials designed for this work are listed below. The basic structure is that of the material B500, which is a p-i-n separate-confinement heterostructure double quantum-well (SCH DQW) material as illustrated in Fig. 2-4. The thickness of the undoped waveguide is 0.2μm. The GaAs quantum-wells are 10nm thick separated by a 10nm thick barrier. The barrier and the waveguide layer are x=0.2 undoped AlGaAs. The p- and n-cladding layers are x=0.4 AlGaAs doped to n or p=5x10^{17} cm^{-3}, respectively. The structure is different from usual p-i-n SCH laser material in that the dopants in the claddings are kept back from the waveguide and QWs by two 0.1μm thick spacer layers. The purpose of this is three-fold. Firstly, the thicker intrinsic layer reduces the characteristic capacitance (capacitance per unit area) to about 300pF/mm^2. For an modulator of the size 5x500μm^2, the capacitance can be kept under 1pF. Secondly, the spacer layers prevent any possible diffusion of dopants into the QWs during the high temperature (~900C) annealing process used for the IFVD, although diffusion is unlikely for the dopants used (Silicon and Carbon). Thirdly, intrinsic layers next to the core of waveguide, where the light intensity is still quite large compare to its maximum in the core, help to reduce optical loss caused by free-carrier absorption and therefore reduce the threshold current of lasers.

Most other materials have similar structures except for small modifications. These are listed below. The materials come from two sources. All material labelled B*** are grown by Molecule Beam Epitaxy (MBE) at University of Glasgow, and all labelled QT*** are grown by Metal Organic Vapour Phase Epitaxy (MOVPE) at Sheffield University. The material B501 is a graded index (GRIN) version of B500. B429 has p-doped (Be:1X10^{17}cm^{-3}) QWs. QT899 is nearly the same as B500 but without a p-side spacer layer because of background doping during the growth of intrinsic material.

The material QT98, however, is a very different one designed as a vertically coupled waveguide structure [1]. It has two x=0.2 AlGaAs waveguide layers spaced by a 0.4mm thick x=0.4 AlGaAs layer. The upper waveguide contains a single quantum-well to form the active layer.

---

[1] Krauss, T. F., 'Integrated semiconductor ring lasers', Ph.D thesis. University of Glasgow, 1992.

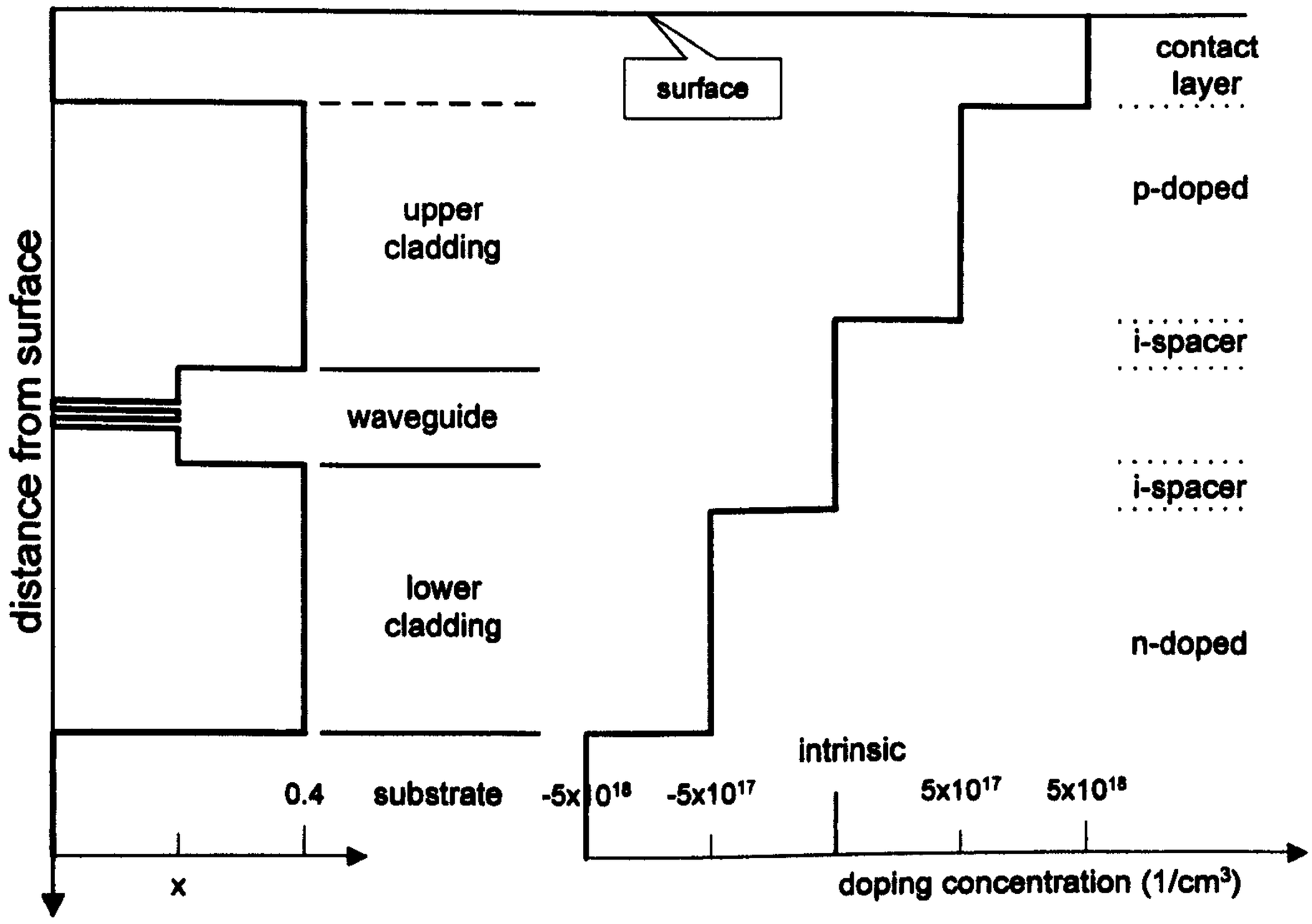

Fig. 2-4 Composition and doping profile of the DQW material.

Material	Well(s)	Barrier	Waveguide	Claddings
B500 **B680**	GaAs DQW 10nm undoped	x=0.2, 10nm undoped	x=0.2, 0.2μm undoped	x=0.4, 1μm
B429	GaAs DQW 10nm p-doped	same	same	same
B501	GaAs DQW 10nm undoped	same	same	x=0.4, 1μm x=0.2-0.4 graded spacer
QT899	same	same	same	x=0.4, 1μm, no p-side spacer
QT98	single QW	x=0.2, undoped	2 waveguides, 1 active, 1 passive	x=0.4, 2μm, no spacer, 0.4μm spacing between waveguides

Table 2-1 AlGaAs/GaAs substrate materials

2.2-2 Characterisation.

The materials must be characterised after growth so that their parameters are known. The characterisation is based on the following formulae of threshold condition (Eq.2-5)and external quantum efficiency of QW semiconductor lasers(Eq.2-6) [1]

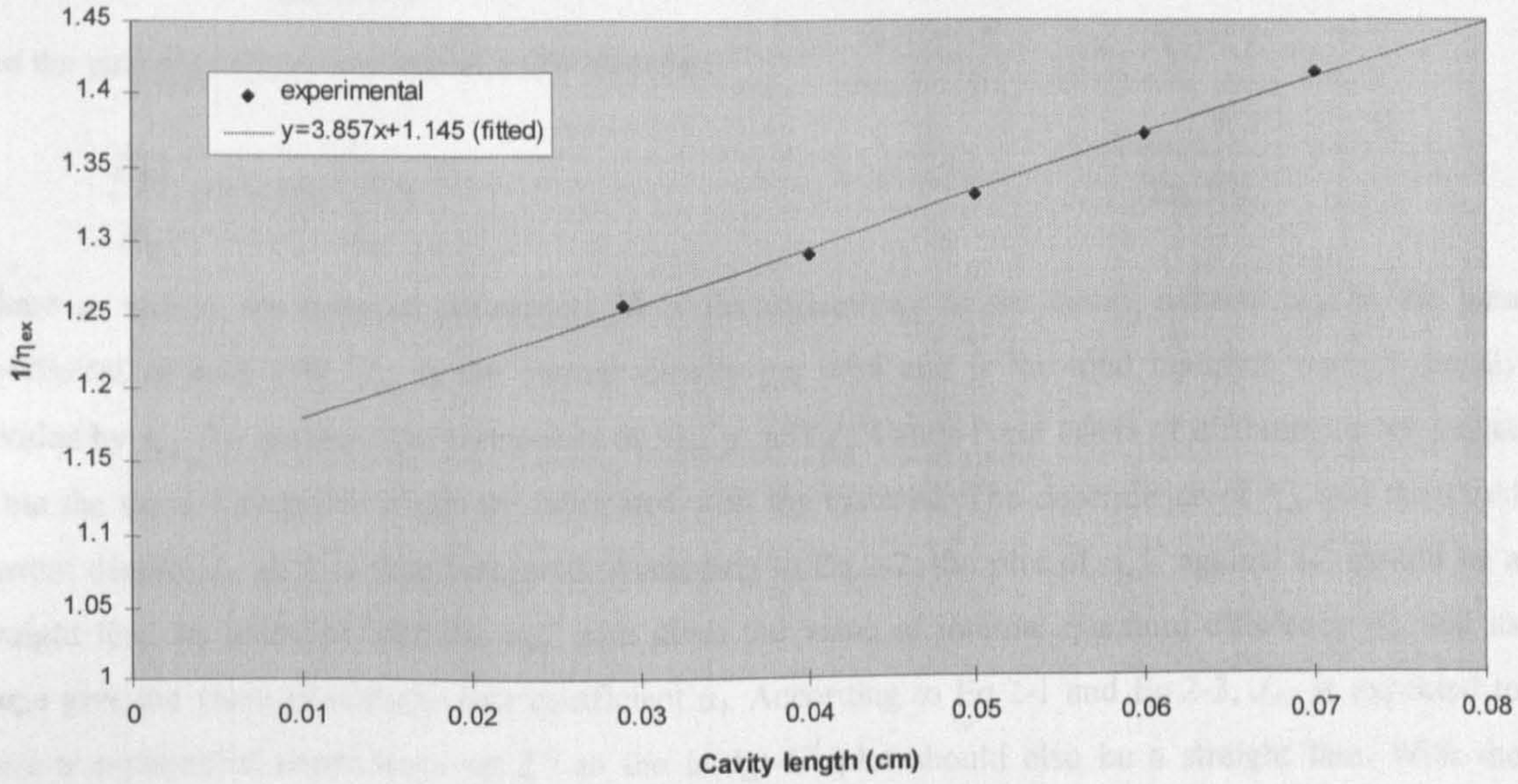

(a)

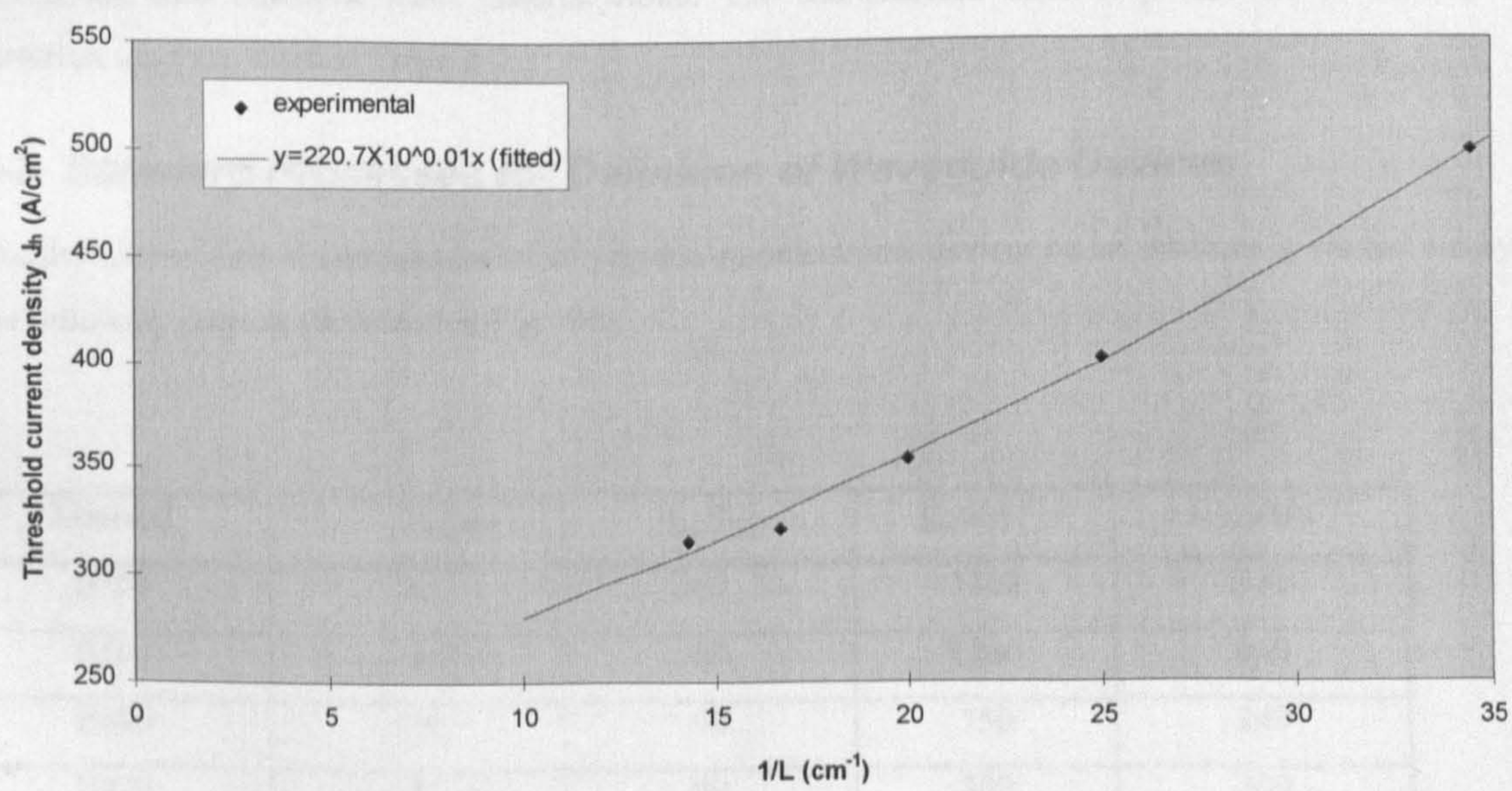

(b)

Fig. 2-5 Characterisation of laser material B680. External efficiency vs. cavity length (a), and threshold current density vs. inverse of cavity length (b).

---

[1] Yariv., A., "Optical Electronics", 4th Edition. Saunders College Pub., 1991.

$$n_{qw}\Gamma_{qw}g_{qw} = \alpha_i + \frac{1}{L}\ln(\frac{1}{R}) \qquad \textbf{Eq. 2-5}$$

$$\eta_{ex} = \frac{\eta_{in}}{1 + \frac{\alpha_i L}{\ln(1/R)}} \qquad \textbf{Eq. 2-6}$$

and the gain-current relationship of a QW structure [1]

$$\frac{g_{qw}}{g_o} = 1 + \ln(\frac{J_{qw}}{J_o}) \qquad \textbf{Eq. 2-7}$$

where g_o and J_o are material parameters. R is the reflectivity of the cavity mirrors. g_{qw} is the gain coefficient of each QW. J_{qw} is the current density per well and is the total injection current density divided by n_{qw}. To measure the parameters α_i, η_{in}, g_o and J_o, Fabry-Perot lasers of different cavity length L but the same waveguide width are fabricated with the material. The dependence of η_{ex} and threshold current density J_{th} on L is then measured. According to Eq.2-2, the plot of η_{ex}^{-1} against L^{-1} should be a straight line. Its intercept with the η_{ex}^{-1} axis gives the value of internal quantum efficiency η_{in} and its slope give the value of material loss coefficient α_i. According to Eq.2-1 and Eq.2-3, J_{th} is expected to have a exponential dependence on L^{-1} so the $\ln(J_{th})$-L^{-1} plot should also be a straight line. With the knowledge of α_i, g_o and J_o can also be determined from the slope and intercept of this straight line. Fig. 2-5 is the data measured from material B680. The characterised material parameters of all DQW materials used are listed in Table 2-2.

2-3 Standard Processes for Definition of Waveguide Devices

The definition of III-V Semiconductor waveguide optoelectronic devices on an substrate is carried out by the following steps as illustrated in Fig. 2-6

Material	α_i (cm^{-1})	η_{in} (%)	g_o (cm^{-1})	J_o (A/cm^2)
B500	4	60	1100	310
B501	4	68	1200	450
B680	3.8	90	750	240
B429	4	90	800	300
QT899	5	80	970	400

Table 2-2 Material Parameters

[1] McIlroy, P. W. A., *et al*, 'Analysis and application of theoretical gain curves to the design of multi-quantum-well lasers', IEEE J. Quantum Electronics, VOL.21, 1985, pp.1958-1963.

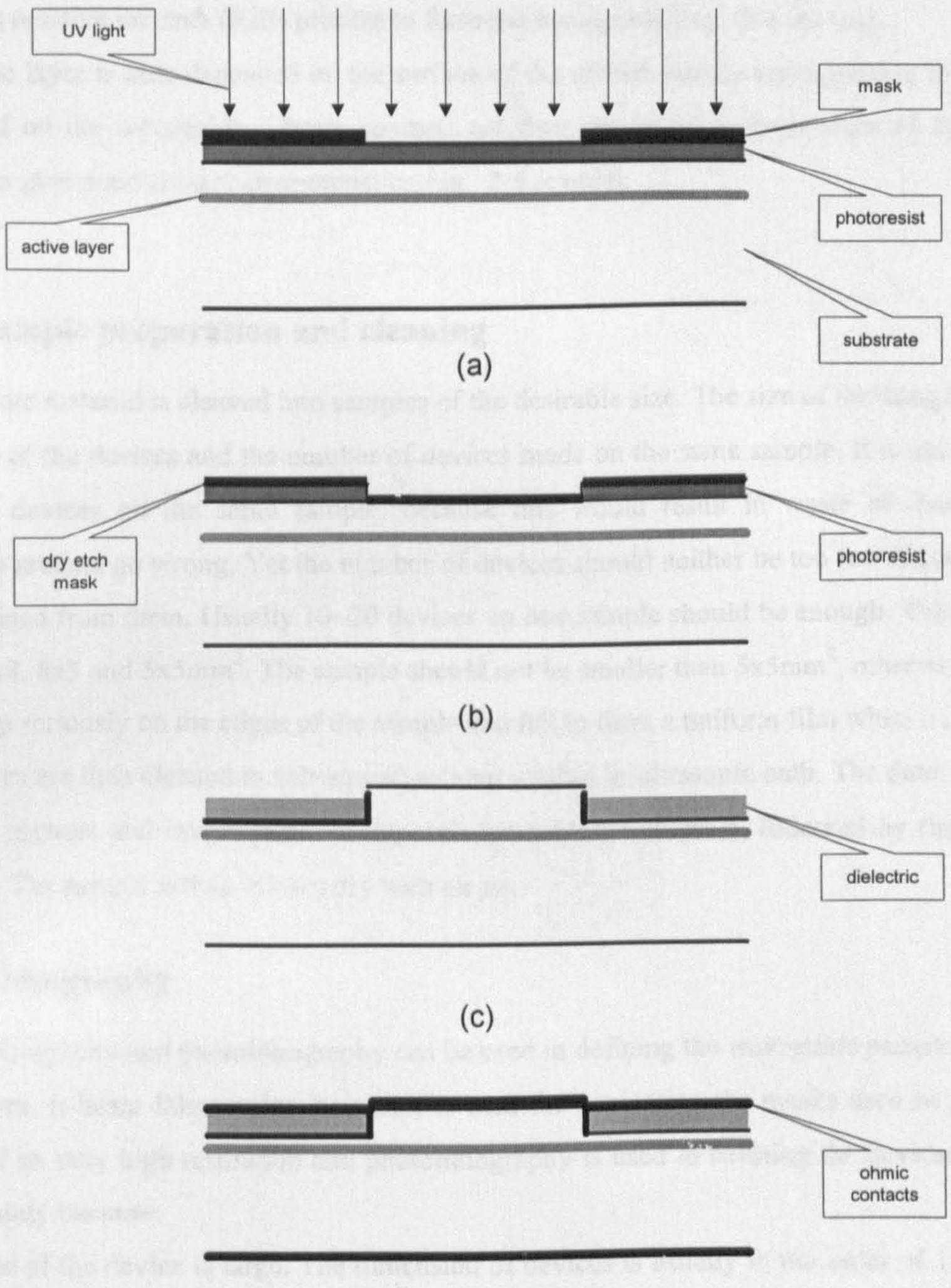

Fig. 2-6 Fabrication process of a optoelectronic waveguide device

In the photolithography step[Fig. 2-6 (a)-(b)], a thin layer of photoresist is first spun on the surface of the sample. The sample is brought into contact with a mask which is transparent in designated areas and is exposed to an ultraviolet (UV) light source. The photoresist exposed to the UV light is then washed away when the patterns are developed.

A dry-etch mask is formed by evaporation of metal film such as Ni/Cr onto the sample then lifting-off the metal over the remaining photoresist by dissolving the photoresist in solvents. The sample is then dry-etched in a reactive ion etch (RIE) process to form the waveguide[Fig. 2-6 (b)-(c)].

A dielectric layer is then deposited on the surface of the etched sample and windows for ohmic contacts are opened on the waveguide. Ohmic contacts are then deposited on both sides of the sample and is annealed to give good contact characteristics[Fig. 2-6 (c)-(d)].

2-3-1 Sample preparation and cleaning

The substrate material is cleaved into samples of the desirable size. The size of the sample depends on the dimension of the devices and the number of devices made on the same sample. It is not suitable to place too many devices on the same sample, because this would result in waste of material should the fabrication process go wrong. Yet the number of devices should neither be too few if convincing data are to be obtained from them. Usually 10~20 devices on one sample should be enough. This result in sample sizes of 8x8, 8x5 and 5x5mm^2. The sample should not be smaller than 5x5mm^2, otherwise the photoresist will pile up seriously on the edges of the sample and fail to form a uniform film when it is spun on.

The samples are then cleaned in subsequent solvent washes in ultrasonic bath. The most popular recipe is methanol, acetone and iso-propanol (IPA), each for at least 4 minutes, followed by rinsing in abundant RO water. The sample is then blown dry with air jet.

2-3-2 Lithography

E-beam lithography and photolithography can be used in defining the waveguide patterns on the samples. In this work, E-beam lithography, however, is used for generating the masks used in photolithography because of its very high resolution and photolithography is used in defining the devices on the samples. This is mainly because:

1) The size of the device is large. The dimension of devices is usually in the order of 1x1mm^2 or larger. This poses the problem of stitching error for e-beam lithography. Stitching error occurs because the e-beam writer can only scan the e-beam spot in an area smaller than 3x3mm^2, therefore for devices with a dimension larger than 3mm, the sample stage must be moved. This is a mechanical movement and the sample could wobble laterally when moved in one certain direction, resulting in misalignment between subsequently written patterns.

2) The required resolution can be achieved with photolithography. The smallest feature encountered in the devices is a waveguide width step of about 0.5μm in MMI couplers. This is well within the resolution of photolithography using UV exposure. The best required repeatability of the waveguide width, which is important in fabricating MMI coupler, is $\pm$ 0.2μm. This is also achievable with photolithography.

3) Photolithography is free of pixelation. In e-beam lithography the spot is scanned stepwise across the sample. At the edges of curved features these steps may result in roughness. Care must be taken to eliminate such an effect. Although the masks in photolithography are generated by e-beam lithography

ard may be pixelised, the roughness is beyond the resolution of photolithography and is smeared out by the diffraction of light.

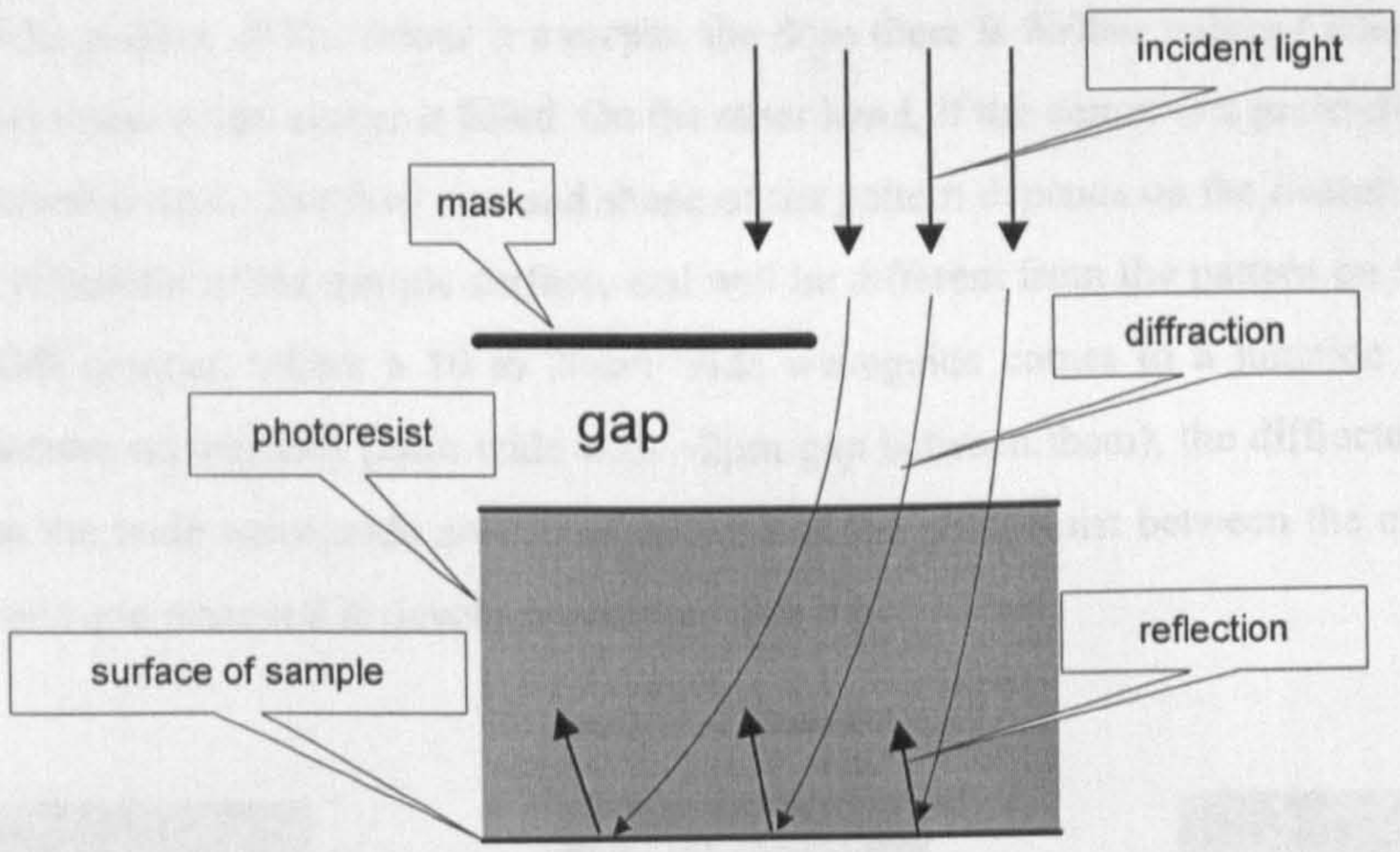

Fig. 2-7 Effects causing the distortion of patterns in photolithography

Throughout the fabrication Shipley Microposit photoresists have been used. In the first photolithographic step when the waveguides are defined, high resolution is the key factor to be considered and therefore thin photoresists (S1400-17 or S1805) must be used. S1400-17 and its safe-solvent substitute S1805 gives film thickness of 0.5μm when spun at 4000rpm (revolutions per minute) for 30 seconds. The recommended exposure dose is 4 seconds at the fixed lamp brightness. This gives good straight line width reproducibility (~0.1μm) in usual applications but is found to be less satisfactory in certain cases. A typical example is the fabrication of MMI couplers where there is a large sudden change of waveguide width.

As illustrated in Fig. 2-7, diffraction of incident light occurs at the edge of the mask because of the fact that there may a gap between the mask and the photoresist and the non-zero thickness of the photoresist.

When the light hits the surface of the sample, part of it will also be reflected back into the photoresist. As a result, the actual exposure profile at the edge of mask is therefore not a ideal step change but a gradual one. The dose near the edge is less than that far from the edge. This effect is particularly significant at a corner of the pattern. If the corner is a recess, the dose there is further reduced than near a straight edge sc the final shape of the corner is filled. On the other hand, if the corner is a protruding one, it will be cut due to increased dose. The final size and shape of the pattern depends on the overall dose, the diffraction and back reflection of the sample surface, and will be different from the pattern on the mask. In the case of the MMI coupler, where a 10 to 20μm wide waveguide comes to a junction with several closely located narrow waveguides (2μm wide with ~2μm gap between them), the diffracted and back reflected light from the wide waveguide area is so strong that the photoresist between the narrow waveguides is also exposed and removed in development[Fig. 2-8(b)].

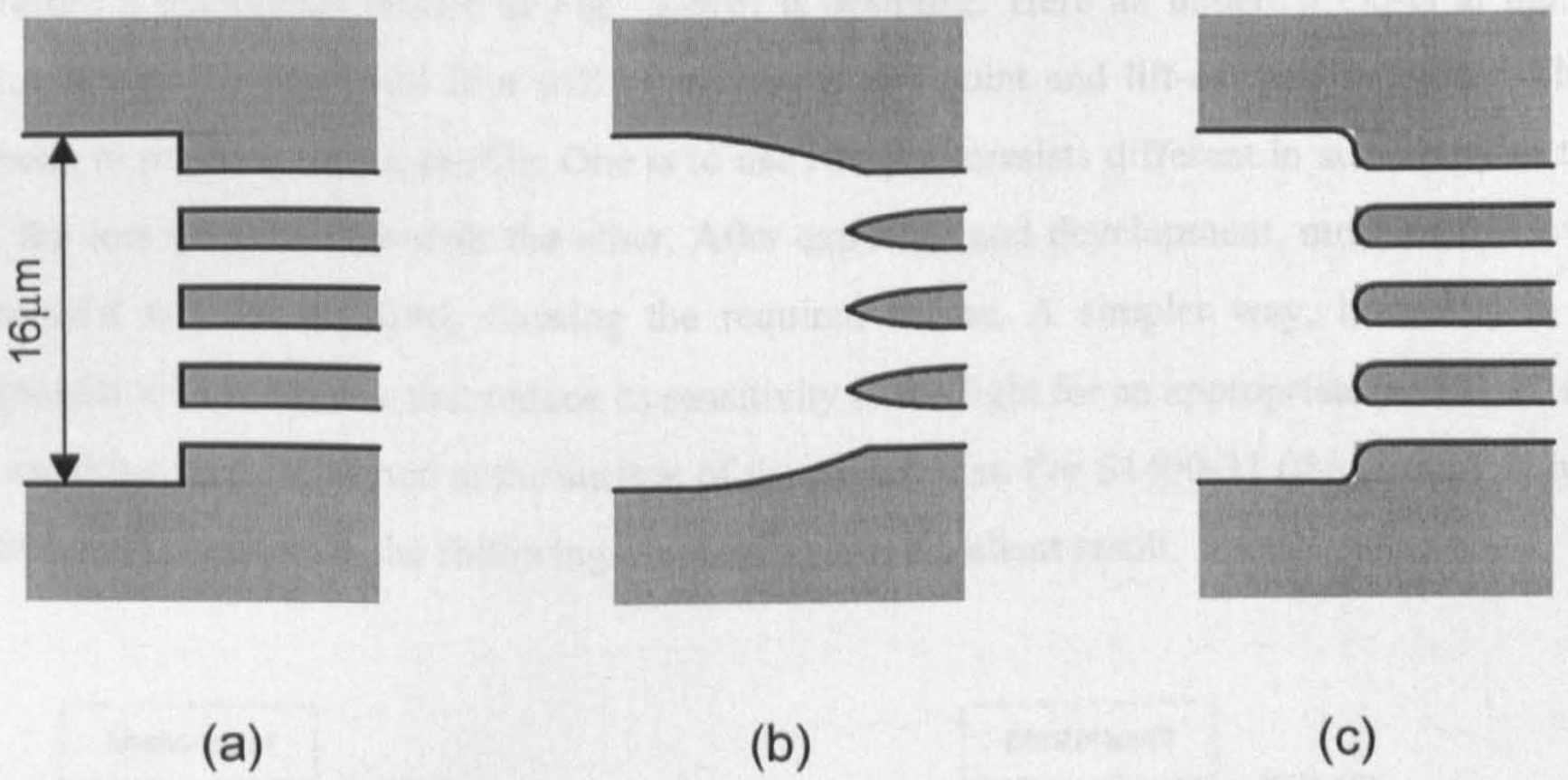

Fig. 2-8 MMI coupler pattern (a)as designed (b)4 sec. exposure (c)2.6 sec. exposure

To minimise the diffraction, the sample must be brought into tight contact with the mask so that there is no gap between them. Thin photoresist must also be used. Back reflection can be reduced by anti-reflective (AR) coating the sample surface. This is usually done by spinning an absorptive film before the photoresist is spun. The AR layer, however, is often difficult to remove after the photoresist is developed. Another effective way to reproduce such a pattern accurately is to reduce the overall exposure dose by reducing the exposure time. Test exposure experiment shows that reductions of up to 40% of the recommended value affect the width of the wide waveguide only slightly (~-0.1mm) when S1400-17 or S1805 are used, because of their small thickness. However, the cuts are extremely effective in improving the reproduction. A nearly square shape at the ends of the photoresist stripe separating the narrow waveguides is obtained at a exposure time of 2.6 seconds[Fig. 2-8(c)].

Second, even third level photolithography may be necessary in the fabrication process. For example, after deposition of a dielectric layer on the sample, windows through the dielectric must be opened above the

waveguides so that ohmic contact can be made. And to electrically isolate devices on the same sample, the ohmic contact may have to be patterned by lift-off, which requires another photolithography step.

2-3-3 Lift-off

Lift-off is a way of patterning thin films by photolithography. The film to be patterned is deposited on the sample after photoresist is exposed and developed. The sample is then soaked in a solvent which dissolves the photoresist. The film on the photoresist is therefore removed, leaving only the film where without photoresist.

When the film to be patterned is thick compared with the thickness of the photoresist (as is the case for lift-off of ohmic contacts), the success of lift-off depends on the profile of the photoresist at its edge. As shown in Fig. 2-9, when the photoresist is exposed and developed in the normal way, its profile will be like Fig. 2-9(a). The deposited material will then form a continuous film, making lift-off very difficult. Therefore a photoresist profile of Fig. 2-9(b) is desirable. Here an undercut exists at the edge of the photoresist so the deposited film will be broken at this point and lift-off will be easier. There are two methods to produce such a profile. One is to use two photoresists different in sensitivity to the light and spin the less sensitive one over the other. After exposure and development, more of the lower layer of photoresist will be removed, forming the required recess. A simpler way, however, is to treat the photoresist with chemicals that reduce its sensitivity to the light for an appropriate period of time so that a less sensitive layer is formed at the surface of the photoresist. For S1400-31 (thickness 1.8μm when spun at 4000rpm, 30seconds), the following procedure gives excellent result.

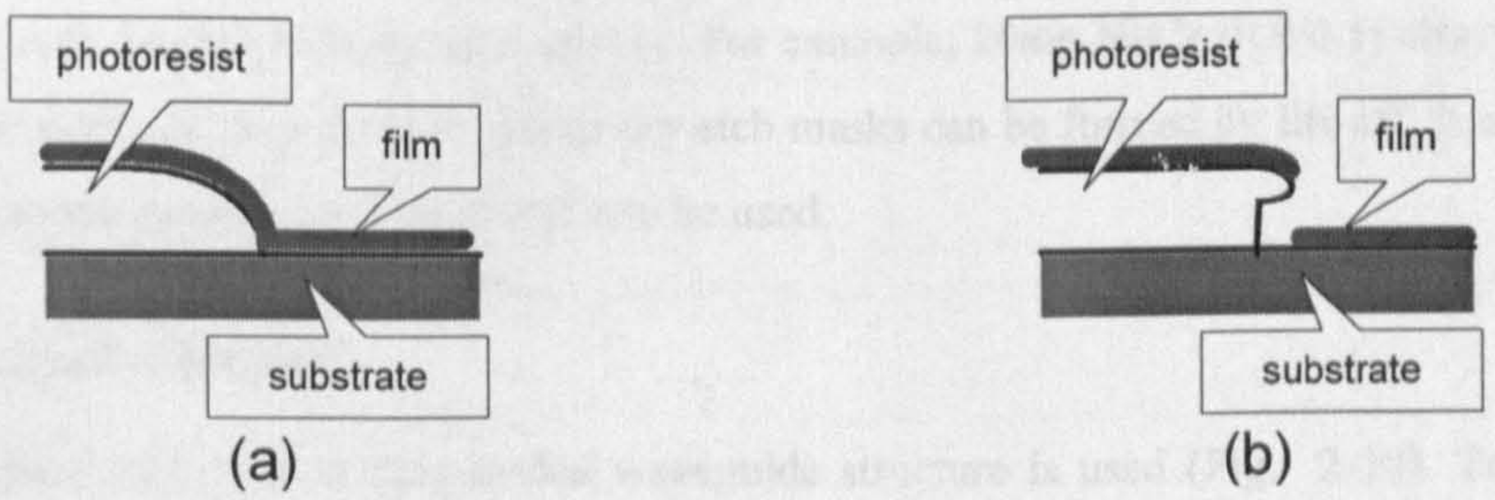

Fig. 2-9 The profiles of photoresist.

step 1	step 2	step 3
bake @90°C for 15 min.	soak in Chlorobenzene for 15min	bake @90°C for 15 min.

Table 2-3

2-3-4 Dry-Etching

Dry etching techniques are ideal for the fabrication of waveguide devices. Compared with wet etching, they have the advantage of being able to be formulated so that the etch will be anisotropic and non-selective, i.e., to have neglectable etch rate along unwanted directions and similar etch rate for different material compositions. This produces highly vertical and smooth waveguide sidewalls.

Silicon Tetrachloride ($SiCl_4$) is used as the etchant in the reactive ion etching (RIE) process to etch GaAs/AlGaAs material. In RIE, the etchant is ionised in a RF discharge plasma. The ions are accelerated by the self-bias voltage generated by the plasma and hit the surface of the sample to react with the sample material. The products of the reaction are volatile and are brought away from the surface by the gas flow. The etched profile depends on the pressure (or gas flow) and the RF power applied to the RIE plasma. When the RF power is kept at 100W, an etching pressure of near 9 millitorr (gas flow 9 sccm) gives nearly rectangular and reproducible waveguide profile. Higher pressure will result in undercut because the ions have more chance to collide with each other, gain lateral momentum and hit the sidewall of the etched profile.

Other dry etching processes used include etching of SiO_2 in C_2F_6 plasma. At an RF power of 100W and gas flow rate of 20sccm, the etch rate is about 50nm/min and gives vertical sidewalls.

Dry etch mask

The profile of the waveguide will also depend on the etch mask. Photoresists erode in the RF plasma at a considerable rate. This fact results in mask shrinking if it is used as the dry etch mask, resulting in inaccurate waveguide width and an overcut profile. Other materials such as metals are more resistant to the dry etch process than the photoresists. For example, 20nm Ni/Cr (0.9/0.1) alloy film can withstand a dry etch depth of 1μm in $SiCl_4$. Metal dry etch masks can be formed by lift-off. It is necessary to reverse the photolithography mask if lift-off is to be used.

Etch depth Control

Throughout this work a strip-loaded waveguide structure is used (Fig. 2-10). To form a strip-loaded waveguide the etch depth of the area surrounding the waveguide must be very close to the guiding layer of the substrate material, i.e., d should be very small (<0.05μm). The effective refractive index of the etched area is very sensitive to d when d is close to zero. For GaAs/AlGaAs material, the refractive index difference between the waveguide and the etched area rises from 0.02 to about 0.05 in a d value range of about 0.1-0μm. To obtain the correct index difference it is important that the d value, or the etch depth is precisely controlled. This is particularly important for devices containing curved waveguides such as SRLs. If the index difference is too small the guiding effect will be too weak and the curved waveguide will have large radiation loss. The smallest possible radius of the curved waveguide is directly related to the index difference. If $1cm^{-1}$ radiation loss is the acceptable standard, For index differences of 0.02 and

0.05 (d=0.1 and 0μm), the corresponding radii are about 450 and 150μm, respectively [1]. To assess whether a strip-loaded waveguide is of the correct etch depth, a set of semiconductor lasers with 180° (half-ring) waveguide [2] of various radius can be fabricated on the same substrate and their threshold current density can be used as a very good indication of the etch depth (see chapter 4 for further detail). An *in-situ* interferometric method has been used to monitor the etch depth, as shown in Fig. 2-10. A laser beam of wavelength λ_0=670nm is projected to the area being etched. The laser beam is reflected by the surface and the internal layer interfaces of the sample. These reflected components interfere with each other to form fringes. As the etching proceeds, the thickness d is changing, so is the light path length of the surface reflection component. This causes the total reflected light intensity to fluctuate periodically. Each period represents an etch depth of λ_0/n, n~3.6 being the refractive index of GaAs. The reaching of an interface can be identified by a sudden change in the phase of the interferometric signal (and often the intensity of the signal, too). The process can be calibrated either by theoretical prediction according to the material layer structure prior to the etching or by the interferometric data recorded in a preliminary etching of the same material. Fig. 2-11 is a typical interferometric trace recorded from a calibration etch of material B680. The interface between the GaAs contact layer (0.2μm thick) and the $Al_{0.4}Ga_{0.6}As$ cladding layer (1.2μm thick) as well as the interface between thc cladding layer and the $Al_{0.2}Ga_{0.8}As$ waveguide layer are clearly identified by the sudden change of signal intensity. This trace can then be used as a reference for future etch of samples using the same material.

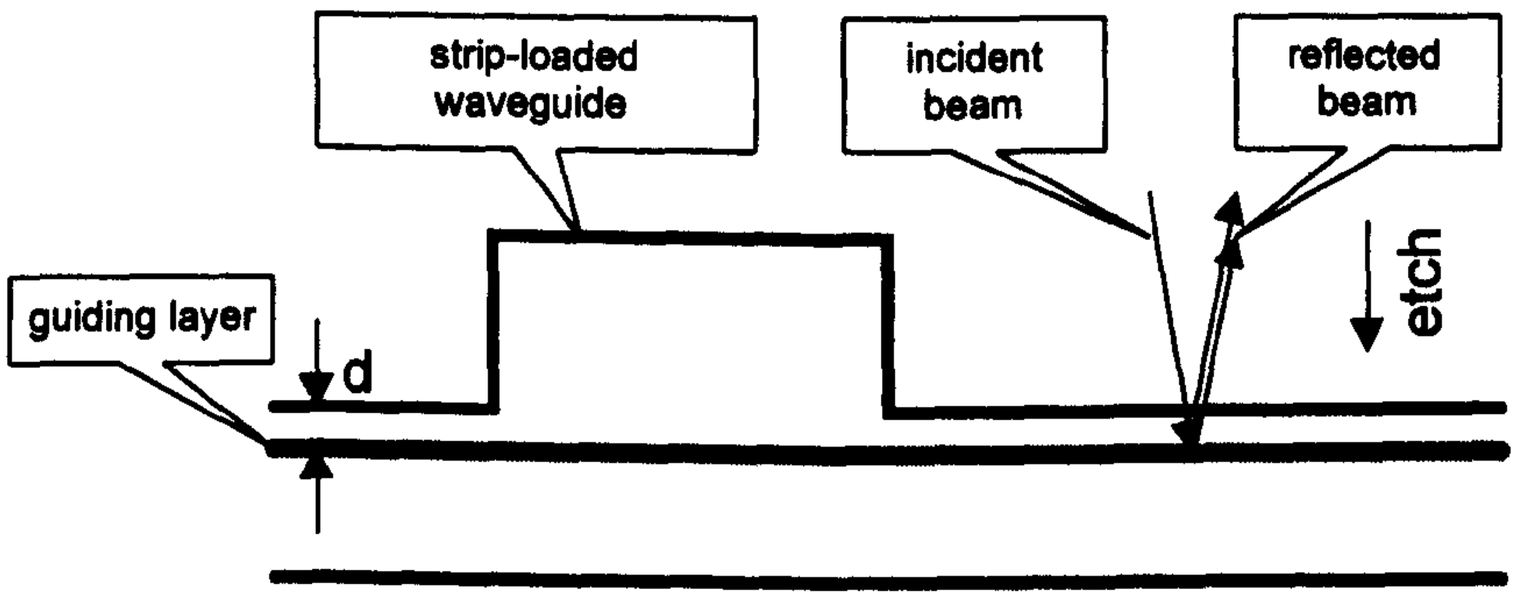

Fig. 2-10 Strip-loaded waveguide and etch-depth control

[1]Krauss, T. F., De La Rue, R. M., Gontijo, I., Laybourn P. J. R., and Roberts, J. S., 'Strip-loaded semiconductor ring lasers employing multi-mode interference (MMI) couplers', Appl. Phys. Lett.,

[2] Krauss, T. F., 'Integrated semiconductor ring lasers', Ph.D thesis. University of Glasgow, 1992.

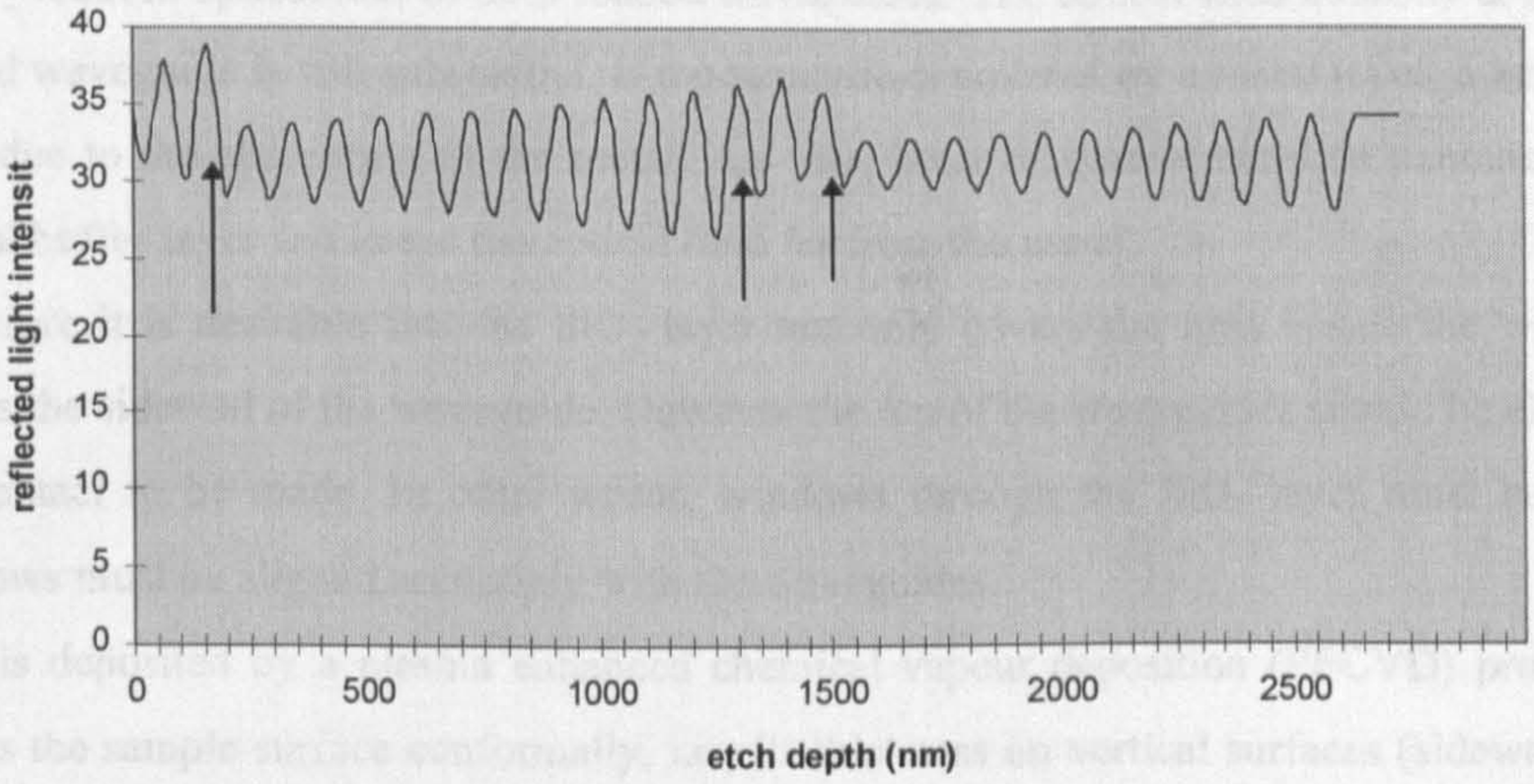

Fig. 2-11 *In situ* interferometric trace of the dry etch process. Interfaces between layers are indicated by arrows.

2-3-5 Metalisation

After the definition of the waveguide devices, ohmic contacts must be deposited where appropriate. The cap layer of the semiconductor materials is heavily doped for good ohmic contacts to be made. The surface of the semiconductor is first treated with diluted HCl (1:4 HCl:H_2O) solution to remove native oxides and other depositives formed during previous fabrication steps. the sample is then rinse in deionised (DI) water.

For p-contact, Ni/Au (70/200nm) can be used. A better choice is Ti:Pd:Au because Ti has better adhesion to the surface and Pd stops Au from diffusing into the semiconductor, which often causes destruction of the device junction. This contact must be annealed, otherwise it forms a Shottky junction with the semiconductor.

For n-contact, Au/Ge/Au/Ni/Au (14/14/14/11/200nm) is a very good combination.

In order to obtain good ohmic contact the contacts must be annealed after deposition so that the metal diffuses into the semiconductor and turns the semiconductor close to the contact degenerate. The typical annealing parameter for these contacts is 400°C for 60 seconds.

2-4 Self-aligned Process for Second-level Lithography

When the waveguide devices are defined by photolithography and dry etching, a layer of SiO_2 is deposited on the sample. This has three purposes:

1)SiO_2 is used as a electrical insulator so that the ohmic contact contacts the semiconductor only on the waveguide. In the case of strip-loaded waveguide, this helps to reduce injection current leakage at the side of the waveguide. If the waveguide is a deeply etched ridge waveguide (i.e., etched through the guiding or active layer), the SiO_2 layer is particularly important because it prevents the active layer from being short circuited by the contact.

2)SiO_2 passivates the surface of the semiconductor. It shields the semiconductor from the atmosphere, reduces degradation and enhances the lifetime of devices.

3)SiO_2 reduces optical loss of strip-loaded waveguides. The optical field intensity at the foot of the strip-loaded waveguide is still substantial. If the structure is covered by a metal layer, a large optical loss may arise due to the absorption of the metal. An SiO_2 layer of several hundred nanometers thick acts as a optical buffer layer and keeps the optical field far from the metal.

Therefore it is desirable that the SiO_2 layer not only covers the area beside the waveguides, but also covers the sidewall of the waveguide. However the top of the waveguides should be clear of SiO_2 in order for contact to be made. In other words, windows through the SiO_2 layer must be opened and these windows must be aligned accurately with the waveguides.

SiO_2 is deposited by a plasma enhanced chemical vapour deposition (PECVD) process. PECVD SiO_2 covers the sample surface conformally, i.e., its thickness on vertical surfaces (sidewalls) is almost equal to that on horizontal surfaces.

The most straightforward way of opening windows through the SiO_2 layer is by performing another level of photolithography. This applies well for straight waveguides over 5μm wide, because the alignment tolerance may be as large as 1μm and alignment is required in only one direction. In the case of very narrow (<3μm) and curved waveguides, the sub-micron and two dimensional alignment is almost impossible to achieve unless e-beam lithography is used. Therefore a self-aligned process must be developed.

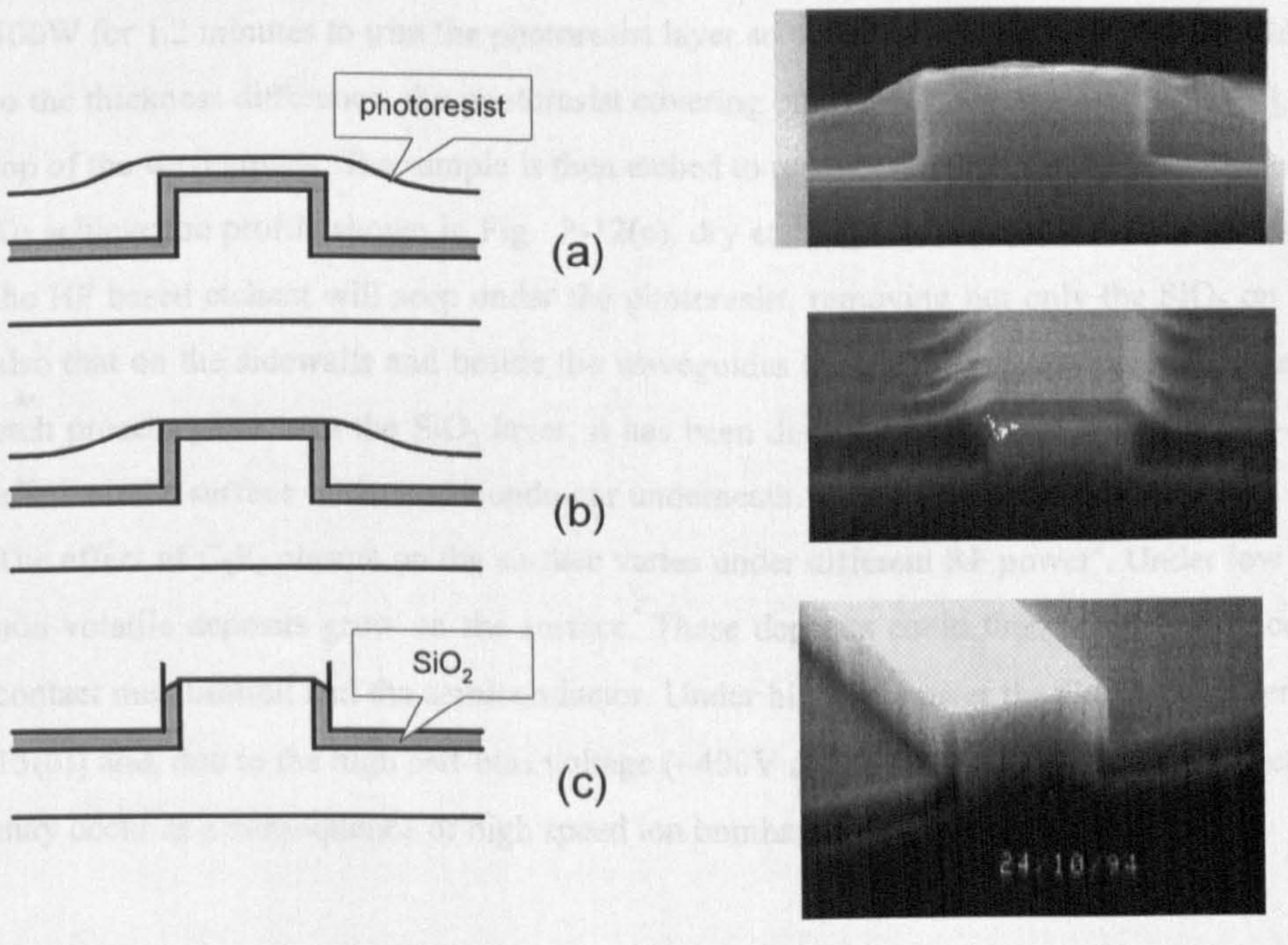

Fig. 2-12 Self-aligned process for o pening windows in SiO_2, (a)as spun, (b) after ashing and (c) window opened.

There was much effort to develop self-aligned processes in the group for various fabrication purposes. Most notably was a process developed by Krauss[1] for fabricating ring lasers. This process employed a so-called 'metal on polymer (MOP)' mask which consisted of a polyimide layer and a metal mask defined by lift-off. The polyimide layer, masked by the metal, was etched in oxygen plasma to expose the semiconductor. Waveguides were then defined by sebsequent dry-etching in $SiCl_4$ plasma. The MOP mask was kept in place while a silica layer was deposited, and was dissolved in boiling xyphenon afterwards to lift-off the silica layer so that windows exactly aligned with the waveguides were opened.

There were several problems associated with this process. Because the silica layer deposited by PECVD was conformal, the sidewalls of the MOP mask was also covered by silica, makes lift-off very difficult (must be done in boiling solvent). The lift-off was particularly difficult for wider waveguides. Besides, the solvent used for polyimide was a quite dangerous substance.

The process used here makes use of the fact that, due to surface tension, photoresist and other polymers, e.g., polyimide, form thinner film on the top of mesas than on flat areas when they are spun on the sample. It is also well known that they can be trimmed by oxygen plasma ashing.

Photoresist S1400-17 is used in this process. When spinning at 4000rpm for 30 seconds, it forms a film of 0.5μm thick on flat surface. However, on narrow waveguides, the film is less than 0.1μm thick [Fig. 2-12(a)]. After baking, the sample is ashed in oxygen plasma at a gas flow of 20sccm and RF power of 100W for 1.2 minutes to trim the photoresist layer so that the thin film on the waveguide is removed. Due to the thickness difference, the photoresist covering other areas remains[Fig. 2-12(b)], exposing only the top of the waveguides. The sample is then etched to remove the SiO_2 on the top of the waveguides.

To achieve the profile shown in Fig. 2-12(c), dry etching of SiO_2 should be used. If wet etching is used, the HF based etchant will seep under the photoresist, removing not only the SiO_2 on the waveguide but also that on the sidewalls and beside the waveguides [Fig. 2-13(a)]. On the other hand, if the usual dry etch process penetrates the SiO_2 layer, it has been discovered that C_2F_6 plasma over-etch has some bad effect on the surface of the semiconductor underneath.

The effect of C_2F_6 plasma on the surface varies under different RF power[2]. Under low RF power (<30W) non-volatile deposits grow on the surface. These deposits could then result in bad contact between the contact metalisation and the semiconductor. Under high RF power the GaAs cap layer is etched [Fig. 2-13(b)] and, due to the high self-bias voltage (~400V at 100W RF power), semiconductor surface damage may occur as a consequence of high speed ion bombardment.

---

[1] Krauss, T. F., De La Rue, R., Laybourn, P. J. R., Vogele, B., and Stanley, C., "Efficient semiconductor ring lasers made by a simple self-aligned fabrication process', IEEE J. of Selected Topics in Quantum Electronics, VOL.1, NO.2, pp.757-761.

[2]Ooi, B. S., Ph.D. Thesis, University of Glasgow, 1994, p26-32.

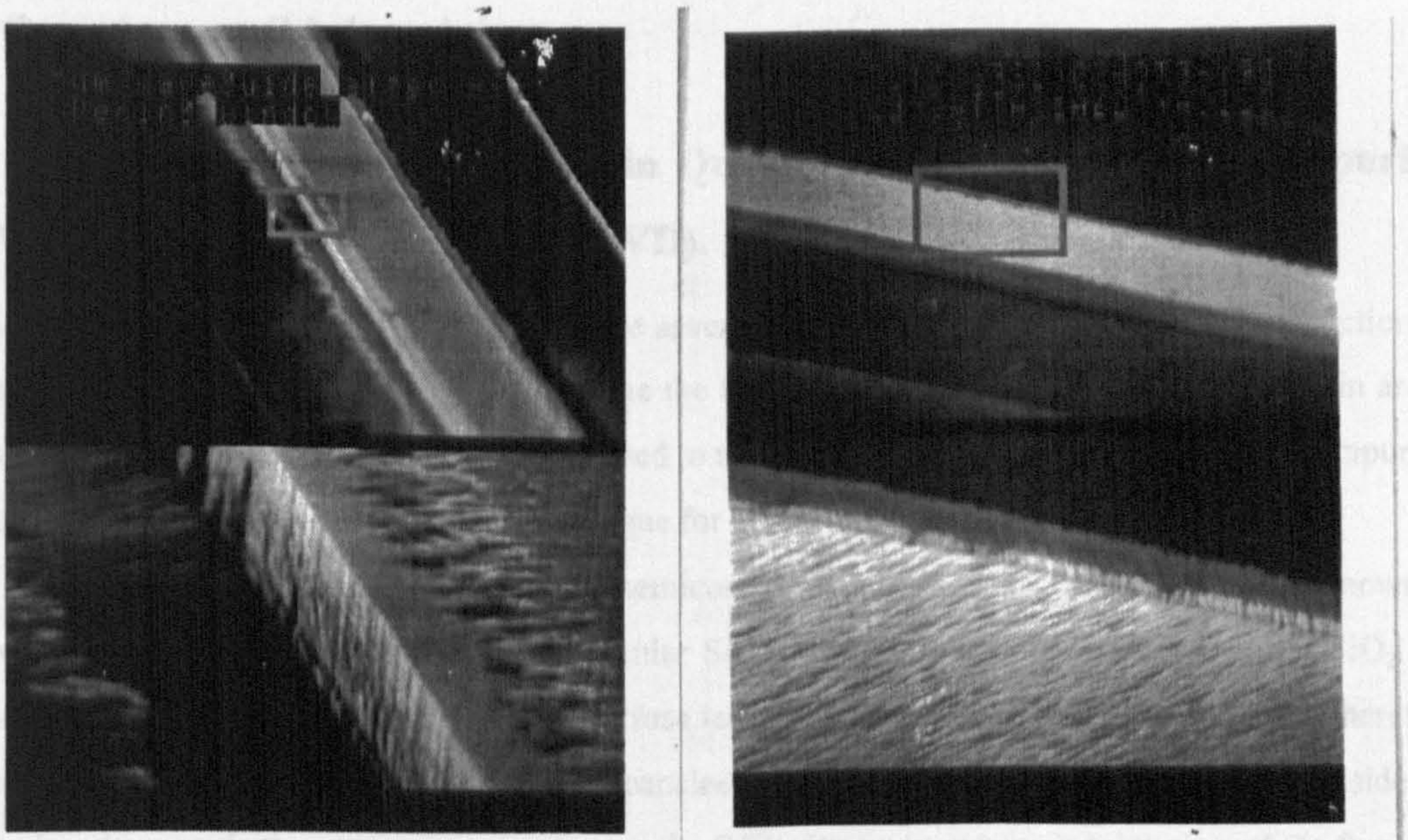

Fig. 2-13 (a)Wet etched window and (b)surface damage on the waveguide caused by C_2F_6 dry etching. The dark material is SiO_2 and the bright material is GaAs. In (a) the SiO_2 layer beside the waveguide has been removed even before the waveguide top is cleared.

A combination of dry and wet etching is therefore used to open the window. After O_2 plasma ashing, the sample is first dry etched in C_2F_6 plasma to remove most of the SiO_2. For a 500nm SiO_2 layer, it is optimal to etch under 100W RF power at a gas flow of 20sccm for 6.5-7 minutes. The etch depth is about 350-400nm, leaving about 100-150nm SiO_2. The sample is then wet etched in 1:4 Silica Etch (an HF based etchant) for a very short time (~5 seconds) to remove the remaining SiO_2. It is important that the wet etching must not exceed 10 seconds so that the etchant has no time to permeate under the photoresist. For best effect, the sample should be post baked for 15 minutes at 90°C after dry etching. This can increase the photoresist's resistance to the wet etchant and cure the possible pinholes in the photoresist formed during dry etching. Wet etchant could have penetrated these pinholes to etch the SiO_2 underneath. Compared with S1400-17, photoresist S1805 is found to have better endurance to the dry etching and better resistance to the permeation of wet etchants. It is slightly more difficult to ash so a longer ashing time should be used.

This process is self-aligned. It eliminates the need for the second level photolithography and the related extremely difficult alignment. It is very reliable and works well on waveguides and mesas less than ~16μm wide. For wider features, the photoresist in the centre of the mesa tends to have the same thickness as on large flat surface and the ashing process will only expose the edge of the mesa. Therefore the method does not apply.

2-5 Quantum-well Intermixing

2-5-1 Principle of Bandgap Tuning in Quantum-well Materials using Impurity-free Vacancy -induced Disordering(IFVD).

As briefly discussed in section 2-1-3, to integrate several optoelectronic devices of different function on the same substrate, it is often necessary to change the bandgap of the substrate material in certain areas. In this section a more detailed discussion is devoted to the main technique used in this work-the impurity-free vacancy-induced disordering (IFVD) technique for bandgap tuning.

IFVD relies on creating vacancies in the III-V semiconductor [1]. The group III element Ga is known to dissolve in certain dielectric materials, in particular SiO_2. When the sample is coated with a SiO_2 cap layer and heated to high temperature, Ga will diffuse into the SiO_2 cap. Group III vacancies are therefore generated near the surface of the sample. The vacancies are filled by Ga ions out-diffused from inside the sample. In other words the vacancies migrate into the QWs due to an outgoing migration of Ga from the QWs, promoting the diffusion of Al into the QWs [2]. A changed Ga/Al composition in the QWs is therefore the result and the shape of the QWs is no longer an abrupt one. These effects elevate the bottom of the QWs to higher energy and consequently lift the quantised state energies, resulting in a widened effective bandgap in the QWs.

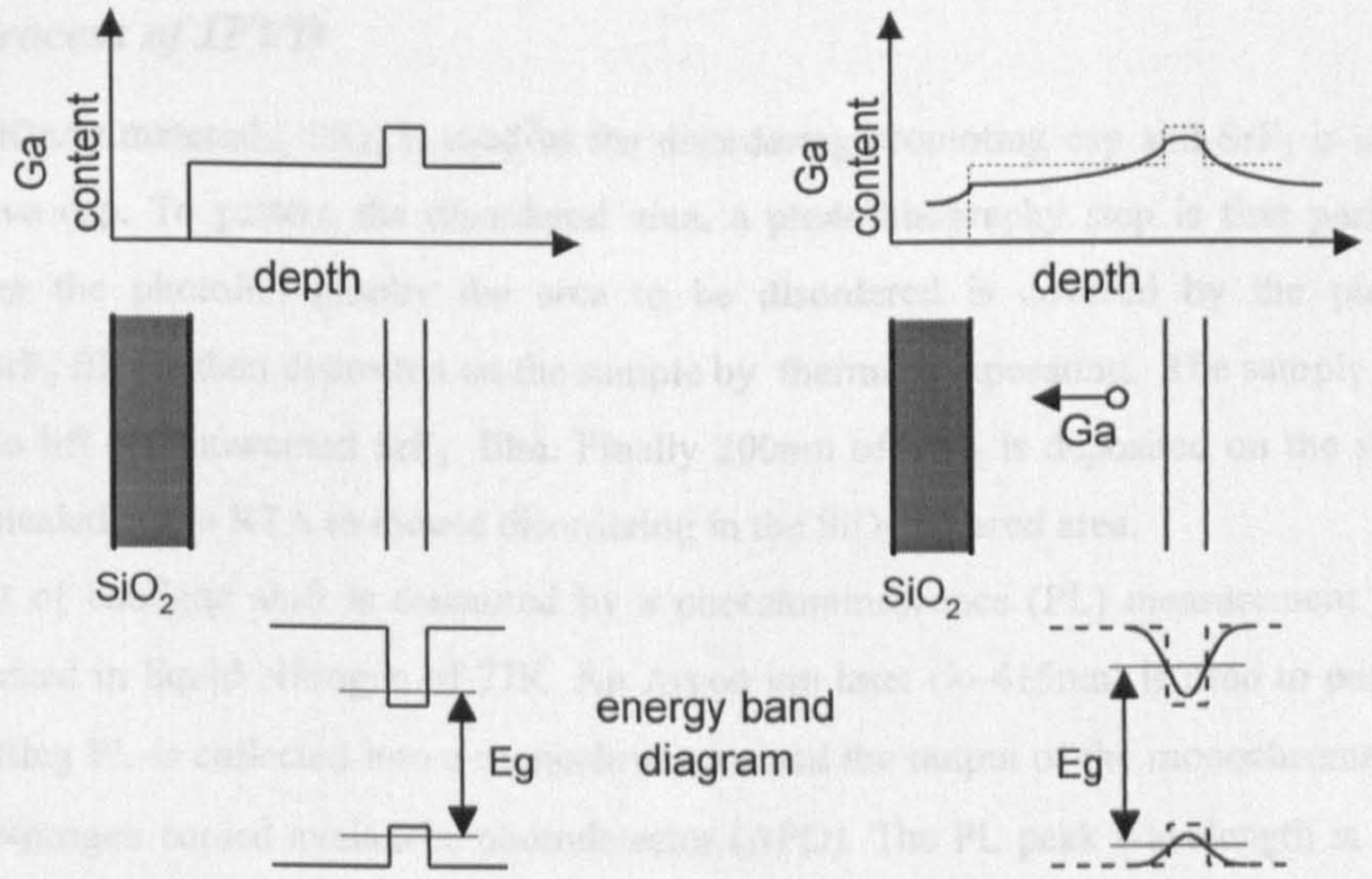

Fig. 2-14 The IFVD process.

Unlike some other disordering techniques (such as impurity-induced disordering-IID), IFVD does not introduce any foreign particles, charged or neutral, into the material. Therefore it has the potential of producing low loss, high quantum efficiency bandgap tuned QW materials. These materials would be

---

[1]Marsh, J. H., 'Quantum Well Intermixing', Semicondutor Sci. and Technology, **8** (1993) pp1136-1155.

[2]Ooi, B. S., Ph.D. Thesis, University of Glasgow, 1994, p100.

suitable for the fabrication of low loss waveguides and active optoelectronic devices such as wavelength tuned lasers and modulators.

2-5-2 IFVD Techniques and Results.

There are a number of practical issues to be solved if IFVD is to be used in device fabrication.

1)Disordering prohibition. The final purpose of IFVD is to produce a reasonable amount of bandgap difference between different parts of the sample. Where bandgap shift is not wanted, a method must be found to prohibit disordering from happening. This is usually achieved by using other kinds of dielectric caps, most notably Strontium Fluoride (SrF_2), which stop the out-diffusion of Ga.

2)Surface quality. IFVD takes place at quite high temperatures (~900°C). Under such temperatures the dielectric caps and the materials expand, usually at different rates, producing very large stress at their interface, i.e., the surface of the material. This stress could result in surface damage. Bad surface morphology can result in roughness ('grass') in later dry etching process. It also prevents good ohmic contact being made in the final stage of fabrication.

3)The parameters of high temperature processing. This process is usually performed in a rapid thermal annealing (RTA) apparatus. The necessary annealing temperature and time to produce a certain amount of bandgap shift must be found. These vary from material to material.

General Process of IFVD

For GaAs/AlGaAs materials, SiO_2 is used as the disordering promoting cap and SrF_2 is usually used as the prohibitive cap. To pattern the disordered area, a photolithography step is first performed on the sample. After the photolithography the area to be disordered is covered by the photoresist. The prohibitive SrF_2 film is then deposited on the sample by thermal evaporation. The sample is then soaked in Acetone to lift off unwanted SrF_2 film. Finally 200nm of SiO_2 is deposited on the sample and the sample is annealed in the RTA to induce disordering in the SiO_2 covered area.

The amount of bandgap shift is measured by a photoluminescence (PL) measurement. The annealed sample is soaked in liquid Nitrogen of 77K. An Argon ion laser (λ~415nm) is used to pump the sample and the resulting PL is collected into a monochromator and the output of the monochromator is detected by a liquid Nitrogen cooled avalanche photodetector (APD). The PL peak wavelength is determined by the bandgap energy of the sample and is compared with both the PL wavelength before annealing and that of the disordering-prohibited area.

After reaching the wanted bandgap shift, which is determined by the purpose of the disordered material, the dielectric caps are removed by wet etching. The SiO_2 cap can be removed by the HF-based SiO_2 Etch solution, although it takes much longer (~1.5 minutes for 200nm) to removed the annealed SiO_2 cap than the usual SiO_2 (<20 seconds for 200nm). SrF_2 can be removed by undiluted HCl acid. For quicker removal, sponge swabs can be used to rub the SrF_2 away from the surface.

Sample loading

For better reproducibility the samples in the RTA are placed face down on a piece of GaAs larger than the samples so that a As-rich vapour exists in the proximity of the sample. Another piece of GaAs covers the back of the sample so that the sample heats up after the As atmosphere is built up (Fig. 2-15). In the RTA the sample is heated by a halogen lamp from the back. Before annealing the chamber is purged and then charged with Nitrogen.

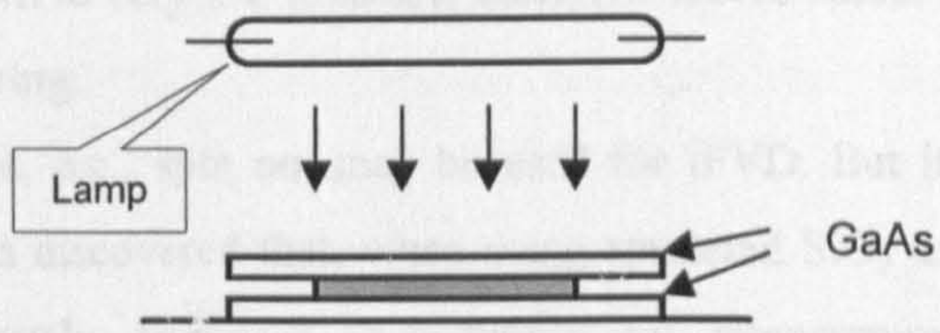

Fig. 2-15 The sample loaded in the RTA

Annealing time and temperature

The bandgap shift caused by IFVD depends on the temperature and time of annealing. For GaAs/AlGaAs materials, there is a threshold temperature in the range of about 850-900°C. The threshold temperature varies from material to material. It is also related to the way the sample is loaded in the RTA. Above the threshold temperature, the amount of PL wavelength shift increase with time and temperature, as shown in Fig. 2-16.

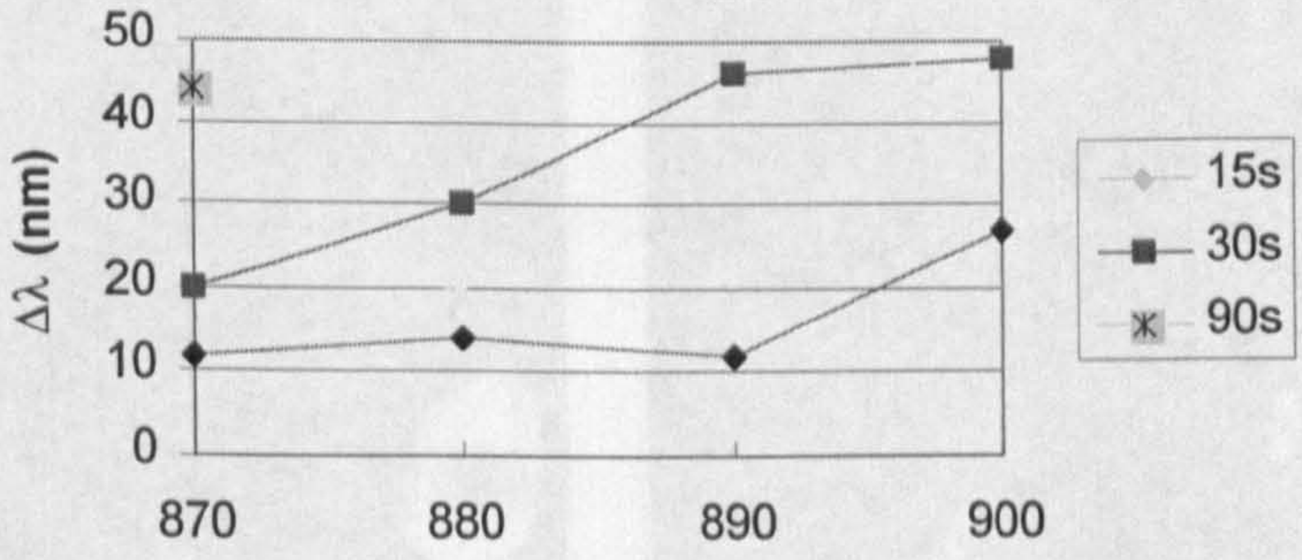

Fig. 2-16 The PL wavelength shift Δλ vs. annealing temperature for different annealing times. Material: B680 (MBE DQW).

For any particular material, a series of test annealing must be carried out to find the threshold temperature. A certain amount of wavelength shift can then be obtained either by a combination of higher temperature and short annealing time or lower temperature and longer annealing time. However, it is

better to choose the latter combination because higher temperature usually results in worse surface morphology. The latter combination is also more controllable and reproducible.

Dielectric caps and surface morphology

Care must be taken in deposition of both promoting and prohibitive caps.

1)The SiO_2 disordering promoting cap layer is deposited by PECVD. During this process the sample is held at a temperature of 400°C. Therefore oxidisation must be avoided using the 'cold load' technique, i.e., the sample should loaded into the machine at room temperature and the temperature is elevated only when the chamber is pumped down to very low pressure, otherwise native oxides of GaAs formed at high temperature will prohibit disordering.

2)SiO_2 deposited by other means, e.g., spin on, may be used for IFVD. But it must be made free of contamination. For example, it is discovered that, when using sputtered SiO_2 as the IFVD cap, the PL intensity of the sample is seriously decreased at relatively low temperature of 800°C and totally extinguished at temperatures above 850°C. This is believed to be due to the contamination of Al from Al_2O_3 residuals in the chamber. These excessive Al atoms may diffuse into the QWs and reduce the radiative recombination efficiency.

2)SrF_2 film should be deposited at a very slow rate (about 0.1-0.2nm/s). SrF_2 is a rather loose and soft material. The slower the deposition rate, the more condensed the film is. This helps the film to stand the stress produced by the annealing. The film should not be too thick because thinner films adapt to the stress better. A thickness more than 50nm is enough to prohibit disordering so usually the thickness should not exceed 200nm.

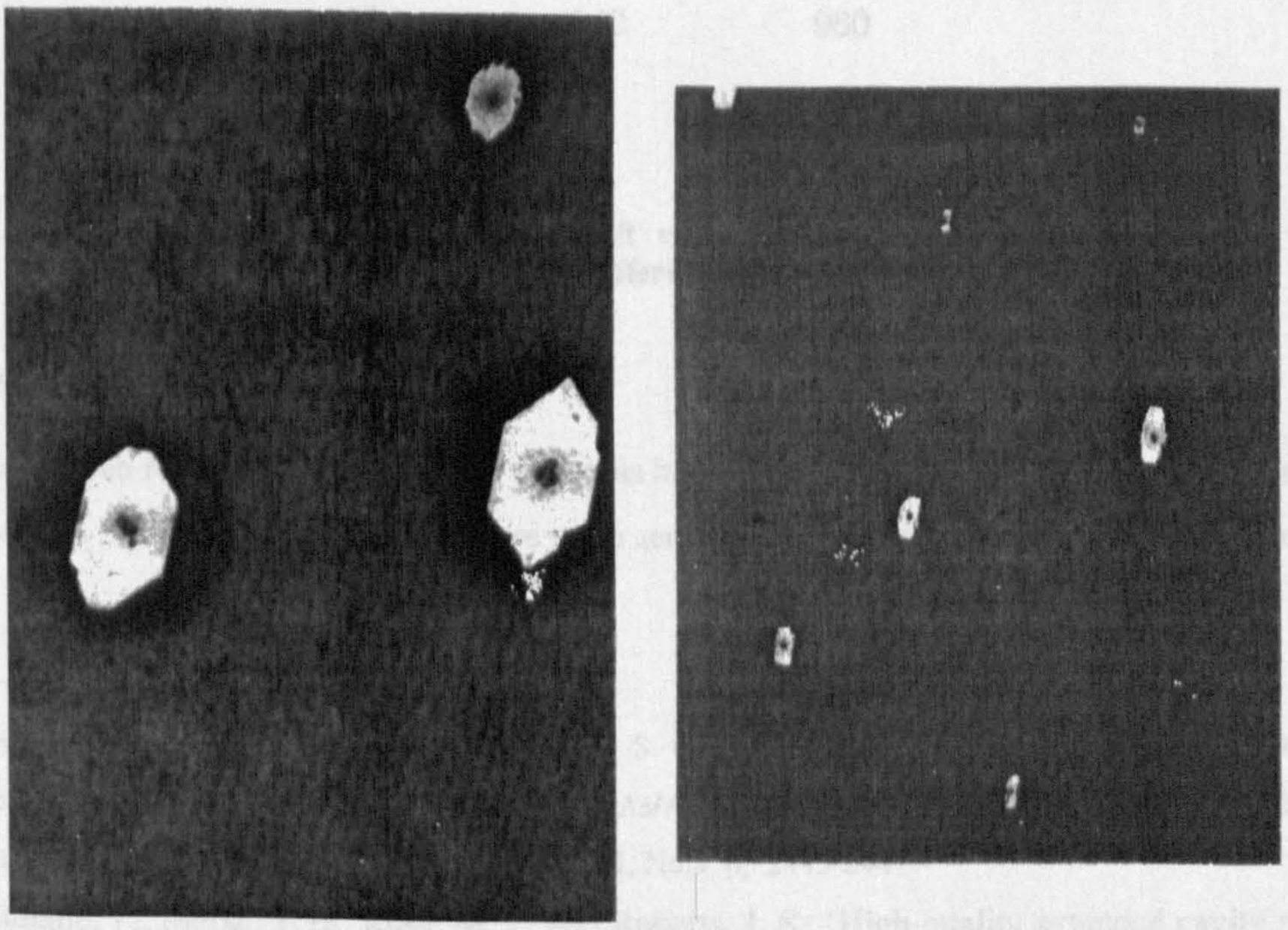

Fig. 2-17 Surface damages in SrF_2 area after annealing. Both hexagonal and near rectangular shapes are observed. The magnification is 1500X and 600X for the left and right pictures, respectively.

In most cases SrF_2 can successfully prohibit disordering. But the surface quality under the SrF_2 film is often less than satisfactory however carefully the film is deposited. The main form of surface damage is a polygonal crater-like defect. The sides of the polygon seem to be conformal with crystal plane directions (Fig. 2-17). Molten material droplets can sometimes be seen on both sides of the rectangle. The cause of such surface damage, which only occurs in SrF_2 covered area, is still unidentified. One possible cause is that low melting point impurity particles exists in the SrF_2 film. When the sample is heated these impurity particles melt. The resulting high pressure vapour causes micro-explosions thereby damaging the surface locally. Apart from this crater-like damage, surface roughness also occurs in most cases. This may result in 'grassy' dry-etched surface later. Observation reveals that, after annealing, microscopic granules may have occurred in the SrF_2 film because tiny reflecting spots can be identified. These micro-granules may be the cause of surface roughness.

A new cap, Phosphor(P)-doped SiO_2, is recently introduced as a prohibitive cap [1]. The P content (~4%) in the SiO_2 greatly reduces the solubility of Ga in the cap thereby prevents disordering. This cap works as well as SrF_2 and leaves a very smooth surface. A P-doped SiO_2 cap produced some of the best extended cavity semiconductor lasers so far and has resulted in a very promising progress in IFVD[2].

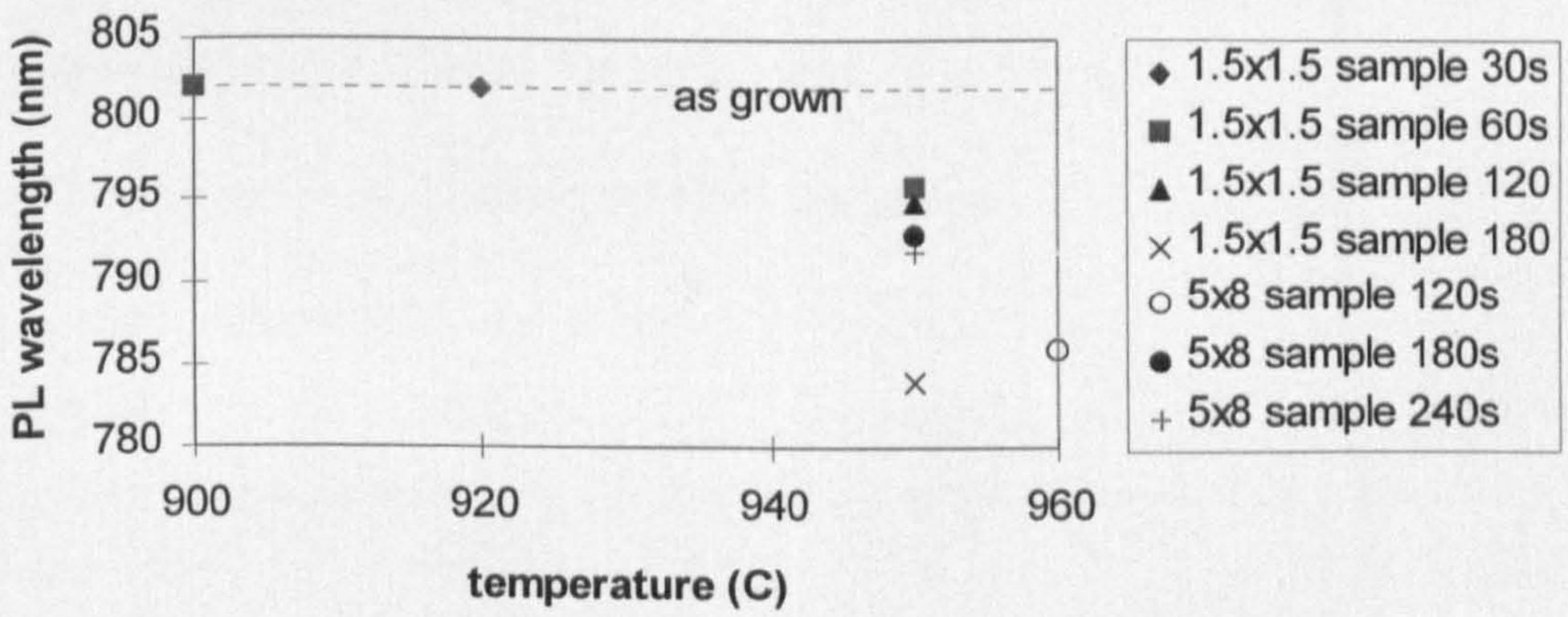

Fig. 2-18 PL wavelength shift vs. annealing time of material QT899 (MOVPE DQW) in different sample sizes.

Material dependence

It has long been recognised that different materials have different sensitivity to the annealing process. On average, it is found that MBE materials are more sensitive, i.e., under the same conditions, they produce

---

[1] Cusumano, P., Ooi, B. S., Helmy, A. S., Ayling, S. G., Bryce, A. C., Marsh, J. H., Voegele, B., Rose, M. J., 'Suppression of quantum well intermixing in GaAs/AlGaAs laser structures using phosphorus-doped SiO2 encapsulant layer', J. of Applied Physics, 1997, Vol.81, No.5, pp.2445-2447.

[2] Cusumano, P., Marsh, J. H., Rose, M. J., and Roberts, J. S., 'High-quality extended cavity ridge lasers fabricated by impurity-free vacancy diffusion with a novel masking technique', IEEE Photonics Technology Letters, 1997, Vol.9, No.3, pp.282-284.

larger bandgap shifts than MOVPE materials. The explanation may be traced to the different background doping in the two materials.

In the nominally 'intrinsic' QWs and barrier layers, background doping resulting from the MOVPE growth is p-type while MBE usually produces n-type background doping. The density of group III vacancies V_{III}, which is the main cause of interdiffusion under the As-rich annealing atmosphere, is proportional to the acceptor (or n-dopant) density in the material[1,2]. Therefore in a p-type background doping, V_{III} is reduced and disordering is suppressed. On the contrary, n-type background doping increases V_{III} hence promotes disordering.

Comparing the data in Fig. 2-16 and Fig. 2-18, this fact is quite obvious. For the MBE material B680 (estimated background n-doping from C-V measurement ~$10^{16}cm^{-3}$), blue shifts up to 40nm can be reached by annealing at 890°C for 30 seconds, whereas for MOVPE material QT899 (background p-doping ~$1X10^{16}cm^{-3}$) , the threshold temperature is above 920°C. Blue shift of about 20nm is reach only when annealed at a temperature as high as 950°C for 180 seconds or 960°C for 120 seconds. Another MBE material, B429 with p-doped QWs, shows moderate sensitivity compared with B680. Blue shifts of about 20-25nm are obtained when B429 is annealed at 925°C for 30 seconds.

---

[1]Guido, L. J., Holonyak, N., Hsieh. K. C., Kaliski, R. W., Plano, W. E., Burnham, R. D., Thornton, R. L., Epler, J. E., and Paoli, T. L., 'Effects of dielectric encapsulation and as overpressure on al-ga interdiffusion in alxga1-xas-gaas quantum-well heterostructures', J. of Applied Physics, 1987, Vol.61, No.4, pp.1372-1379.

[2] Marsh, J. H., "Quantum-well intermixing', Semiconductor Sci. & Tech., 1993, 8, pp.1136-1155.

3 Multi-mode Interference (MMI) Couplers

The self-imaging property of a multimode wavegide as result of multimode interference (MMI) effect was first discussed as early as 1975[1]. In recent years MMI couplers has attracted much attention because of their certain advantages over other kind of couplers, such as directional couplers. The research carried out by Pennings and Soldano et al [2,,3,4] has taken MMI couplers into practical use and various devices have been fabricated. In the meanwhile, the research by Bachmann, Besse and Melchior[5, 6] contributed much to the understanding of the principles of the MMI couplers and their general properties, and revealed the existence of new structures with arbitrary power splitting ratios[7].

One of MMI couplers' outstanding feature is that they allow multiple access, therefore are very suitable for the purpose of multiplexers and demultiplexers. The size of a multiple access MMI coupler would be more compact than a group of directional couplers performing the same function. The purpose of this chapter is to investigate the property of MMI couplers used as power multiplexers. The operational principle and design method of MMI couplers will be discussed. Guidelines for fabrication will also presented. These should also apply to the MMI couplers used as output couplers for ring lasers The advantages and problems associated with that application are discussed in chapter 4.

3-1 Theory and Modelling of MMI Couplers

3-1-1 Principle of MMI couplers

As shown in Fig. 3-1, the input field $E_{in}(x, 0)$ to a multimode waveguide will in general excite all the eigenmodes $E_k(x)$ of the waveguide. The input field $E_{in}(x)$ can be expressed as[1]

---

[1] Ulrich, R., 'Image formation by phase coincidences in optical waveguides', Optics Communications, VOL.13, NO.3, 1975, pp.259-264.

[2] Penning, E. C. M., et al, 'Ultracompact, low-loss directional-couplers on InP based on self-imaging by multimode interference', Applied Physic Letters, VOL.59, NO.16, 1991,pp.1926-1928.

[3] Soldano, L. B. et al, 'Planar monomode optical couplers based on multimode interference effects', Journal of Light wave Technology, 1992, 12, pp.1843-1849.

[4] Soldano, L. B., and Penning, E. C. M., 'Optical multimode interference device based on self-imaging - priciples and applications', J. of Lightwave Technology, VOL.13, NO.4, 1995, pp.615-627.

[5] Bachmann, M., Besse, P. A., and Melchior, H., 'General self-imaging properties in NXN multimode interference couplers including phase-relations', Applied Optics, VOL.33, NO.18, 1994, pp.3905-3911.

[6] Bachmann, M., Besse, P. A., and Melchior, H., 'Overlapping-image multimode interference couplers with a reduced number of self-images for uniform and nonuniform power splitting', Applied Optics, VOL.34, NO.30, 1995, pp.6898-6910.

[7] Lai, Q., Bachmann, M., Hunziker, W., Besse, P. A., and Melchior, H., 'Arbitrary ratio power splitters using angled silica on silicon multimode interference couplers', Electronics Letters, VOL.32, NO.17, 1996, pp.1576-1577.

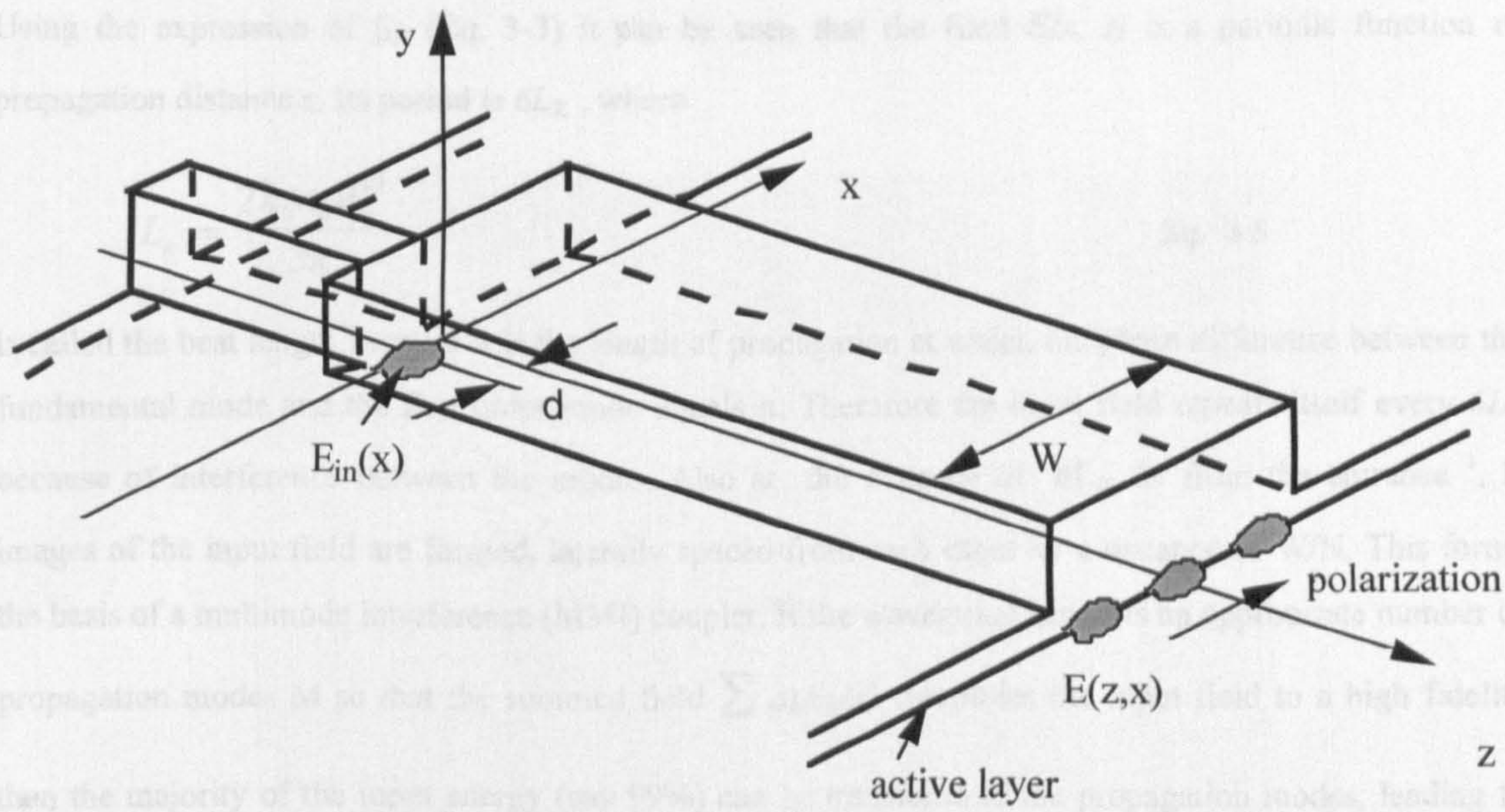

Fig. 3-1 An MMI coupler with input waveguide

$$E_{in}(x,0) = \sum_{k=0}^{M} a_k E_k(x) \qquad \textbf{Eq. 3-1}$$

with [1]

$$a_k = \frac{\int E_{in}(x,o) E_k^*(x) dx}{\int E_k(x) E_k^*(x) dx} \qquad \textbf{Eq. 3-2}$$

The eigenmodes $E_k(x)$ includes propagating modes which will travel along the waveguide in their own propagation constants β_k and radiative modes which result in loss. When input field $E_{in}(x,0)$ is real $E_k(x)$ can also be a set of real functions. In a step-index profile planar waveguide the propagation constants can be approximated by a Taylor expansion [2]

$$\beta_k = \left[k_0^2 n_0^2 - \frac{\pi^2 (k+1)^2}{W^2} \right]^{1/2} \approx k_0 n_0 - \frac{\pi^2 (k+1)^2}{2 k_0 n_0 W^2} \qquad \textbf{Eq. 3-3}$$

where k=0,1,2,...M is the mode number, k_0 is the wave vector of the vacuum, n_0 is the refractive index of the waveguide core material, W is the waveguide width. So the field in the waveguide at any cross section z is

$$E(x,z) = \sum_{k=0}^{M} a_k E_k(x) \exp(-j\beta_k z) \qquad \textbf{Eq. 3-4}$$

---

[1]Snyder, A. W., and Love, J. D., 'Optical Waveguide Theory', Chapmen and Hall, 1983.

[2]Soldano, L. B., *et al*, 'Planar monomode optical couplers based on multimode interference effects', Journal of Light wave Technology, 1992, 12, pp.1843-1849.

Using the expression of β_k (Eq. 3-3) it can be seen that the filed *E(x, z)* is a periodic function of propagation distance *z*. Its period is $6L_\pi$, where

$$L_\pi = \frac{2k_0 n_0 W^2}{3\pi} \qquad \textbf{Eq. 3-5}$$

is called the beat length because it is the length of propagation at which the phase difference between the fundamental mode and the first order mode equals π. Therefore the input field repeats itself every $6L_\pi$ because of interference between the modes. Also at the distance of $6L_\pi$ /N from the entrance [1], N images of the input field are formed, laterally spaced from each other by a distance of W/N. This forms the basis of a multimode interference (MMI) coupler. If the waveguide supports an appropriate number of propagation modes M so that the summed field $\sum a_k E_k(x)$ resembles the input field to a high fidelity then the majority of the input energy (say 99%) can be transfered to the propagation modes, leading to low energy loss and low back-reflection. This is important in practical device design.

3-1-2 Modelling of MMI couplers

The MMI waveguide is approximated by a simple model of one-dimensional slab waveguide despite the factor that the practical strip-loaded waveguide structure (Fig. 3-1) is two dimensional and not symmetric in the y direction. The width of the slab waveguide core equals that of the strip-loaded waveguide. The effective core and cladding refractive indices n_0 and n_c are deduced from the propagation constants of the y direction fundamental mode in the corresponding areas. This method is called the effective index (EI) method.

Rather than using the approximated Eq. 3-3, the eigenfunctions [2] of the wave equation in such a waveguide with TM polarization (the electric field vector lies in the x direction, which is TM for the MMI waveguide) is solved numerically to find the β_k values up to the highest mode number M supported by the waveguide.

$$M = \text{int}\left(\frac{4V}{\pi}\right) \qquad \textbf{Eq. 3-6}$$

where *V* is the normalised frequency of the slab waveguide

$$V = \frac{k_0 W}{2}\left(n_0^2 - n_c^2\right)^{1/2} \qquad \textbf{Eq. 3-7}$$

---

[1]Heaton, J. M. *et al*, 'Novel 1-N way integrated optical beam splitter using symmetric mode mixing in GaAS/AlGaAs multimode waveguides', Applied Physics Letters, 1992, 15, pp1754-1756.

[2]Snyder, A. W., and Love J. D., 'Optical Waveguide Theory', Chapmen and Hall, 1983.

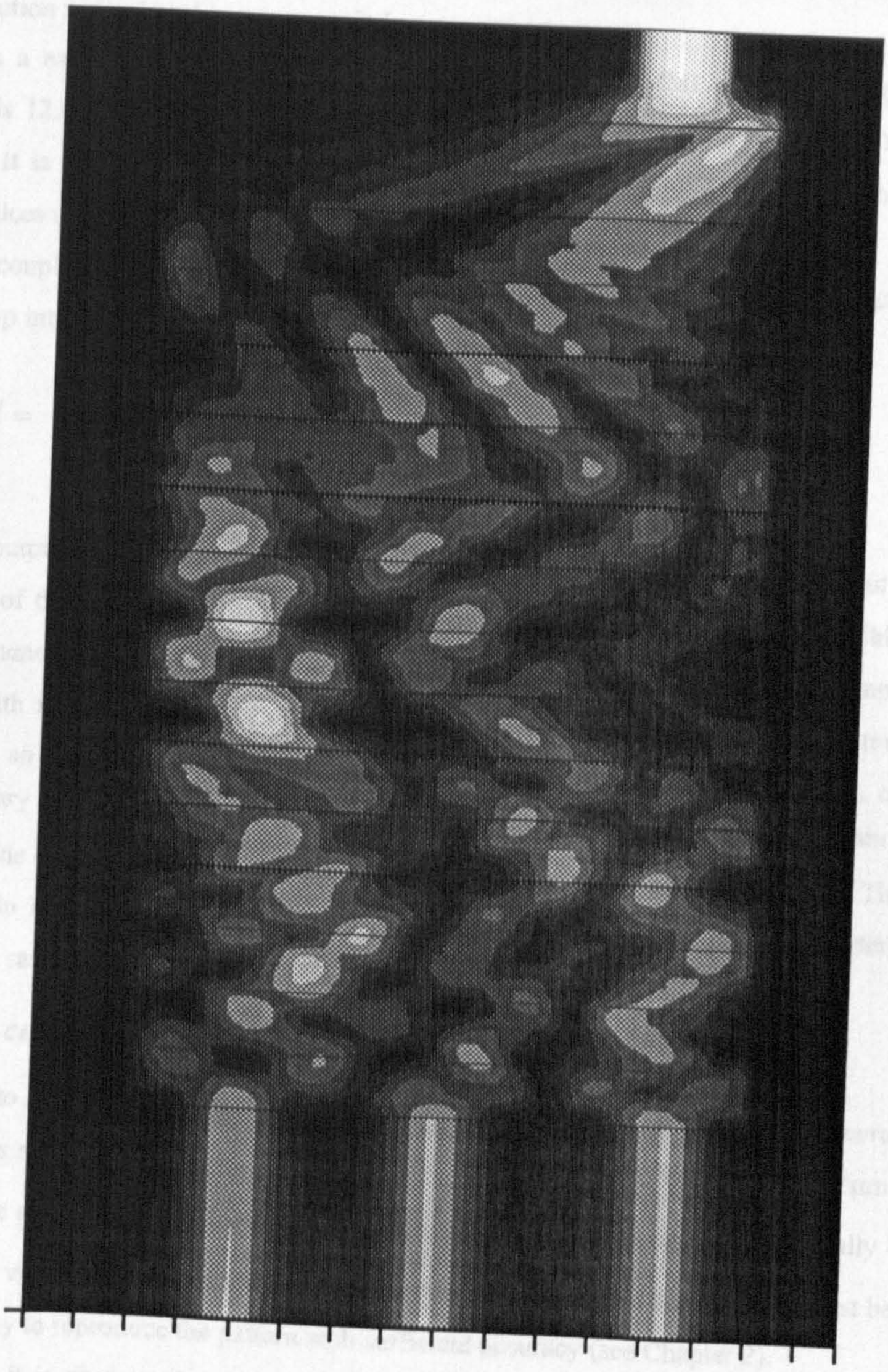

Fig. 3-2 Field distribution in 3x3 MMI coupler waveguides.

The coefficients a_k of the modes are calculated according to Eq. 3-2. The field distribution in the MMI waveguide is calculated according to Eq. 3-1 by stepping the co-ordinate z in 5μm step length and the field distribution is displayed in a grey-scaled contour chart.

Fig. 3-2 is a example of calculated field distribution in 3x3 MMI coupler waveguide. The MMI waveguide is 12.0μm wide, the centre of input waveguide is 4.0μm from the central line of the MMI waveguide. It is shown that the position of the 3x image is at about 810μm from the entrance. The effective indices used in the calculation are n_0=3.56 and n_c=3.61.

The energy coupling coefficient between the MMI images and the output waveguides can be calculated by the overlap integral [1]

$$Ovl = \frac{\int \left| E(x,L)E_{out}(x) \right| dx}{\int \left| E(x,L)E^*(x,L) \right| dx \bullet \int \left| E_{out}(x)E^*_{out}(x) \right| dx} \qquad \text{Eq. 3-8}$$

between the output field $E(x,L)$ of the MMI waveguide and the field $E_{out}(x)$ of the output waveguides. L is the length of the MMI waveguide and * denotes the complex conjugate. It is possible to refine the structural parameters, e.g., the length of the MMI section L, the position of the input and output waveguide with respect to the centre of the MMI waveguide, and, when necessary, the width of the waveguide W so that the output is maximised. Usually the length and the position of input/output waveguides vary slightly from the value predicted by $6L_\pi$ /N and W/N due to, for example, the actual MMI waveguide being wider than it nominal width W because of Goos-Hanchen shift. These variations are indicated in Fig. 3-3. The sensitivity of the output light power to these parameters can also be obtained at the same time.

Fabrication considerations

It is important to know the tolerance of the geometric parameters because fabrication accuracy is limited. Fig. 3-3 shows some of the important position tolerances. For MMI couplers with 2μm input/output waveguides, the calculated -1dB tolerance to the position of these waveguides is typically $\pm$0.4μm. The tolerance to the width of the MMI waveguide, however, is only about $\pm$0.2μm. Care must be taken in the photolithography to reproduce the pattern with sufficient accuracy (see Chapter 2).

From Fig. 3-2 it is obvious that the larger the number of images N, the shorter is the length of the images (the 'focal depth'). Therefore it is more important for an MMI section of the correct length to be defined. This fact poses problems in term of both fabrication error and the changing refractive index in active media (see Chapter 2 and Chapter 4). The main sources of fabrication error here are the width W and the etch depth of the strip-loaded waveguide which affect the propagation contants of the modes. To make sure a 'well-matched' MMI coupler is fabricated, especially when N is large (greater than 3 or 4), a series of device with the same width but different lengths covering the vicinity of the calculated length should be fabricated on the same sample.

3-2 Results

3x3 and 4x4 MMI couplers were fabricated on the MBE DQW material B500. The designed width of the MMI waveguides is 12.0 and 16.0μm for 3x3 and 4x4 couplers, respectively. Five lengths covering ±20μm arround the calculated lengths of 800 and 1050μm are used for both kind of devices to ensure that optimum lengths are hit. The input/output waveguides are 2μm wide with 2μm space between each other. This is carried to near the limit of the definition of the photolithographic technique (see chapter 2) used in the department, because the width W of the MMI coupler must be made as small as possible in order to reduce its length which is proportional to W^2. The output waveguides curve out by 400μm radius bends so that there is a reasonable distance between the outputs, which makes characterisation easier. The junction between the straight and the bent waveguides have a displacement of 0.3μm in order to reduce the coupling loss due to the fact that the field distribution in bent waveguides shifts towards the outer boundary [1,2]. The position of the bent waveguides with respect to the MMI waveguide was also shifted accordingly.

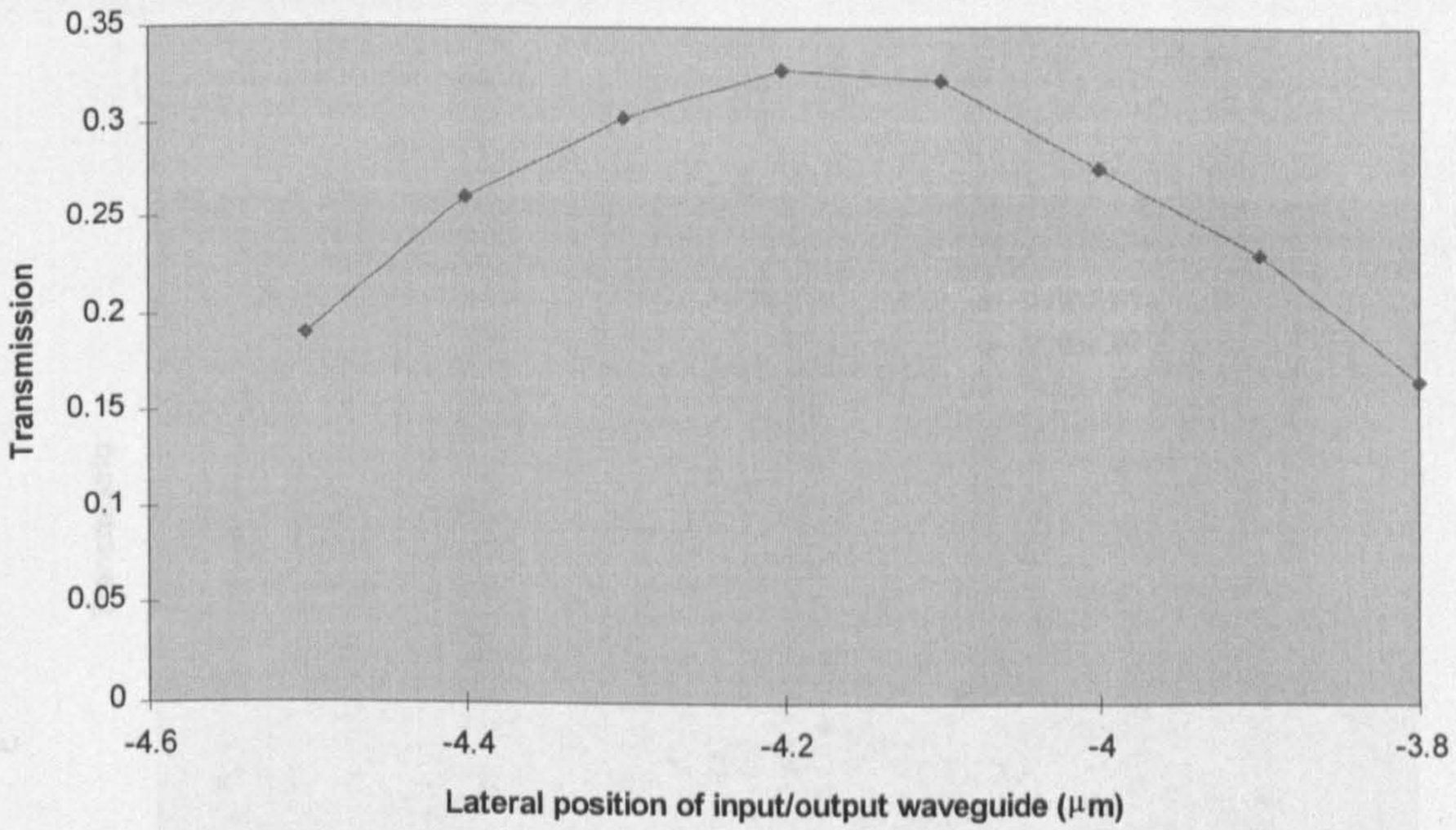

(a)

[1] Krauss, T. F., 'Integrated semiconductor ring lasers', Ph.D thesis. University of Glasgow, 1992.

[2] Garth, S. J., 'Modal behaviour of bent waveguides', IEE Proceeding-Optoelectronics, VOL.142, No. 2, April 1995, pp.115-120.

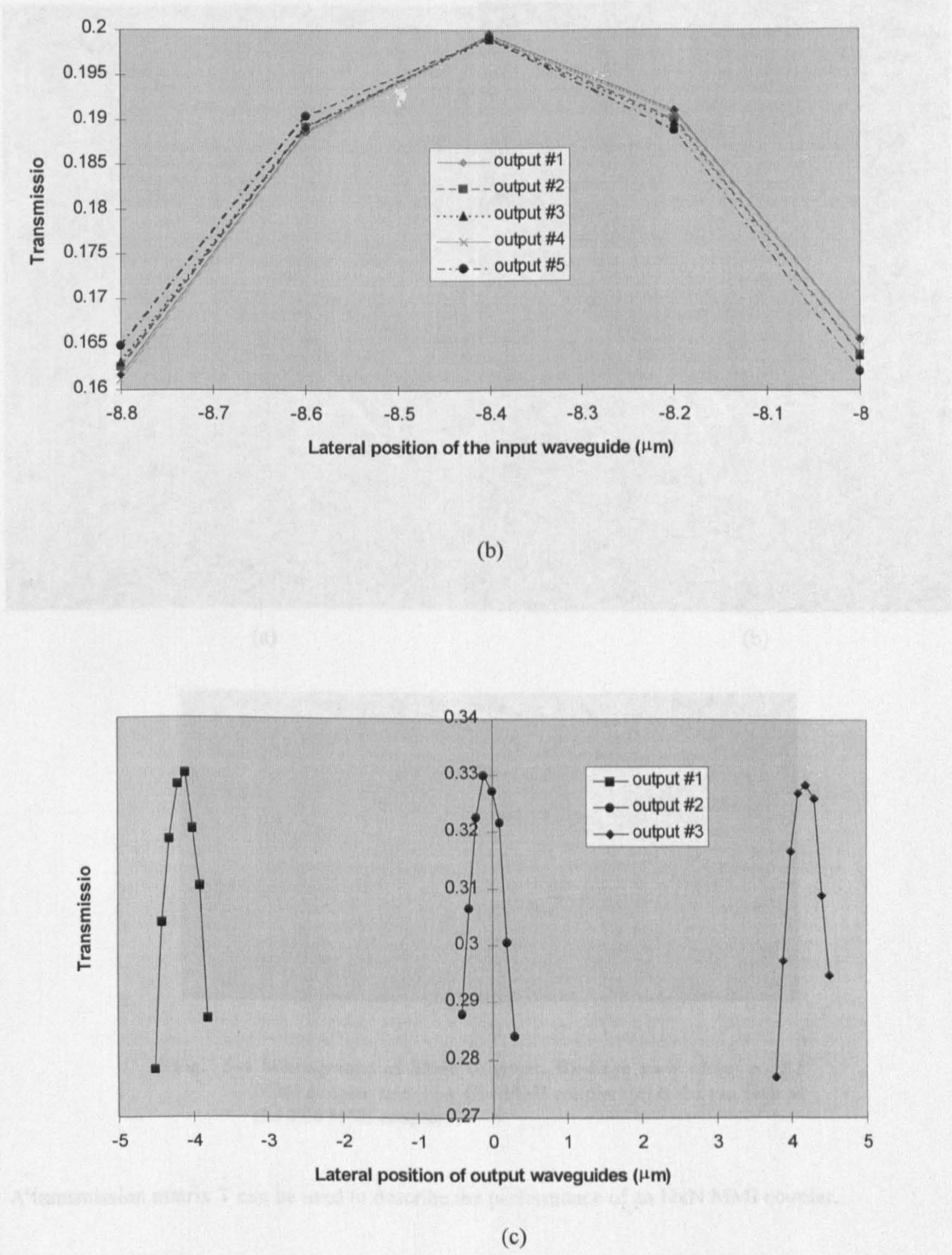

Fig. 3-3 The sensitivity of MMI transmission to waveguide positions. (a) The transmission of a 3x3 MMI coupler(W=12.0μm) when input and output waveguides are both displaced at the same direction, (b) the transmission of a 5x5 MMI coupler (W=20.0μm) when input waveguide is displaced, and (c) the transmission of a 3x3 MMI (W=12.0μm) coupler when it output waveguides are displaced

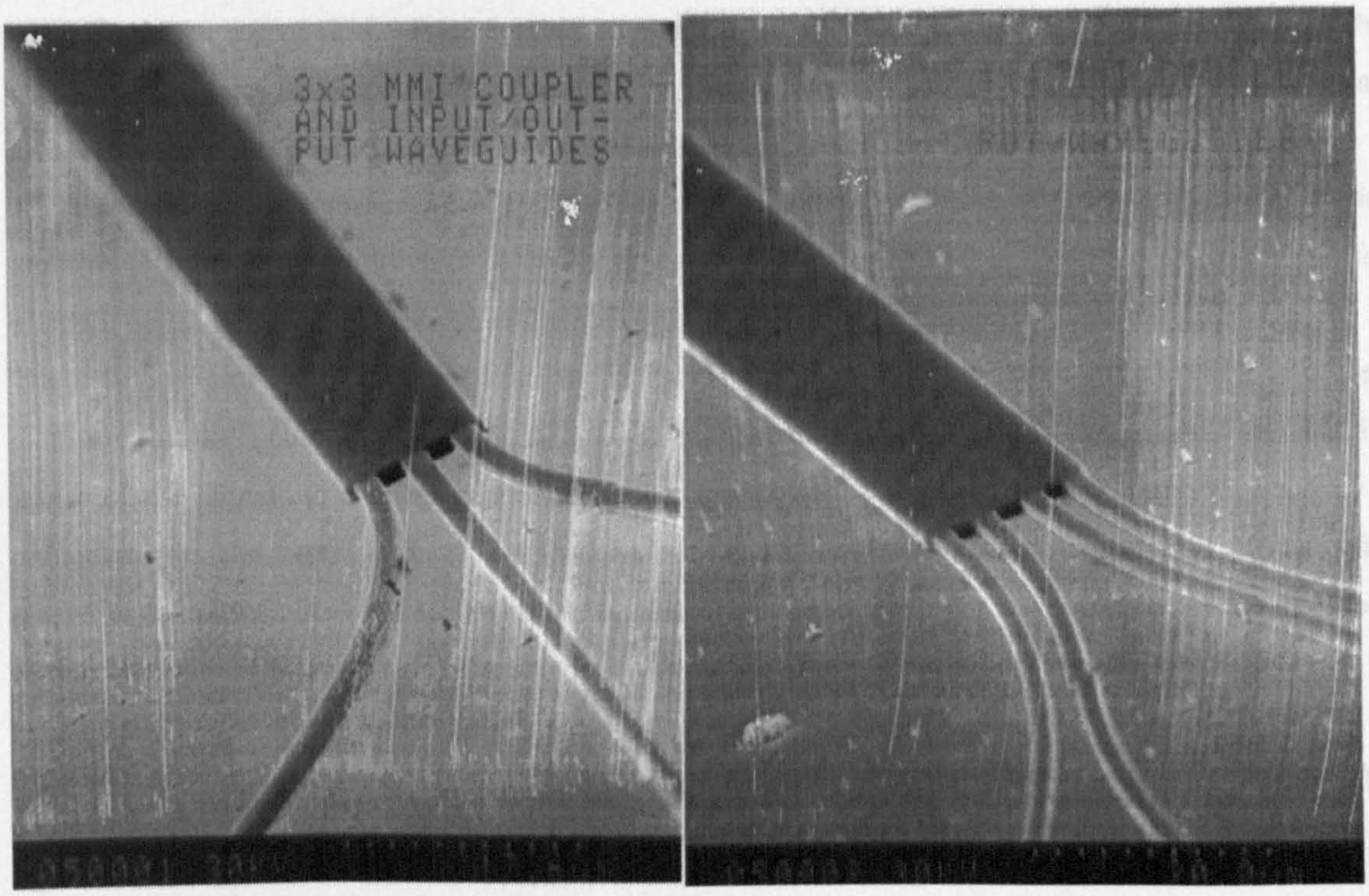

(a) (b)

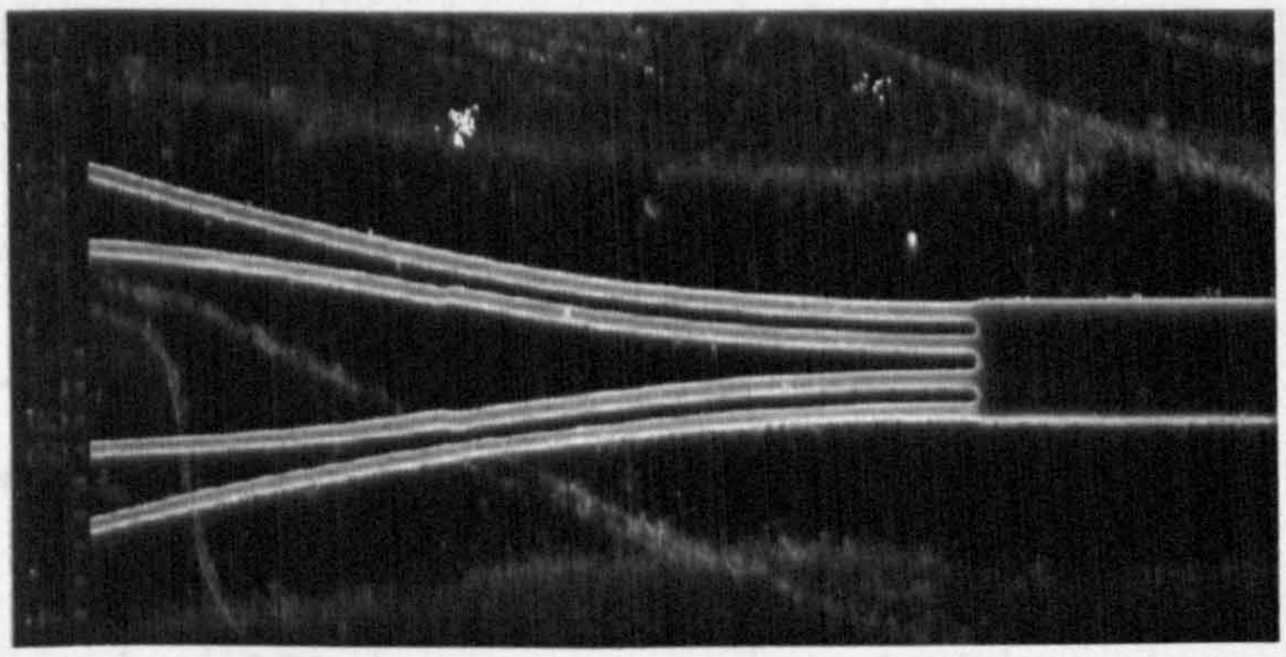

(c)

Fig. 3-4 Micrographs of MMI couplers. Bird-eye view of (a) a 3X3 MMI coupler and (b) a 4X4 MMI coupler. (c) is the top view of the 4X4 MMI coupler.

A transmission matrix T can be used to describe the performance of an NxN MMI coupler.

$$\begin{bmatrix} P_{01} \\ P_{02} \\ P_{03} \\ \vdots \\ P_{0N} \end{bmatrix} = \begin{bmatrix} T_{11} & T_{12} & T_{13} & \cdots & T_{1N} \\ T_{21} & T_{22} & T_{23} & \cdots & T_{2N} \\ T_{31} & T_{32} & T_{33} & \cdots & T_{3N} \\ \vdots & \vdots & \vdots & \ddots & \vdots \\ T_{N1} & T_{N2} & T_{N3} & \cdots & T_{NN} \end{bmatrix} \begin{bmatrix} P_{i1} \\ P_{i2} \\ P_{i3} \\ \vdots \\ P_{iN} \end{bmatrix} \qquad \textbf{Eq. 3-9}$$

where P_{0j} is the output power from output port j and P_{ik} is the input power from input port k. T_{jk} is the power transmission factor from input k to output j. Ideally the value of T_{jk} equals 1/N if there is no insertion loss in the coupler and the input light power is uniformly distributed among the N outputs.

The MMI couplers are characterised by coupling a Ti:Sapphire laser beam of λ=860nm into one of the input ports and measuring the relative output power from each output ports. The process is repeated for all input ports. The system is illustrated in Fig. 3-5.

The chopped laser beam is launched into the input waveguide by a 40x objective lens. A polariser is used to ensure that the input beam is polarised in the sample plane. Another 40x objective is used to project the image of the outputs to a image plane. An iris is used to select the output image to be detected by a photodetector. The signal is measured by a lock-in amplifier. For a quick observation a CCD can be placed in the image plane to find the output beams. The sample is cleaved into bars containing a number of couplers with different length. The sample holder stage can be manipulated in five dimensions (x, y, z, rotation and tilt) to maximise the input coupling and also to move different device into the spot.

Because the input coupling condition is not always repeatable, one should only expect the outputs to be equal while each input is excited. That is, all elements in each column in the matrix T are equal.

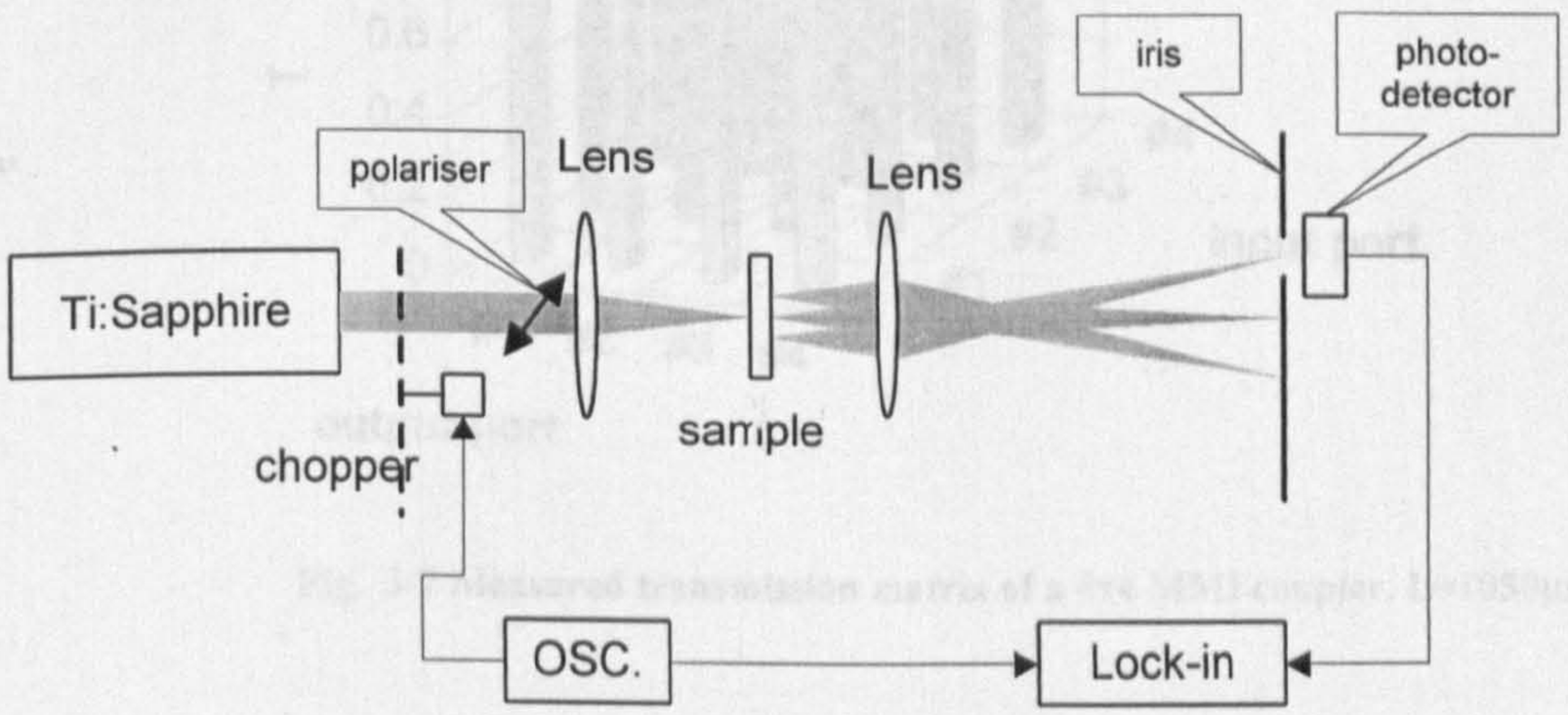

Fig. 3-5 Characterising MMI couplers.

Fig. 3-6 is the measured trasmission matrix of a 3x3 MMI coupler. The elements in each column is normalised to the largest element in that column. The result indicate that the inhomogeneity among outputs are within 1.3dB.

Similar results for a 4x4 MMI coupler is shown in Fig. 3-7. The best homogeneity achieved in 4x4 MMI couplers is about 3dB.

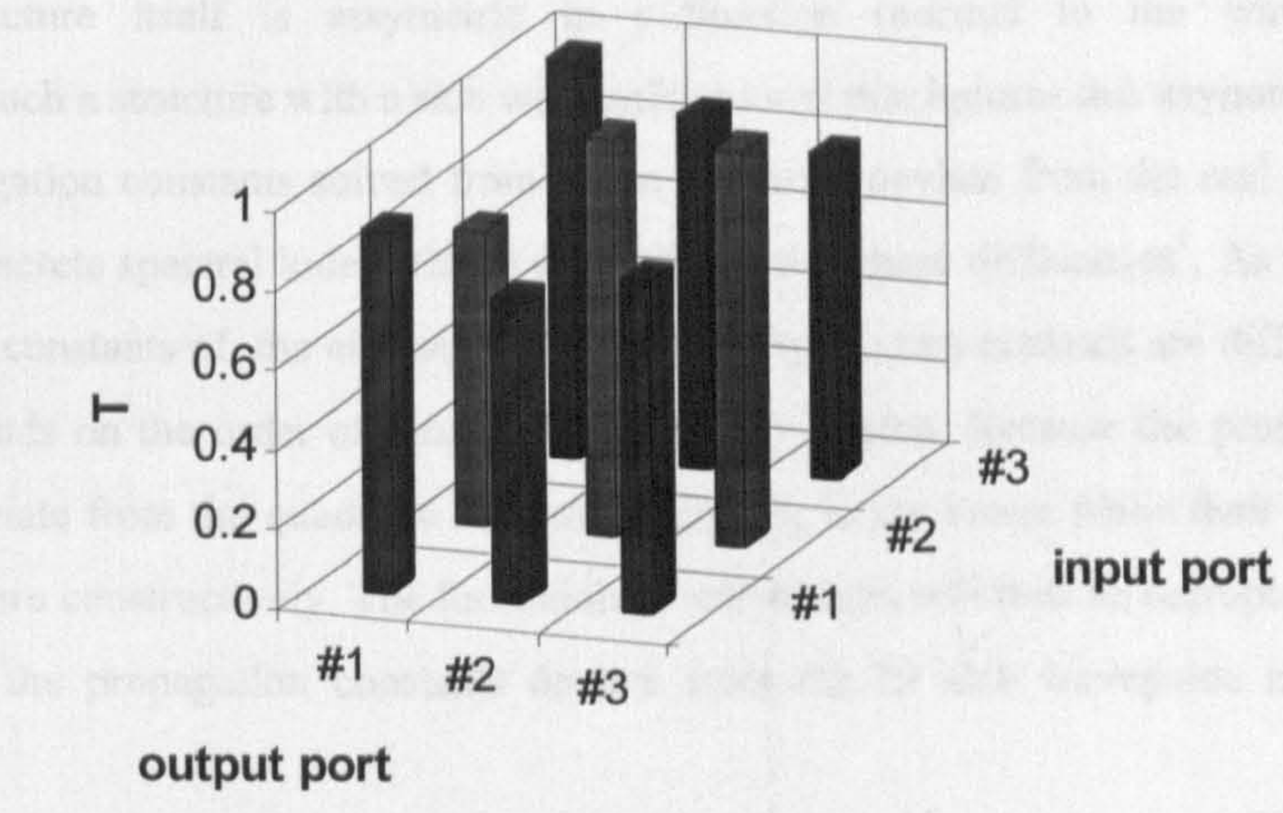

Fig. 3-6 Measured transmission matrix of a 3x3 MMI coupler. L=810μm.

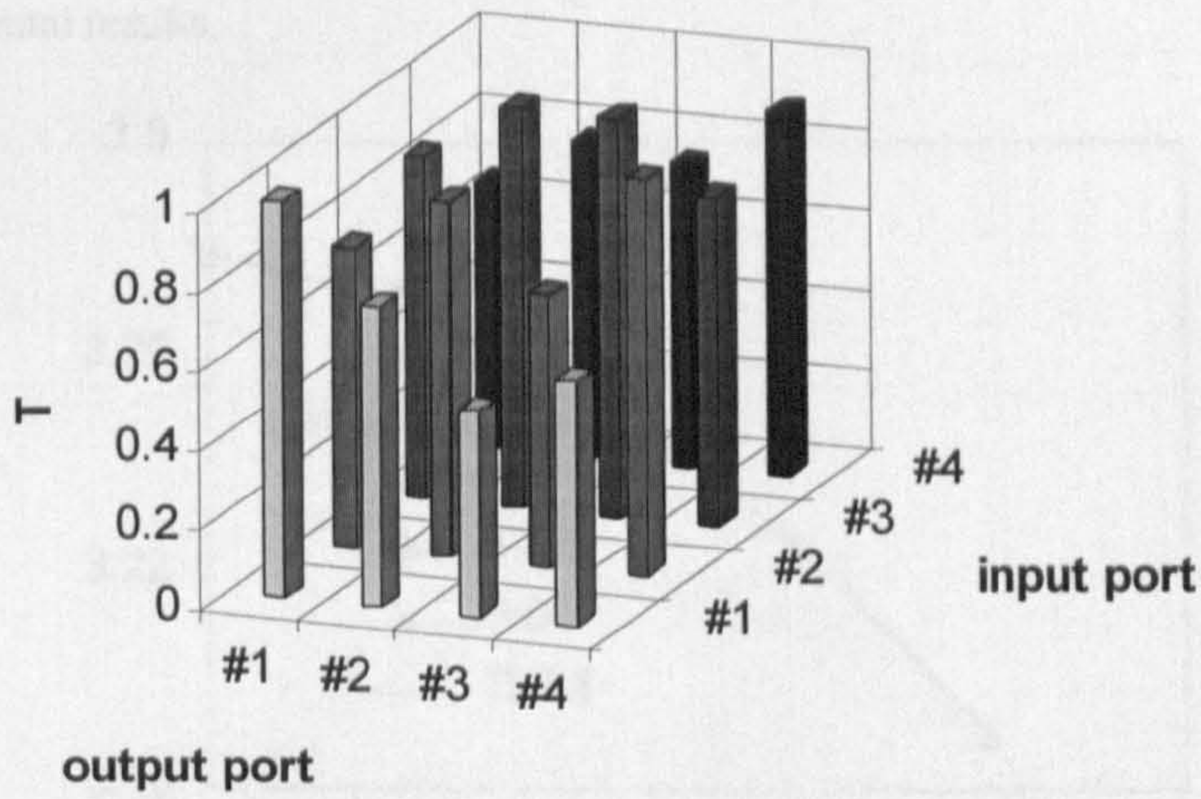

Fig. 3-7 Measured transmission matrix of a 4x4 MMI coupler. L=1050μm.

The MMI section length L of the couplers seem to be in good agreement with the calculated value. The best performance of 3x3 MMI coupler is measured in a L=810μm device which is slightly longer than the calculated value of 800μm. The best 4x4 coupler has exactly the calculated length of 1050μm.

3-3 discussion

There are several factors affecting the operation of the MMI couplers.

The strip-loaded waveguide structure

The effective index (EI) method is used in the modelling of MMI couplers with a strip-loaded structure. While they seem to give the correct length of an MMI section, it is doubtful whether they give the correct field distribution in the MMI section.

The problem lies in the fact that the field distribution in the cross-section plane perpendicular to the direction of propagation of the strip-loaded waveguide is asymmetric about the active layer because the

waveguide structure itself is assymetric in y-direction (normal to the waveguide plane). By approximating such a structure with a slab waveguide model that ignores this asymmetry, the eigenmodes and their propagation constants solved from the model must deviate from the real ones. A recent study employing a 'discrete spectral index' (DSI) method revealed these differences[1]. As depicted in Fig. 3-8, the propagation constants of the eigenmodes calculated by the two methods are different. The amount of difference depends on the order of modes and the depth of etch. Because the propagation constants of eigenmodes deviate from the quadratic relation of Eq.3-3, in the image plane their phases are no longer correct to interfere constructively. The formation of self-images will thus be corrupted. The shallower the etch, the more the propagation constants deviate from the EI slab waveguide model, the worse the corruption.

Another effect of the strip-loaded structure is the length of MMI section will be longer than the value calculated with the EI method [1]. However, in our devices, because the etch is very close to the active layer of the material (~0.05μm), the influence on the length of the MMI section is slight, which is proved by the experimental results.

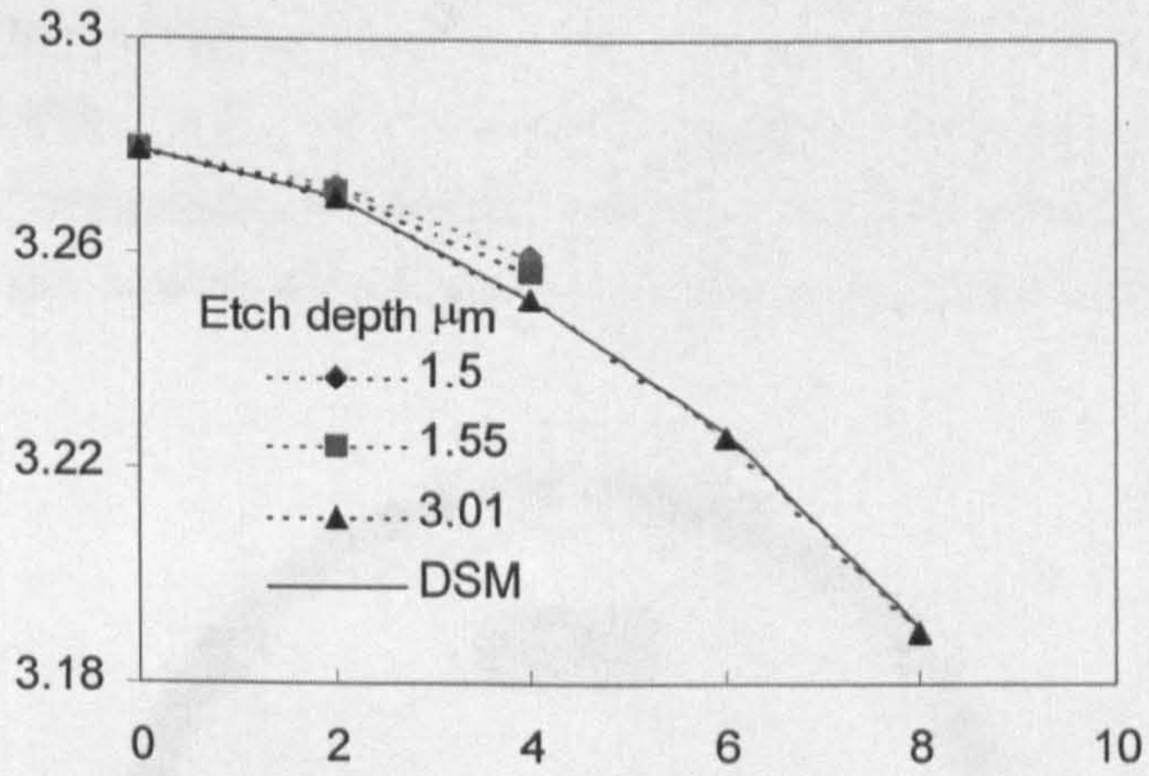

Fig. 3-8 The difference between propagation constants calculated by DSI and EI methods [1].

Material Loss

Because the material has a lasing wavelength of 860nm, it has a high absorption coefficient at this wavelength when not pumped. As a result the devices have very high insertion losses. The complex refractive index of a material with high absorption or gain could also change the optimum parameters of the MMI section because a real refractive index is used in the modelling. In practical devices, the MMI sections should be fabricated in low loss material such as bandgap tuned material so that low insertion loss and homogeneous coupling ratio can be achieved.

---

[1]Berry, G. M., and Burke, S. V., 'Analysis of optical rib self-imaging multimode interference (MMI) waveguide devices using the discrete spectral index method', Optical and Quantum Electronics, VOL.**27** (1995) pp.921-934.

4 Light Source I-Semiconductor Ring Lasers (SRLs) and Its Improvement

4-1 Review

The reasons for studying the use of semiconductor ring lasers (SRLs) has been presented in I-4. In this chapter, the development of SRLs will be reviewed. The factors governing their performance will be discussed and methods of improving the performance and adapting the device for use in a OTDM system will be presented.

4-1-1 Whispering Gallery Mode and Micro-disc ('pillbox') SRLs

'Whispering Gallery' wave-guiding effect

Most early semiconductor ring lasers were based on the 'whispering gallery' waveguiding effect. It is believed that this effect was observed more than 500 years ago as a phonic phenomenon in the Temple of Havens in Beijing (Fig. 4-1). The first scientific discussion was made by Lord Rayleigh[1]. The 'whispering gallery' mode propagates along the inner side of a curved wall due to total reflection. If the medium is a laser gain material the structure can be used as a resonant cavity to produce stimulated emission.

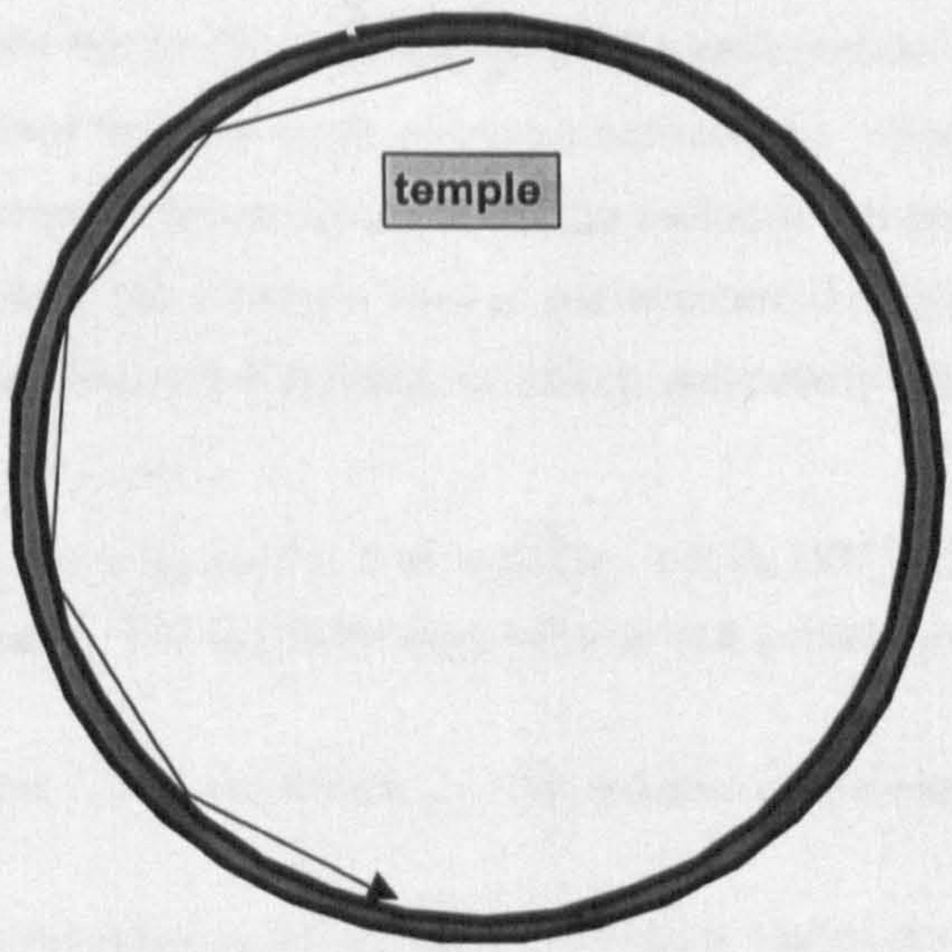

Fig. 4-1 The whispering gallery mode

The concept of whispering gallery mode semiconductor laser was first demonstrated in half-ring or quarter-ring [2] devices, which still relied on facet reflection for optical feedback. Full ring laser were

---

[1] Lord Rayleigh, SCI. PAPERS, 1912 Vol.5 p.617.

[2] Ury, I., *etc*, Applied Physics Letters, 1980, Vol.36 p.629.

realised later[1] and a Y-junction output coupling mechanism was introduced [2]. The first CW operating SRL was made in Glasgow in 1990 [3].

The geometric structure of these whipering-gallery mode devices was a 'pillbox'-a semiconductor disc. For total internal reflection to happen, the refractive index difference at the sidewall should be large. This was usually realised by deep etching through the active layer so that the total reflection happened at the semiconductor-air interface. Because the light field concentrated close to the sidewall, a smaller dielectric disc covering the central part of the pillbox was introduced to restrict the injection current at an outer annulus of about 4μm wide[4]. This reduced the CW threshold current to as low as 12.5mA.

A deeply etched structure (i.e., etched through the waveguide core layer) allowed very small SRLs to be made because of its high refractive index contrast at the semiconductor-air interface. Most of the micro-disc SRLs had diameter in the order of 100μm. A small diameter was necessary in early stages to reduce the threshold current of the devices. Despite the use of injection current confining structure as described above, 'pillbox' or micro-disc SRLs still had the problem of current spreading [5] towards the centre of the disc, which resulted in high threshold current. Small diameter narrow waveguide ring lasers [6] were introduced to eleminate this problem. But sidewall scattering loss was larger in narrow waveguide structure because two sidewalls interact with the light. Yet this structure has been pursued further later on to produce so-call 'optical bandgap' ring lasers which are as small as 2.5μm in diameter [7].

Output coupler

In the early stages of development Y-junctions were mainly used as the output coupler of SRLs. The idea was a straight-forward one but performance was poor. The main problems were the high radiation loss and back-reflection resulted from the mode mismatch between the 'whispering gallery' modes and the modes of the output waveguide. It was estimated that this radiation loss could be as high as 50% [8], which would significantly increase the threshold current and decrease the external quantum efficiency (see section 4-2-1: Theory of External Efficiency of SRLs), particularly when the device was small. The

---

[1] Matsumoto, N. and Kumabe, K., Japanese J. of Appl. Phy., Vol.16, 1977, p.1395.

[2]Liao, A. S-H. and Wang, S., 'Semiconductor injection lasers with a circular resonator', Appl. Phy. Lett., Vol.36, 1980, pp.801-803.

[3]Krauss, T. F., Laybourn, P. J. R. and Roberts, J., 'CW operation of semiconductor ring lasers', Electron. Lett., Vol.26, 1990, .2095-2097.

[4]Krauss, T. F., 'Integrated semiconductor ring lasers', Ph.D thesis. University of Glasgow, 1992.

[5]Dumke, W. P., 'Current threshold in stripe-contact injection lasers', Solid-State Electronics, Vol.16, 1973, pp.1279-1281.

[6]Jezierski, A. F. and Laybourn, P. J. R., 'Polyimide embedded semiconductor ring lasers', Proc. SPIE Vol.1141, 1989, pp.9-13.

[7] Zhang, J. P., Chu, D. Y., Wu, S. L., Bi, W. G., Tiberio, R. C., Tu, C. W., and Ho, S. T., 'Directional light output from photonic-wire microcavity semiconductor-lasers', IEEE Photonics Technology Letters, 1996, Vol.8, No.8, pp.968-970.

[8]Krauss, T. F., 'Integrated semiconductor ring lasers', Ph.D thesis. University of Glasgow, 1992.

back-reflection is very harmful because it causes coupling between the two counter-propagating modes, resulting in complicated interference between the cavity modes and the back-reflected field which adversely influences the output light-injection (L-I) relationship. What made things worse was that the coupling ratio of the Y-junction coupler is very sensitive to the change of injection current because the refractive index is related to the varying injection current via both carrier density and temperature variations. This effect alters the lateral modal distribution of the micro-disc ring cavity[1].

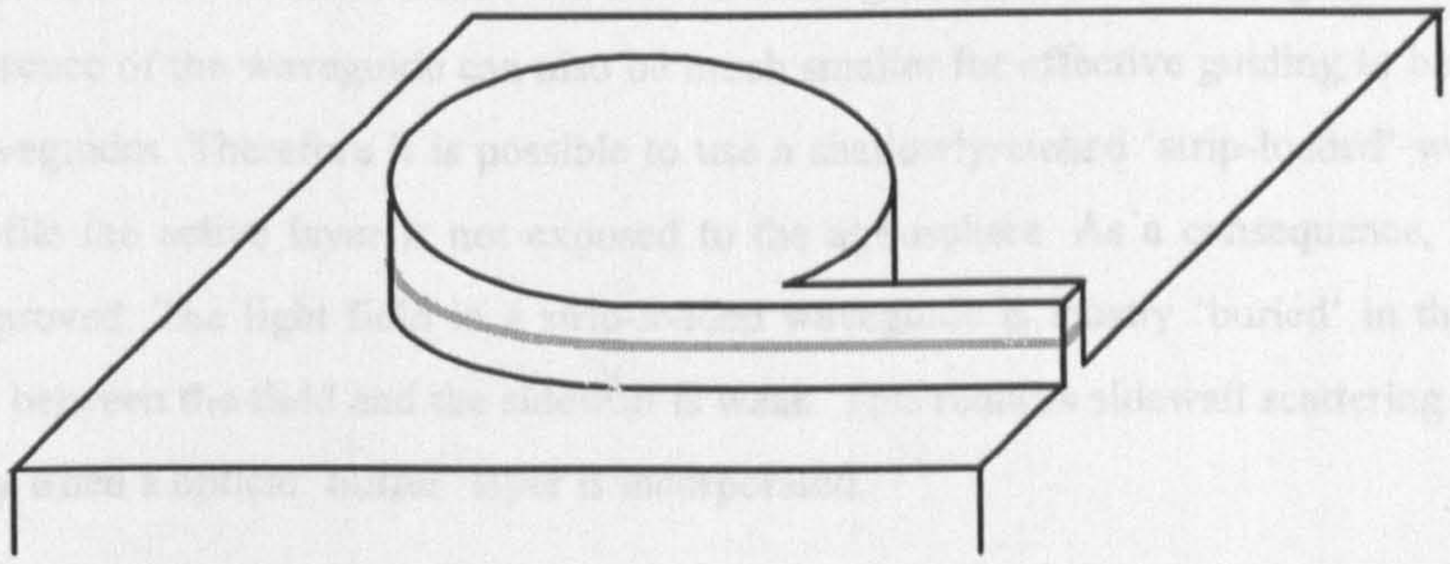

Fig. 4-2 Micro-disc or 'pillbox' SRL with Y-junction output coupler

4-1-2 Large SRLs with Curved Waveguides

Output coupler

In this work, however, large SRLs, the diameter of which is in the order of millimeters, are to be studied. In such a case, other output couplers can be introduced. It is possible to use couplers that have small radiation loss, small back-reflection and insensitive to the change of injection. Such couplers are refered as 'well-matched' couplers.

The use of directional couplers [2] and multi-mode interference (MMI) couplers [3] (see also chapter 3) in SRLs has been investigated in several works. Compared with Y-junction coupler, MMI couplers and directional couplers not only had almost negligible radiation loss and very small back-reflection, they were also more stable when injection current changed. While directional couplers were still somewhat injection-dependent at high currents, MMI couplers demonstrated robustness when properly designed and

---

[1] Krauss, T. F., 'Integrated semiconductor ring lasers', Ph.D thesis. University of Glasgow, 1992. p.65-70.

[2] Krauss, T. F., De La Rue, R. M., and Laybourn, P. J. R., "Impact of Output coupler Configuration on the Operating Characteristics of semiconductor Ring lasers". J. of lightwave Technology, VOL. 13, No.7, JULY 1995, pp.1500-1507.

[3] Van Roijen, R., Pennings, E. C. M., Van Stalen, M. J. N., Van Dongen, T., Verbeek, B. H., and Van der Hejiden, J. M. M., 'Compact InP-based ring lasers employing multimode interference couplers and combiners', Appl. Phys. Lett., Vol.64 (14), 1994, pp.1753-1755.

fabricated (or 'well-matched'). SRLs with MMI couplers produced the best external quantum efficiency (16%) [1] and linearity in the output L-I characteristics prior to this work. However, the fabrication tolerance of the directional coupler was very stringent that it was difficult to fabricate a device with a designed coupling ratio. On the other hand, MMI couplers were more tolerant to fabrication errors.

Waveguide

Because of the large diameter of the device, it is obvious that the 'pillbox' structure is unsuitable. Waveguides of several microns wide would be useful. Again because of the large diameter, the refractive index difference of the waveguide can also be much smaller for effective guiding to be achieved even in curved waveguides. Therefore it is possible to use a shallowly-etched 'strip-loaded' waveguide[1] profile. In this profile the active layer is not exposed to the atmosphere. As a consequence, device lifetime is greatly improved. The light field in a strip-loaded waveguide is mostly 'buried' in the material, so the interaction between the field and the sidewall is weak. This reduces sidewall scattering loss significantly, particularly when a optical 'buffer' layer is incorporated.

4-2 External Efficiency

One of the main reasons for which SRLs are not yet considered as practical devices has been the lower total external quantum efficiency η_{ex} (~16%) compared with Fabry-Perot lasers. In this section methods of improving η_{ex} are discussed and significant improvements are presented.

4-2-1 Theory of External Efficiency of SRLs

The low efficiency of previous SRLs can be traced back to several factors. These are material loss, cavity length and the feedback coupling ratio of their output couplers.

Similar to F-P lasers, the external efficiency η_{ex} of SRLs is described by the following formula [2]

$$\eta_{ex} = \frac{\eta_{in}}{1 + \frac{\alpha_i L}{\ln(1/\sqrt{F})}} \qquad \text{Eq. 4-1}$$

where η_{in} is the internal quantum efficiency of the laser medium, α_i is the loss coefficient of the medium, L is the length of the ring cavity and F is the feedback coupling ratio (i.e., the fraction of light power coupled back into the ring cavity in each round-trip). $\sqrt{F}$ is equivalent to facet reflectivity R in F-P lasers.

---

[1]Krauss, T. F., De La Rue, R. M., Gontijo, I., Laybourn P. J. R., and Roberts, J. S., 'Strip-loaded semiconductor ringlasers employing multi-mode interference (MMI) couplers', Appl. Phys. Lett., VOL.64, 1994, pp.2788-2790.

[2]Yariv., A., "Optical Electronics", 4th Edition. Saunders College Pub., 1991.

Eq.4-1 applies at the exit of the coupler, i.e., the junctions between the coupler and the output waveguide. What can be measured, however, are the L-I relationships at the output facets. So the influence of the output waveguides and the facets should be taken into account.

Effect of Output Waveguides

The effect of the output waveguide on the external efficiency is simple if the waveguides are not pumped or are 'passive'. They act as attenuators. so the value of external efficiency is reduced by a factor of the attenuation of the waveguides. However, when the output waveguides are pumped, the problem is rather more complicated.

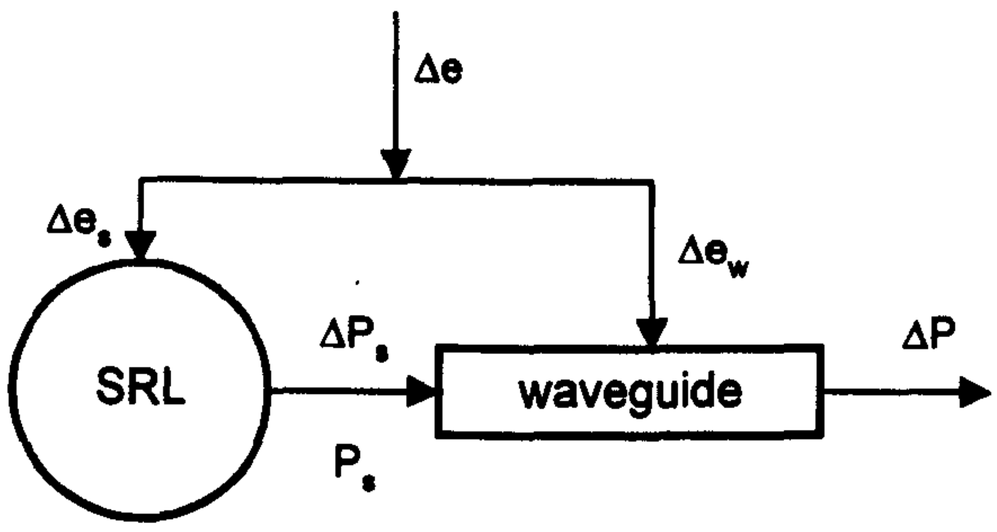

Fig. 4-3 The model of SRL with pumped output waveguide

As shown in Fig. 4-3, the external efficiency measured at the output of the device is

$$\eta_{ex} = \frac{\Delta P}{\Delta e} = \frac{\Delta P_s \cdot A + P_s \cdot \Delta A}{\Delta e_s + \Delta e_w} \qquad \textbf{Eq. 4-2}$$

where ΔP is the increment of the output photon rate resulting from the increment of injected electron rate Δe. The injected electrons devide into two parts, Δe_s and Δe_w, which are the electrons entering the ring laser cavity and the output waveguides, respectively. The increment of the output photon rate is the result of two effects. The first is the increment of the output rate of photons from the ring cavity ΔP_s multiplied by the gain of the output waveguide A. The second part is the result of the total photon rate coming out of the ring cavity multiplied by gain increment ΔA in the output waveguide due to injection increment Δe_w. Eq.4-2 can be re-arranged as

$$\eta_{ex} = \frac{A\left(\Delta P_s / \Delta e_s\right)}{1+\left(\Delta e_w / \Delta e_s\right)} + \frac{P_s \cdot \Delta A / \Delta e_w}{1+\left(\Delta e_s / \Delta e_w\right)} \qquad \textbf{Eq. 4-3}$$

In Eq.4-3 the first term represent the effect of the output waveguide as an amplifer on the external efficiency of the whole device. Inside the parenthesis of its numerator is the external efficiency of the ring laser described by Eq.3-1. Its contribution to the overall external efficiency is increased by the

amplifier gain A but is reduced by the fact that not all the injection increment goes into the ring cavity (the parenthesis in the denominator). The numerator of the second term is the electron-photon converting efficiency of the output waveguide or the amplifier. Its contribution to the overall external efficiency is again reduced by the fact that not all the injection increment goes into the waveguide.

The overall external efficiency is therefore a complicated function of many factors, e.g., the proportion of current injected into the cavity and the gain A of the output waveguide, which is influenced by the extent of saturation of the output waveguide by its input (i.e., the ring cavity's output) photon number P_s, etc. However, in practical situations these factors often tend to cancel each other. Experiments suggested that the influence of the pumped output waveguide could often be ignored.(see section IV-2-2) and Eq.3-1 can be used to approximate the external efficiency.

Output Facet

The effect of the output facet on external efficiency is straight forward when the reflected light is NOT coupled back into the ring cavity. It attenuates the external efficiency by a factor of 1-R, R being the reflectivity of the facet.

In Y-junction micro-disc SRLs the loss coeficient α_i was large due to the high radiation loss at the Y-junction. This radiation loss increased the average loss coefficient significantly when the cavity length was short. High loss was also due to the sidewall scattering loss.

In directional coupler SRLs, theoretically it is possible to design devices with low loss and high external efficiency simply by decreasing feedback coupling ratio F. However, in the device investigated in a previous study [1] the coupling length between the ring cavity and the output waveguide was not long enough to allow more light power to be coupled out of the cavity, i.e., the feedback coupling ratio F was still large.

The 2x2 MMI couplers used in previous devices which have been shown to be superior in other aspects (see IV-1-2) only allow a fixed feedback coupling ratio F of 0.5 (which determined that η_{ex} of the SRL"s was about 16% when devices with 3mm long cavities were fabricated on materials with η_{in}~90% and α_i~4cm^{-1}). Considering the cavity length of these devices, a much lower feedback coupling ratio F is required for efficient operation.

4-2-2 Approaches for Improving External Efficiency

Bearing in mind the purpose of this work, i.e., developing a light source to be used in an integrated optical time-division multiplexing (OTDM) system, the cavity length L of the SRL is determined by the pulse rate and cannot be changed. Therefore the only means of improving the external efficiency is to

---

[1]Krauss, T. F., De La Rue, R. M., and Laybourn, P. J. R., "Impact of Output coupler Configuration on the Operating Characteristics of semiconductor Ring lasers". J. of Lightwave Technology, VOL. 13, No.7, July 1995, pp.1500-1507.

reduce the feedback coupling ratio F by altering the structure of the output coupler. The physical nature of this action is to couple more light out of the laser cavity. Although this may result in increased threshold gain, the threshold current will increase only slightly due to the steep gain-current relationship of the QW materials.

SRLs with asymmetric MMI couplers

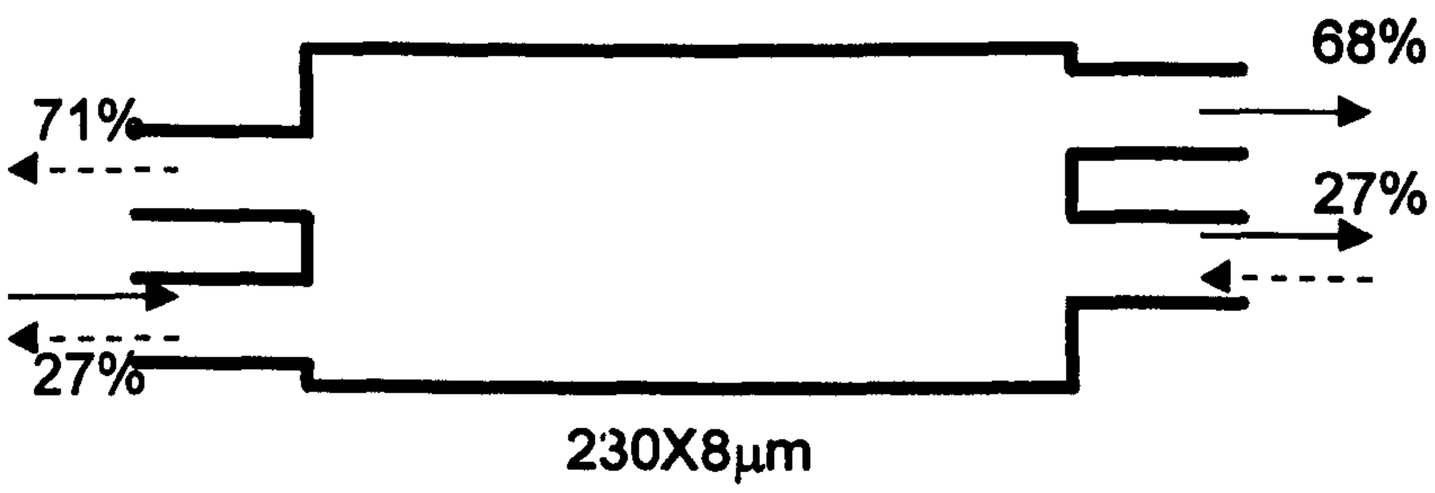

Fig. 4-4 Asymmetric MMI coupler

Because MMI couplers are based on the self-imaging property of multi-mode waveguides, coupling ratios other than 0.5/0.5 are not readily available. However, a 2x2 MMI coupler structure with approximately 0.3/0.7 coupling ratio does exist and was proposed in a previous study [1] (Fig. 4-4).

The following figures (Fig. 4-5) compare the test results of SRLs made on GaAs/AlGaAS MBE double quantum-well (DQW) materials B429. Device No.1-d-2 is a typical F=0.5 device. The external efficiency is about 16% (8% per output). Device 2-f-3 is a SRL with an asymmetric F=0.3 MMI coupler. On average the F=0.3 devices have external efficiency values of about 9-10% per output, or 18-20% overall, which is very close to the theoretical estimation. (Using F=0.3, L=3mm, α_i=4cm^{-1} and η_{in}=90% in Eq.4-1, the external efficiency of an SRL employing the asymmetric MMI coupler should be about 26%. The facet reflection should reduce this value to about 18%). The increase of efficiency due to reduced feedback ratio is clearly evident.

The typical threshold current of the 0.5/0.5 MMI coupler devices was about 80mA (the lowest being only about 70mA). The pumped waveguide length is about 4.5mm (comprising 3.1mm ring circumference and about 1.4 mm output waveguide) and its width is 2μm, giving a 'nominal' threshold current density J_{th} of less than 900A/cm^2 , which compares well with about 600A/cm^2 measured in 50μm wide, 500μm long stripe FP lasers fabricated on the same material. In a narrow strip-loaded waveguide there is the problem of lateral current spreading in the active layer [1], so the actual pumped width is wider than the width of the waveguide and the actual current density is smaller than the nominal current density.

---

[1]Dumke, W. P., 'Current threshold in stripe-contact injection lasers', Solid-State Electronics, Vol.16, 1973, pp.1279-1281.

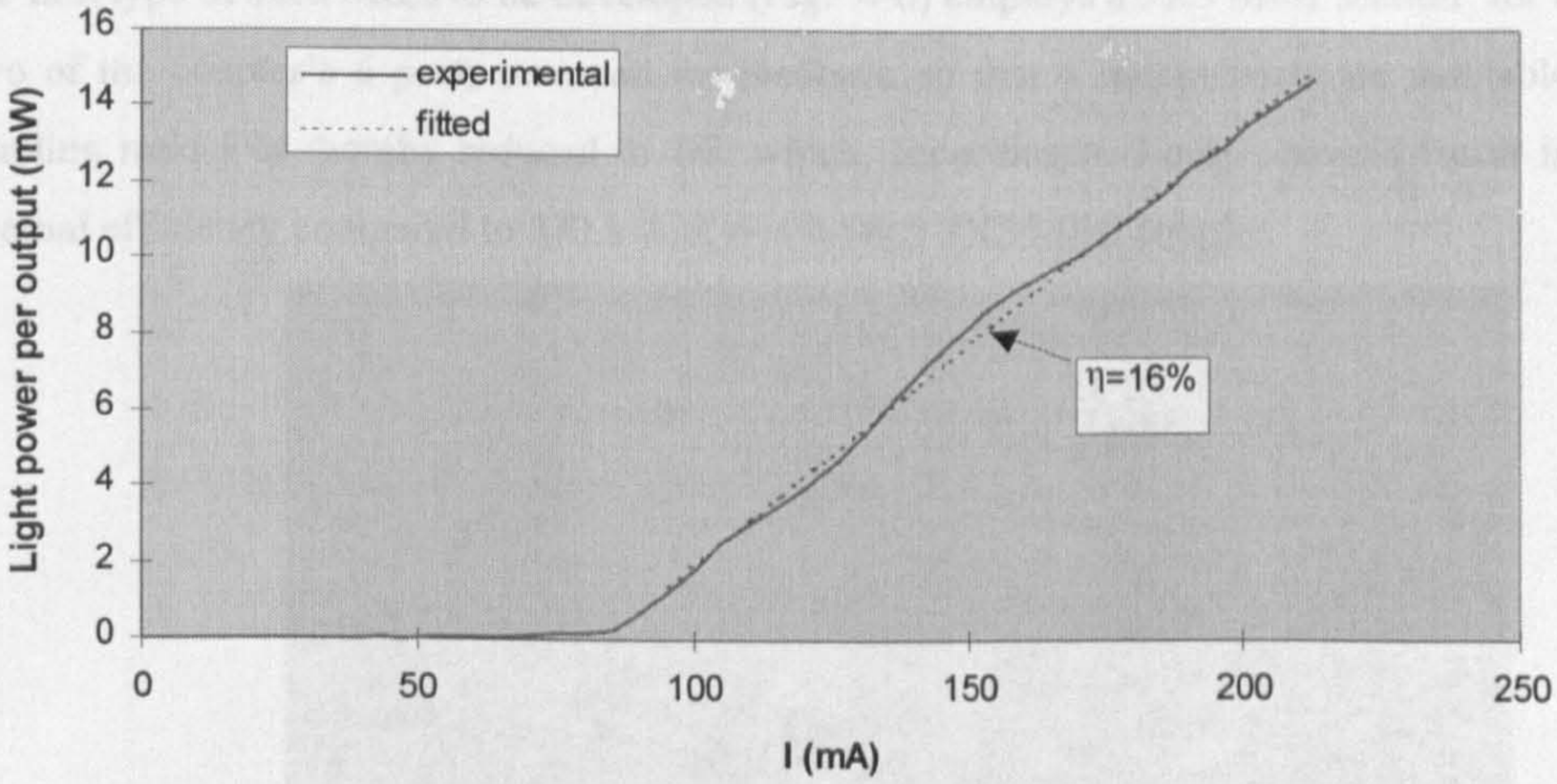

(a)

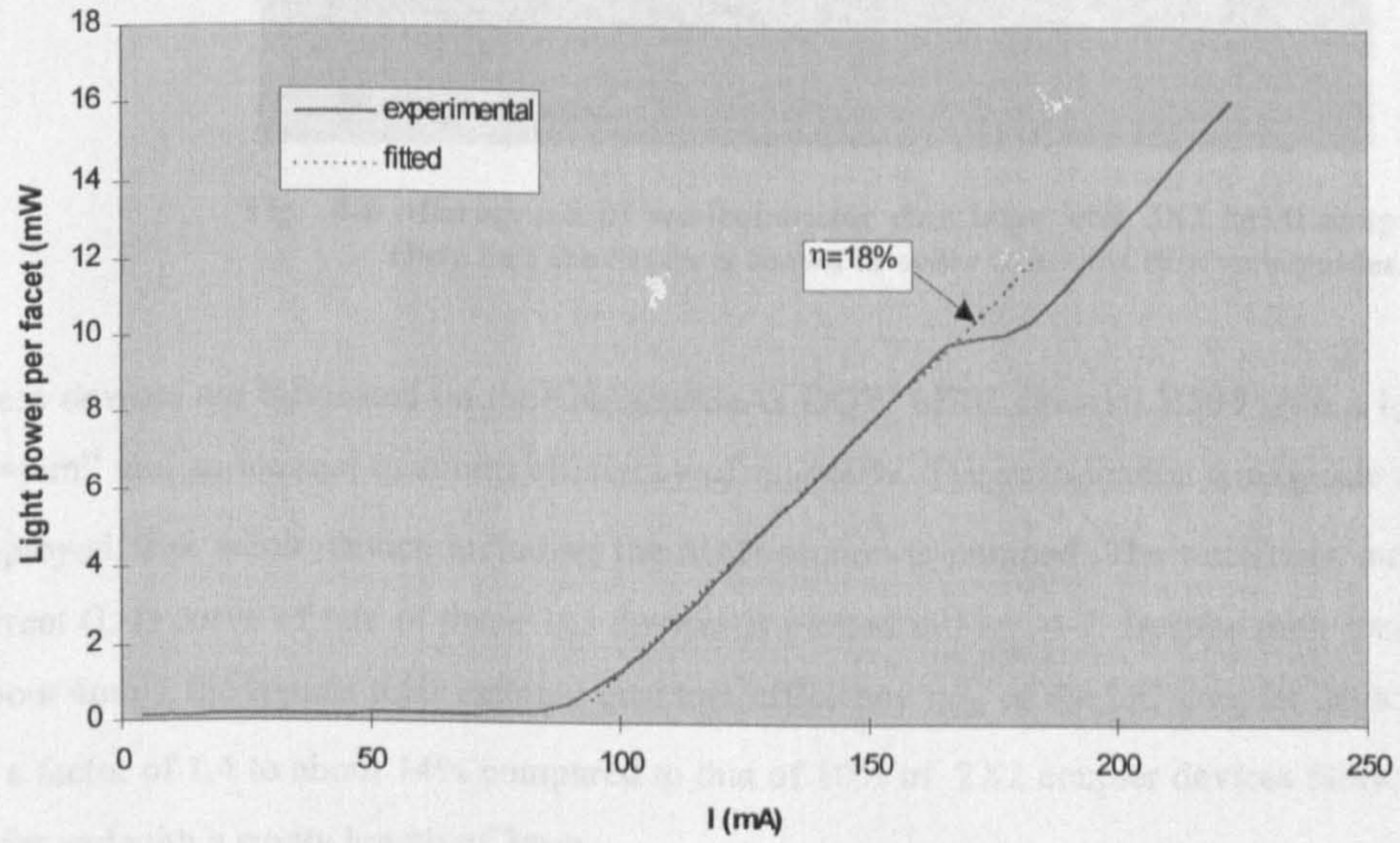

(b)

Fig. 4-5 The L-I curves of F=0.5 (a), and F=0.3 (b) MMI coupler SRLs.

SRLs employing 3X3 MMI couplers

In an OTDM system the output of the light source will have to be split into several parallel beams. However, it would be better that the light source could produce these beams without using a beam splitter. This will save the output light from insertion loss of the beam splitter. The space to place the beam splitter and the waveguides to connect the light source to the beam splitter are also saved. SRL devices with multiple output ports are therefore developed, which also extract more light out of the ring cavity than the 0.5/0.5 MMI coupler SRLs.

The first type of such SRLs to be developed (Fig. 4-6) employs a 3X3 MMI section[1] for output coupling. Two of the coupler's 6 ports are used for feedback so that 4 output ports are available. The feedback coupling ratio F is thereby reduced to 1/3, which, according to Eq.4-1, should result in higher overall external efficiency compared to SRLs with one 0.5/0.5 2X2 MMI coupler.

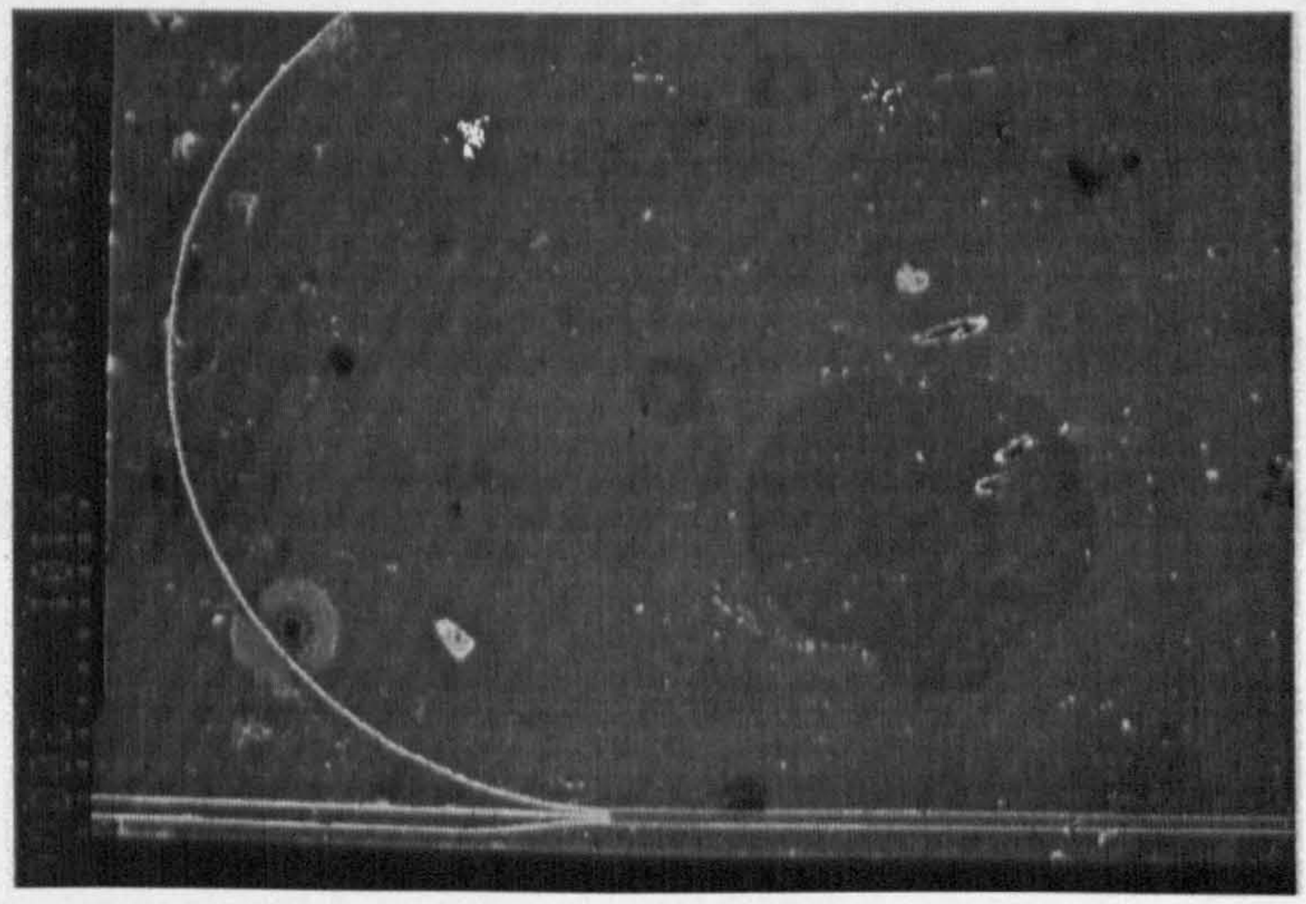

Fig. 4-6 Micrograph of semiconductor ring laser with 3X3 MMI coupler. Only half the device is shown in order to see the thin waveguides.

These devices are fabricated on the GaAs/AlGaAs DQW MBE material B500 with a loss coefficient of α_i=4cm^{-1} and an internal quantum efficiency of η_{in}=60%. The strip-loaded waveguide structure is again employed. The whole device including the MMI section is pumped. The total light output vs. injection current (L-I) curve of one of these 3x3 devices is plotted in Fig. 4-7. Despite their longer cavity length (about 4mm), the typical total external quantum efficiency η_{ex} of the 3x3 coupler devices was improved by a factor of 1.4 to about 14% compared to that of 10% of 2X2 coupler devices fabricated on the same wafer and with a cavity length of 3mm.

Fig. 4-7 also compares the L-I curves of two SRLs with 3x3 MMI couplers of different MMI section length. These L-I curves are measured from the individual outputs of each device. In the device with 810μm MMI section, although the values of output power from each output are not equal, the L-I curves are nearly linear and they all start at the same threshold current value. In devices with shorter MMI sections, however, the L-I curves tend to be 'switched on' at different injection current values and the onset of one output is often accompanied by the reduce of slope in another output's L-I curve. This is a clear indication of changing coupling ratio due to injection variation (see IV-4-1) and suggests that these MMI couplers are not 'well-matched'. Similar behaviour is also observed in devices with longer MMI couplers. The 810μm MMI section length is therefore believed to the 'well-matched' value and agrees excellently with the Ti:Sapphire laser characterisation results described in Chapter 3.

---

[1]Bachmann, M., Besse, B. A. and Melchior, H., "General Self-imaging Properties in NxN Multimode Interference Couplers Including Phase Relations", Applied Optics, VOL.33, No.18, 1994, pp.3905-3911.

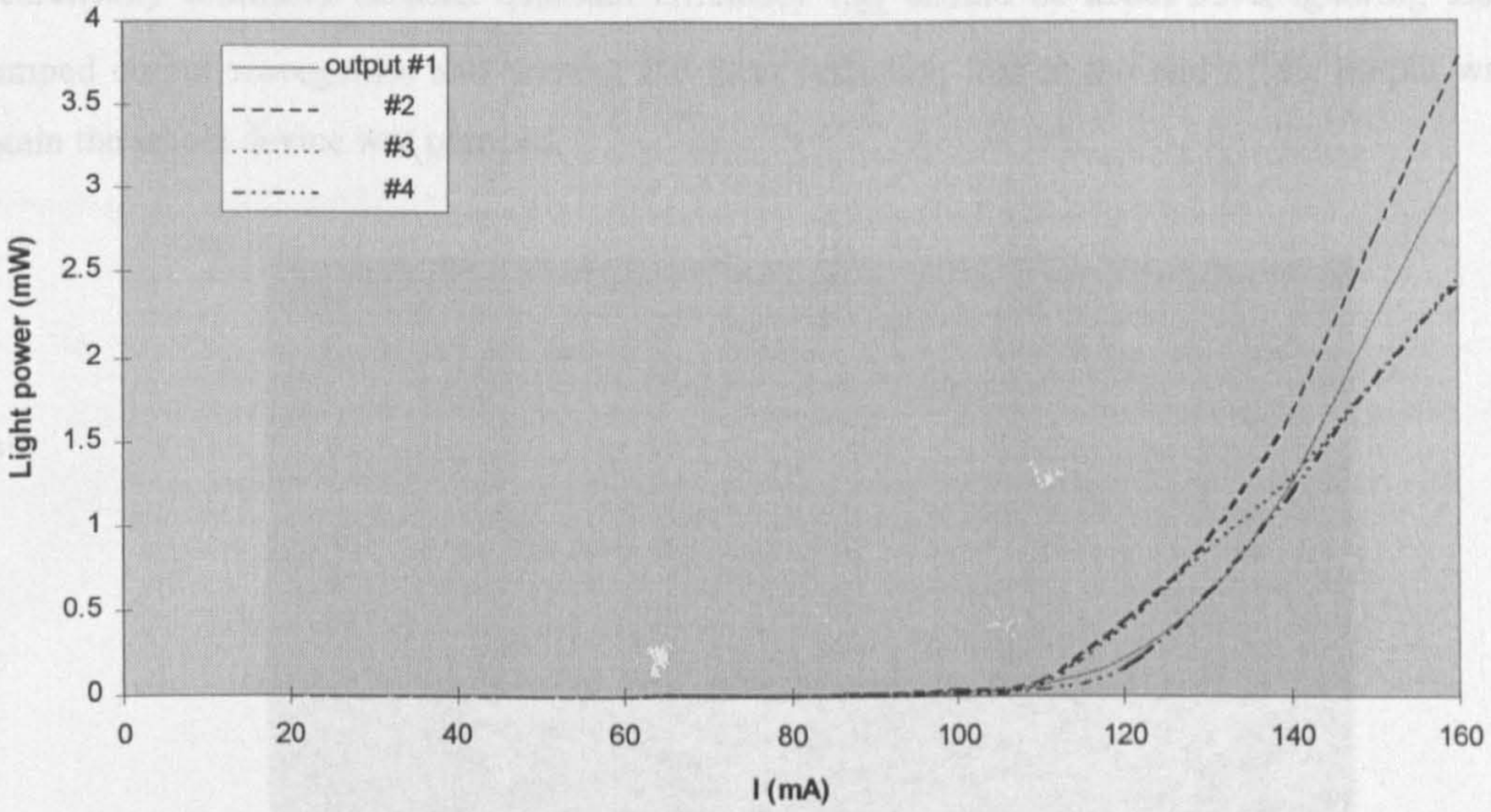

(a)

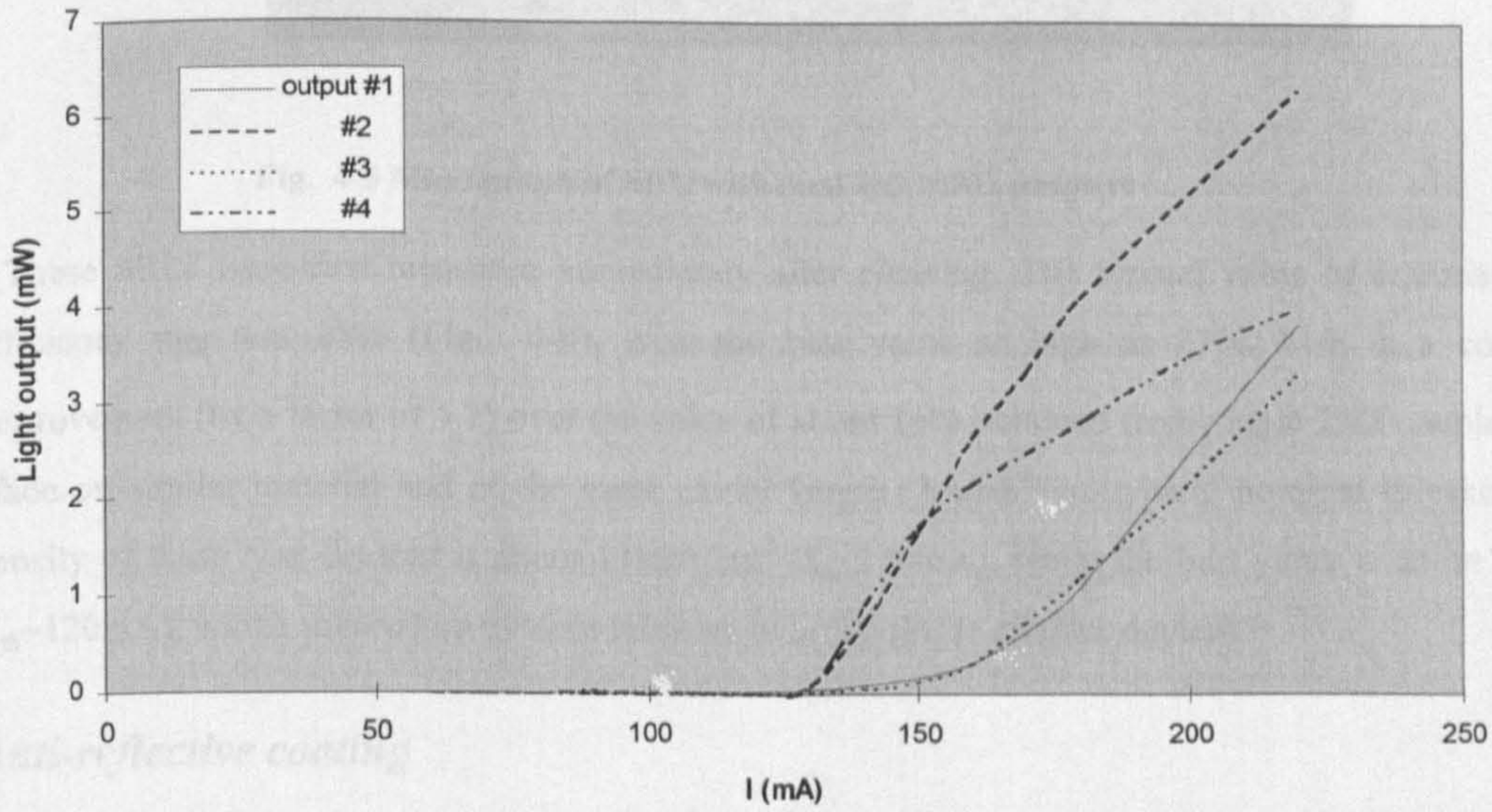

(b)

Fig. 4-7 The L-I curves of 3x3 MMI coupler SRLs with different MMI section length, (a)L=810μm, (b)L=780μm.

Dual 2X2 coupler SRLs

The second type of SRL (Fig. 4-8) employs two 2X2 MMI couplers of 0.5/0.5 coupling ratio to obtain four outputs and a further reduced feedback coupling ratio F of 0.25. Among all the coupler structures used, 0.5/0.5 2X2 MMI couplers were shown to be the most robust for use in SRLs for reasons discussed in Chapter 3. Due to the use of an improved MBE DQW material B680 (α_i=4cm^{-1}, η_{in}=90%),

theoretically estimated external quantum efficiency η_{ex} should be about 33%, ignoring the effect of pumped output waveguides and without the facet reflection loss at the end of the output waveguides. Again the whole device was pumped.

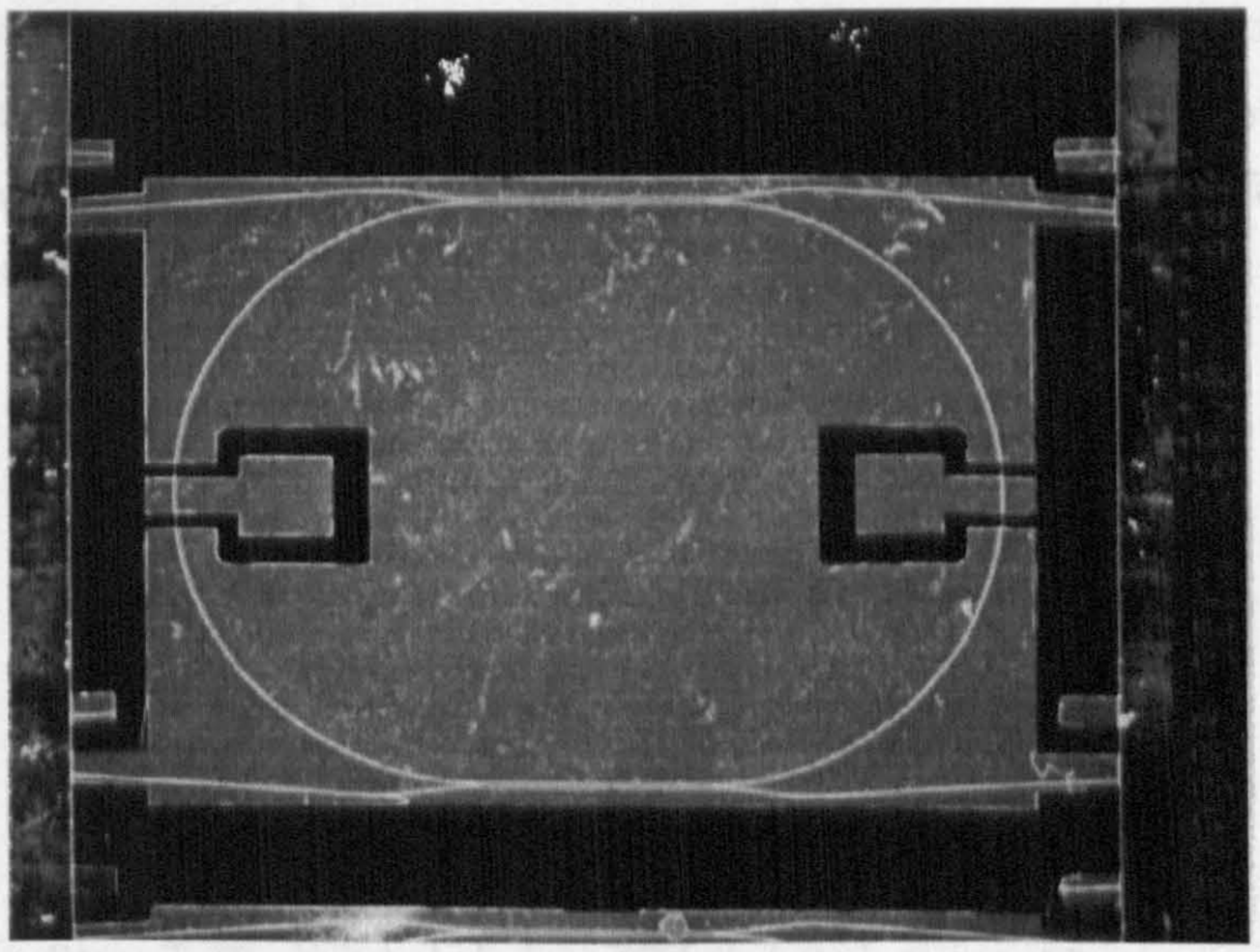

Fig. 4-8 Micrograph of SRL with dual 2x2 MMI couplers

These SRLs were first measured immediately after cleaving. The typical value of external quantum efficiency η_{ex} was 25% (Fig. 4-9), with the best value as high as 27%. This is a considerable improvement (by a factor of 1.7) over the value of about 16% obtained from single 2X2 coupler devices[1] made on similar material and of the same cavity length (3mm). The typical nominal threshold current density of these new devices is about 1100A/cm^2 (I_{th}~150mA), while the best value is about 880A/cm^2 (I_{th}~120mA), which showed no evident increase over the single coupler devices.

Anti-reflective coating

The output facet reduces the external efficiency by a factor of about 0.7 (R=0.3). To eliminate this loss an anti-reflective coating can be applied to the facet.

The same dual 2x2 MMI devices were anti-reflective (AR) coated on both output facets. The AR coatings were sputtered Al_2O_3 $\lambda/4$ film. The external efficiency improved to above 30% for almost all devices and the best value was 33%, which was in excellent agreement with the theoretical prediction using Eq.4-1. It also caused changes of threshold current in some devices and a redistribution of light power among the outputs (Fig. 4-19). These later phenomena suggested that, in an uncoated device, although the output waveguides were tilted 4° from normal to the cleaved facet, facet feedback could still not be ignored and

---

[1]Krauss, T. F., De La Rue, R., Laybourn, P. J. R., Vögele, B., and Stanley, C., "Efficient Semiconductor Ring Lasers Made by a Simple Self-Aligned Fabrication Process", IEEE J. of Selected Topics in Quantum Electronics, VOL. 1, No.2, pp.757-761.

played a role in the operation of the devices. This judgement was also justified by the fact that the η_{ex} values measured before AR coating varied considerably from device to device. The η_{ex} values measured before and after AR coating were not related to each other simply by a factor of 1-R (R=0.3 is the reflectivity of uncoated facet). This is because before AR coating, the coupling between the ring cavity and the sub-cavity formed by facets' reflection would affect the light power distribution in the devices and therefore their output characteristics. After AR coating, however, the efficiency values tended to vary less from device to device, all fell in the range of 30-33%(Fig. 4-9). Thus the facet feedback was believed to be greatly reduced.

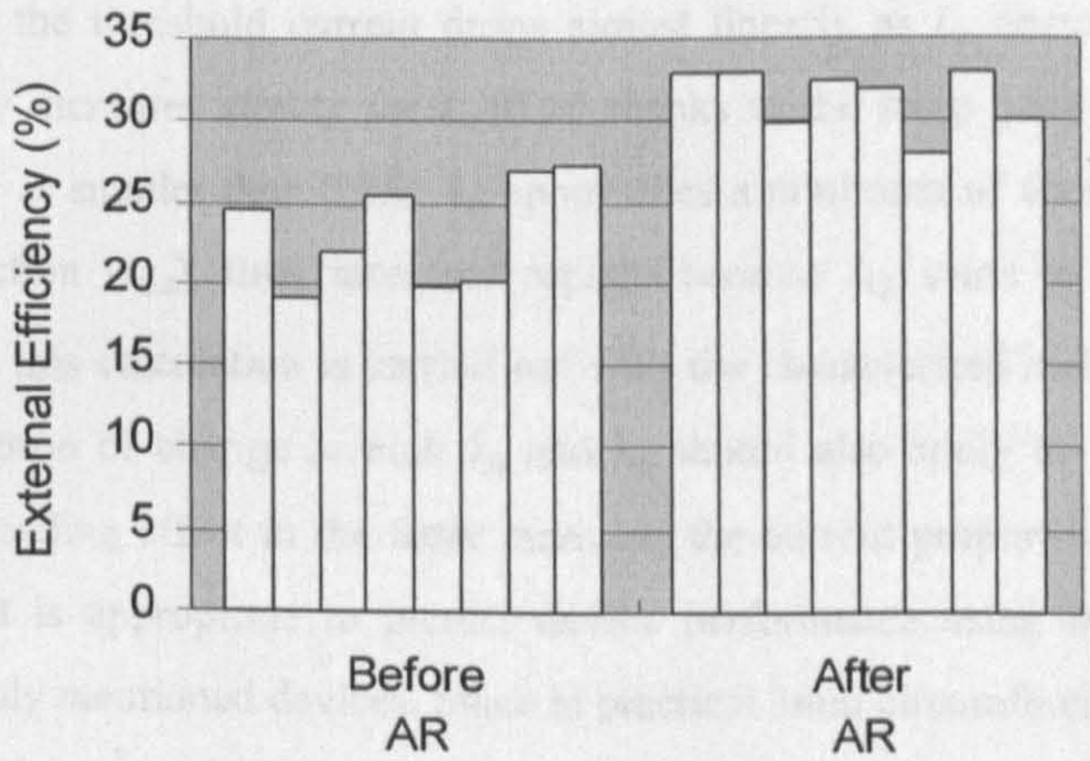

Fig. 4-9 External Efficiency before and after AR coating, measured from 8 device on the same wafer.

4-3 Extended Cavity Semiconductor Ring Lasers

As presented in II-1-2, in order to operate the semiconductor ring laser mode-locked at 10GHz, the cavity circumference L will be about 8.6mm long. It is impossible to operate it without making most of its cavity length passive (i.e., without current injection) because the threshold current would be too large.

4-3-1 Reducing the Threshold Current of Semiconductor Lasers by Introducing Passive Sections.

Consider a semiconductor QW laser with a passive section in its cavity. Suppose that the passive waveguide has the same loss coefficient α_i as the active waveguide. The threshold condition of such a laser will be

$$n_{qw}\Gamma_{qw}g_{qw}L_a = \alpha_i L + \ln(1/R) \qquad \textbf{Eq. 4-4}$$

where n_{qw} is the number of QW's in the material, Γ_{qw} is the light confinement factor of each QW, g_{qw} is the gain coefficient of each QW, L_a is the length of the active (pumped) section, $L=L_a+L_p$ is the total

cavity length and R is the reflectivity of the cavity mirrors. The gain coefficient g_{qw} can be expressed by the following formula (see II-1)

$$\frac{g_{qw}}{g_0} = 1 + \ln(\frac{J_{qw}}{J_0}) \qquad \textbf{Eq. 4-5}$$

Use the typical parameter values of the presently used DQW materials $\alpha_i = 4.5\text{cm}^{-1}$, Γ_{qw}=4%, saturation parameters J_0=300A/cm^2 and g_0=900cm^{-1}, the reduction of threshold current and the increase of threshold current density for a 0.3:0.7 coupling ratio ring laser (R=$\sqrt{0.3}$) are shown in Fig. 4-10 as the fraction of active section length varies.

It can be seen that the threshold current drops almost linearly as L_a decreases because the threshold current density only increases slowly for L_a>0.2L thanks to the steep gain-current relationship in QW materials. When L_a is smaller then 0.2L, I_{th} approaches a minimum of about 1/5 the threshold current without passive section (I_{th0}), then increases rapidly because J_{th} starts to rise sharply, which is not desirable. Although this calculation is carried out with the characterised material parameters from wide area lasers, the fraction of change in both J_{th} and I_{th} should also apply to narrow waveguide devices, because current spreading effect in the latter increases the current proportionally for any active section length. Therefore it is appropriate to predict device performance using the nominal current density obtained in previously mentioned devices. Since in practical 3mm circumference SRLs the measured J_{th} is in the order of 1000A/cm^2, and if 1.5 times that value is considered as acceptable, it is sensible to make an active section no shorter than 0.15L, which is about 1.2mm for 8.6mm cavity length, and no longer than 0.5L (4.3mm). This would result in a threshold current density in the range of 1000-1500A/cm^2 and a threshold current of about 100mA.

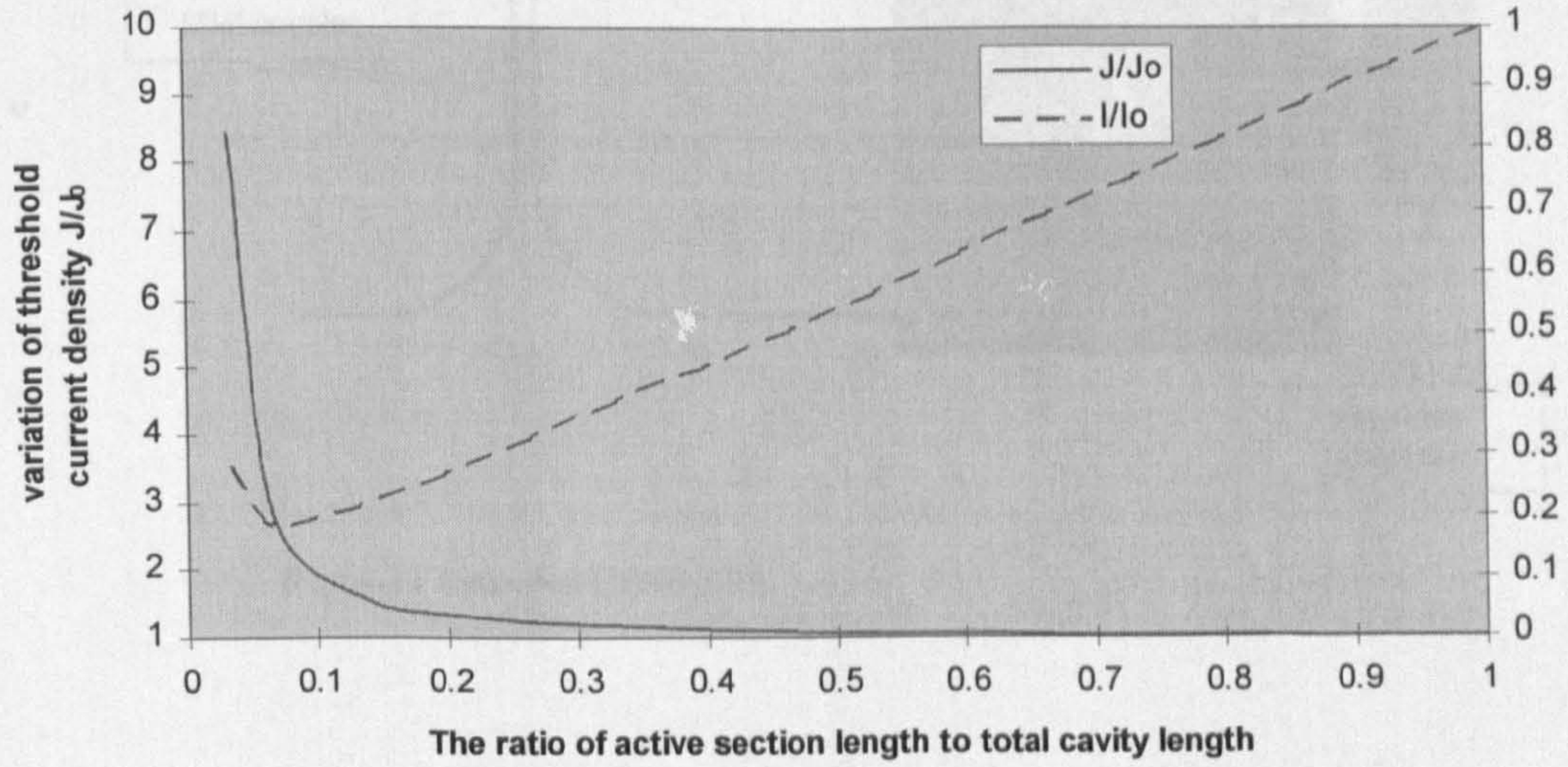

Fig. 4-10 Variation of threshold current I_{th} and threshold current density J_{th} of extended cavity ring lasers as the fraction of active section length is changed.

4-3-2 Extended Cavity Ring Laser Results

Device

The extended cavity SRLs have been designed to have 0.5:0.5 feedback/output MMI couplers, 7.5 mm ring circumference, and active section length variable from 1.75-3.75mm. The passive section of the cavity has been designed to be bandgap-tuned by the IFVD technique before the waveguide is defined. A saturable absorber is placed in the middle of the active section to operate the device mode-locked. The device is illustrated in Fig. 4-11.

Results

The devices are made on both MBE DQW material B429 with p-doped GaAs QWs and MOVPE material QT899. Fig. 4-12 is the measured photoluminescence (PL) curve of the material B429 before and after the process. The SiO_2 coated area has a wavelength shift of 30nm relative to the material as grown and the SrF_2 coated area has a shift of only about 4nm so the differential wavelength shift between the two areas was about 26nm. For QT899 samples the differential wavelength shift was about 20nm. The samples then undergo the same fabrication process as usual SRLs to form the extended cavity ring lasers. The pumped active section is 3.75mm long (or half the cavity circumfenrece).

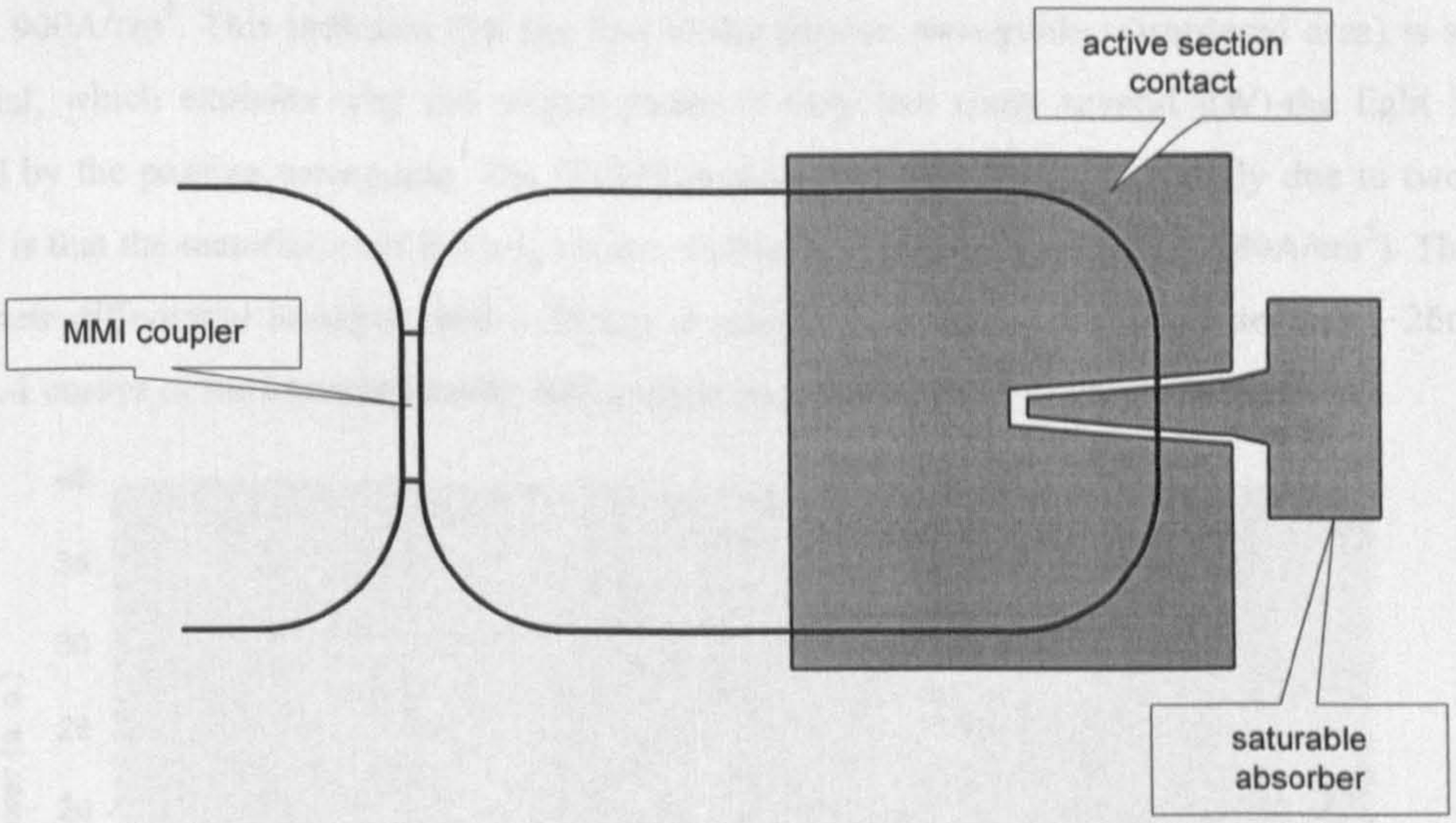

Fig. 4-11 Extended Cavity SRL

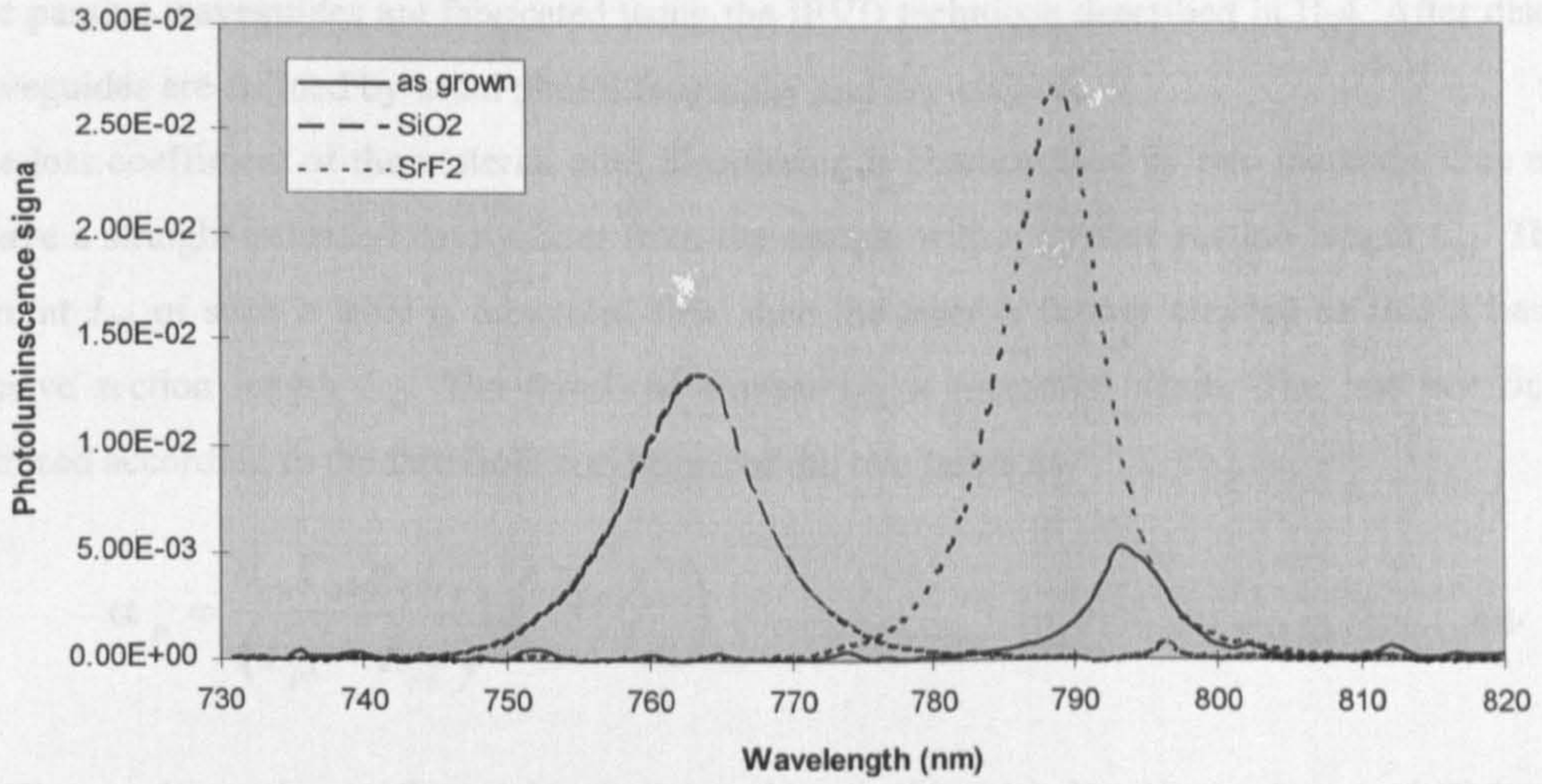

Fig. 4-12 Photoluminscence (PL) results of material B429 after IFVD. Annealed 30seconds @900°C.

The typical threshold currents are about 100mA and 240mA for B429 and QT899 devices respectively, corresponding to threshold current densities J_{th} of about 1350A/cm^2 and 3240A/cm^2. In contrast, non-extended cavity SRLs fabricated on B429, with 3.1mm ring circumference (4.5mm total pumped waveguide length), the same output coupler and the same waveguide width, have a much lower J_{th} value of about 900A/cm^2. This indicates that the loss of the passive waveguide (disordered area) is still quite substantial, which explains why the output power is very low (only several μW)-the light has been absorbed by the passive waveguide. The QT899 devices had even higher J_{th} mainly due to two factors. The first is that the material itself has a J_0 value (~400A/cm^2) higher than B429 (~180A/cm^2). The second is that their differential bandgap shift (~20nm) is smaller than that of the B429 devices (~26nm). The pulsed L-I curves of the extended cavity SRLs made on material B429 is shown in Fig. 4-13.

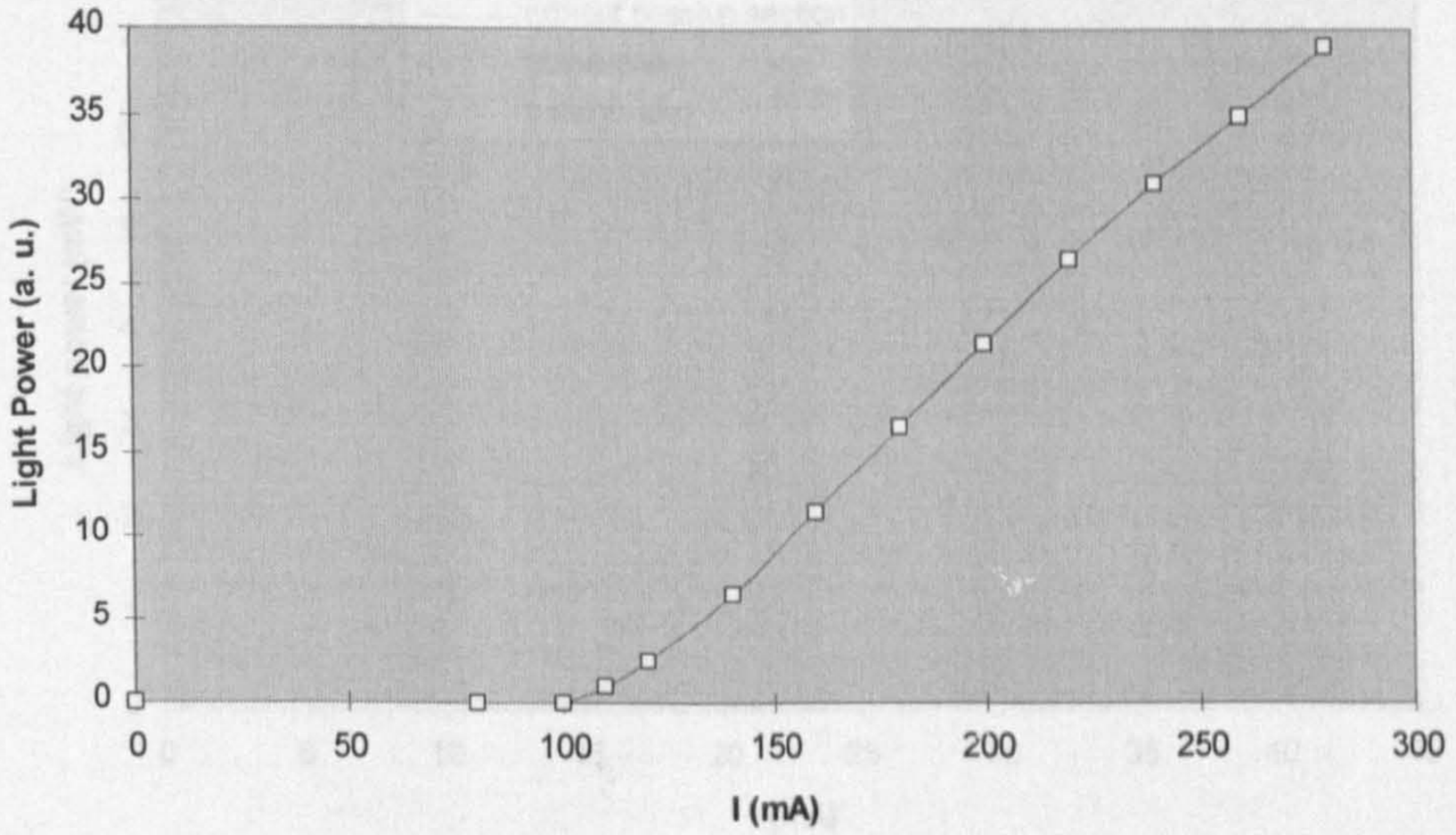

Fig. 4-13 L-I curve of an extended cavity SRL fabricated material B429 by IFVD.

4-3-3 Characterisation of Waveguide Loss

The passive waveguides are fabricated using the IFVD technique described in II-4. After disordering the waveguides are defined by usual photolithography and dry-etching.

The loss coefficient of the material after disordering is characterised by two methods. One method is to cleave a straight extended cavity laser from the sample with a passive section length L_{p1}. The threshold current I_{th1} of such a laser is measured first, then the laser is further cleaved so that it has a different passive section length L_{p2}. The threshold current I_{th2} is measured again. The loss coefficient can be deduced according to the threshold conditions of the two lasers as

$$\alpha_p = \frac{n_{qw}\Gamma_{qw}g_0 L_a}{(L_{p1} - L_{p2})} \ln\left(I_{th1} / I_{th2}\right) \qquad \text{Eq. 4-6}$$

The result can be confirmed by the second method, which launches a beam of Ti:Sapphire laser emission at the semiconductor laser's lasing wavelength (860nm) into a passive waveguide cleaved from the sample. By changing the temperature of the waveguide or fine tuning of the Ti:Sapphire wavelength, the output of the waveguide will change due to Fabry-Parot resonance between the two end facets of the waveguide. The peak-trough ratio of this change is related to the transmittance T of the waveguide material by the following equation

$$\frac{P_{\max}}{P_{\min}} = \frac{(1+RT)^2}{(1-RT)^2} \qquad \text{Eq. 4-7}$$

where

$$T = \exp(-\alpha_p L_p) \qquad \text{Eq. 4-8}$$

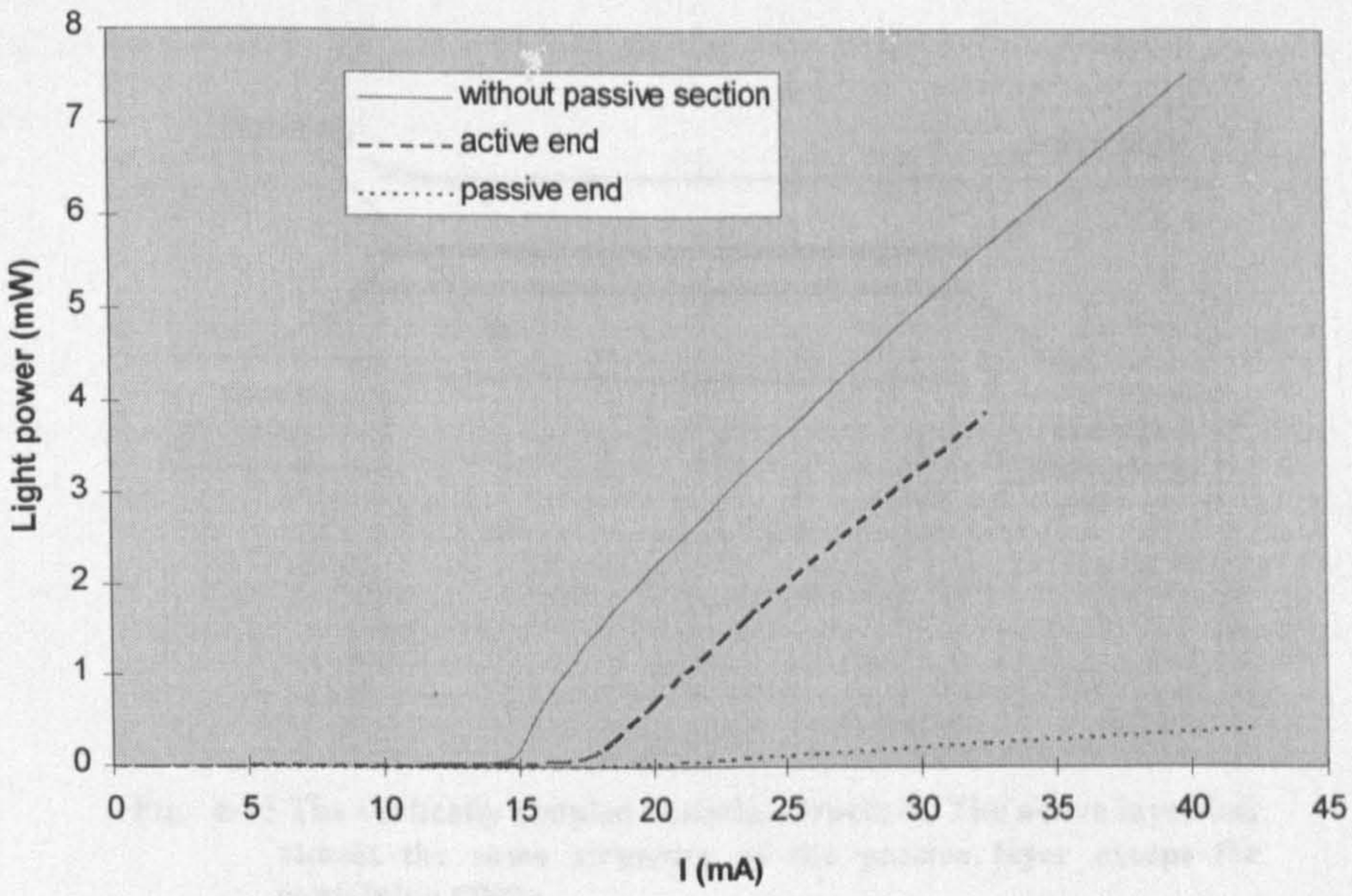

Fig. 4-14 The L-I curves of a straight extended cavity laser formed on the same sample as the extended cavity SRL.

By method one a straight extended cavity laser of L_a=381μm, L_{p1}=348μm is formed on the same B429 sample. I_{th1} and I_{th2} are measured as 17.81 and 14.57mA (L_{p2}=0μm) respectively (Fig. 4-14). Using material parameters n_w=2, Γ_w=0.04 and g_0=1250cm^{-1}, the loss coefficient is calculated as α_p=23.91cm^{-1}.

By method No.2 a 536μm long waveguide was used and the peak-trough ratio is measured as 1.37. Taking facet reflectivity R=0.32 the loss coefficient was calculated as α_p=25.13cm^{-1}.

These two values agreed very well. They corresponded to a loss of more than 90dB/cm., which was very high. One possibility is that the differential bandgap shift was not enough and interband absorption still exists to a large extend. Another possibility is that during the IFVD process sub-micron defects were created in the material. If the density of such defects was higher than one in 10X10μm area , then they would almost certainly cause large scattering loss in a long narrow waveguide.

4-3-4 Alternative Structure for Extended Cavity SRLs

Despite recent progress in techniques such as phosphor-doped SiO_2 disordering prohibitive capping, there are many problems related to disordering process remain unsolved. Among them are reproducibility, material quality after annealing, and device lifetime. Because disordering often involves processing the material under very high temperature and relies on the production of lattice vacancies or point defects, doubts as to its practicability in real devices remain until further investigations prove otherwise.

An alternative way of constructing a PIC comprising both active and passive devices without incuring the use of regrowth can be found by growing both the passive and active waveguides successively in one growth process. The two guiding layers then form a vertically coupled waveguide structure which can be tailored into either passive or active waveguide components. The idea is illustrated in Fig. 4-15 and was first implemented in an earlier SRL for output coupling[1].

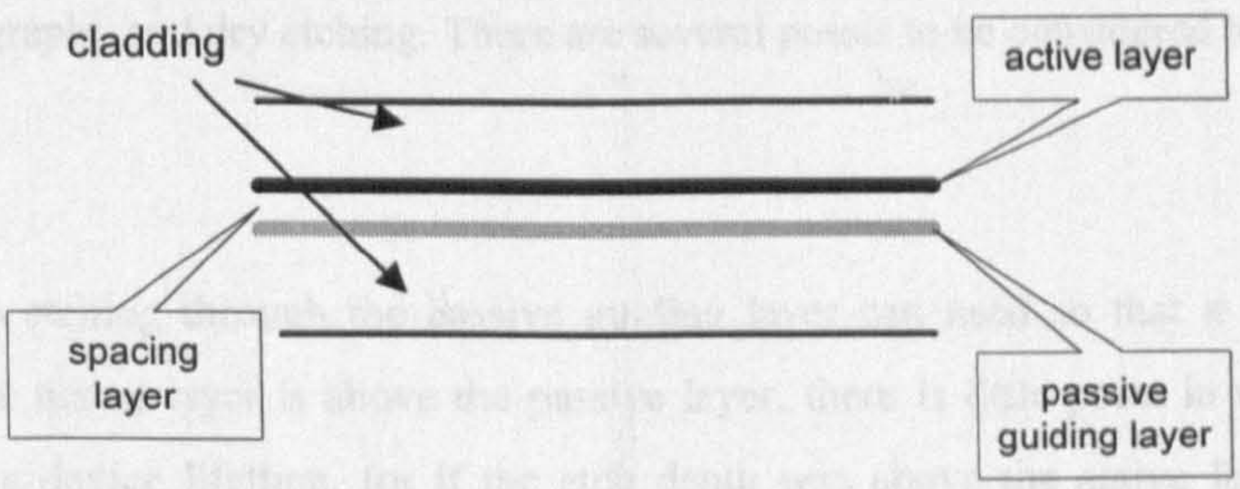

Fig. 4-15 The vertically coupled material structure. The active layer has almost the same structure as the passive layer except for containing QW's.

[1]Krauss, T. F., 'Integrated semiconductor ring lasers', Ph.D thesis. University of Glasgow, 1992..

The light propagation in such a structure is described by the coupled waveguide. The light intensity in each waveguide is a sinusoidal function of the propagation length and the pitch of the sinusoidal is determined by the thickness of the spacing layer or the strength of coupling. If the structure is completely symmetric both geometrically and optically (i.e., the refractive indices of the two waveguide layers are equal), the switch is complete. Otherwise only part of the propagating light intensity switches between them. Using a Beam Propagation Method (BPM) numerical simulation [1], the light intensity distribution of a structure with 0.2μm thick $Al_{0.2}Ga_{0.8}As$ guiding layers and 0.4μm $Al_{0.4}Ga_{0.6}As$ spacing layer (i.e., the structure of MOVPE material QT98) is calculated and depicted in Fig. 4-16. The pitch of the structure is about 50μm.

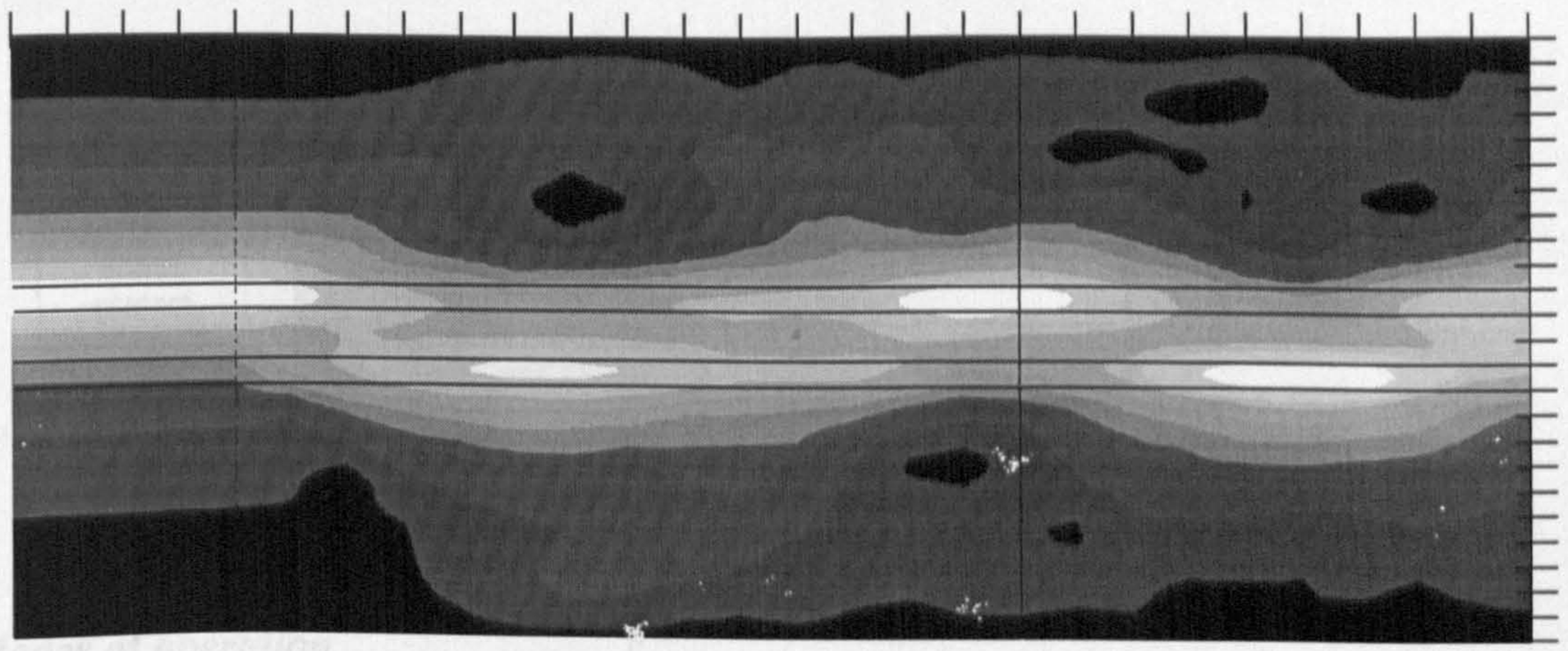

Fig. 4-16 The light intensity distribution in a coupled waveguide structure. The horizontal and vertical scale s are 5μm/div and 0.2μm/div, respectively. The horizontal solid lines mark the boundaries of the waveguide layers. The vertical dashed line marks the starting point of the coupling.

Extenernal cavity F-P lasers and ring lasers can be fabricated using this material structure. The scheme for exended cavity F-P lasers is shown in Fig. 4-17. laser waveguides are formed on the material by standard photolithography and dry etching. There are several points to be considered here.

Etch Depth

For simplicity deep etching through the passive guiding layer can used so that a ridge waveguide is formed. Because the active layer is above the passive layer, there is little point in using a strip-loaded structure to improve device lifetime, for if the etch depth was above the active layer there would be insufficient lateral optical confinement for the passive waveguide, and if the etch depth came to near the passive guiding layer the active layer would be exposed to the atmosphere anyway. Low loss passive waveguide is obtained simply by removing the active waveguide layer above the passive guiding layer by a second etch step using the ohmic contact as the etch mask. The depth of the second etch should be

---

[1] Krauss, T. F., "Impact of Output coupler Configuration on the Operating Characteristics of semiconductor Ring lasers". J. of Lightwave Technology, VOL. 13, No.7, July 1995, pp.1500-1507.

controlled very carefully so that the etch stops immediately when the active layer is removed, because the spacing layer is only 0.4mm thick and should be kept to form the upper cladding of the passive waveguide.

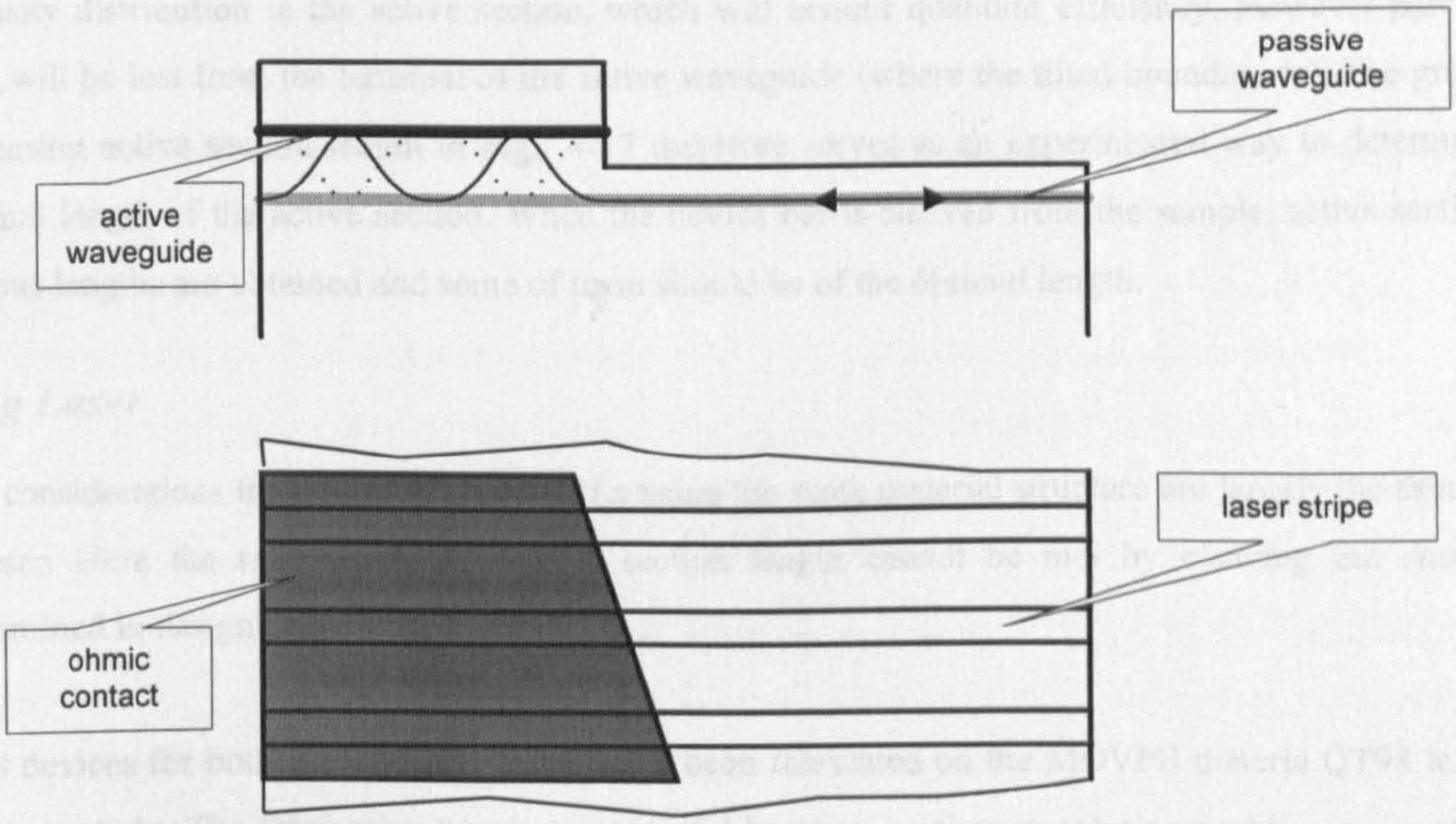

Fig. 4-17 The extended cavity laser scheme using vertical coupled structure. Top: cross-section, bottom: top view of sample.

Modes of operation

Two modes of operation can exist in this structure as shown by solid and dashed lines in the top diagram of Fig. 4-17. The solid line is the wanted extended cavity mode and the dashed line is the sub-cavity mode in the active section. Unfortunately in this structure the former suffers more loss than the latter if the etch end facet of the active layer is vertical and smooth enough, so the favoured mode of operation is the latter. To prevent the sub-cavity mode from lasing, the boundary between the active and the passive section is tilted against the crystal axis (bottom diagram in Fig. 4-17). The subcavity is then destroyed by the tilted etched facet.

Cavity length, Threshold and Efficiency

In this structure, the length of the active section will have to be carefully designed. One obvious choice is to make it multiple times of half the pitch, i.e., $L_a = kP/2$. This ensures that the extended cavity mode will be fully coupled back into the passive waveguide after being amplified by the active section in each roundtrip.

In this configuration, however, the lasing mode effectively only stays in the active layer for half the active section length so the overall gain it experiences is only $e^{-\frac{1}{2}} \approx 0.6$ times the value the active section can provide. For QW materials with steep gain-injection relationship this could mean ony a small increase in the threshold current. However, when above threshold, because half the injected carriers do not interact with the light field at all, the quantum efficiency could be halved.

If active section length not equal to kP/2 is used, the light intensity distribution in the active sevtion tends to be very complicated by the composition between the waves travelling in opposite direction and coupling between the two waveguide. At some lengths it is possible to have a more uniform light intensity distribution in the active section, which will benefit quantum efficiency. However part of the light will be lost from the terminal of the active waveguide (where the tilted boundary is). The gradually increasing active section length in Fig. 4-17 therefore serves as an experimental way to determine the optimal length of the active section. When the device bar is cleaved from the sample, active sections of various lengths are obtained and some of them should be of the optimal length.

Ring Laser

The considerations for extended cavity SRLs using the same material structure are largely the same as F-P laser. Here the requirement for active section length cannot be met by cleaving but should be determined in design stage.

Trial devices for both F-P and ring lasers have been fabricated on the MOVPE materia QT98 left from previous study. The fabrication was not successful because a polymer polution problem occured in the first dry etch process. Further investigation could not go shead because of lack of material. However, there is no reason why the scheme should not work. Despite the disadvantage concerning threshold and quantum efficiency, when compared with the uncertainties in the disordering process, the controllability, the non-damaging nature of the process and the possibly very low loss passive sections capable of producing by this scheme are very attractive and worth further study.

4-4 Linearity of L-I characteristics and Spectral Properties.

4-4-1 Sources of Nonlinearity in L-I characteristics

Apart from low external efficiency, another disadvantage of semiconductor ring lasers which has prevented their application for practical purpose was that their L-I characteristics were nonlinear[1]. Previous studies revealed that the causes of the nonlinearity have been:

1)The unstability of the output coupler. As discussed in Section IV-1, the coupling ratio of some couplers, in particular Y-junctions and directional couplers, is sensitive to the variation of injected current. When properly designed, 2x2 MMI couplers are more robust to the variation, but the self-imaging length of MMI couplers still depends on the refractive index. The use of strip-loaded waveguide structure imposes new question on the robustness of MMI couplers. The problem is particularly serious

---

[1]Krauss, T. F., De La Rue, R. M., and Laybourn, P. J. R., "Impact of Output coupler Configuration on the Operating Characteristics of semiconductor Ring lasers". J. of Lightwave Technology, VOL. 13, No.7, July 1995, pp.1500-1507.

when the 3x3 MMI coupler is used. This kind of nonlinearity appears as a gradual change (either increase or decrease) of the slope of individual L-I curves measured at each output as shown in IV-2.

2)Unwanted back scattering or reflection. Experiment revealed that, while the overall trend of the L-I curves are straight, sudden 'kinks' exist at certain injection currents. Detailed studies [1] suggested that these 'kinks' were accompanied by longetudinal mode hopping. Between the 'kinks' the SRL usually operated single moded. Given the SRLs long cavity length, which should have very close longitudinal mode spacing, it would have operated multi-moded should no mode selecting mechanism exist. Since there was no other elements in the cavity, the mode selection was attributed to the feedback due to back scattering at discontinuities of the waveguides, particularly the back reflection of output facets.

The light reflected by the output facet couples into the counter-propagating cavity mode of the SRL. The two directions are no longer independent but coupled. The output waveguide and the ring cavity form a coupled cavity. Lasing happens at the optical frequency where the two sets of sub-cavity modes coincide. As the injected current increases, the effective refractive indices of the ring and the output waveguides change, their sub-cavity modes no longer co-incide at the lasing frequency. Instead they may coincide at another ring cavity mode frequency. Mode hopping occurs as a result.

To reduce the facet back reflection into the ring cavity, in some earlier devices the output waveguides were tilted at about 4° from normal. It was estimated that the facet feedback into the output waveguide was reduced to about 1%. However, this still did not eliminate the kinks. The reason was that the output waveguides were pumped and had optical gain. The actual feedback into the ring cavity was therefore amplified by the output waveguide and was greater than 1%. Yet in a semiconductor laser a external feedback in the order of 0.1% is enough to change its spectral property[1].

4-4-2 Improving linearity of L-I characteristics by Anti-reflective (AR) Coating

Having identified the source of nonlinearity, measures can be taken to reduce it. Fig. 4-18 shows the L-I curves of a dual 2x2 MMI coupler SRL before and after AR coating. The light output is the sum of its four outputs. The output waveguides are tilted. Before AR the kinks were clearly present. After AR coating, the kink at the smaller injection current value has almost disappeared while the one at the higher injection current is still visible but has become less obvious. The experiment has therefore proved that the facet feedback is the cause of the kinks. Because the AR coating was aimed at improving the external efficiency and was applied without *in situ* monitoring, the residual facet reflectivity is estimated to be of the order of several percent. The total facet feedback must therefore be of the order of 10^{-3} -10^{-4}.

4-4-3 Improving Linearity of L-I Characteristics by Using Improved Couplers

Studying the L-I curves from individual outputs reveals that, even after AR coating, these curve are still not smooth (Fig. 4-19 and Fig. 4-7). They have variations between the 'kinks'. These variations of light

---

[1] Krauss, T. F., De La Rue, R. M., Gontijo, I., Laybourn P. J. R., and Roberts, J. S., 'Strip-loaded semiconductor ringlasers employing multi-mode interference (MMI) couplers', Appl. Phys. Lett., VOL.64, 1994, pp.2788-2790.

power in individual L-I curves are due to the change of coupling ratio in the MMI coupler as a result of refractive index changes caused by carrier injection. These variations, however, tended to cancel each other out when the outputs are added together, because the reduced light power from one output would appear in another, giving a relatively fixed total stimulated emission rate in the whole device. Thus, when added up, they result in a smooth total L-I characteristic.

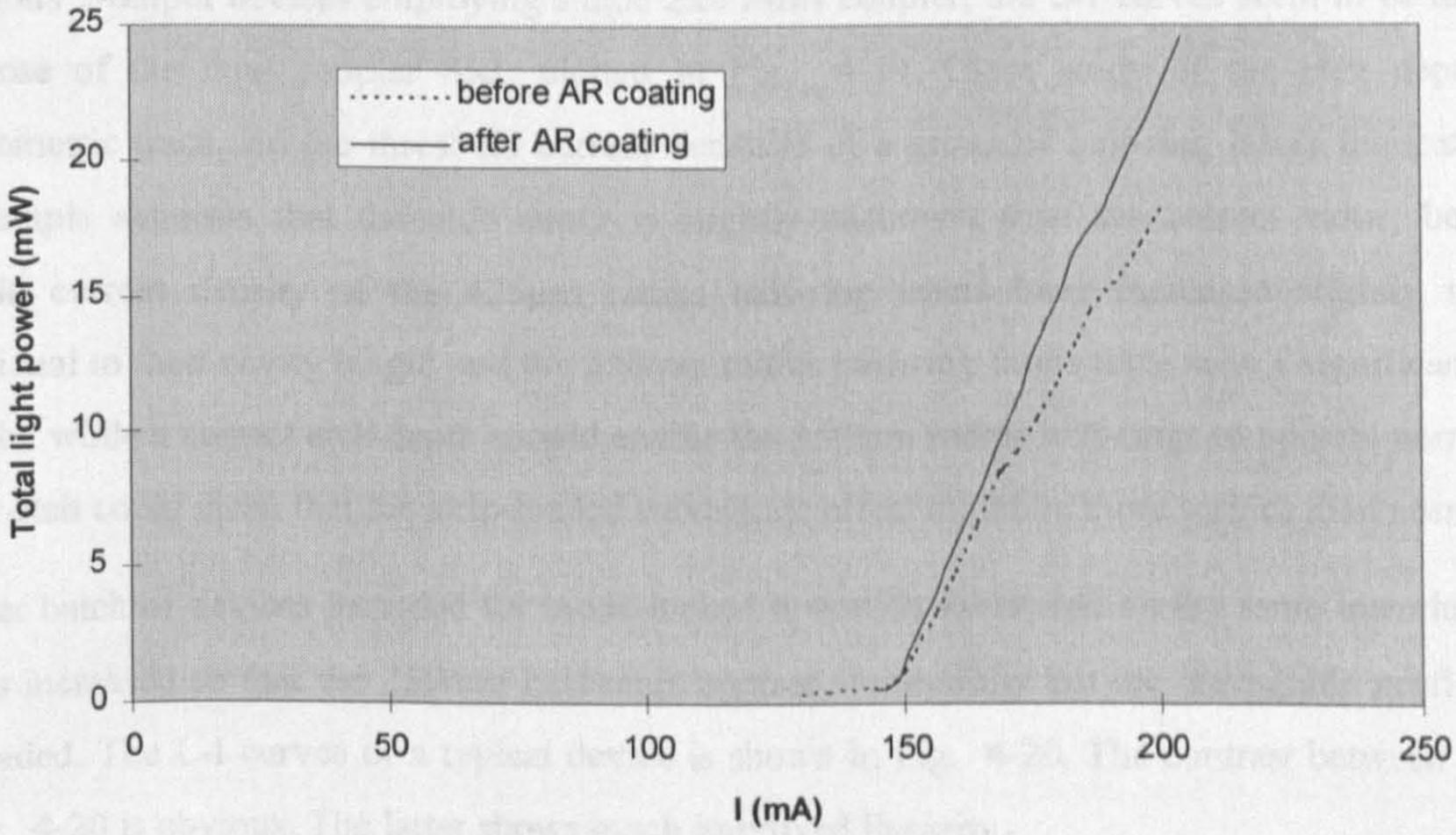

Fig. 4-18 Total light output vs. injection current of dual 2x2 MMI coupler SRL before and after AR coating.

Problems related to 3x3 MMI couplers

As have been discussed in Chapter 3, for MMI couplers, fabrication tolerances become more stringent as the number of ports increases, because of the fact that the self-images will only appear in a shorter 'focal depth' [1] for higher-order self-imaging and are therefore more vulnerable to fabrication errors and refractive index variations, i.e., any small such variations, which would be of little consequence in 2x2 MMI couplers, could have a substantial effect in 3x3 MMIs. One of the fabrication errors is the inaccuracy of etch depth of the strip-loaded waveguide structure which results in a refractive index step different from that used in the calculation of MMI section length. As a consequence, it is more difficult to fabricate a 'well-matched' [2] 3x3 MMI coupler.

---

[1]Heaton, J. M., Jenkins, R. M., Wight, D. R., Parker, J. T., Birbeck J. C. H. and Hilton, K. P., "Novel 1-to-N Way Integrated Optical Beam Splitters Using Symmetric Mode Mixing in GaAs/AlGaAs Multimode Waveguides", Applied Physics Letters, VOL.61, (15), October 1992, pp.1754-1756.

[2]Krauss, T. F., De La Rue, R. M., and Laybourn, P. J. R., "Impact of Output coupler Configuration on the Operating Characteristics of semiconductor Ring lasers". J. of Lightwave Technology, VOL. 13, NO.7, JULY 1995, pp.1500-1507.

Perhaps more importantly, the modal behaviour in a strip-loaded waveguide structure deviates significantly from that of an one-dimensional waveguide model upon which the MMI couplers are designed and disrupts the self-imaging property of MMI couplers, as detailed in Chapter 3. This effect, again, is more serious in 3x3 MMI couplers than in a 2X2's.

2x2 MMI couplers

In previous 2-output devices employing single 2x2 MMI coupler, the L-I curves seem to be more linear than those of the dual coupler SRL plotted in Fig. 4-19. Close study of the etch depth control interferometric trace and the threshold current densities of a group of half-ring lasers fabricated on the same sample suggests that the etch depth is slightly shallower than the correct value, because the threshold current density of the 425μm radius half-ring lasers have increased slightly more than proportional to their cavity length and the 350mm radius half-ring lasers have seen a significantly higher threshold, while a correct etch depth should enable the 350mm radius half-rings to operate normally. The shallow etch could mean that the strip-loaded waveguide effect might be more serious than normal.

In a later batch of devices intended for mode-locked operation fabricated on the same material, the etch depth is increased so that the 350mm half-rings operate successfully but the waveguide profile remains strip-loaded. The L-I curves of a typical device is shown in Fig. 4-20. The contrast between Fig. 4-19 and Fig. 4-20 is obvious. The latter shows much improved linearity.

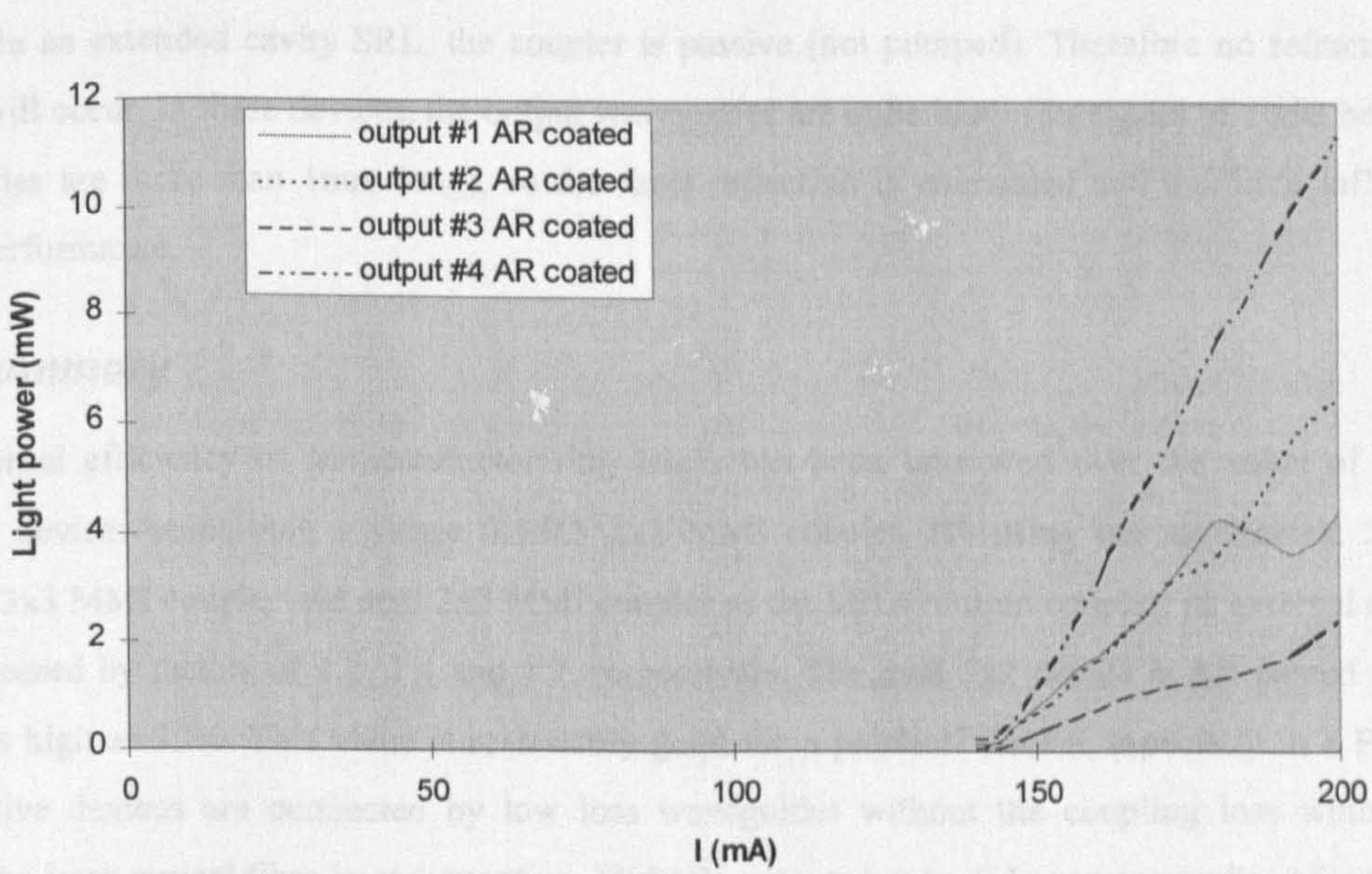

Fig. 4-19 The L-I curves from individual outputs of an AR coated dual 2x2 coupler SRL.

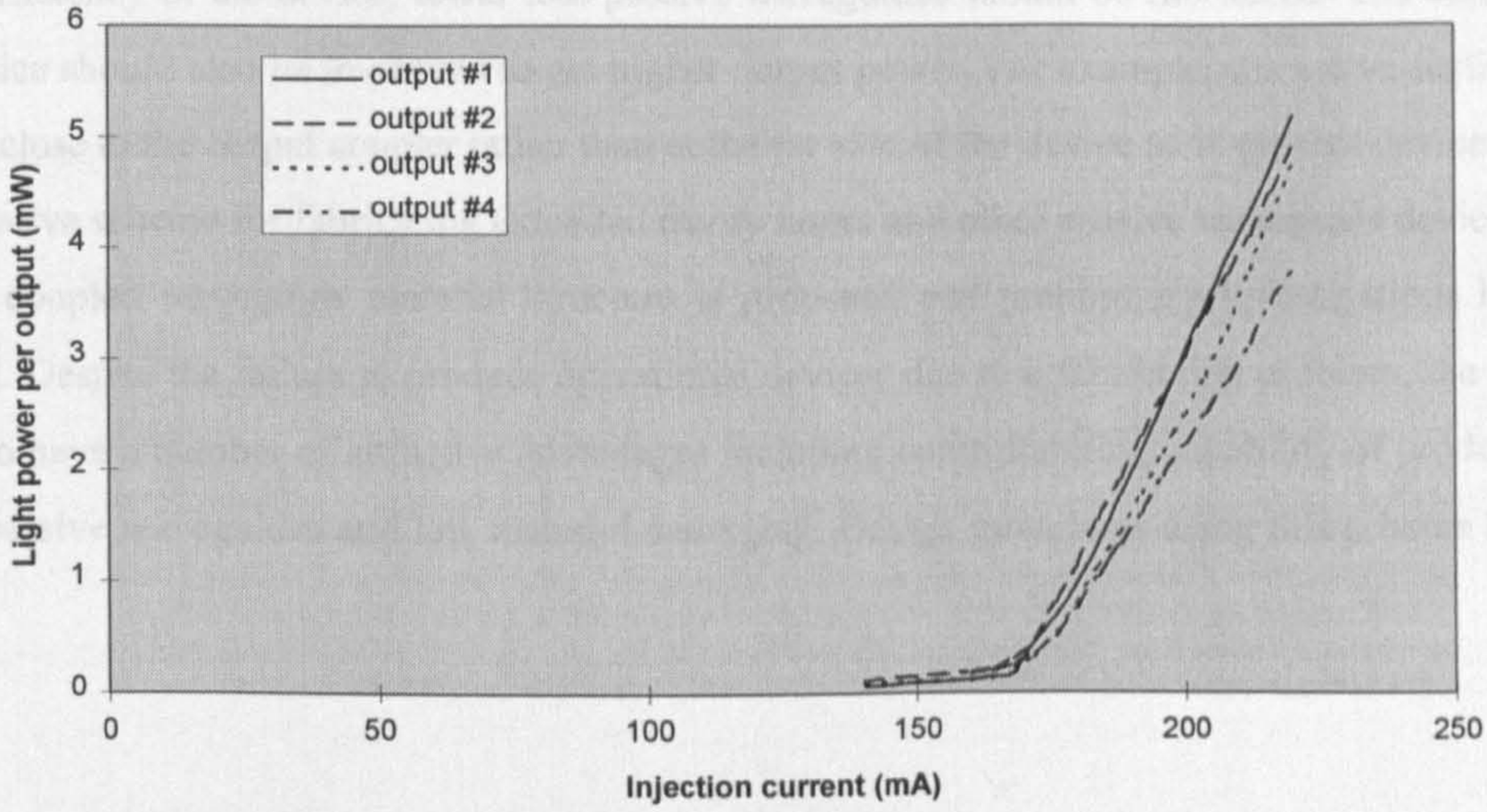

Fig. 4-20 The L-I curves measured from a deeper etch dual 2x2 coupler SRL.

Extended Cavity SRL with Passive MMI coupler

Studying the L-I curves of extended cavity SRLs (Fig. 4-13) fabricated on both the B429 and the QT899 material suggests that they are almost perfectly linear and kink-free, similar to that of a F-P laser. This is because in an extended cavity SRL, the coupler is passive (not pumped). Therefore no refractive index change will occur. In these devices, the output waveguides are quite lossy (in excess of 10dB because the waveguides are more than 1mm long), so the facet reflection is attenuated and has little influence on device performance.

4-5 Summary

The external efficiency of semiconductor ring lasers has been improved over the value of ~16% of previous devices employing a single 0.5/0.5 2x2 MMI coupler. By using the asymmetric 2x2 MMI coupler, 3x3 MMI coupler and dual 2x2 MMI coupler as the SRLs' output coupler, its external efficiency was increased by factors of 1.2, 1.4 and 1.7, respectively. The dual 2x2 device is AR coated to get η_{ex} values as high as 33%. This value is reasonably good for a practical device, especially in a PIC where consecutive devices are connected by low loss waveguides without the coupling loss which usually occurs at a laser-optical fibre interconnection. Multiple outputs (up to 4) have been realised for the device to be used in an OTDM system as the light source. The performance of the dual MMI coupler SRL is close to a practical level in terms of external efficeincy.

The mechanisms causing non-linearity in SRLs L-I characteristics are studied and the linearity is shown to be improved by several means including AR coating, a reasonably deeper waveguide profile and passive output coupler.

Extended cavity SRLs with very long cavity length have been fabricated by the IFVD technique and successfully operated. The linearity of their L-I characteristics is as good as F-P lasers. To improve the

external efficiency of the device, lower loss passive waveguides should be fabricated. The configuration of the device should also be improved to get higher output power. For example, the active section should be placed close to the output coupler rather than at the far side of the device as in present devices.

An alternative scheme for fabricating extended cavity lasers and other passive waveguide devices using a vertically coupled waveguide material structure is proposed and preliminary investigations have been conducted. Despite the failure to produce operational devices due to a fabrication problem, the scheme is believed to have a number of attractive advantages including controllability, capability of producing very low loss passive waveguides and low material damaging. Design guidelines using this scheme have been discussed.

5 Light Source II: Mode-locked Operation of Semiconductor Ring Lasers

Optical short pulse can be generated from semiconductor lasers in several ways including Q-switching or gain-switching, mode-locking and direct external modulation of CW light.

Q-switching and gain switching semiconductor lasers can produce high power pulse (up to 10W peak) and reasonably narrow pulse width (typically in the order of 10ps). Because the carrier density and light intensity in the laser cavity undergo very drastic relaxation during the switching process, the pulse produced is highly chirped. Therefore the pulse quality is poor in terms of bandwidth-pulse width product and pulse timing jitter[1]. The pulse-to-pulse repeatability of pulse parameters such as pulse power, width, shape, etc., is also poor.

External modulation of CW light[2] generally produces the best pulse quality of all methods. This is because most external modulators have very small linewidth enhancement factor [3]compared with semiconductor laser medium. Therefore the phase modulation (or 'chirp') accompanying light intensity modulation is small. However, the method is wasteful in terms of light power because most of the power is 'chopped' out. The peak power of the pulse is in the order of milliwatts.

Mode-locked semiconductor lasers have satisfactory performance in most aspects and therefore received the most attention. Various experimental and theoretical studies have been carried and documented in numerous literature [4]. Semiconductor ring lasers, however, are less studied than other semiconductor laser structures. There have been several scattered reports on the experimental work concerning mode-locked SRLs in other groups[5, 6] as well as in the group[7]. But in general the research is far from systematic. It is

---

[1]Vasil'ev, P. P., 'High-power, high-frequency Picosecond pulse generation by Passively Q-switched 1.55μm diode lasers', IEEE Journal of Quantum Electronics, VOL.29, No.36, June 1993, pp.1687-1692.

[2]Suzuki, M., et al, 'Transform limited optical pulse generation up to 20 GHz repetition rate by a sinusoidally driven InGaAsP electroabsorption modulator', J. of Lightwave Technology, 1993, No.3, pp.48-473.

[3]Henry, C. H., 'Theory of the linewidth of semiconductor-lasers', IEEE J. of Quantum Electronics, Vol.18, No.2, 1982pp.259-264.

[4] To name only a few, the works carried out by Chen, Y. K. et al, e.g.,'Monolithic colliding pulse mode-locked multiple quantum well lasers', Applied Physic Latters, 1991, pp.1253-1255, and Derickson, D. J., et al, e.g., "Short pulse generation using multisegment mode-locked semiconductor lasers," IEEE J-QE, VOL.28, NO. 10, pp.2186-2202, Oct. 1992, and the theoretical work by Haus, et al.

[5] Hohimer, J. P., and Vawter, G. A., 'Passive mode-locking of monolithic semiconductor ring lasers at 86GHz', Applied Physic Letters, 1993, 11, pp.2457-2459.

[6] Hansen, P. B., et al, 'A 1.54-μm monolithic semiconductor ring laser: CW and mode-locked operation', IEEE Photonic Technology Letters, 1992, 5, pp.411-413.

[7] Krauss, T. F., Martins-Filho, J. F., Ironside, C. N., Laybourn, P. J. R., and De La Rue, R. M., 'Mode-locked semiconductor ring lasers with two saturable absorbers', Proceeding of ECIO'95. p.55-58.

necessary to achieve a more comprehensive and systematic understanding of the mode-locking process in SRLs.

5-1 Theory and Computer Modelling of Passively Mode-locked Semiconductor Ring Lasers

5-1-1 The time-domain description of pulse propagation in semiconductor laser medium

The partial differential equation describing the propagation of the light in the gain (or absorptive) medium can be derived from the wave equation as[1]

$$\frac{\partial A}{\partial z}+\frac{1}{v_g}\frac{\partial A}{\partial t}+\frac{i}{2}\beta_2\frac{\partial^2 A}{\partial t^2}=\frac{1}{2}(1-i\alpha)gA-\frac{1}{2}\alpha_i A \qquad \text{Eq. 5-1}$$

where A is the amplitude of the light field and β_2 is the material dispersion parameter. α_i is the material loss co-efficient. The gain coefficient g which contains a dispersive element can be assumed to have a frequency response approximated to the second order as

$$g(\omega)=g(\omega_o)+\frac{1}{2}g''(\omega-\omega_o)^2 \qquad \text{Eq. 5-2}$$

which converts to a time domain operator as

$$g=g_p(1+T_2^2\frac{\partial^2}{\partial t^2}) \qquad \text{Eq. 5-3}$$

where T_2 is the measure of the gain bandwidth of the media and therefore the strength of gain dispersion. Substituting this into Eq.4-1 and ignore the small material dispersion β_2 results in the following equation

$$\frac{\partial A}{\partial z}+\frac{1}{v_g}\frac{\partial A}{\partial t}=\frac{1}{2}(1-i\alpha)g_pA+\frac{1}{2}(1-i\alpha)g_pT_2^2\frac{\partial^2 A}{\partial t^2} \qquad \text{Eq. 5-4}$$

The variation of peak gain coefficient g_p is governed by the gain saturation and recovery behaviour in the semiconductor and is described by

$$\frac{dg}{d\tau}=\frac{g_0-g}{t_c}-\frac{gP}{E_{sat}} \qquad \text{Eq. 5-5}$$

with $P=|A|^2$ the power of the light field.

---

[1]Agrawal, G. P., "Effect of Gain Dispersion on Ultrashort Pulse Amplification in Semiconductor Laser Amplifiers", IEEE J-QE VOL. 27, NO. 6, June 1991, pp.1843-1849.

5-1-2 The Lumped Element Model of Mode-locked Semiconductor Ring Laser

The semiconductor ring laser (SRL) can be configured to operate in the passive or active mode-locked mode. This kind of structure usually includes one or more saturable absorber/modulator section in the ring cavity, as shown in Fig. 1.

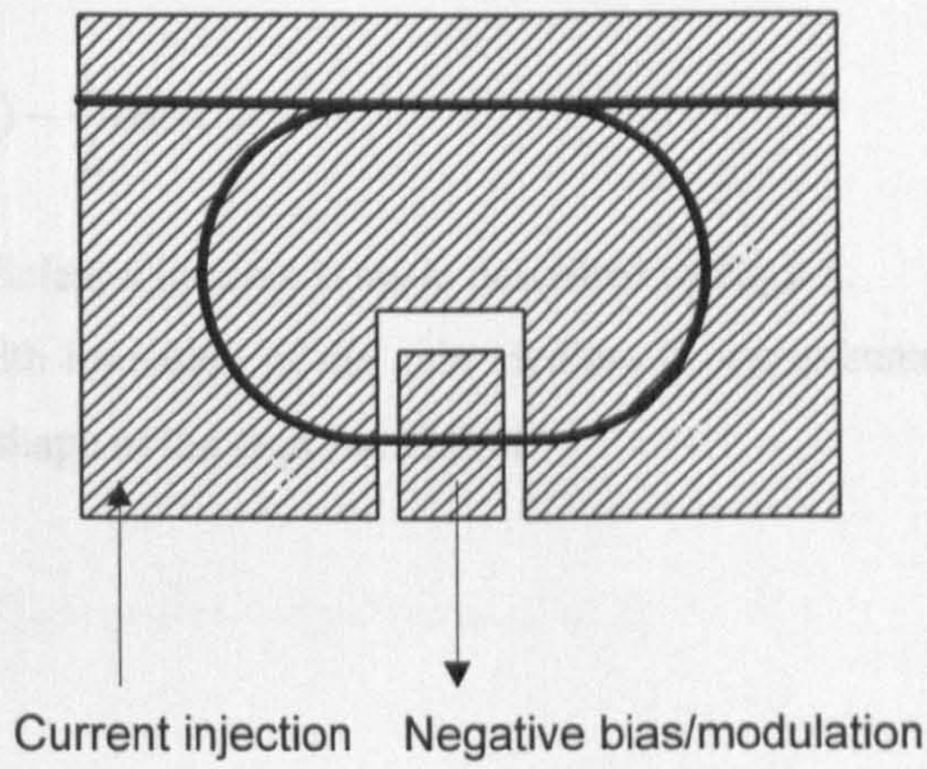

Fig. 5-1 A sketch of mode-locked SRL.

The combined system of gain and absorber/modulator sections can be described in many ways as in numerous literature both in the time/space domain or in the frequency domain. In this work two time domain approaches have been taken to deal with the case of passive mode-locking where saturable absorbers are used.

The first approach, presented in this section, treats the gain section as a nonlinear saturable amplifier with unlimited bandwidth. A system of two coupled ordinary differential equations derived from the propagation equation Eq.5-1 is used to describe the behaviour of light intensity and phase when propagating in such a gain medium [1]. The time derivatives in the propagation equation are removed by transforming the time co-ordinate into one ($\tau=t-z/v_g$) that moves with the light pulse [2], which results in the following equations

$$\frac{\partial P}{\partial z} = (g - \alpha_i) P \qquad \textbf{Eq. 5-6}$$

$$\frac{\partial \Phi}{\partial z} = -\frac{1}{2}\alpha g \qquad \textbf{Eq. 5-7}$$

---

[1] Agrawal, G. P. and N. A. Olsson, "Self-Phase Modulation and Spectral Broadening of Optical Pulses in Semiconductor Laser Amplifiers", IEEE J-QE VOL. 25, NO. 11, Nov. 1989, pp.2297-2306.

[2] Siegman, A. E., "Lasers", Oxford University Press, 1986.

where P is the light intensity, g is the gain coefficient, α_i is the material loss coefficient. Φ is the phase of the light field, α is the linewidth enhancement factor, v_g is the group velocity of the light in the medium. When α_i is much smaller than g, the above equations can be integrated over the length of the gain section so that the gain section can be treated as a lumped amplifier element.

$$P_{out}(\tau) = P_{in}(\tau)\exp[h(\tau)] \qquad \textbf{Eq. 5-8}$$

$$\Phi_{out}(\tau) = \Phi_{in}(\tau) - \frac{1}{2}\alpha h(\tau) \qquad \textbf{Eq. 5-9}$$

The change of the gain coefficient with time is again described by Eq.5-5.

The dispersion and bandwidth limitation of the gain medium is approximated by a filter synthesised to simulate the Lorentzian lineshape of the gain coefficient

$$g(\omega) = \frac{1}{1 + j\frac{\omega}{\omega_o}} \qquad \textbf{Eq. 5-10}$$

and

$$A_{out}(\omega) = A_{in}(\omega) \times \exp[g(\omega)L_g] \qquad \textbf{Eq. 5-11}$$

where L_g is the length of the gain section and $A_{in,out}(\omega) = \mathcal{F}\{A_{in,out}(\tau)\}$ $= \mathcal{F}\{\sqrt{P_{in,out}(\tau)}\exp(j\Phi_{in,out})\}$ are the Fourier transform of the input and output pulse electric field envelopes, respectively. ω_o is the bandwidth of the gain lineshape. The filter consists of a second order low-pass filter

$$H(\omega) = \frac{1}{b_0 + b_1\omega + b_2\omega^2}$$

and a direct feed-through so the transfer function is approximated by $1+H(\omega)$. The coefficients in the denominator of $H(\omega)$ are determined by a fit in a least square root error sense.

The saturable absorber is treated in a similar way to the amplifier except that the gain coefficient now takes a negative value and the recovery time is different from that of the amplifier. The saturable absorber is also assumed to have unlimited bandwidth and no dispersion .

The resulting model is solved by MATLAB's Simulink Toolbox. Fig. 5-2 is a simplified model diagram based on these equations.

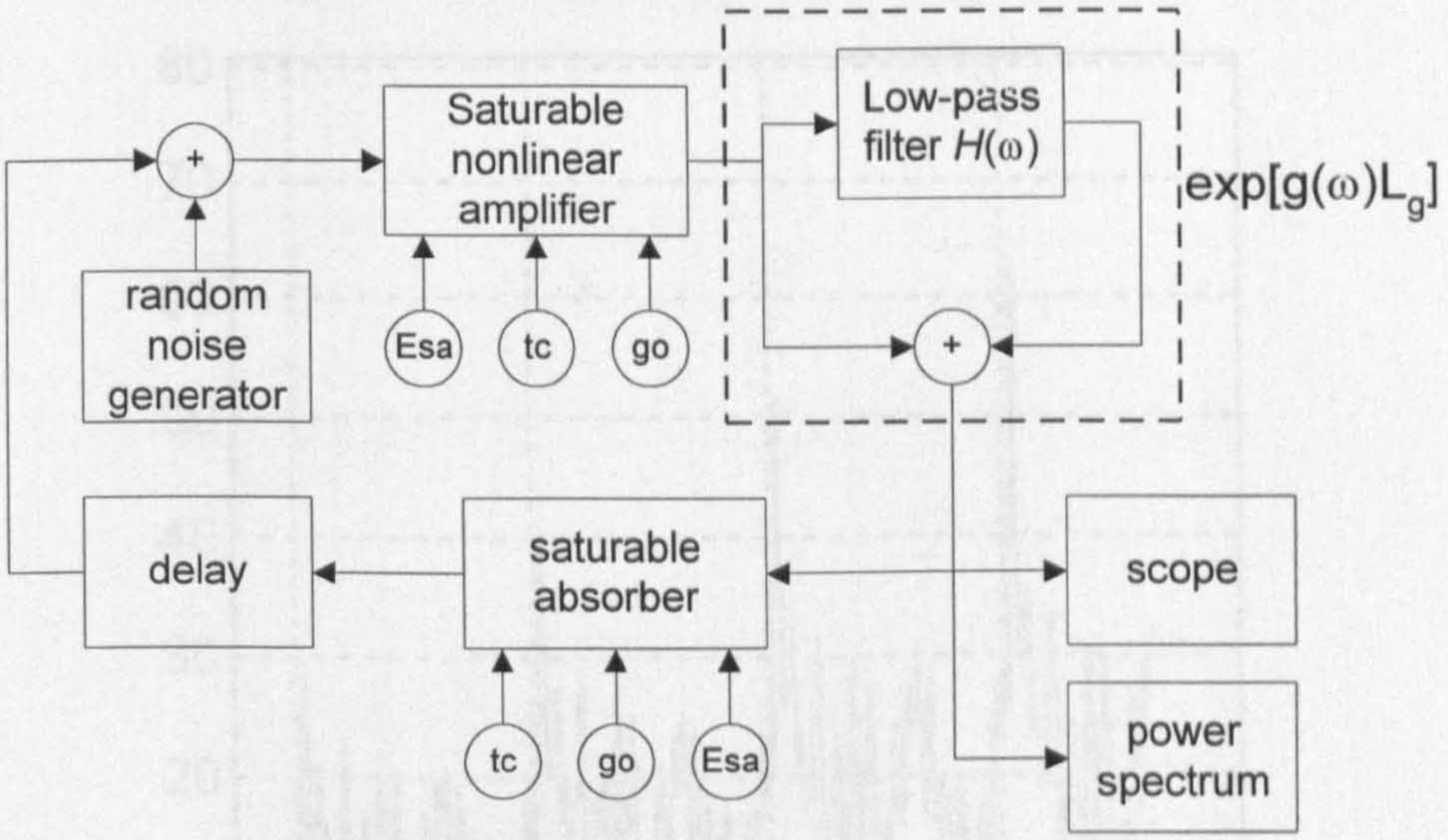

Fig. 5-2 Diagram of the lumped element model.

Results.

Fig. 3 shows an example of the pulse building-up process in the mode-locked SRL. The parameters used in the model are summarised in table.1. All the time parameters are normalised to the round trip (delay) time which is 1. All the energy and power values are normalised to the saturation energy E_{sat} of the gain media which is 10.

parameters	description	value
E_{sat}	Saturation energy	10 for gain, 2.5 for absorber
t_c	recovery time	0.6 for gain, 0.1 for absorber
G_o	unsaturated transmission	exp(4) for amplifier, exp(-3) for absorber
α_i	loss in the cavity	exp(-1)
ω_o	bandwidth of the Lorentzian lineshape g(ω)	200π

Table 5-1 The normalised parameters used in the model of Fig. 5-2.

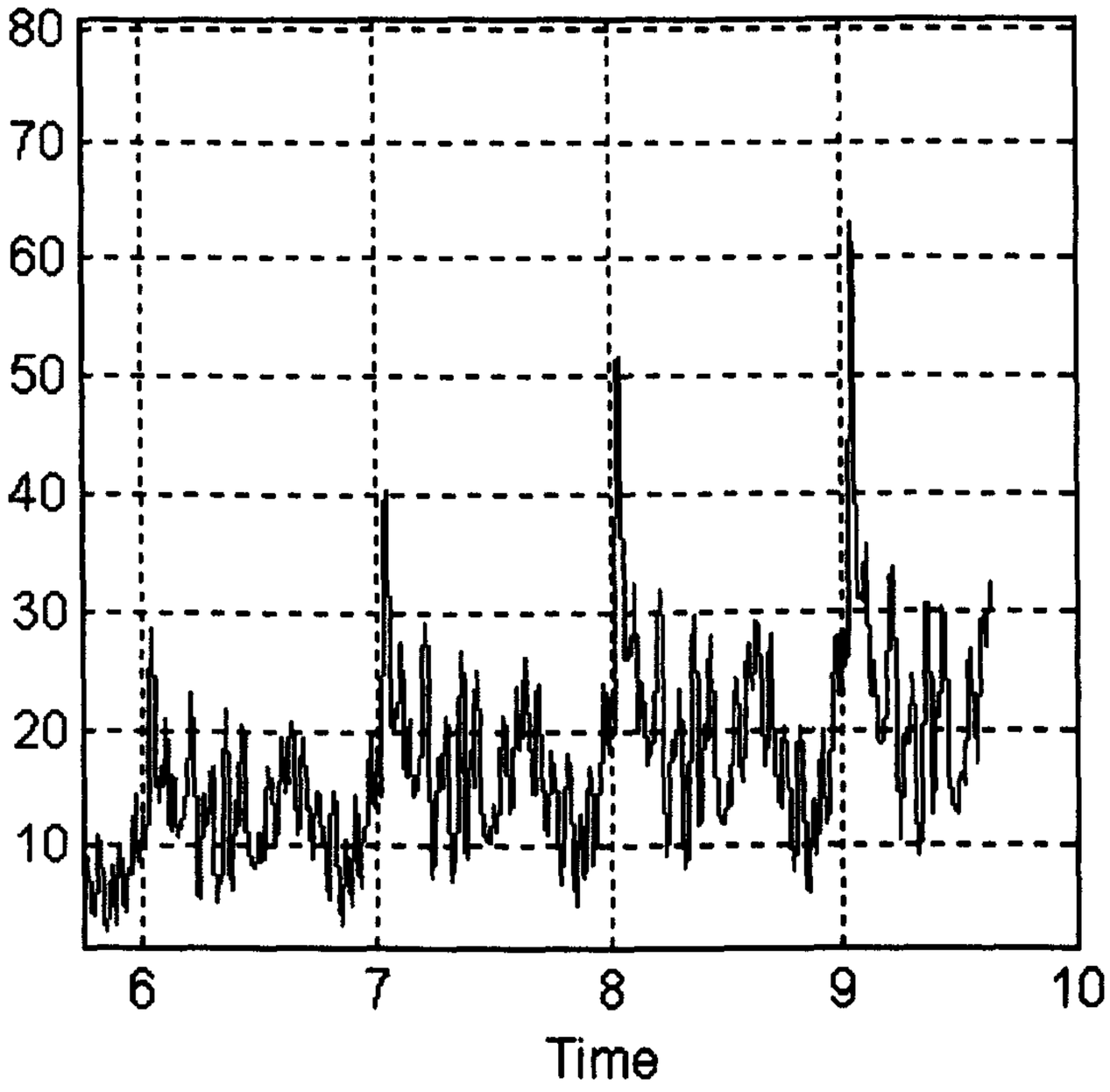

Fig. 5-3 Development of mode-locked pulse from spontaneous emission noise.

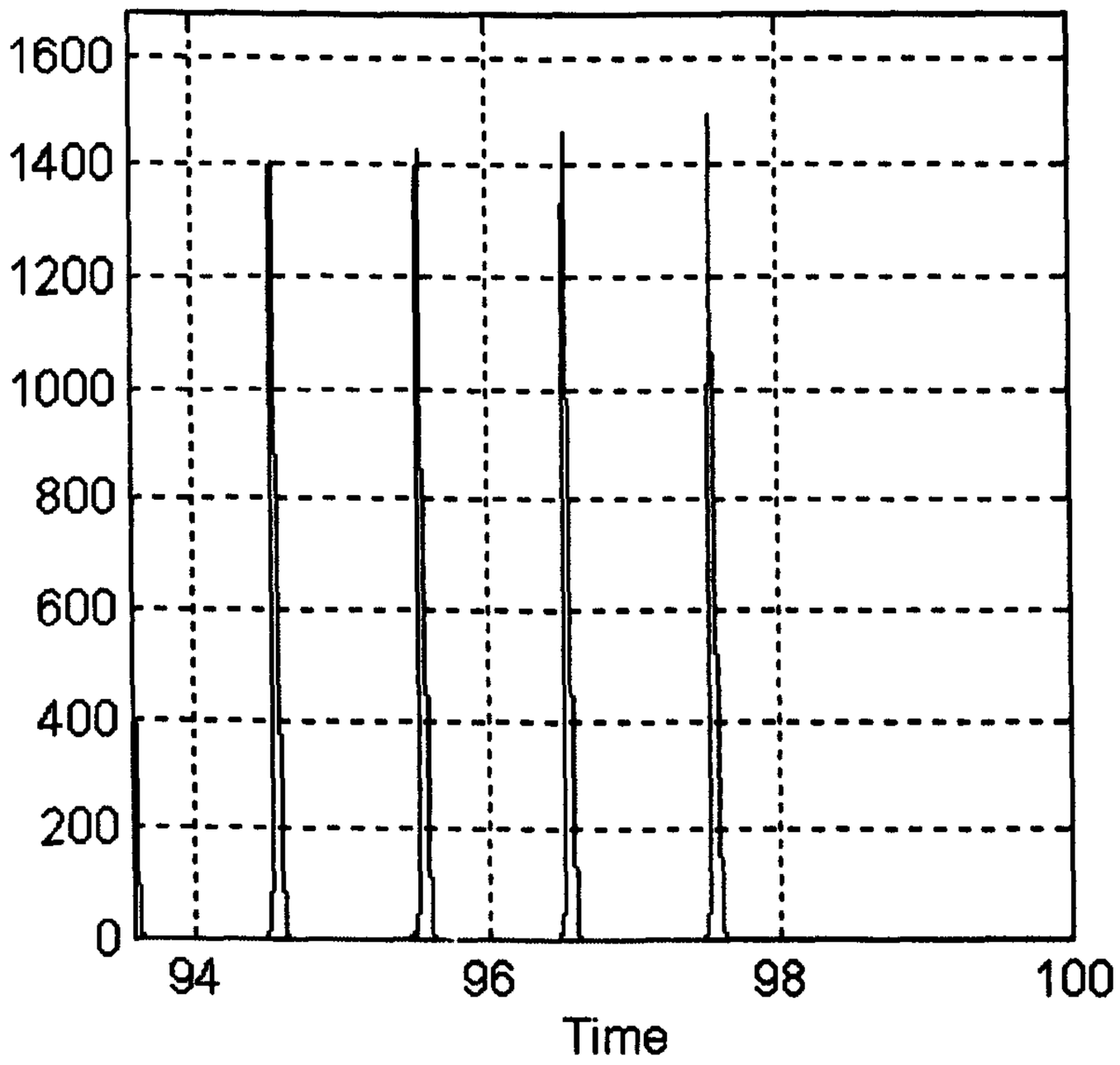

(a)

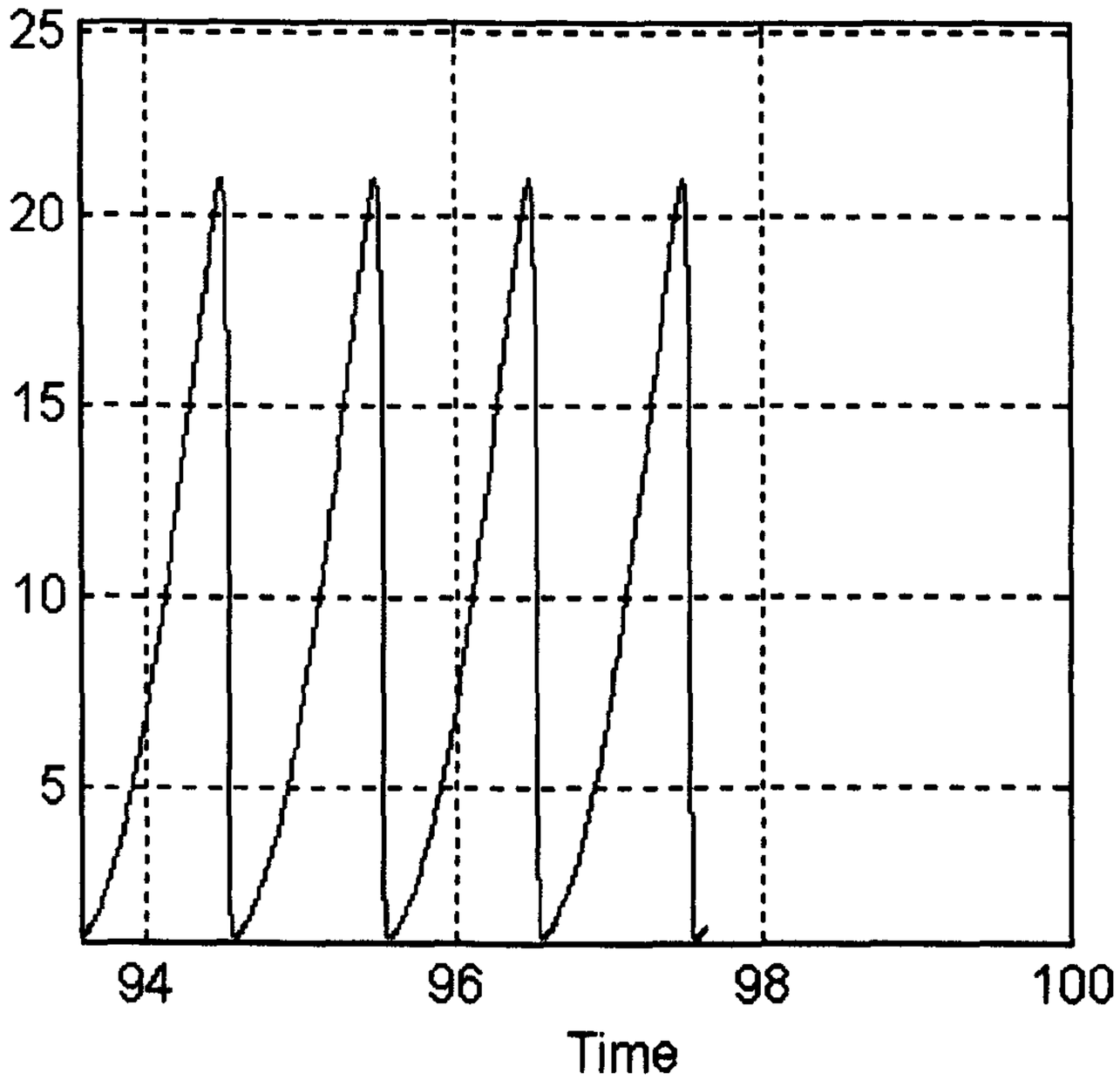

(b)

Fig. 5-4 The mode-locked pulse (a) and gain recovery process (b) calculated by the lumped element model.

Fig. 5-3 shows the building-up process of the pulse from noise after the system is turned on at time 0. Fig. 5-4(a) shows the steady-state pulse train and (b) the depletion and recovery process of the amplifier gain. It is clearly demonstrated that the gain is saturated by the pulse and recovers, after the pulse, to a intermediate value.

The mode-locking condition

Whether mode-lock happens and stabilises depends on the interplay of several parameters, i.e., the unsaturated gain g_0 and absorption α_0 of the amplifier and absorber sections (which are determined by the injection current and reverse bias voltage of respective sections) and their recovery times, which are again dependent on the injection and reverse bias. The bandwidth (or dispersion) of the system also plays an important role in the mode-locking process.

The advantage of the lumped element model is that it allows analytical results to be obtained after introducing certain approximations. Haus [1,2] has used this approach to give some very revealing results.

---

[1] Haus, H. A., 'Theory of mode-locking with a slow saturable absorber', IEEE J. of Quantum Electronics, VOL.11, No.9, 1975, pp.736-746.

[2] Haus, H. A., 'Theory of mode-locking with a fast absorber', J. of Applied Physics, VOL.64, No.7, 1975, pp.3049-3058.

Based on the same lumped element model, Koumans and Van Roijen[1] have discussed comprehensively the stable mode-locking conditions of semiconductor lasers with both the ring cavity and the linear cavities, including the influence of gain dispersion and self-phase modulation. The stable mode-locking area has been charted on the normalised unsaturated gain vs. normalised unsaturated absorption plane for different dispersion, linewidth enhancement factor and gain/absorption relaxation time constants. An example is shown in Fig. 5-5 [2].

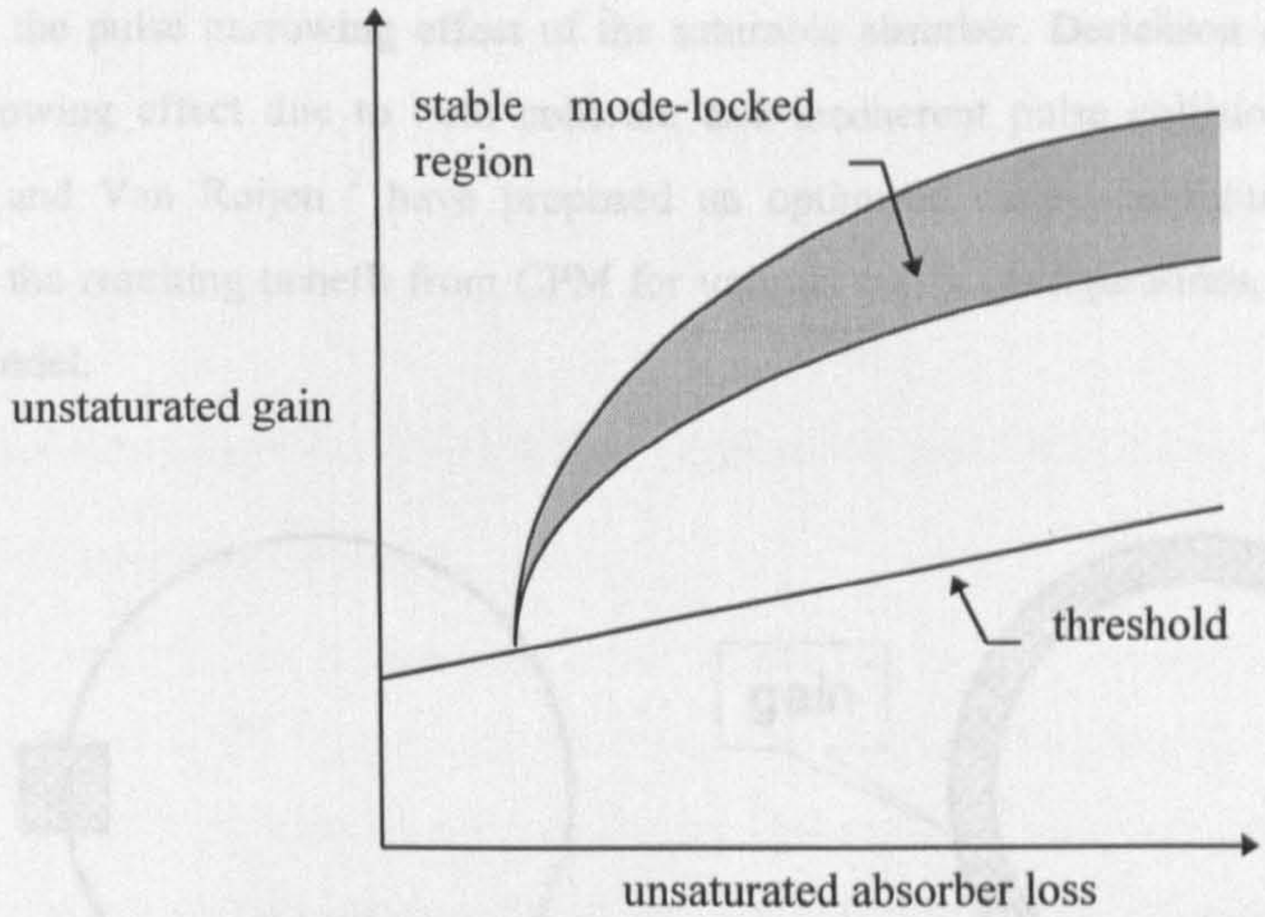

Fig. 5-5 The stable mode-locked region of uni-directional SRL predicted by lumped element model.

The results of the above mentioned studies are limited in two senses. Firstly, the lumped element model, which results from the moving time coordinate transformation, can only treat *unidirectional* propagation problems. All the conclusions therefore apply only to that situation. Secondly, although wide value ranges of the main internal parameters (of gain section: initial gain, gain saturation energy, gain relaxation time constant, linewidth enhancement factor, and gain bandwidth, of absorber section: initial absorption, absorption saturation energy, absorption relaxation or recovery time constant) involved in mode-locking mechanism are discussed, in fact there are only four external parameters that can be varied in designing a real device, i.e., the lengths of gain and absorber sections, the injection current of the gain section and the reverse bias voltage of the absorber. Many parameters are related to each other. For example, the recovery time and the initial absorption of the absorber both depend on its reverse bias voltage. The gain and gain relaxation time constant are determined by the carrier density in the gain section which in turn is determined by the injection current density. There exists a possibility that for a particular laser material, the stable mode-locking values of the internal parameters cannot be satisfied simultaneously in some or all external parameter value ranges. The stable mode-locking area in terms of

---

[1]Koumans, R. G. M. and Van Roijen, R., 'Theory for passive mode-locking in Semiconductor laser structures including the effect of self-phase modulation, dispersion, and pulse collisions', IEEE J-QE, VOL.32, NO.3, March 1996, pp.478-492.

the external parameters will then be fragmented or even non-existent. Therefore from a practical point of view it would be necessary that, instead of being able to predict the mode-locked region in a normalised internal parameter space, the behaviour of a given mode-locked laser structure can be predicted in real external parameter space, i.e., for specific injection current and reverse bias voltage.

CPM and cavity configuration

The colliding pulse mode-locking (CPM) scheme has also received much discussion for its advantage of enhancing the pulse narrowing effect of the saturable absorber. Derickson *et. al.* [1] have calculated the pulse narrowing effect due to both coherent and incoherent pulse collisions in a saturable absorber. Koumans and Van Roijen [2] have proposed an optimised cavity configuration for a ring laser and calculated the resulting benefit from CPM for various cavity configurations, again based on the lumped element model.

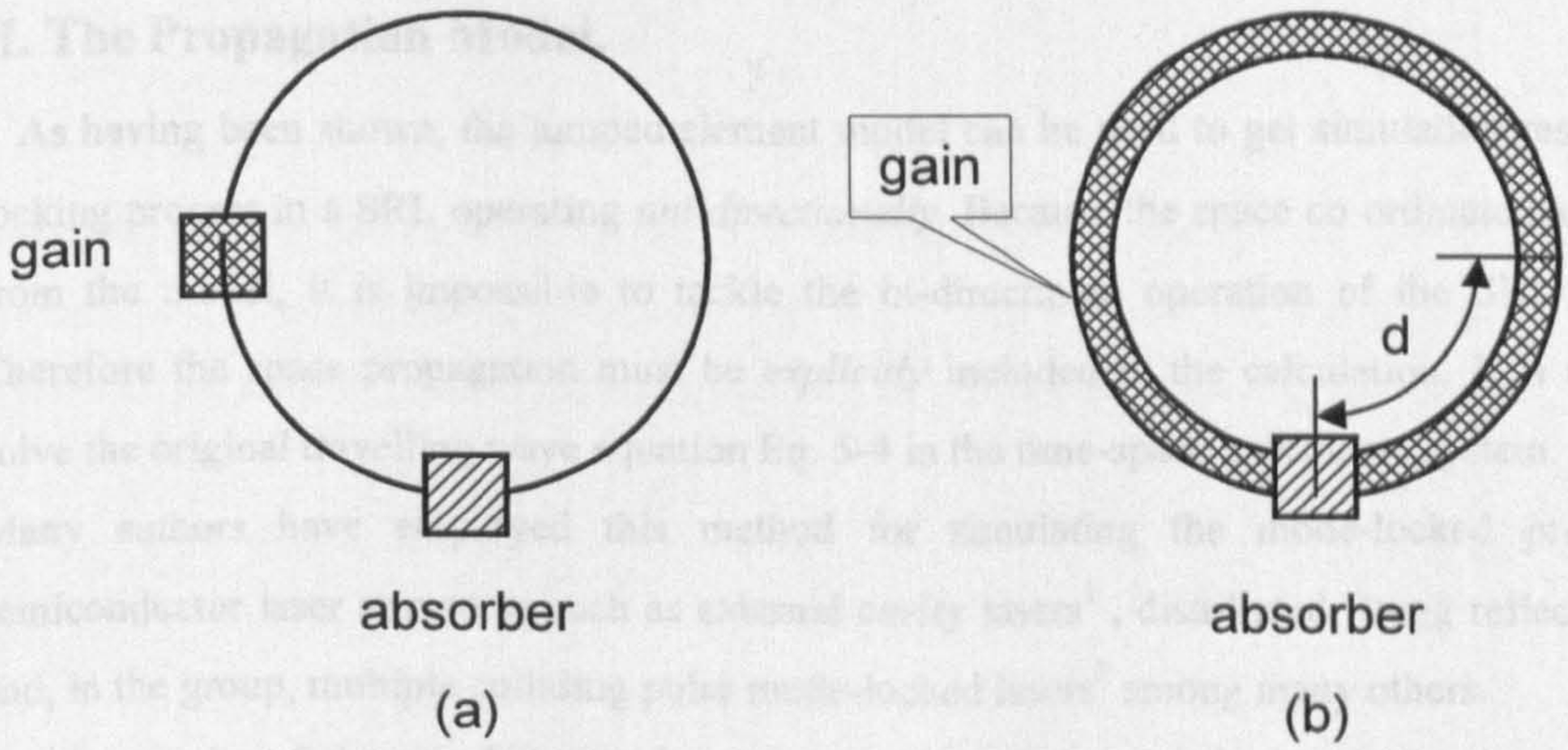

Fig. 5-6 (a)The optimised lumped element ring cavity configuration which take advantage of CPM and avoids pulse collision in the gain section which broadens the pulses. (b)A usual ring cavity with distributed gain section.

While these calculations for the colliding pulse (CP) effect are correct because they are based on the formation of a transient grating due to interference between the waves travelling in the opposite directions, the idea of displacing the gain element from where the pulses will collide again (they will collide once in the absorber because this gives the largest round-trip gain for both pulses) is not possible if the whole cavity length with the exception of the absorber is pumped. Even if a passive section is

---

[1] Derickson, D. J., Helkey, R. J., Mar, A., Karin, J. R., Wasserbauer, J. G., and Bowers, J. E., "Short pulse generation using multisegment mode-locked semiconductor lasers," IEEE J-QE, VOL.28, NO. 10, pp.2186-2202, Oct. 1992.

[2]Koumans, R. G. M. and Van Roijen, R., 'Theory for passive mode-locking in Semiconductor laser structures including the effect of self-phase modulation, dispersion, and pulse collisions', IEEE J-QE, VOL.32, NO.3, March 1996, pp.478-492.

introduced for this purpose, the gain section now experiences a saturation process that is more complicated. Unlike the unidirectional case, at different points in the gain section, the time interval between the arrival of consecutive pulses now is different. This time interval can be calculated by

$$\delta T = \begin{cases} v_g \cdot (L - 2d) & \text{when} \quad d \geq L/4 \\ v_g \cdot 2d & \qquad\quad d \leq L/4 \end{cases}$$

where L is the cavity length and d is the distance of the point from the centre of the absorber. δT ranges from 0 to $v_g L/2$ or half the round-trip time, while in the unidirectional case it always equals the round-trip time. So even if the pulses do not collide in the gain section, they will still influence each other's propagation in the gain section by causing additional gain saturation to that existing in a unidirectional ring cavity. The benefit of CPM therefore is still partly negated.

5-1-3 The Propagation Model and Bi-directional Operation

II. The Propagation Model.

As having been shown, the lumped element model can be used to get simulation results of the mode-locking process in a SRL operating *uni-directionally*. Because the space co-ordinate has been eliminated from the model, it is impossible to tackle the bi-directional operation of the SRL with this model. Therefore the space propagation must be *explicitly* included in the calculation. It is then necessary to solve the original travelling wave equation Eq. 5-4 in the time-space coordinate system.

Many authors have employed this method for simulating the mode-locked process in various semiconductor laser structures such as external cavity lasers[1] , distributed Bragg reflector (DBR) lasers[2] and, in the group, multiple colliding pulse mode-locked lasers[3] among many others.

For the results of the simulation to be representative of the real device situation, material and device parameters must be incorporated into the calculation. The gain rate equation of Eq. 5-5, however, is derived by using a linear approximation of the gain-carrier density relation and is particularly inaccurate for quantum-well structures. Therefore instead of using Eq. 5-5 the carrier density rate equation in the QW

---

[1] Schell, M., et al, 'Chirp and stability of mode-locked Semiconductor lasers', IEEE Journal of Quantum Electronics, VOL.32, No.7, July 1996, pp.1180-1190.

[2] Zhu, B., White, I. H., Penty R. V., Wonfor, A., Lach, E. and Summers H. D., 'Theoretical analysis of timing jitter in monolithic multisection mode-locked DBR laser diodes', IEEE J. Quantum Electronics, VOL.33 NO.7, July 1997, to be published.

[3] Martins-Filho, J. F., Avrutin, E. A., Ironside, C. N., Roberts, J. S., 'Monolithic multiple colliding pulse mode-locked quantum-well lasers-experiment and theory',IEEE J. of Selected Topics in Quantum Electronics, 1995, VOL.1, NO.2, pp.539-551.

$$\frac{dn}{dt} = \frac{\eta_i J}{n_{qw} d_{qw} e} - \frac{n}{\tau_c(n)} - g(n)|A|^2 \qquad \textbf{Eq. 5-12}$$

is used. n_{qw} is the number of quantum-wells in the laser material, d_{qw} is their thickness, e is the electron charge, η_i is the internal quantum efficiency and J is the injected current density. The travelling wave equation Eq.5-4 is re-written in the following form

$$\frac{\partial A}{\partial z} + \frac{1}{v_g}\frac{\partial A}{\partial t} = \frac{1}{2}(1 - i\alpha) n_{qw} \Gamma_{qw} g(n) A + \frac{1}{2}(1 - i\alpha) n_{qw} \Gamma_{qw} g(n) T_2^2 \frac{\partial^2 A}{\partial t^2} \qquad \textbf{Eq. 5-13}$$

where Γ_{qw} is the optical confinement factor of each quantum-well. By definition $|A|^2$ will have the unit of $cm^{-2}s^{-1}$, which means that it represents the photon flux density in the laser waveguide.

The gain relaxation time constant τ_c is determined by the total carrier recombination rate in the QW and has the following relationship with the carrier concentration n in the QW

$$\tau_c = \frac{1}{A + Bn + Cn^2} \qquad \textbf{Eq. 5-14}$$

where the terms in the denominator stand for the non-radiative, the spontaneous radiative and the Auger recombinations in that order, respectively. Use Eq. 5-14 in Eq. 5-12, the steady-state carrier density of the active section at a particular injection current can be calculated by solving the equation

$$Cn^3 + Bn^2 + An - \frac{\eta_i J}{n_{qw} e d_{qw}} = 0 \qquad \textbf{Eq. 5-15}$$

Determination of Gain Section Parameters

The following procedure is used in determining gain section parameters from experimentally characterised data.

First of all, device geometry is defined. The circumference of the ring cavity, the positions (with respect to the output coupler) and lengths of the gain, passive (if any) and absorber sections L_g, L_p and L_a are defined. The output coupler is assumed to be located at a certain point in the ring rather than a distributed component. The power feedback/coupling ratio F is represented by a fixed attenuator.

For the gain section, the QW material parameters g_o and J_o combined with its geometry can be used to determine its steady-state (initial) gain coefficient g at certain injection current I according to

$$\frac{g}{g_o} = \ln\left(\frac{J}{J_0}\right) \qquad \textbf{Eq. 5-16}$$

J is the injected current density

$$J = \frac{I}{n_{qw} W L_G} \qquad \text{Eq. 5-17}$$

where W is the width of the waveguide and $L_G=\Sigma L_g$ the total length of the active sections. Here a gain expression different from that used in Chapter 2 is employed. The value of g_0 and J_0, however, can still be calculated from the characterised data. Typical values for the MBE materials used (e.g., B680) are $g_0=620\text{cm}^{-1}$ and $J_0=100\text{A/cm}^2$. Substituting equations 5-15 into 5-16 gives

$$g = g_o \ln\left(\frac{An + Bn^2 + Cn^3}{An_o + Bn_o^2 + Cn_o^3}\right) \qquad \text{Eq. 5-18}$$

Where n_o is the carrier density corresponding to the gain value of g_0 and injection current density of J_o

$$Cn_o^3 + Bn_o^2 + An_o - \frac{\eta_i J_0}{n_{qw} e d_{qw}} = 0 \qquad \text{Eq. 5-19}$$

The saturation energy as inversely proportional to dg/dn is inherently defined by Eq. 5-18.

Determination of Absorber Section Parameters

For the absorber section, the initial absorption coefficient as a function of reverse bias voltage V_b can be found from the measured absorption data described in Chapter 6. Ideally the absorption saturation energy and the recovery time constant of the absorber should be determined by pump-and-probe measurements. However, because the unavailability of the experiment, other ways must be find to define these parameters.

The recovery time is often assumed to be determined by the thermionic emission and tunnelling escaping of the carriers from the QW into the barrier. However, the calculated recovery time due to these effects from a $GaAs/Al_{0.2}Ga_{0.8}As$ quantum well structure under reasonable reverse bias electric field is about 1-10ps which is in clear contradictory to available experimental results [1, 2]. It is therefore necessary to take into consideration the transient electric field screening effects caused by the electric charge induced by the optically generated carriers which transport through the intrinsic layer towards the doped regions. This screening effect reduces the electric field in the QW and results in a reduced absorption coefficient through quantum-confined Stark effect (QCSE). The reduced absorption will hold until the carriers begin to arrive at the doped region. Therefore the transport time will dominate the recovery of the absorption after the original fast relaxation of carriers out of the QW. The time will then be strongly dependent on

---

[1] Bradley, P. J., Rigo, C., and Stano, A., "Carrier Induced Trasient Electric Fields in a p-i-n InP-InGaAS Multiple-Quantum-Well Modulator", IEEE J. QE, VOL.32, NO.1, Jan. 1996, pp.43-52.

[2] Brovelli, L. R., Hugi, J., Jackel, H., and Melchior, H., "Optical pulse mixing measurement of carrier lifetime and absorption recovery time in reverse-biased GaAs/AlGaAs single quantum well laser structures", J. Applied Physics, VOL.76 (12), Dec. 1994, pp.7713-7719.

the structure of the material and its doping profile, as well as the applied reverse bias voltage. The most reliable way to determine the recovery time is again by experiment. Here the result from Karin *et. al.* [1]

$$\tau_c = 86 \cdot \exp[-(V_{bias} + V_{bi}) / 2.1] \text{ (ps)} \qquad \textbf{Eq. 5-20}$$

is used because the device structure used in there is quite similar to the structure used in this work.

The absorption coefficient is related to the carrier density by [2]

$$\alpha = \alpha_0 - \sigma n \qquad \textbf{Eq. 5-21}$$

where α_0 is the unsaturated absorption coefficient. The value of the absorption cross-section σ, which determines the saturation energy, varies from 1-7X10^{-14} cm^2 depending on wavelength and reverse bias voltage. This is the only parameter that is left free in the model.

Algorithm

The travelling wave equation Eq. 5-13 is a non-linear partial differential equation (PDE) essentially of the hyperbolic type. It is solved using the centred difference scheme where the partial derivatives are approximated by the following finite differences

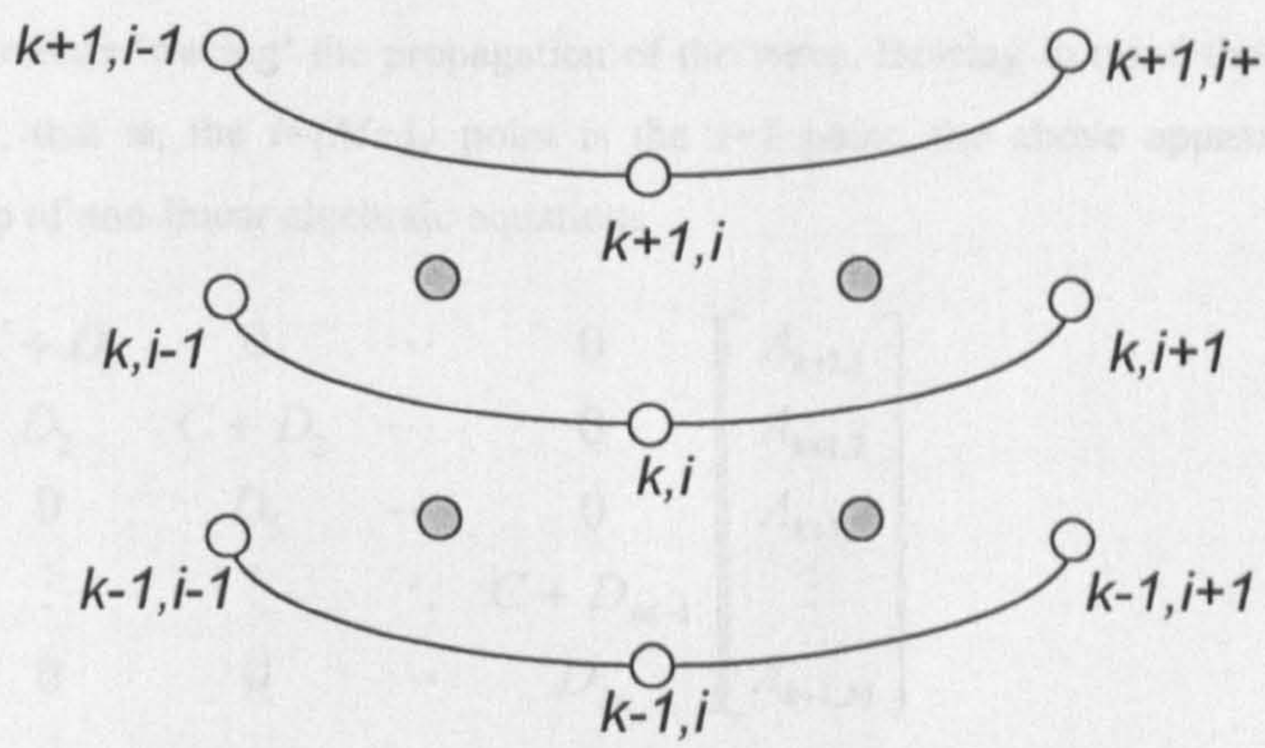

Fig. 5-7 The nomenclature of the algorithm.

$$\frac{\partial A}{\partial z} = \frac{1}{2}\left(\frac{A_{k+1,i+1} - A_{k+1,i}}{\Delta z} + \frac{A_{k,i+1} - A_{k,i}}{\Delta z}\right) \qquad \textbf{Eq. 5-22}$$

---

[1] Karin, J. R., Helkey, R. J., Derickson, D. J., Nagarajan, R., Allin, D. S., Bowers, J. E., and Thornton, R. L., "Ultrafast dynamics in field-enhanced saturable absorbers", Applied Physics Letters, Vol.64 (6), Feb. 1994, pp.676-678.

[2] Schmitt-Rink, S., *et al,* 'Linear and non-linear optical properties of semiconductor quantum wells', Advances in Physics, 1989, VOL.12, No.2, pp.89-188.

$$\frac{\partial A}{\partial t} = \frac{1}{2}\left(\frac{A_{k+1,i+1} - A_{k,i+1}}{\Delta t} + \frac{A_{k+1,i} - A_{k,i}}{\Delta t}\right) \qquad \textbf{Eq. 5-23}$$

$$\frac{\partial^2 A}{\partial t^2} = \frac{1}{2}\left(\frac{A_{k+1,i+1} - 2A_{k,i+1} + A_{k-1,i+1}}{\Delta t^2}\frac{A_{k-1,i+1}}{} + \frac{A_{k+1,i} - 2A_{k,i} + A_{k-1,i}}{\Delta t^2}\right) \qquad \textbf{Eq. 5-24}$$

Where Δz is the space step size and Δt is the time step size. The subscript $k=1,2,\ldots$ denotes the discrete time level and $i=1,2,\ldots,M$ denotes the discrete space points. $\mathrm{M} = \dfrac{(\mathrm{L_G} + \mathrm{L_p} + \mathrm{L_a})}{\Delta \mathrm{Z}}$ is the number of slices that the cavity is divided into. The nomenclature is shown in Fig. 5-7.

The first order derivatives are centred at the half time level, half space step point $(k+\frac{1}{2}, i+\frac{1}{2})$ which is denoted by the filled circle. The second order derivative is centred at the point $(k, i+\frac{1}{2})$.

The centred difference method is stable at any ratio between Δz and Δt. However it is proved that [1] using step sizes related by $\Delta z = v_g \Delta t$ gives the smallest truncation error and the simplest form of algebraic equations to solve when the amplification (zero order) and the dispersion (second order) terms are small. Physically this means 'tracing' the propagation of the wave. Bearing in mind the boundary condition of the ring cavity, that is, the $i=(M+1)$ point is the $i=1$ point, the above approximation results in the following group of non-linear algebraic equations

$$\begin{bmatrix} D_1 & C+D_1 & 0 & \cdots & 0 \\ 0 & D_2 & C+D_2 & \cdots & 0 \\ 0 & 0 & D_3 & \cdots & 0 \\ \vdots & \vdots & \vdots & \ddots & C+D_{M-1} \\ C+D_M & 0 & 0 & \cdots & D_M \end{bmatrix} \begin{bmatrix} A_{k+1,1} \\ A_{k+1,2} \\ A_{k+1,3} \\ \vdots \\ A_{k+1,M} \end{bmatrix}$$

$$= \begin{bmatrix} C+G_1+2D_1 & 2D_1 & 0 & \cdots & 0 \\ 0 & C+G_2+2D_2 & 2D_2 & \cdots & 0 \\ 0 & 0 & C+G_3+2D_3 & \cdots & 0 \\ \vdots & \vdots & \vdots & \ddots & 2D_{M-1} \\ 2D_M & 0 & 0 & \cdots & C+G_M+2D_M \end{bmatrix} \begin{bmatrix} A_{k,1} \\ A_{k,2} \\ A_{k,3} \\ \vdots \\ A_{k,M} \end{bmatrix}$$

$$- \begin{bmatrix} D_1 & D_1 & 0 & \cdots & 0 \\ 0 & D_2 & D_2 & \cdots & 0 \\ 0 & 0 & D_3 & \cdots & 0 \\ \vdots & \vdots & \vdots & \ddots & \vdots \\ D_M & 0 & 0 & \cdots & D_M \end{bmatrix} \begin{bmatrix} A_{k-1,1} \\ A_{k-1,2} \\ A_{k-1,3} \\ \vdots \\ A_{k-1,M} \end{bmatrix} \qquad \textbf{Eq. 5-25}$$

[1] Mitchell, A.R. 'Computational methods in partial differential equations', London : Wiley, 1969.

where

$$C = (\frac{1}{\Delta z} + \frac{1}{v_g \Delta t}) \qquad \textbf{Eq. 5-26}$$

$$D_i = -\frac{(1 - i\alpha)T_2^2}{2(\Delta t)^2} n_{qw} \Gamma_{qw} g_i \qquad \textbf{Eq. 5-27}$$

$$G_i = [(1 - i\alpha) n_{qw} \Gamma_{qw} g_i - \alpha_{in}] \qquad \textbf{Eq. 5-28}$$

Here α_{in} is used instead of α_i for the material loss coefficient to avoid confusion.

Similar equations can be established for the light travelling in the *-z* direction. The only differences are that the position of the *i*th and the *(i+1)*th point in the space derivative equation Eq. 5-22 should be swapped.

For obvious physical and algorithmic reasons, the grid point set for the carrier density *n* is chosen at the $(k + \frac{1}{2}, i + \frac{1}{2})$ point so that it represents the carrier density in a gain slice which locates between the field grid point *i* and *i*+1 at the time the light travelled half its length. Hence the field points $A_{k,l}$ and $A_{k+1,i+1}$ are the input and output of the slice. The forward finite difference equation for the carrier density in the gain section is

$$n_{k+1} = n_k + dt(\frac{J}{n_{qw} e d_{qw}} - \frac{n_k}{\tau_c(n_k)} - \frac{1}{2} g \left| A_{k,i}^{+} + A_{k,i+1}^{+} + A_{k,i}^{-} + A_{k,i+1}^{-} \right|^2) \qquad \textbf{Eq. 5-29}$$

where the + and - superscripts stand for waves propagating along +z and -z directions, respectively. For the absorber section, Eq. 5-21 is substituted into the carrier density rate equation to get equation for α itself, i.e., the same form as in Eq. 5-5

$$\frac{d\alpha}{d\tau} = \frac{\alpha_0 - \alpha}{\tau_c} - \alpha\sigma |A|^2 \qquad \textbf{Eq. 5-30}$$

Backward finite difference must used to approximate this equation in order for the algorithm to be stable when non-linearity is present. The resulting equation is

$$\alpha_{k+1} = \frac{\alpha_k + \frac{\alpha_0 \Delta t}{\tau_c}}{1 + \frac{\Delta t}{\tau_c} + \frac{1}{2}\sigma\Delta t \left| A_{k,i}^{+} + A_{k,i+1}^{+} + A_{k,i}^{-} + A_{k,i+1}^{-} \right|^2} \qquad \textbf{Eq. 5-31}$$

Iteration is used to deal with the non-linearity of the equations. A trial value for field amplitude $A_{k+1}^{(0)}$ is first calculated using old values of A_k, $g(n_k)$ and α_k. The value is then averaged with the old value A_k and the average value is used to determined the new values of n_{k+1}, $g(n_{k+1})$ and α_{k+1}. These in turn are averaged with their old values to calculated the new value of $A_{k+1}^{(1)}$. The process goes on until the

consecutive values of $A_{k+1}^{(j)}$ and $A_{k+1}^{(j+1)}$ are close enough. Usually the iteration converges in about 2-3 circles.

Eq. 5-25 only has non-zero values in its diagonal and first upper-diagonal terms so can be considered sparse when the number of sections M is large. It pays off in terms of memory size and speed to employ sparse matrix techniques to store and handle the matrices. The same applies to the equation's -z direction counterpart. For M =55 the sparse algorithm in average uses only one third the calculation time of its full matrix rival.

Operation Modes and Stable mode-locking Region of Mode-locked SRLs

The computer model is used to simulate the operation of the following SRL configurations.

1) The symmetric configuration in which the saturable absorber is situated 180° from the output coupler[Fig. 5-8(a)].
2) The asymmetric configuration in which the saturable absorber is situated 90° from the output coupler [Fig. 5-8(b)].
3) The dual saturable absorber configuration in which the saturable absorbers are situated +90° and -90° respectively from the output coupler [Fig. 5-8(c)].

The symmetric configuration is an important test case for the algorithm. As a result of symmetry the output waveforms associated with the two counter-propagating modes are expected to be identical, which can be used to check the convergence of the algorithm. In order to start the laser, non-zero initial light

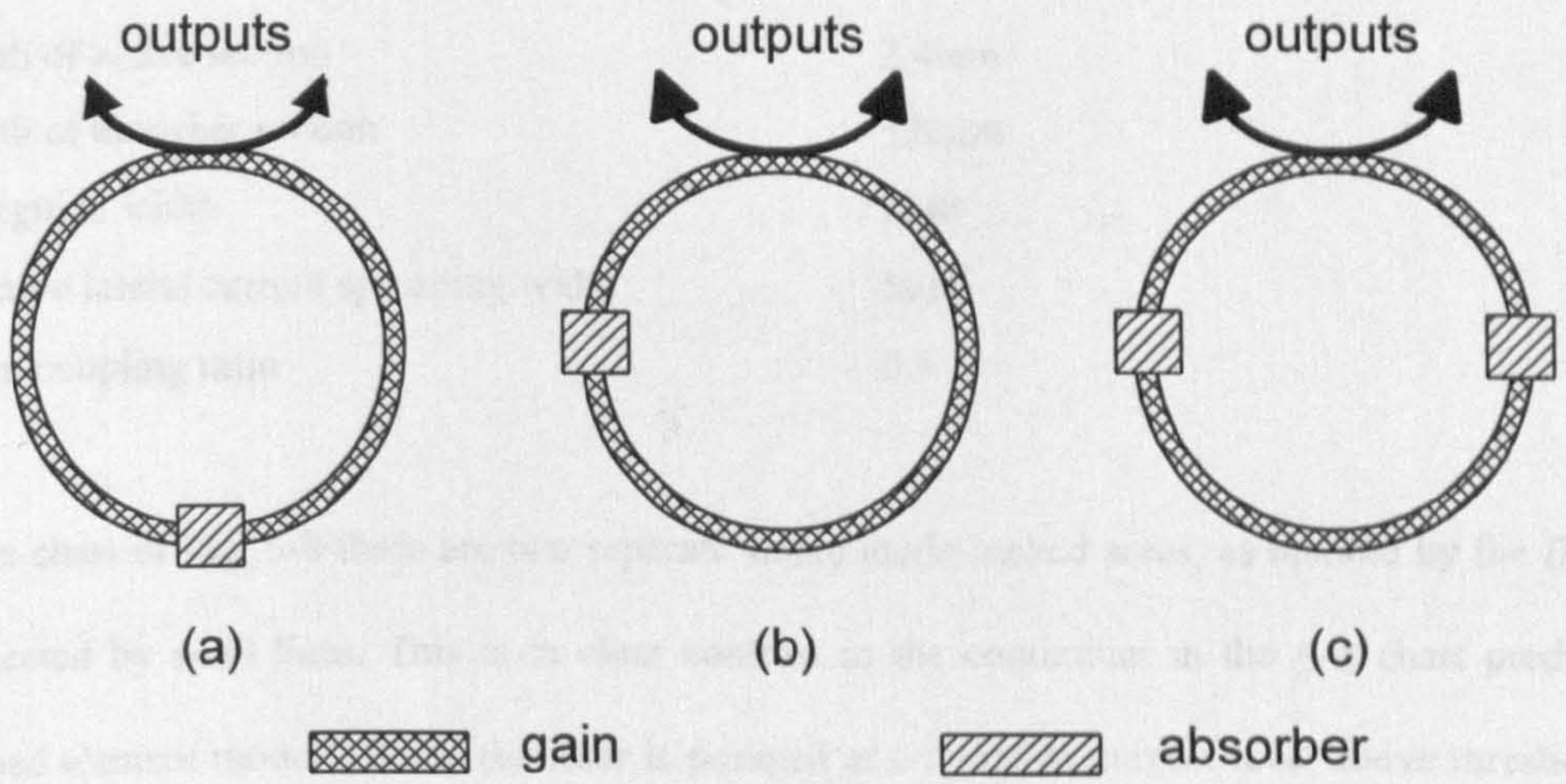

Fig. 5-8 Mode-locked SRL with (a) symmetric configuration, (b)asymmetrically placed saturable absorber and (b) two saturable absorbers.

distribution (initial condition) is needed. With whatever random initial conditions for both directions, the solutions should converge to two identical output pulse trains from the two outputs.

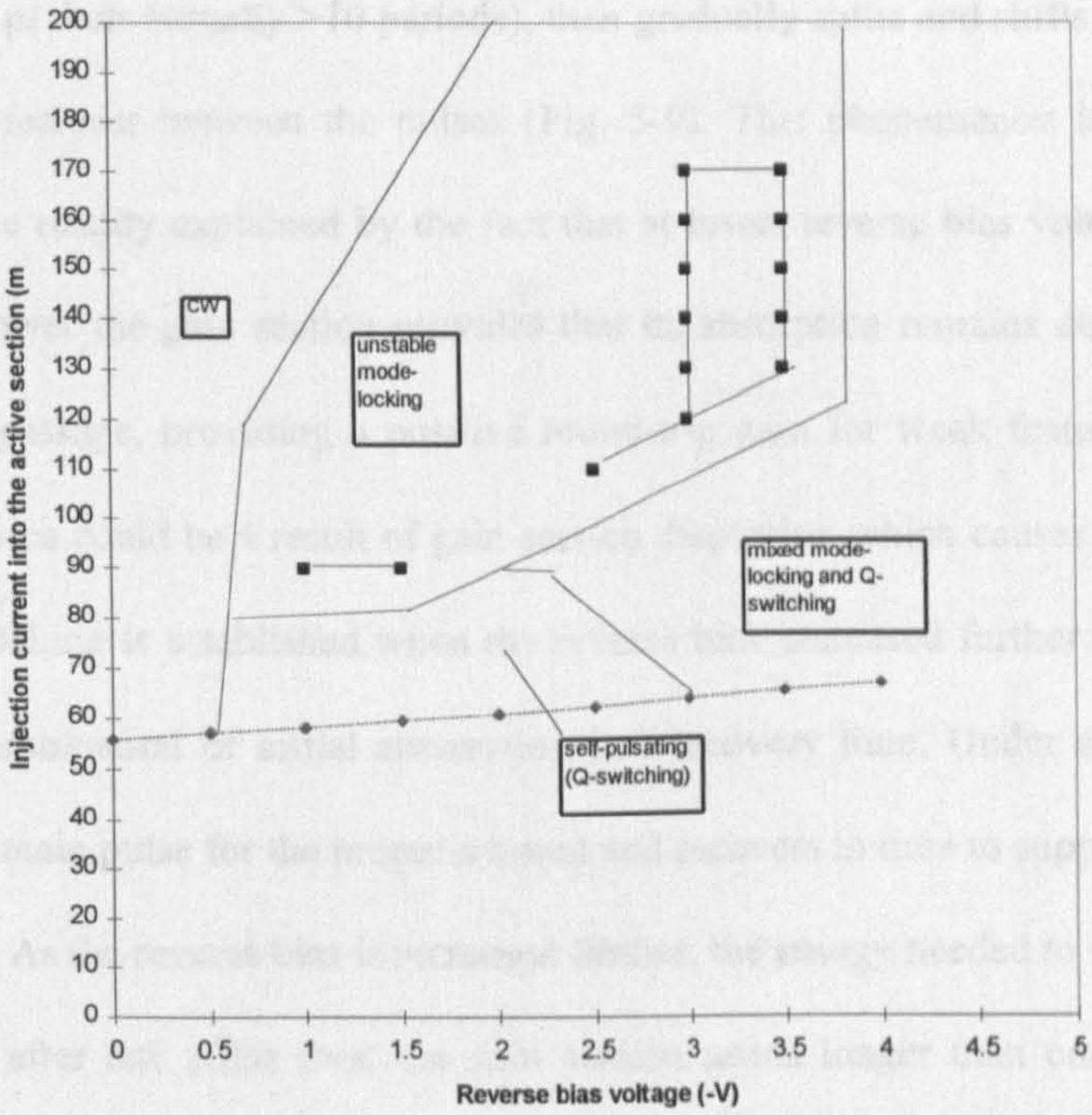

Fig. 5-9 The operation mode of a symmetric mode-locked SRL of Fig. 5-8(a). Black squares indicate stable mode-locked operation.

The operational modes of a SRL with symmetric mode-locked configuration is mapped in the reverse bias-injection current plane (Fig. 5-8). The geometric parameters of the laser are listed below

Length of active section	2.4mm
Length of absorber section	120μm
Waveguide width	2μm
Effective lateral current spreading width	5μm
output coupling ratio	0.5

In the chart of Fig. 5-8 there are two separate stable mode-locked areas, as marked by the filled squares connected by solid lines. This is in clear contrast to the continuum in the g-α chart predicted by the lumped element model[1]. When the laser is pumped at a injection current level above threshold at which stable mode-locking exists, what happens when absorber reverse bias voltage magnitude is increased is that the laser transfers from CW operation into an unstable mode-locking state in which the pulse may

---

[1]Koumans, R. G. M. and Van Roijen, R., 'Theory for passive mode-locking in Semiconductor laser structures including the effect of self-phase modulation, dispersion, and pulse collisions', IEEE J-QE, VOL.32, NO.3, March 1996, pp.478-492.

sustain for a number of periods (usually >10 periods), then gradually splits and shifts to an adjacent peak due to the rise of sub-features between the pulses (Fig. 5-9). This phenomenon is observed in other simulations [1] and can be readily explained by the fact that at lower reverse bias voltage, the absorber is overwhelmed by the power the gain section provides that its absorption remains deeply saturated even after the main pulse's passage, providing a positive round-trip gain for weak features that follows the main pulse. These features could be a result of gain section dispersion which causes the pulse to deform or split. Stable mode-locking is established when the reverse bias increased further so that the absorber provides the right recombination of initial attenuation and recovery time. Under such a condition the absorber attenuates the main pulse for the proper amount and recovers in time to suppress any feature that follows the main pulse. As the reverse bias is increased further, the energy needed to saturate the absorber becomes so high that, after one pulse shot, the gain section needs longer than one round-trip time to recover to provide this energy. Longer time scale fluctuations in pulse energy set in as a result and finally mixed Q-switching and mode-locking takes place. In this region the laser typically gives a giant pulse encapsulating several mode-locked pulses and has to wait for a time determined by bias voltage before another giant pulse is produced.

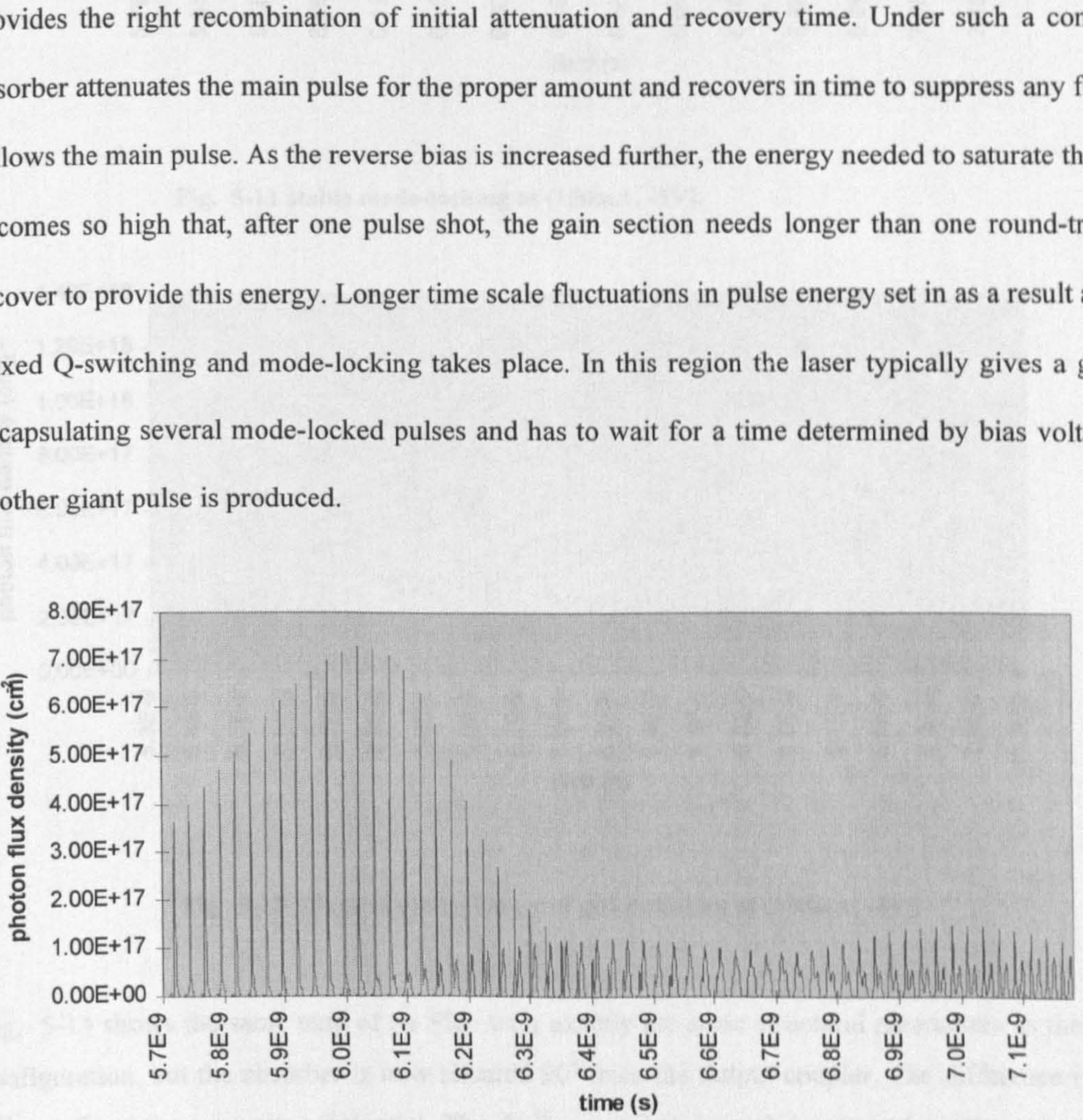

Fig. 5-10 unstable mode-locking at (150mA, -2.5V).

---

[1]Schell, M., et al, 'Chirp and stability of mode-locked Semiconductor lasers', IEEE Journal of Quantum Electronics, VOL.32, No.7, July 1996, pp.1180-1190.

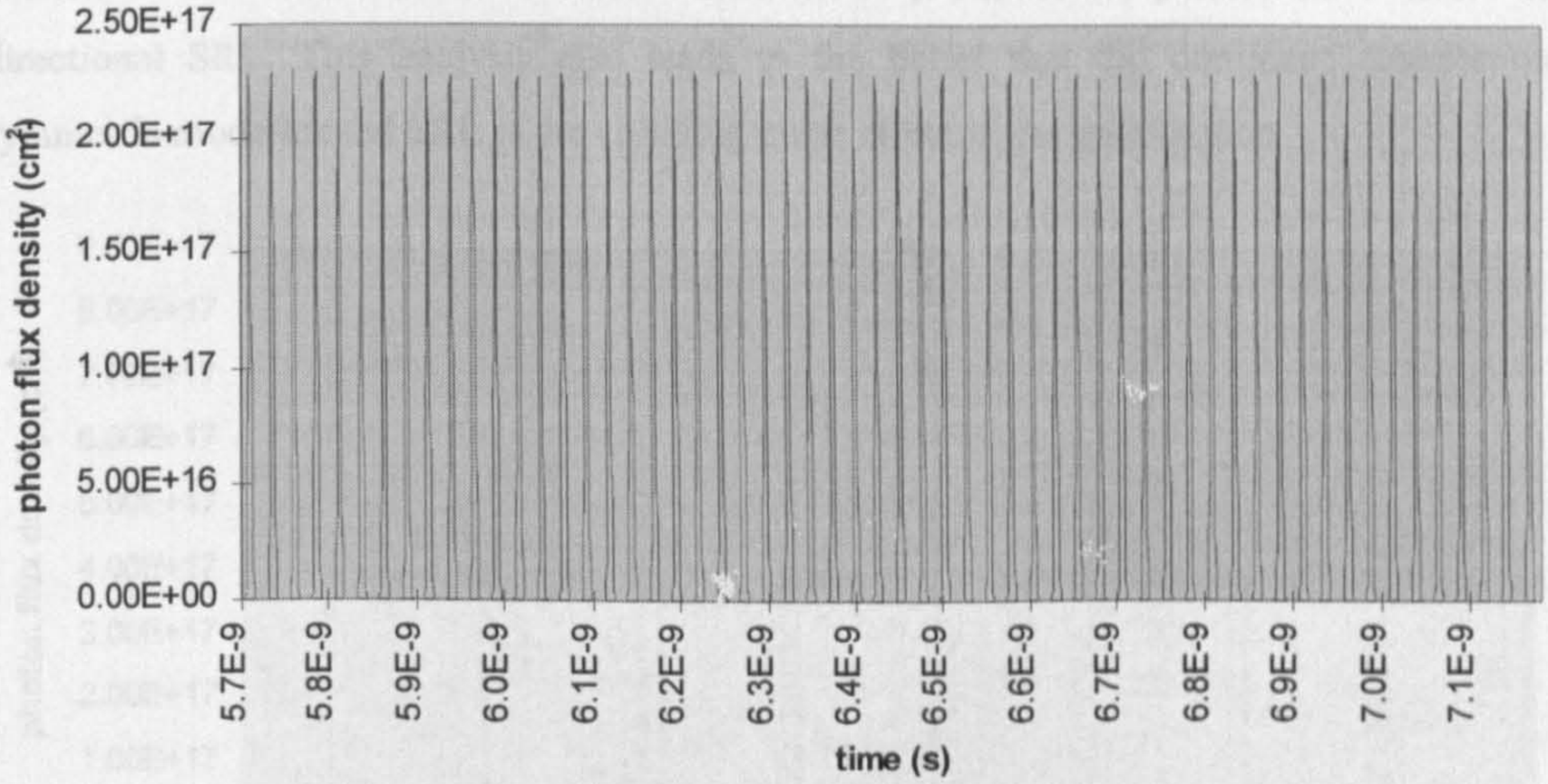

Fig. 5-11 stable mode-locking at (150mA, -3V).

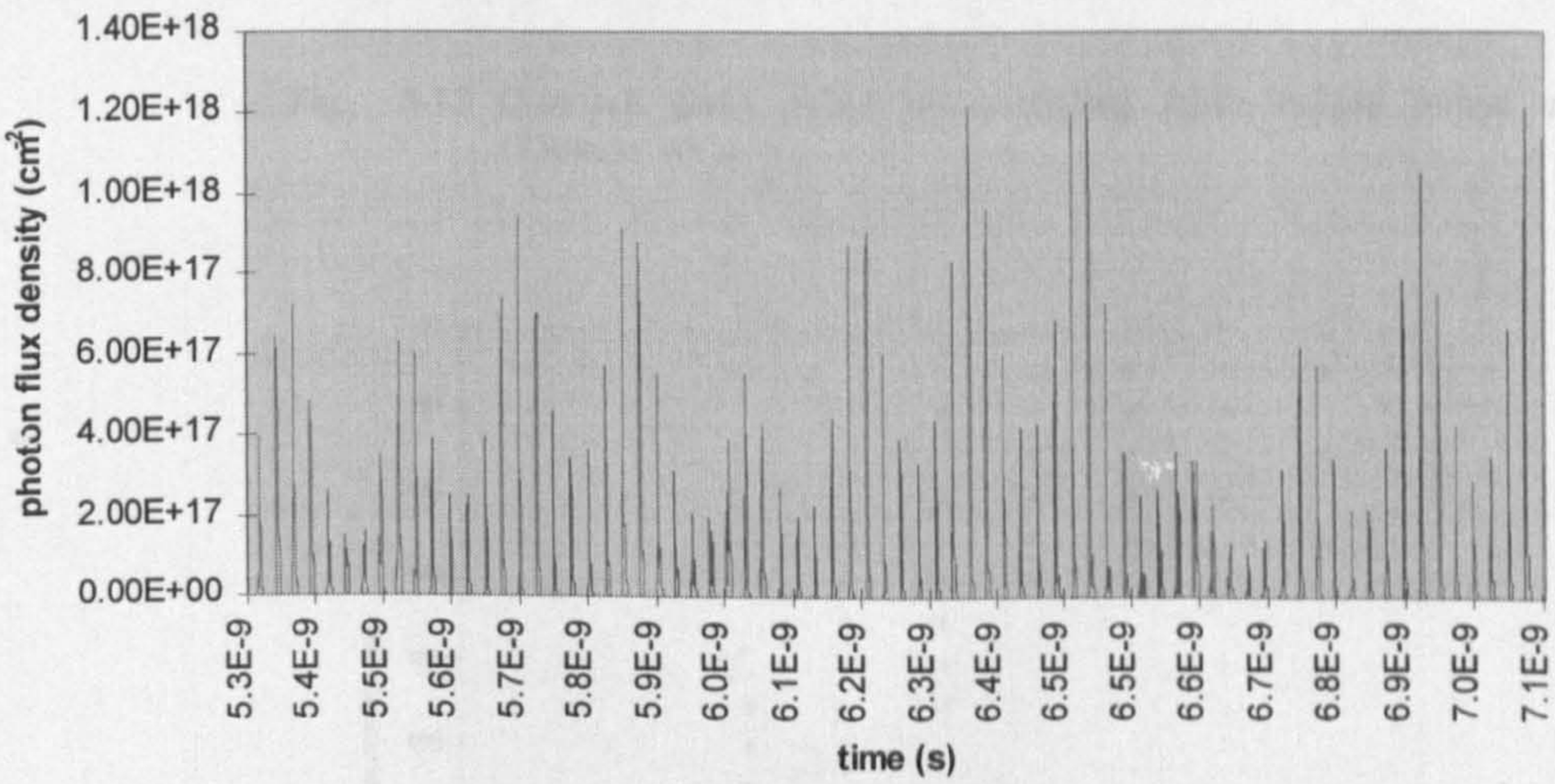

Fig. 5-12 Mixed mode-locking and self-pulsation at (150mA, -4V).

Fig. 5-14 shows the same map of an SRL with exactly the same structural parameters as the symmetric configuration, but the absorber is now situated 90° from the output coupler. The difference between the two configurations is very substantial. The device now has a much larger and continuous stable mode-locking region almost resembling that predicted by the lumped element model. This reveals that in the asymmetric configuration, although the counter-propagating pulses still collide in the active section, the adverse effect of the collision has been reduced significantly due to the fact that the two pulses are very unequal in their energy when they collide in the gain section because, since the last collision, one of them has travelled through the output coupler and has been significantly attenuated. As a result at both collision points (one at the absorber and the other opposite the absorber in the gain section), the saturation

behaviours of the two media are more dominated by one of the pulses, close to the case of an uni-directional SRL. This analysis also leads to the belief that the dominant deteriorating effect in a symmetric mode-locked SRL is the colliding pulse effect in the gain section.

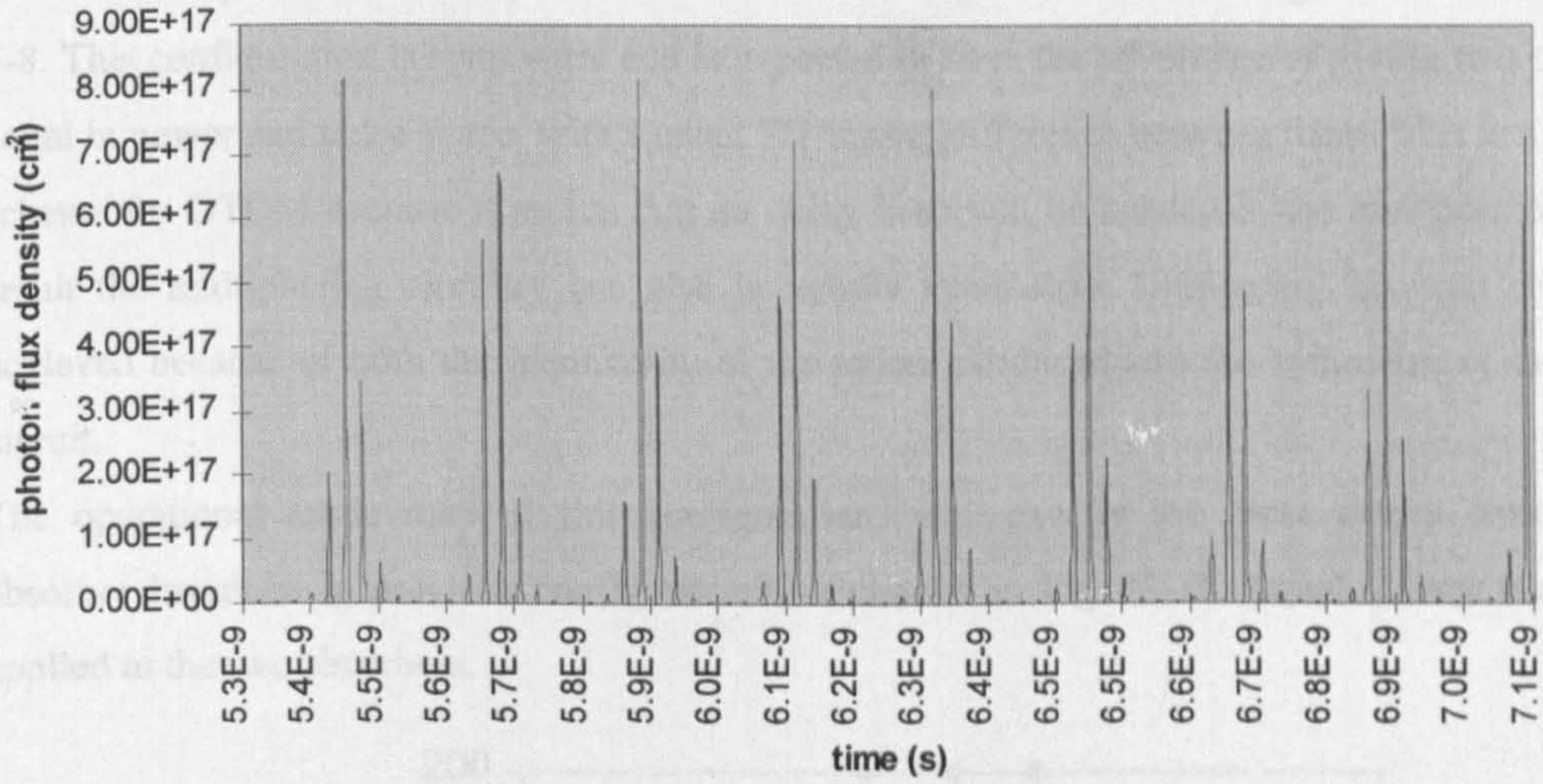

Fig. 5-13 Q-switch giant pulses encapsulating mode-locking pulses at (130mA, -4V).

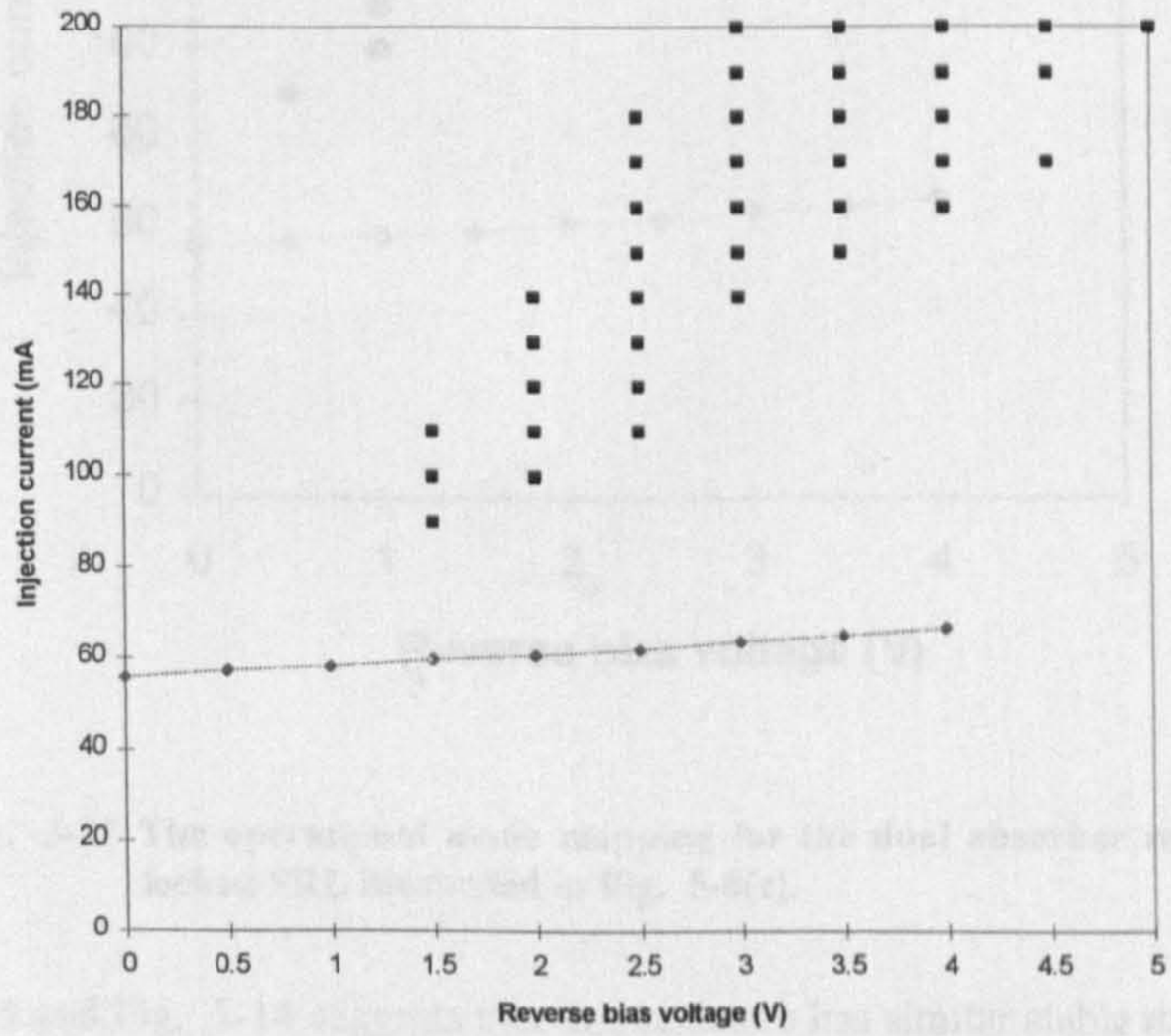

Fig. 5-14 The operation mode mapping for asymmetric mode-locked SRL of Fig. 5-8(b).

While the asymmetric configuration has the clear advantage of large stable mode-locking region and narrower pulse width, it has the disadvantage that the two output pulse trains are unequal in power and pulse shape. The two pulse train also do not have the timing difference of T/2 as expected from the configuration. This is because that the two directions experience different propagation conditions,

although at the output point their apparent optical path difference from the absorber is half the cavity circumference.

To finally eliminate the problem of pulse collision in the gain section, another saturable absorber can be placed in the place where the pulses collide, thus leading to the third configuration as illustrated in Fig. 5-8. This configuration is symmetric and is expected to have the advantage of giving two outputs that are equal in power and pulse shape, with a exact T/2 timing difference between them. This is a very attractive scheme for OTDM because it means that no delay lines will be needed in the multiplexing circuit. As a result the multiplexing circuitry can also be totally symmetric. Uniformity between channels can be achieved because of both the identicality of the pulses produced and the symmetry of the multiplexing circuit.

The operational mode map of this configuration, with exactly the same cavity circumference and absorber length as in previous configurations, is charted in Fig. 5-15. Equal reverse bias voltages are applied to the two absorbers.

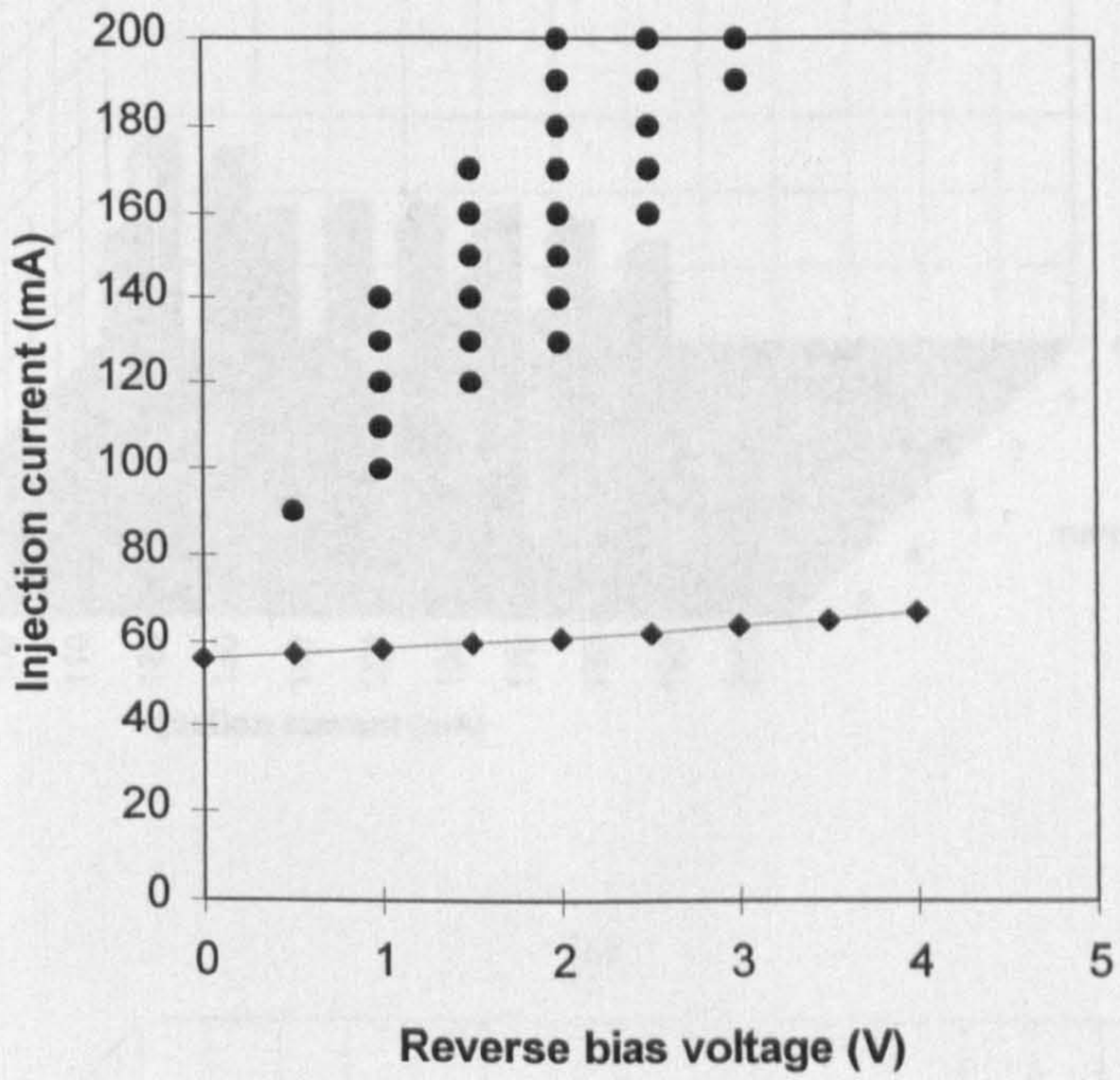

Fig. 5-15 The operational mode mapping for the dual absorber mode-locked SRL illustrated in Fig. 5-8(c).

Comparing Fig. 5-15 and Fig. 5-14 suggests that this structure has similar stable mode-locking region as the asymmetric configuration. The stable mode-locking region here has moved towards the low voltage side and are narrower in the horizontal direction. However, bearing in mind that the same bias voltage now correspond to about double the unsaturated absorber attenuation, if the two charts are translated into g-α charts, the stable mode-locking region of the dual absorber configuration is wider than that of the asymmetric configuration.

Pulse Width

Although a mode-locked laser can operate stable with a wide range of injection and bias parameters, narrow pulse width is usually sought after. The pulse width as a function of injection current and reverse bias voltage for the three structures is charted in Fig. 5-16. In the three configurations the pulse widths are highly dependent on the reverse bias but are relatively independent of injection current at high injection levels. The shortest pulse width in the mapped region (I=70 to 200mA, V_b=0 to 5 V) appears in the asymmetric configuration at (200mA, 5V), with a value of 0.9ps. However, when comparing the asymmetric configuration and the dual absorber configuration at the same injection current and bias voltage, the latter produces narrower pulses because of the stronger pulse compression effect by two rather than one absorber .

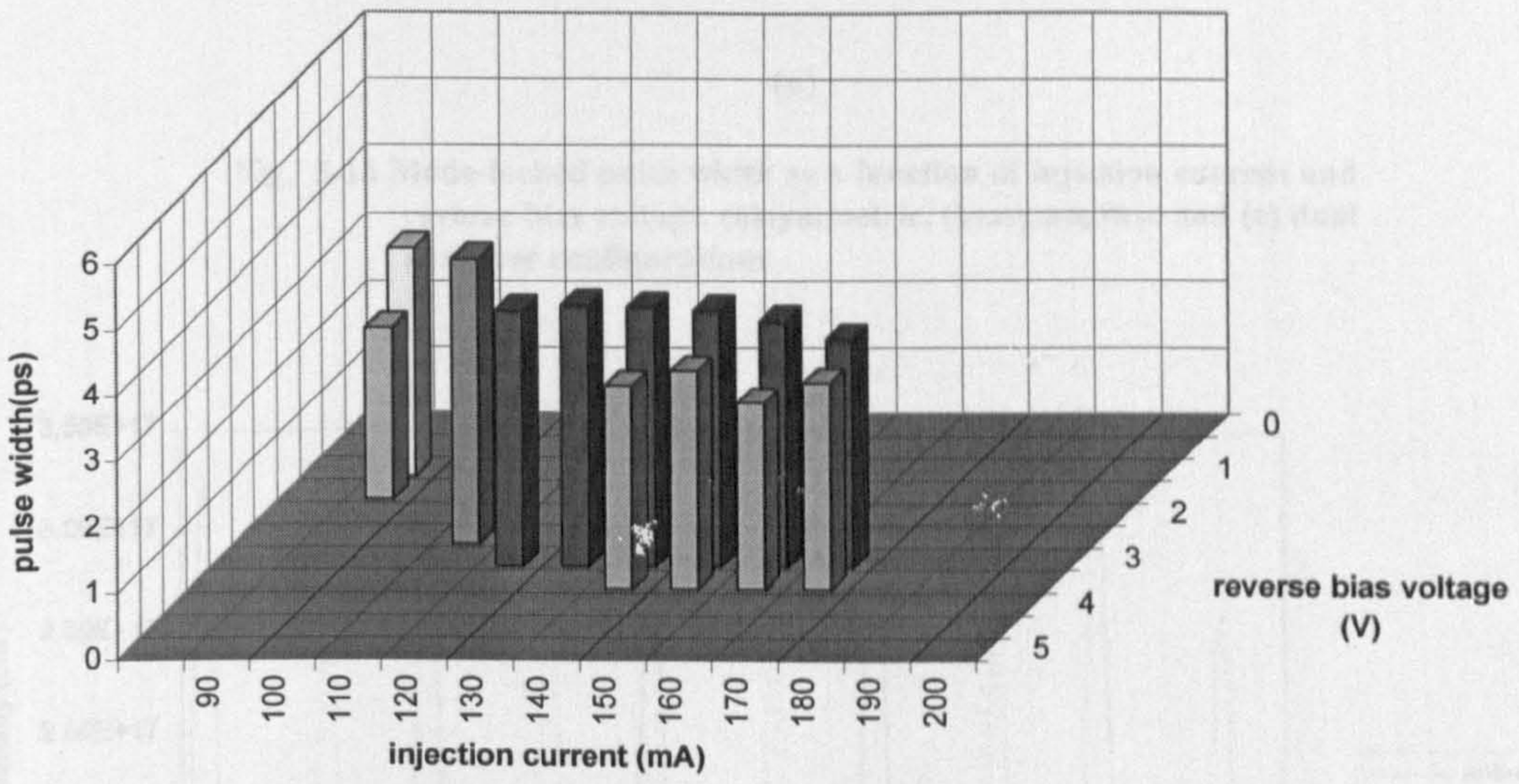

(a)

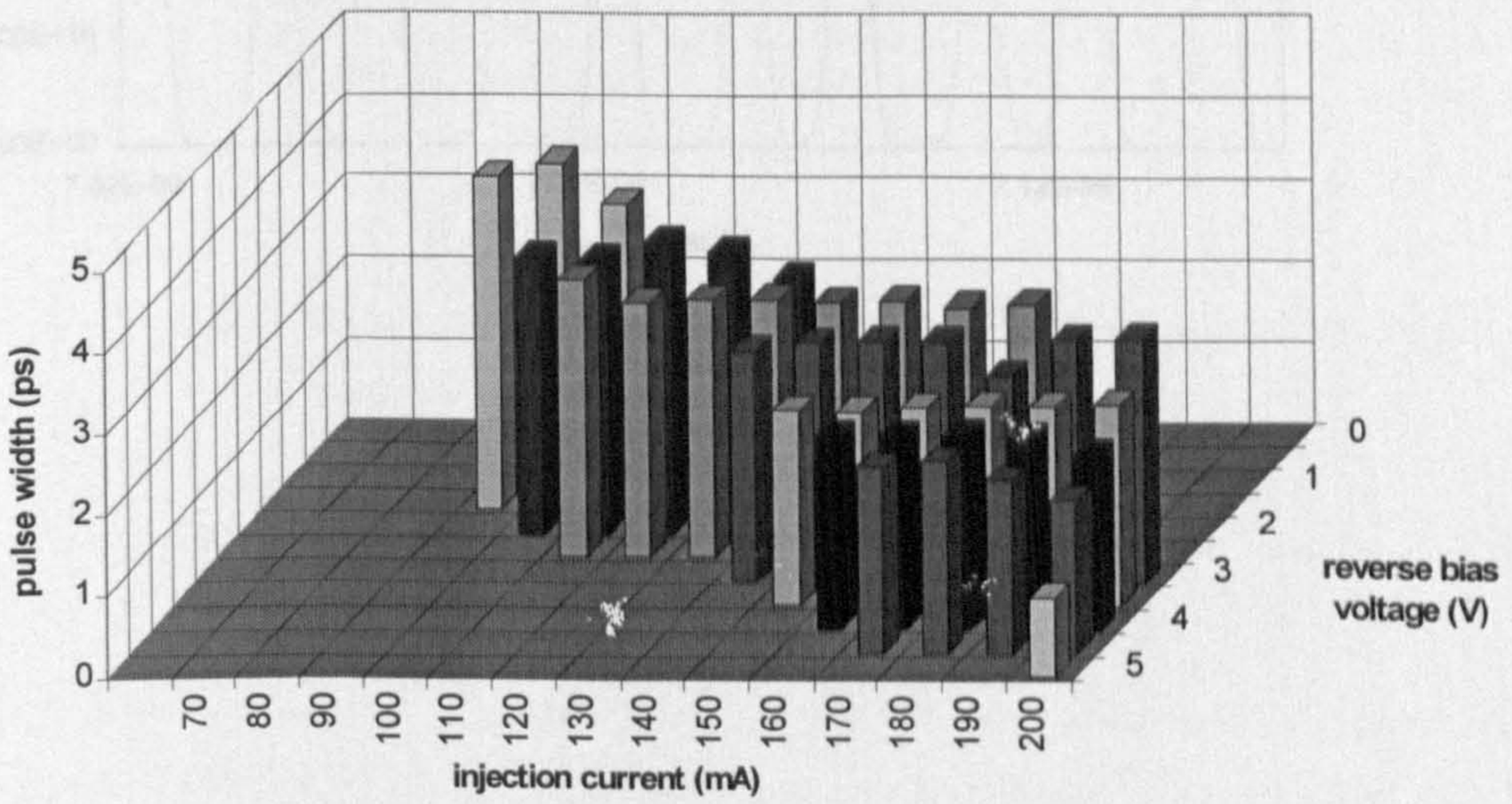

(b)

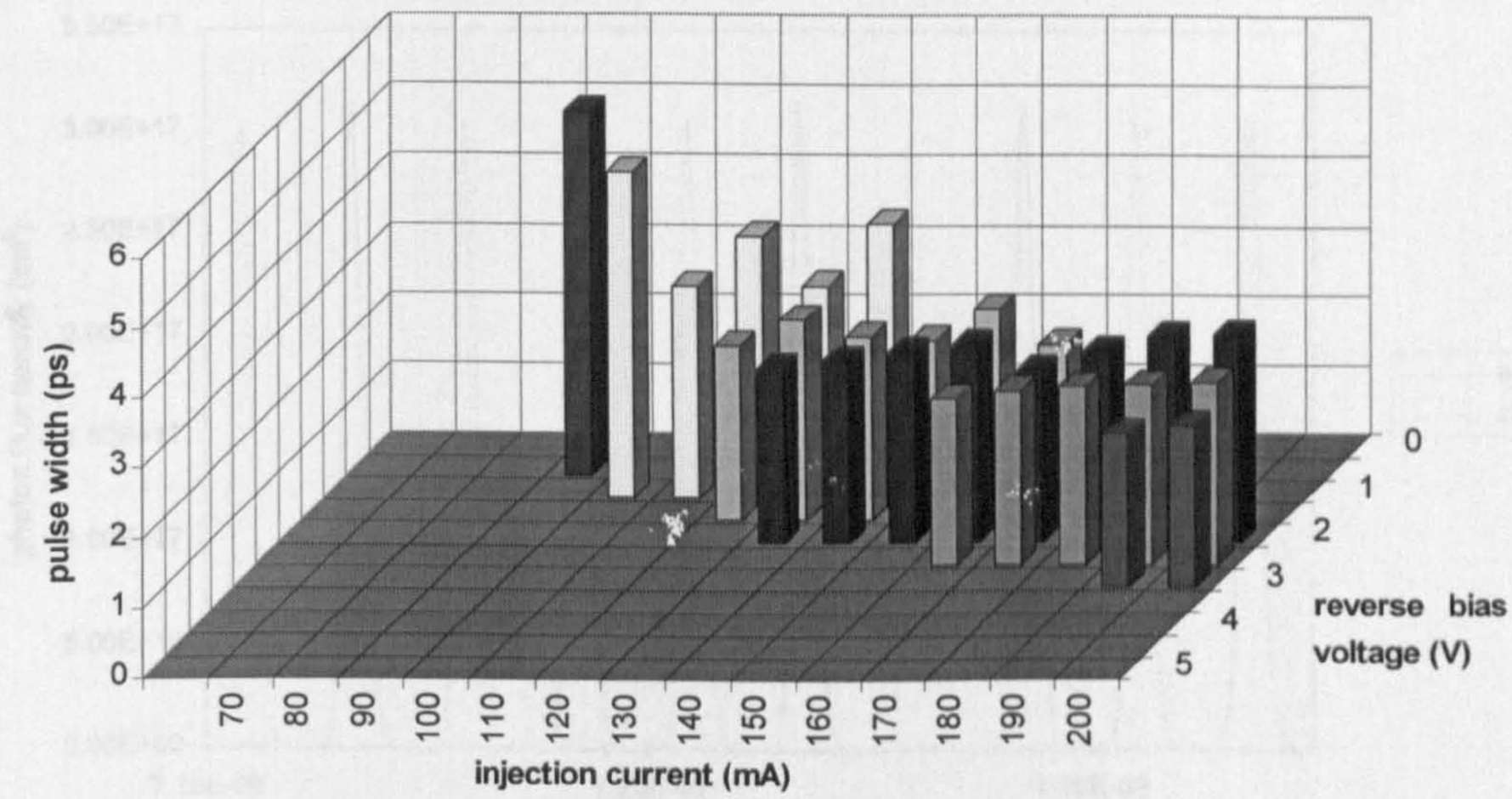

(c)

Fig. 5-16 Mode-locked pulse width as a function of injection current and reverse bias voltage. (a)symmetric, (b)asymmetric and (c) dual absorber configurations

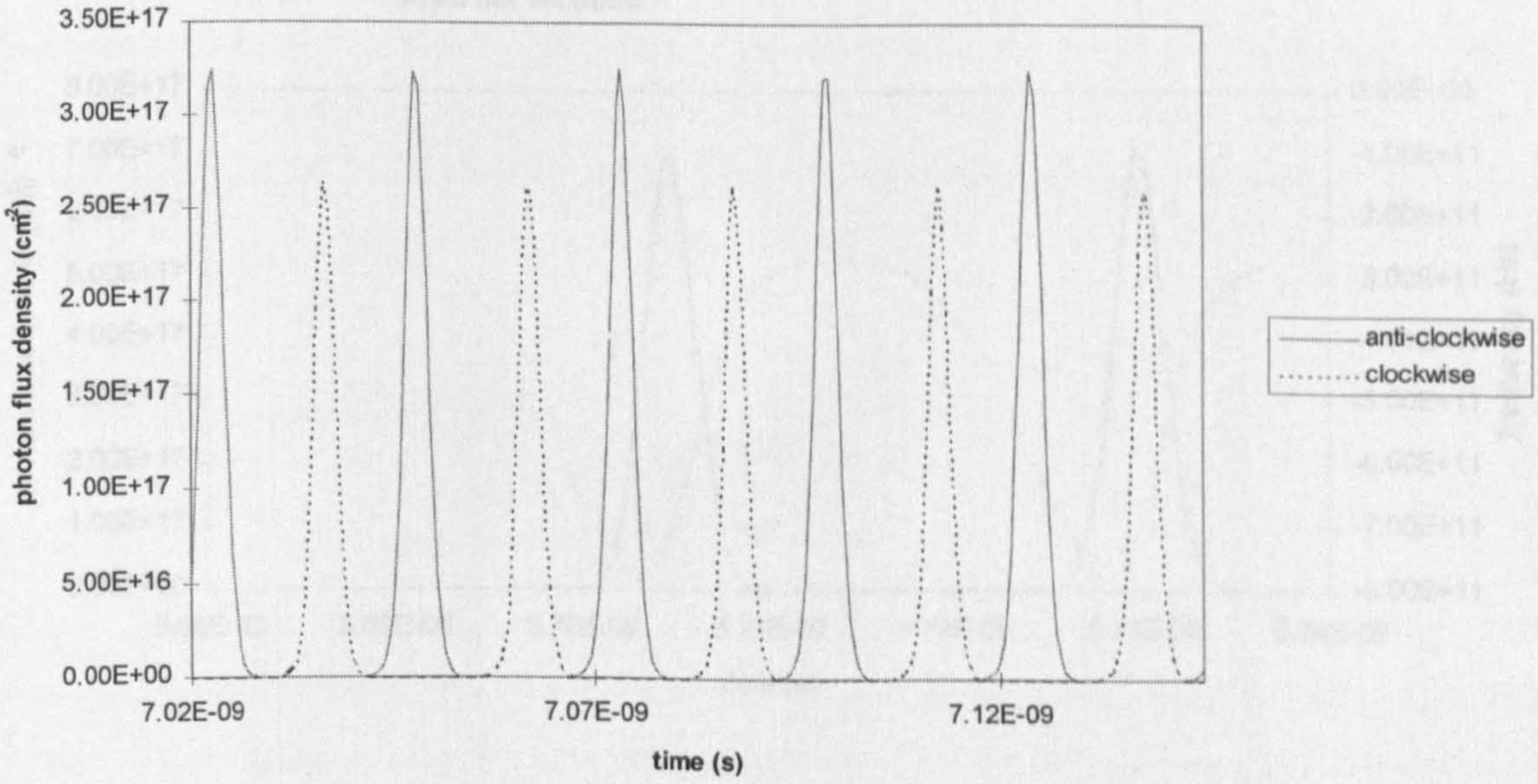

(a)

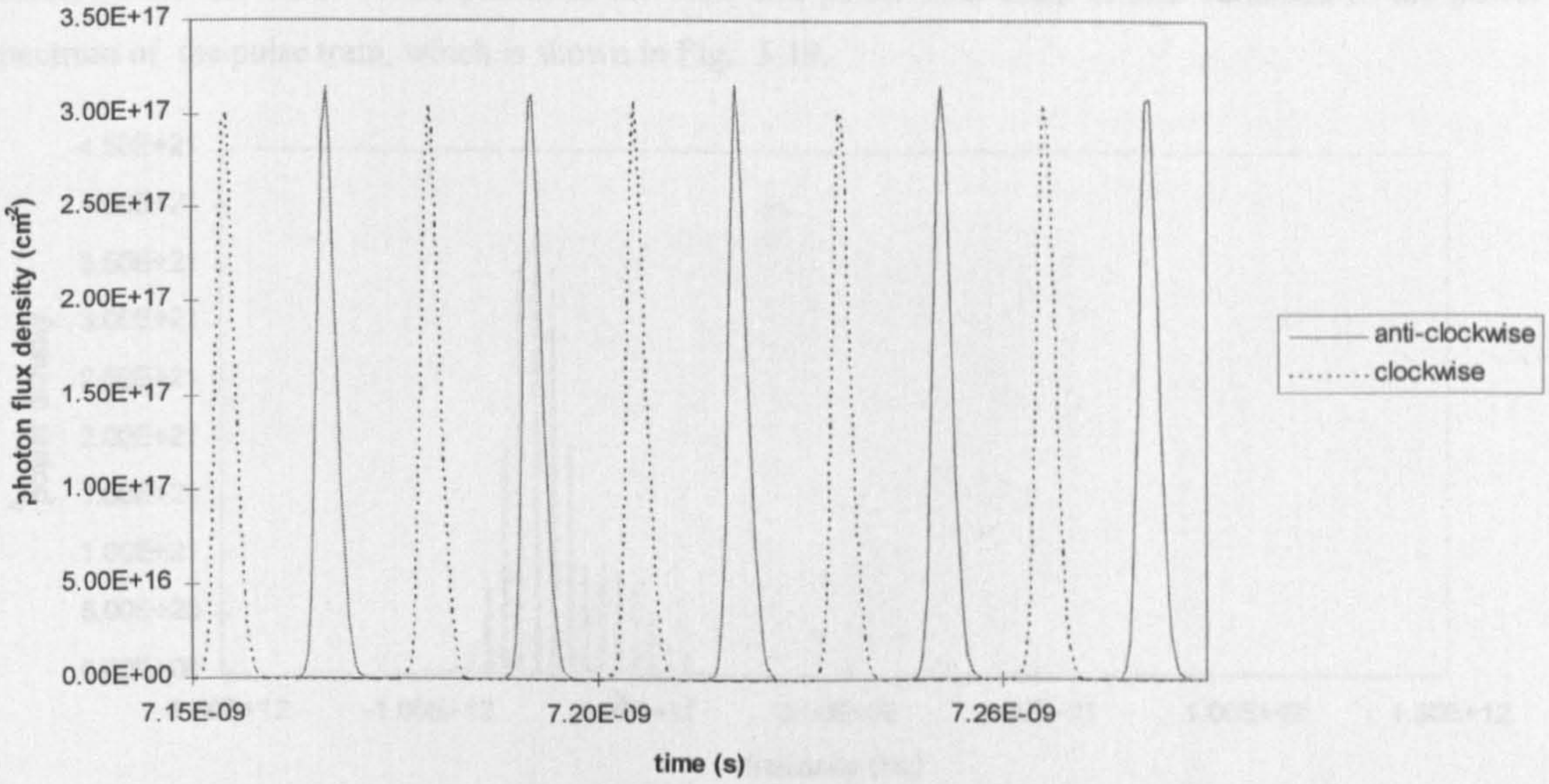

(b)

Fig. 5-17 Output mode-locked pulse train from (a)asymmetric, and (b)dual absorber mode-locked SRLs at 140mA gain section injection current and 2V reverse bias voltage on the saturable absorber sections.

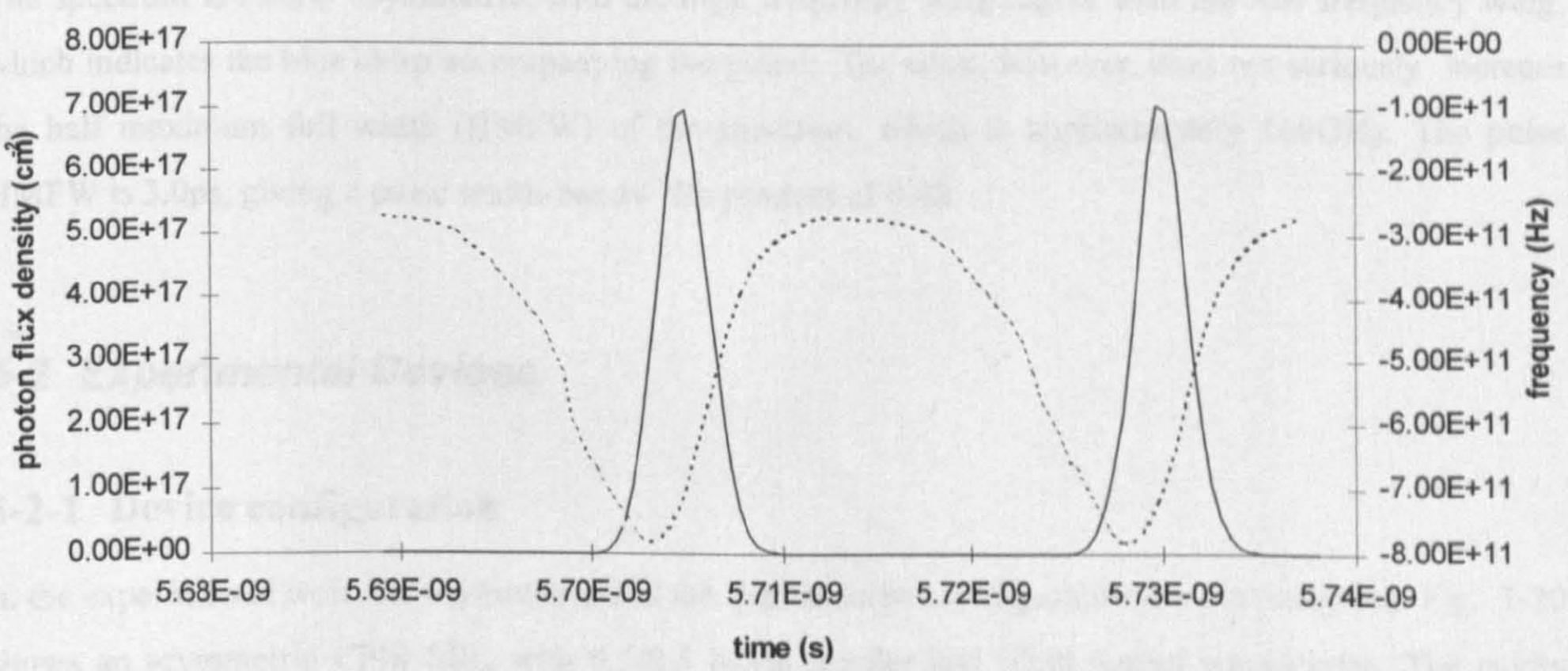

Fig. 5-18 The output pulse train (solid line) and corresponding transient frequency change (chirp) (dashed line) of the asymmetric mode-locked SRL.

Power Spectrum, Chirp and Pulse Width-Bandwidth Product

Fig. 5-18 shows mode-locked pulses and the frequency chirp accompanying the pulses, for asymmetric configuration at (200mA, -3V). It is clear that the pulses have a blue chirp, i.e., there is a frequency

increase from the onset of the pulses to the their end point. This chirp is also reflected in the power spectrum of the pulse train, which is shown in Fig. 5-19.

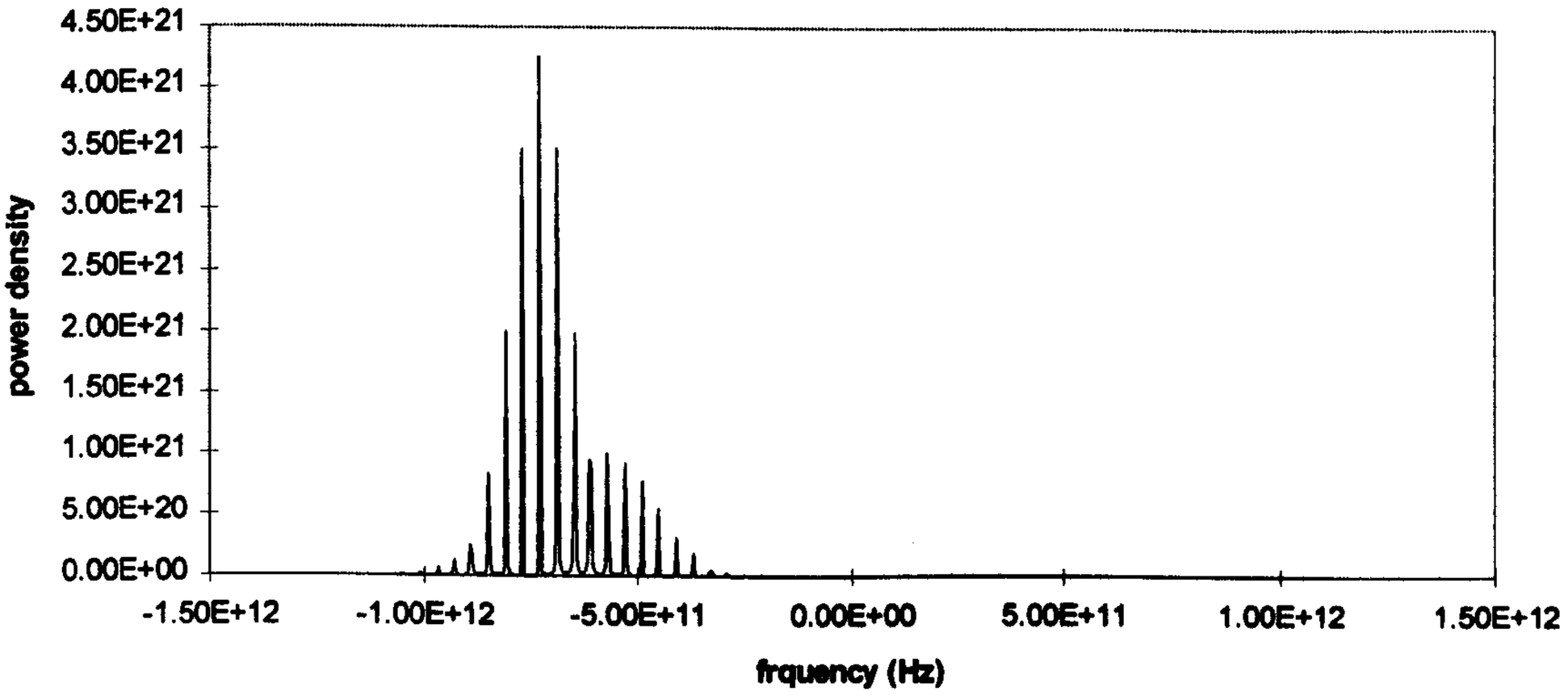

Fig. 5-19 The power density spectrum of the pulse train shown in Fig. 5-18.

The spectrum is clearly asymmetric, with the high frequency wing higher than the low frequency wing, which indicates the blue chirp accompanying the pulses. The chirp, however, does not seriously increase the half maximum full width (HMFW) of the spectrum, which is approximately 160GHz. The pulse HMFW is 3.0ps, giving a pulse width-bandwidth product of 0.48.

5-2 Experimental Devices

5-2-1 Device configuration

In the experimental work the asymmetric and the dual absorber configurations are investigated. Fig. 5-20 shows an asymmetric CPM SRL with 0.5/0.5 MMI coupler and tilted output waveguides. The cavity circumference is 3.1mm. The length of the saturable absorber is 50μm not including the 20μm separation zone on both sides of it. The saturable absorber is placed at a quarter circumference from the centre of the coupler.

The dual absorber CPM SRL shown in Fig. 5-21 is a modified design combining the dual MMI coupler SRL and the two absorber structure of Krauss[1], and is capable of producing 4 outputs. The two saturable absorbers are placed exactly half the circumference from each other and quarter the circumference from the centre of the couplers. The pulse collision should always happen in the absorbers and the four outputs

---

[1] Krauss, T. F., 'Mode-locked semiconductor ring lasers with two saturable absorbers', Proceeding of ECIO'95. p.55-58.

should have such a timing relation that the two outputs from one facet are in phase. They should be out of phase with those from the other facet if the output waveguides are of the same length. This means that, apart from being able to generate four outputs and eliminating the need for power splitters to form a 4 channel OTDM, only T/4 (T the mode-locked pulse period) delay lines are necessary.

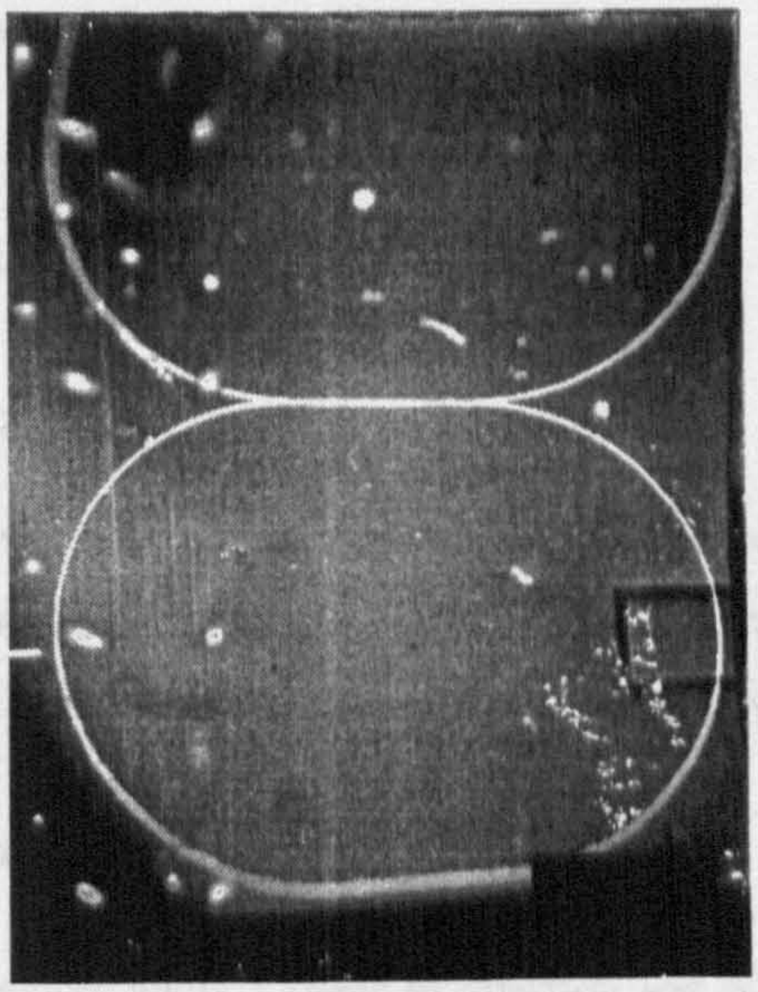

Fig. 5-20 Asymmetric mode-locked semiconductor ring laser.

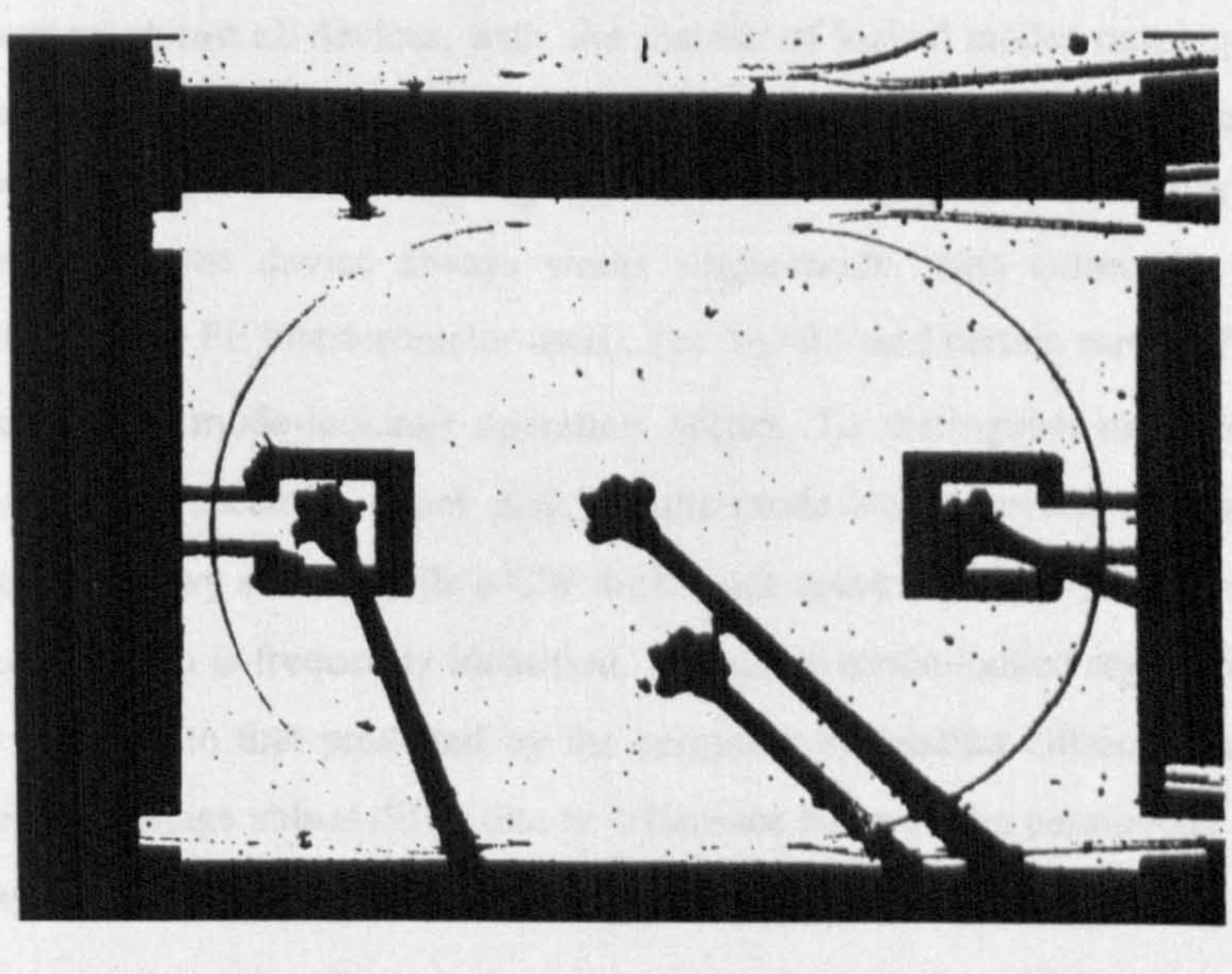

Fig. 5-21 Micrograph of a wire bonded dual MMI coupler CPM SRL.

5-2-2 Fabrication

The definition of passive mode-locked SRLs is by the same process used for usual SRL devices. The separation between the saturable absorber section and the gain section is achieved by lift-off of the p-contact. This exposes the waveguide between the two sections. After lift-off the samples are dry-etched in the RIE for about 2.5 minutes to remove the p^+-cap layer between the two sections so that a high isolation resistance (>5kΩ) is achieved. If the isolation resistance between the absorber and the gain sections is too

small, the reverse bias will draw a considerable amount of current from the gain section and the device will not work mode-locked. For the devices to work CW, the samples are thinned to about 150μm thick to reduce the thermal resistance. After cleaving the devices are mounted on gold-plated copper heatsinks and gold wires are bonded to the contact pads with an ultrasonic wire bonder. CW operation is necessary for the characterisation of mode-locked SRLs.

5-3 Experimental Results

5-3-1 Asymmetric CPM SRL with 2x2 MMI couplers

The material used for these devices is MBE DQW material B429. After bonding these devices typically have CW threshold currents ranging from 100 to 160 mA when the absorbers are open circuited. Fig. 5-22 is the CW L-I curves of one such device with different absorber bias voltage.

Frequency domain characterisation

The optical spectrum of these devices under a range of injection and bias conditions has been studied using a Fabry-Perot interferometer. By varying the bias voltage on the saturable absorber, the sudden broadening of the spectrum from a single longitudinal mode to a group of locked longitudinal modes has been widely observed on almost all devices, with the number of locked modes ranging from about 5 up to more than 20 depending on the bias condition, and also varying from device to device. The change of threshold current with absorber bias voltage V_b and the mode-locked area of one device is depicted in Fig. 5-23. For V_b<0.5V, the device always works single-mode, with extremely narrow linewidth (beyond the resolution of the FP interferometer used). For V_b>0.5 and certain range of injection current, multimode (not necessarily mode-locking) operation occurs. To distinguish mode-locking from CW multimode operation on the spectrum is not easy, but the mode-locked spectrum usually rises abruptly from a single mode and is very stable, while a CW multimode spectrum usually has gradually rising side modes and mode competition is frequently identified. The stable mode-locked region mapped in Fig. 5-23 is very similar in shape to that predicted by the computer simulation although the actual injection current and reverse bias voltage values differ due to difference between the parameters values used in the computing and actual material values.

Fig. 5-24 is a typical mode-locked spectrum measured from the device. The frequency (horizontal) axis in all the spectra measured are reversed (frequency increases from right to left). Because the whole spectral range is wider than one free-spectral range (FSR) of the F-P interferometer, the interferometer is driven to scan for two FSRs so two groups of the same spectrum are displayed. The mode spacing is about 25GHz. The half-maximum full width (HMFW) of the spectrum is about 8 mode spacings or 200GHz. The shape of the spectral envelope is Gaussian-like. Detailed study reveals that the side mode on the left side of the main modes are slightly higher than those on the right, so the mode-locked pulses

are slightly blue chirped, which is very similar to the spectrum calculated by the simulation. But the chirp is not large enough to significantly increase the pulse width-spectral width product $\Delta\tau\Delta f$. If the simulation $\Delta\tau\Delta f$ value of 0.48 is used, the corresponding pulse width should be about 2.4ps.

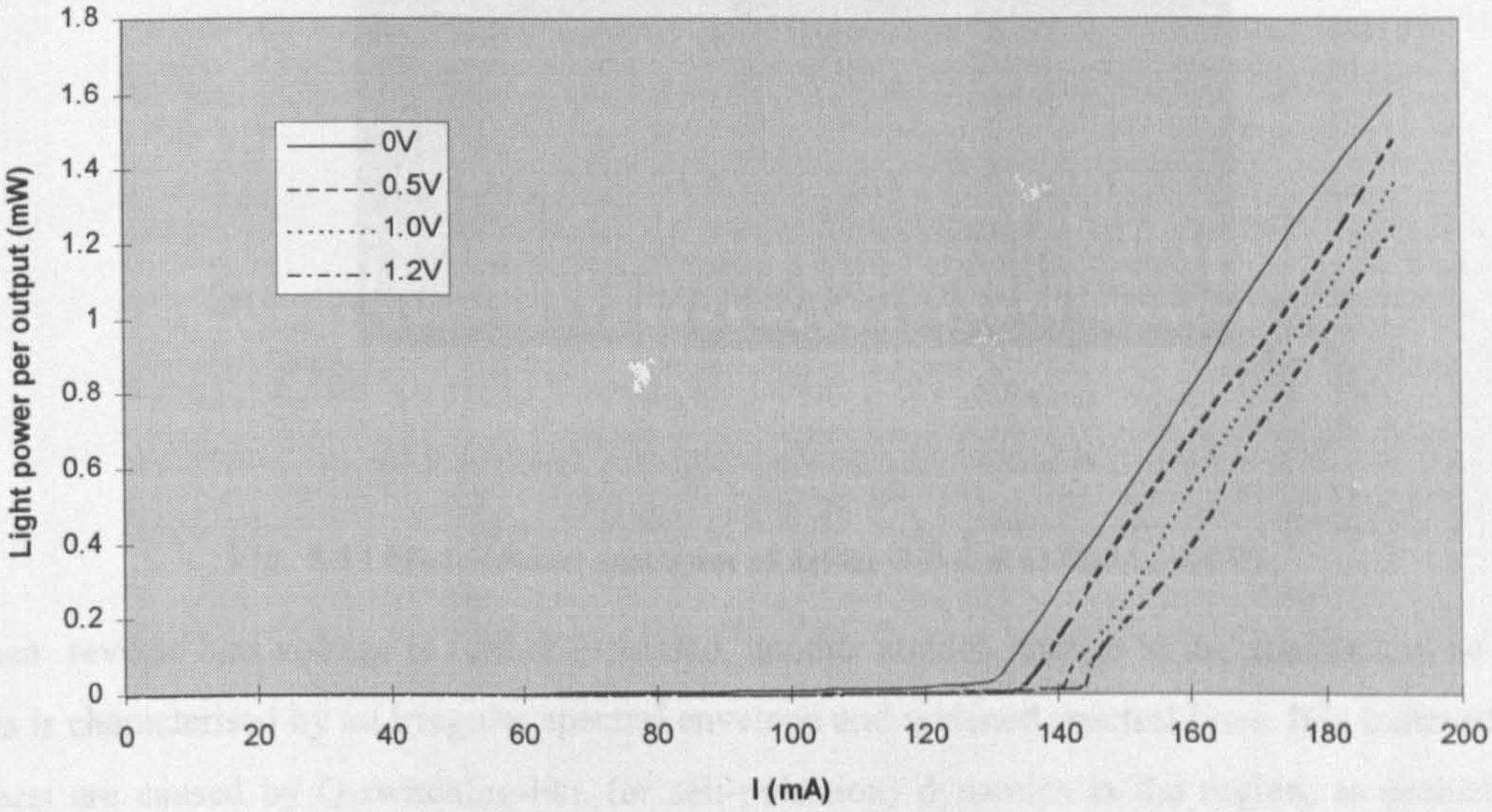

Fig. 5-22 CW L-I curve of asymmetric mode-locked SRL No.6-B-1.

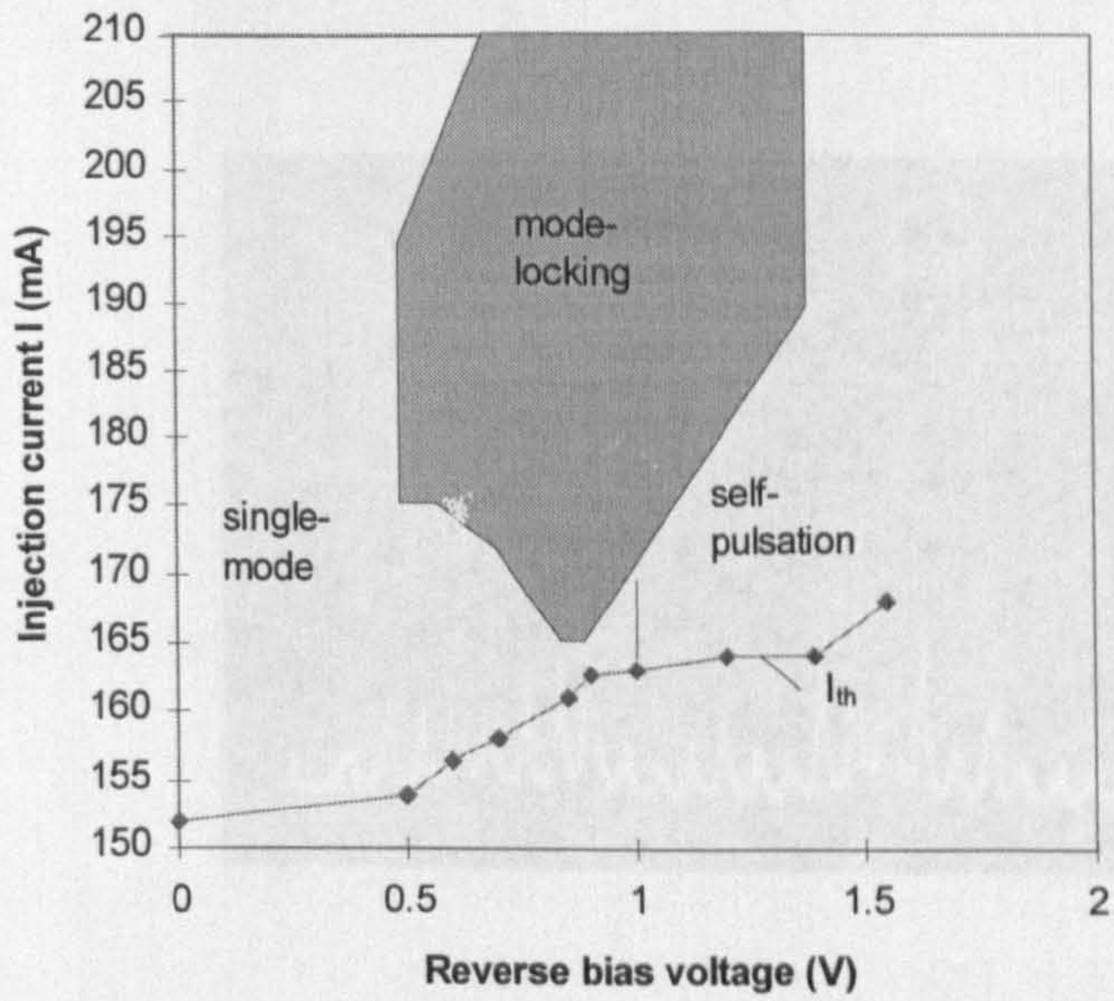

Fig. 5-23 Threshold vs. absorber bias voltage and mode characteristics chart of asymmetric mode-locked SRL No.6-B-2.

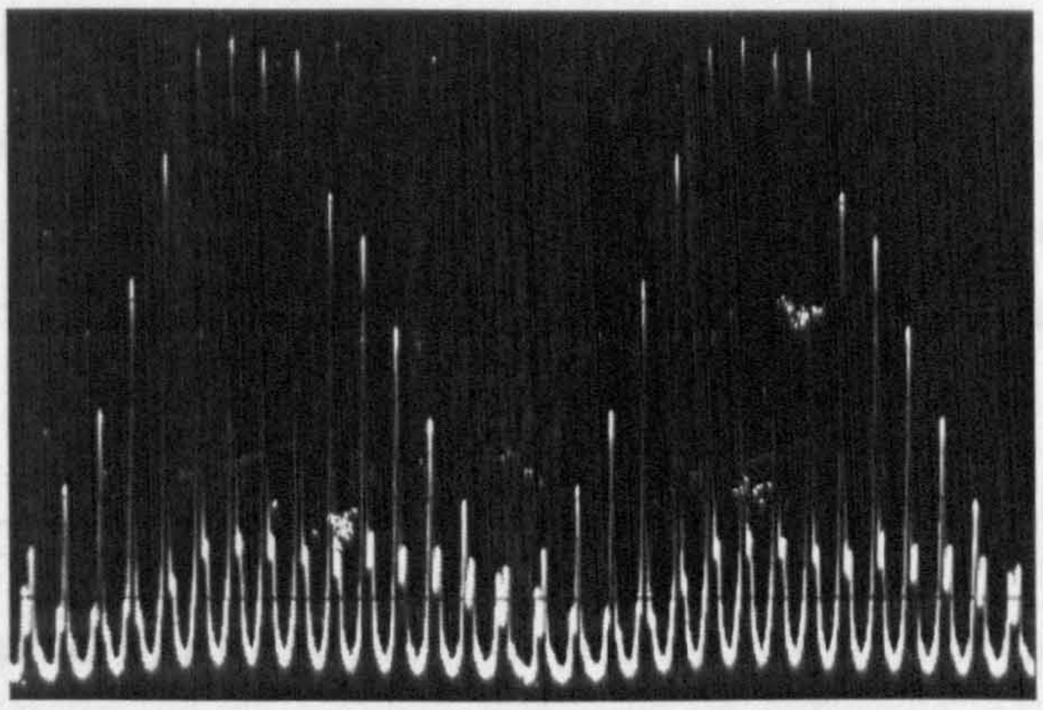

Fig. 5-24 Mode-locked spectrum of device 6-B-2 at (178mA, -1.0V).

When reverse bias voltage is further increased, another sudden change in the spectra can be observed. This is characterised by an irregular spectral envelope and widened spectral lines. It is believed that both effects are caused by Q-switching-like (or self-pulsation) dynamics in the region, as predicted by the simulation, which widen the spectral lines by pulse magnitude modulation at frequencies in the order of several GHz and disrupts the spectral envelop by introducing large chirp effect.

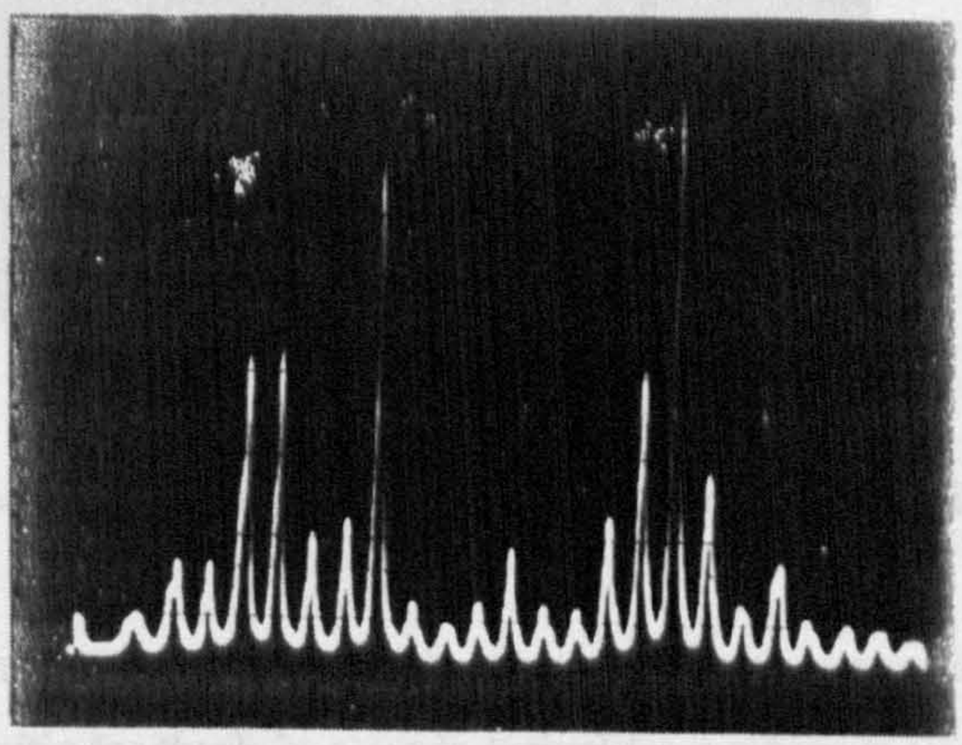

Fig. 5-25 The spectrum of the same device at (178mA, -1.28V)

Since the absorber is displaced from the symmetric centre, it is expected that the two spectra from the two outputs will differ. It is observed that the spectrum from the output closer to the absorber has a wider HMFW and a smaller energy. This can be explained as the pulse from this output experiencing less amplification after leaving the absorber, which increases the energy of the pulse but reduces its bandwidth.

5-3-2 CPM SRL with dual 2x2 MMI couplers

These devices are fabricated on the MBE DQW material B680 with undoped well and barrier layers (see Chapter 2). The device circumference is again 3.1mm, the same as the asymmetric configuration. Their typical CW threshold current is only about 120mA. Several lengths of absorbers ranging from 30-90μm are experimented.

Frequency domain Characterisation

The study on the spectrum of the dual coupler CPM SRLs reveal that mode-locking happens in a much smaller area than that of the single coupler CPM SRLs. The best spectrum available is shown in Fig. 5-26, which is observed from a device with 90μm long absorbers at a injection current of 190mA and reverse bias voltages of V_{b1}=-4.0V and V_{b2}=-3.8V, where only 6 modes are present and the HMFW of the envelope is about 2 mode spacings or 50GHz.

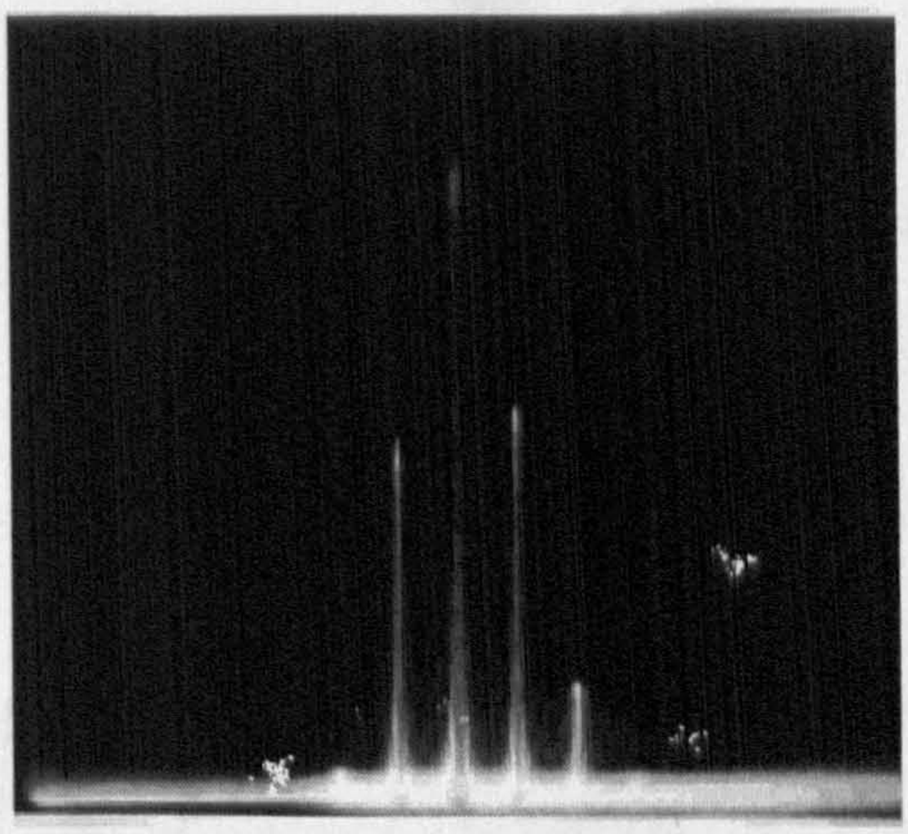

Fig. 5-26 Mode-locking spectrum of a dual absorber dual MMI SRL.

A possible explanation for the reduced mode-locking region and the narrower spectrum width is the effect of facet feedback. Parasitic feedback in a mode-locked laser cavity is known to introduce 'etalon effect'[1] which seriously reduce the spectrum bandwidth. The same effect exists in the two output asymmetric configuration, but the situation would be worse in the dual MMI coupler device because there are now four outputs and therefore four sources of facet feedback. This makes extremely complicated (and virtually unpredictable) interference between these feedback to take place and may result in serious damage in mode-locked operation. A recent study carried out in the department[2] suggested that such feedback may induce high order harmonic mode-locking (at the 8th harmonic

---

[1] Siegman, A. E., "Lasers", Oxford University Press, 1986.

[2] Avrutin, E. A., Kauss, T. F., Pottinger, H., De La Rue, R. M., and Button, C. C., 'Harmonic mode-locking effects in 1.5μm ring laser diodes: experiment and theory', Proceed. SIOE'97, March 1997, Cardiff. Wales, UK.

frequency of about 256GHz) and suppress mode-locking at foundamental ring cavity freguency. It would therefore be necessary to apply anti-reflective coating on the facets to eliminate feedback in order for successful mode-locking at the ring cavity mode separation frequency.

Time domain characterisation

The corresponding time domain characteristics of the CPM SRLs are studied by means of a streak camera. The streak image corresponding to the spectrum in Fig. 5-26 is shown in Fig. 5-27. Fig. 5-28 is the corresponding intensity profile.

Fig. 5-27 The Streak camera image of the mode-locked pulses corresponding to Fig. 5-26

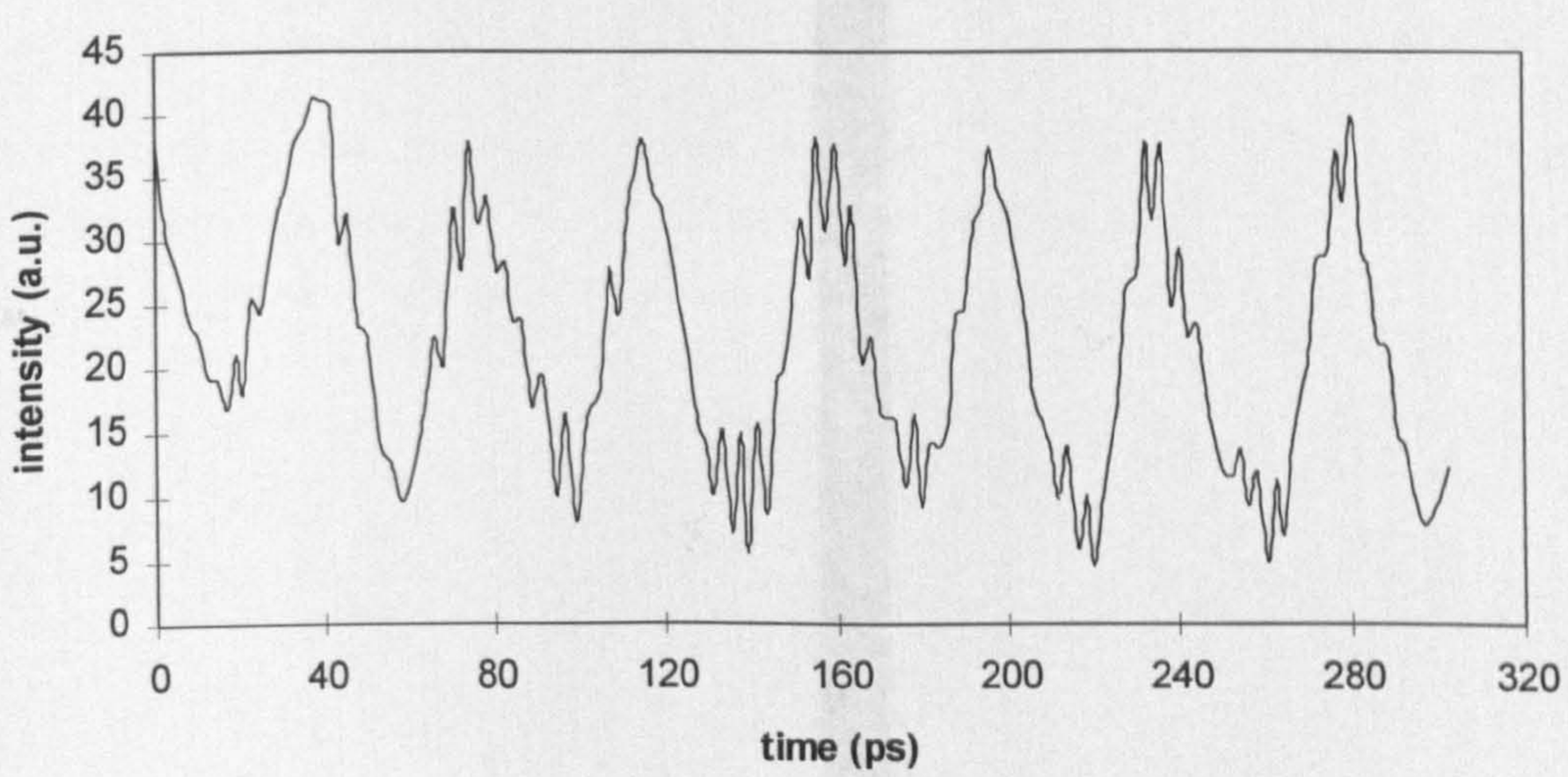

Fig. 5-28 Intensity profile corresponding to the image in Fig. 5-27.

Because the device is operated CW the streak camera can only work in the single shot mode, i.e., the camera is switched on for a time window of 1ns and the light intensity profile in this period of time is recorded. The signal/noise ratio cannot be improved by averaging due to the lack of trigger signal to synchronise the camera to the pulses. The recorded signal is therefore quite noisy. The consequence is that the pulse width values vary. The pulse train passes through the pumped output waveguide before

arriving at the streak camera. Except for the amplification and possible pulse shaping effects, the spontaneous emission in the output waveguide will affect the property of the pulse train. One of the effects is that it forms a background light intensity, so that the measured intensity modulation depth of the output pulses is not 100%. Another effect is that the spontaneous emission imposes both random phase (adding to their timing jitter) and amplitude noises onto the pulses.

To determine the pulse parameters from the intensity profile, the resolution of the streak camera has to be considered. The measurement is carried out with a time window of 1ns. In the 1ns window mode the resolution of the streak camera is about 12ps HMFW. This result in a broadening of measured pulse profile.

Fig. 5-29 The streak camera image of mixed mode-locking and self-pulsation observed in dual absorder CPM SRL.

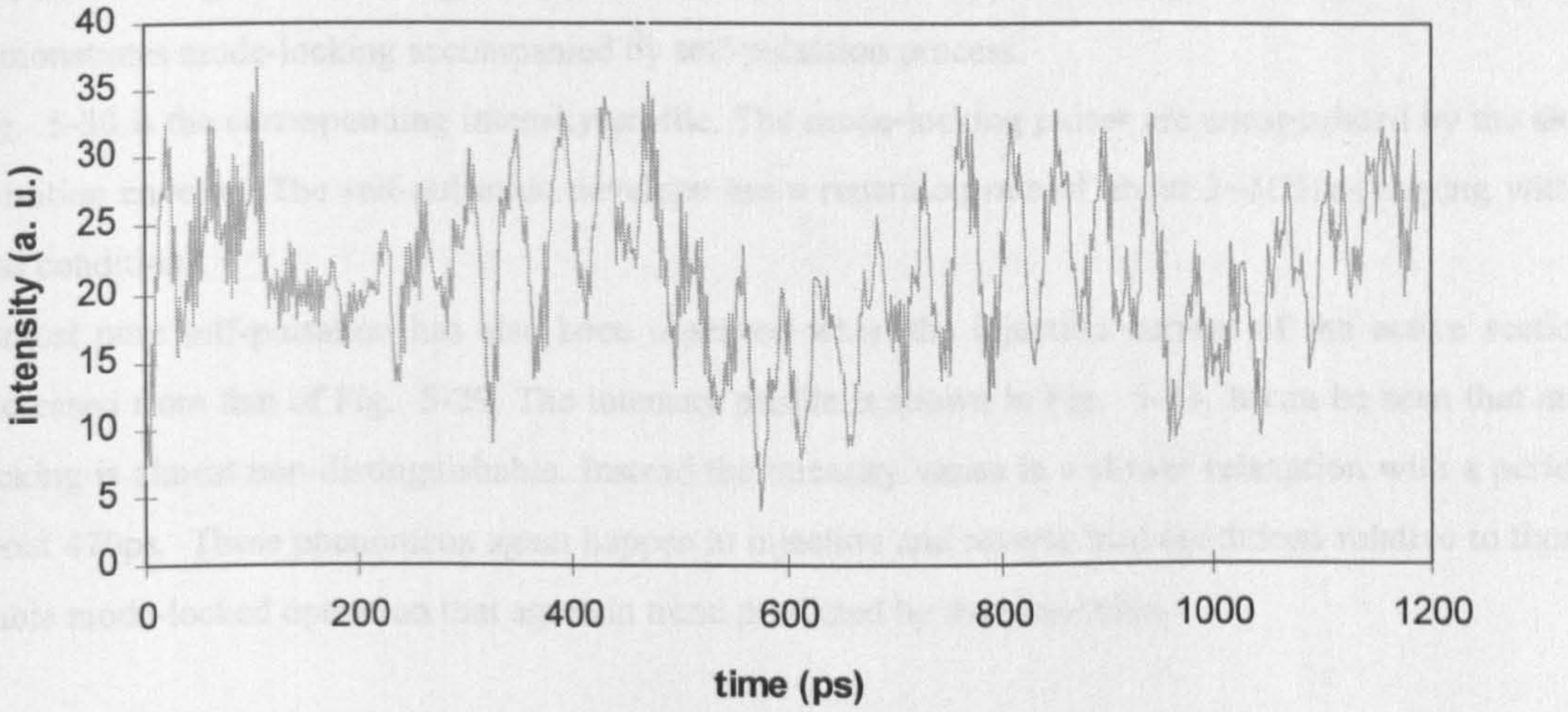

Fig. 5-30 The intensity profile of the mixed mode-locking and self-pulsation pulses shown in Fig. 5-29.

The real pulse width $\Delta\tau$ should be deduced by averaging the pulse width values measured from many peaks in the signal to get a measured pulse width value $\Delta\tau_m$, and be calculated according to the following formula (assuming near-Gaussian pulse shape)

$$\Delta\tau = \sqrt{\Delta\tau_m^2 - \tau_s^2} \qquad \text{Eq. 5-32}$$

where τ_s is the resolution of the streak camera. The typical value of $\Delta\tau_m$ is 15ps so the real pulse width $\Delta\tau$ should be about 9ps. The pulse width-bandwidth product is therefore about 0.45, which agrees with the computer simulation value well and is reasonably close to the ideal value of 0.316.

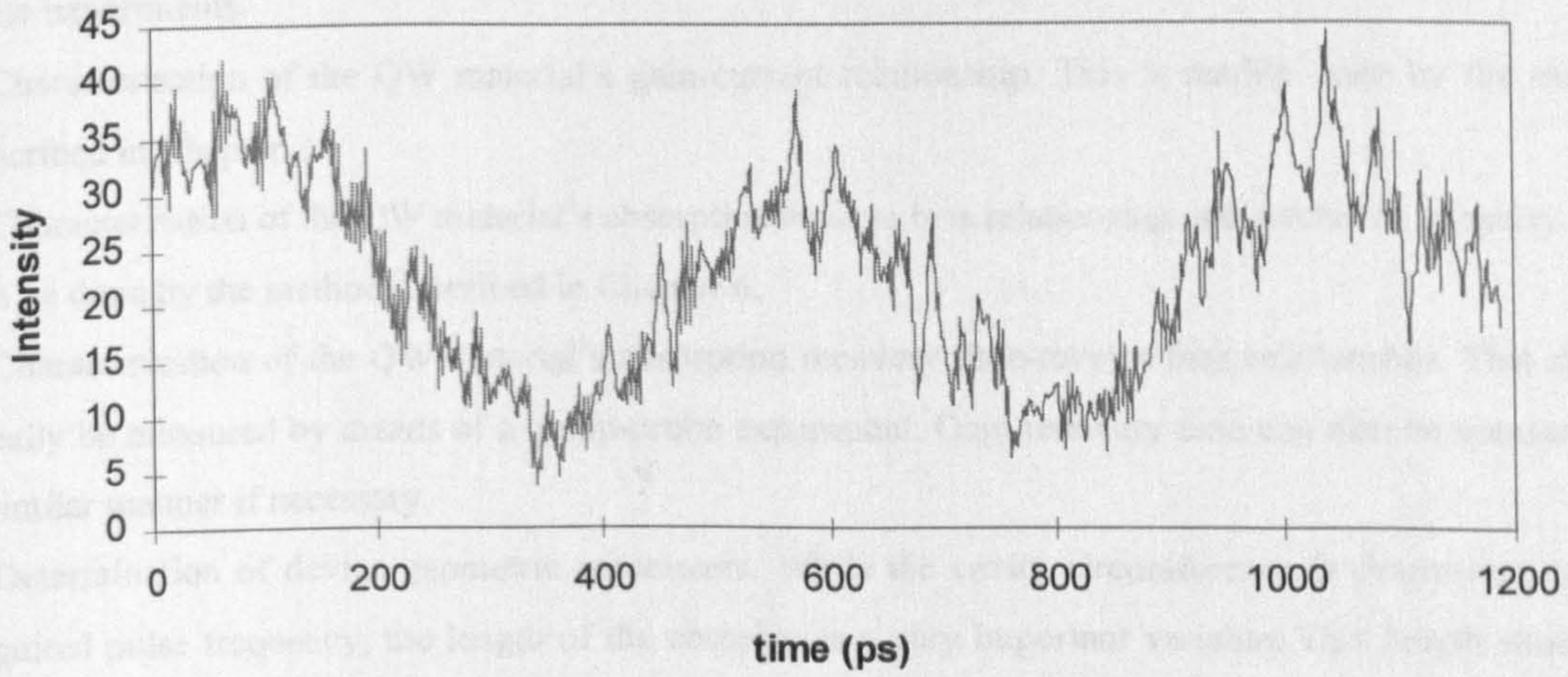

Fig. 5-31 The intensity profile of self-pulsation.

The streak image shown in Fig. 5-29, taken at increased reverse bias voltage as compared to Fig. 5-27, demonstrates mode-locking accompanied by self-pulsation process.

Fig. 5-30 is the corresponding intensity profile. The mode-locking pulses are encapsulated by the slower pulsation envelop. The self-pulsation envelope has a repetition rate of about 2~3GHz (varying with the bias condition).

Almost pure self-pulsation has also been observed when the injection current of the active section is decreased from that of Fig. 5-29. The intensity profile is shown in Fig. 5-31. It can be seen that mode-locking is almost non-distinguishable. Instead the intensity varies in a slower relaxation with a period of about 470ps. These phenomena again happen at injection and reverse bias conditions relative to those of stable mode-locked operation that agree in trend predicted by the simulation.

5-4 Summary

The mode-locking properties of semiconductor ring lasers has been studied both theoretically and experimentally. In the theoretical side, by means of computer simulations based on both the lumped element model and the travelling wave model, an in-depth understanding of the passive mode-locking process in SRLs has been achieved. The mode-locking properties of three cavity configurations, namely the symmetric configuration, the asymmetric configuration and the newly proposed dual absorber configuration, have been compared. It is shown that in terms of all major considerations, i.e., wider mode-locked region, shorter pulse width and also suitability for OTDM application, the dual absorber configuration is superior to the others.

The study enables the prediction of the operational modes of an SRL with intra-cavity saturable absorber given the gain section injection current and absorber reverse bias voltage, provided sufficient information concerning the semiconductor QW material is used. The following procedures for designing passive mode-locked SRL are therefore recommended, although some of them were not available in the course of these experiments.

1)Characterisation of the QW material's gain-current relationship. This is readily done by the method described in Chapter 2.

2)Characterisation of the QW material's absorption-reverse bias relationship and saturation property. This can be done by the method described in Chapter 6.

3)Characterisation of the QW material's absorption recovery time-reverse bias relationship. This should ideally be measured by means of a pump-probe experiment. Gain recovery time can also be measured in a similar manner if necessary.

4)Determination of device geometric parameters. While the cavity circumference is determined by the required pulse frequency, the length of the absorber is a very important variable. This length should be chosen so that sufficient unsaturated absorption is available at a reasonable reverse bias voltage and so that the device can be operated stable mode-locked at a reasonably high injection current, to give high pulse power and short pulse. Yet the unsaturated absorption should not be not too large for the pulse to

saturate the whole absorber. The length of the absorber should therefore be carefully optimised by means of the computer simulation.

Experimentally, mode-locked SRLs with both asymmetric and dual absorber, dual MMI coupler configurations have been successfully fabricated and operated. The former configuration shows operational properties very similar to those predicted by the computer simulation. The pulse width of the la"er configuration has been measured by means of a streak camera to be about 9ps with a time-band width product of 0.45. Mode-locking mixed with self-pulsation and pure self-pulsation are also observed in injection and reverse bias conditions, agreeing with simulation.

6 Electro-absorption (EA) Modulators

6-1 The Operational Principle of EA Modulators

In a semiconductor quantum-well (QW) structure, the motion of carriers (electrons and hole) in the direction perpendicular to the QW is confined by the potential well so they exist in bound states, if their kinetic energy is not enough to overcome the potential barrier[1,2]. These bound states have discrete energies, marked by E_n, with n=1,2,...,N the number of the quantum states, and the distribution of carriers in a bounded state is described by the state's wave function, which can be found by solving the one-dimensional (1-D) Schrodinger Equation under the boundary condition at the walls of the well. A square QW system is illustrated in Fig. 6-1 with electron states in the conduction band and the hole states in the valence band.[3]

The energies E_n are usually measured relative to the lowest energy of the band in which the particle exists, i.e., for electrons E_n are from the bottom of the conduction band and for holes E_n are from the top of the valence band. E_1, the lowest of all, has non-zero values because of the principle of uncertainty.

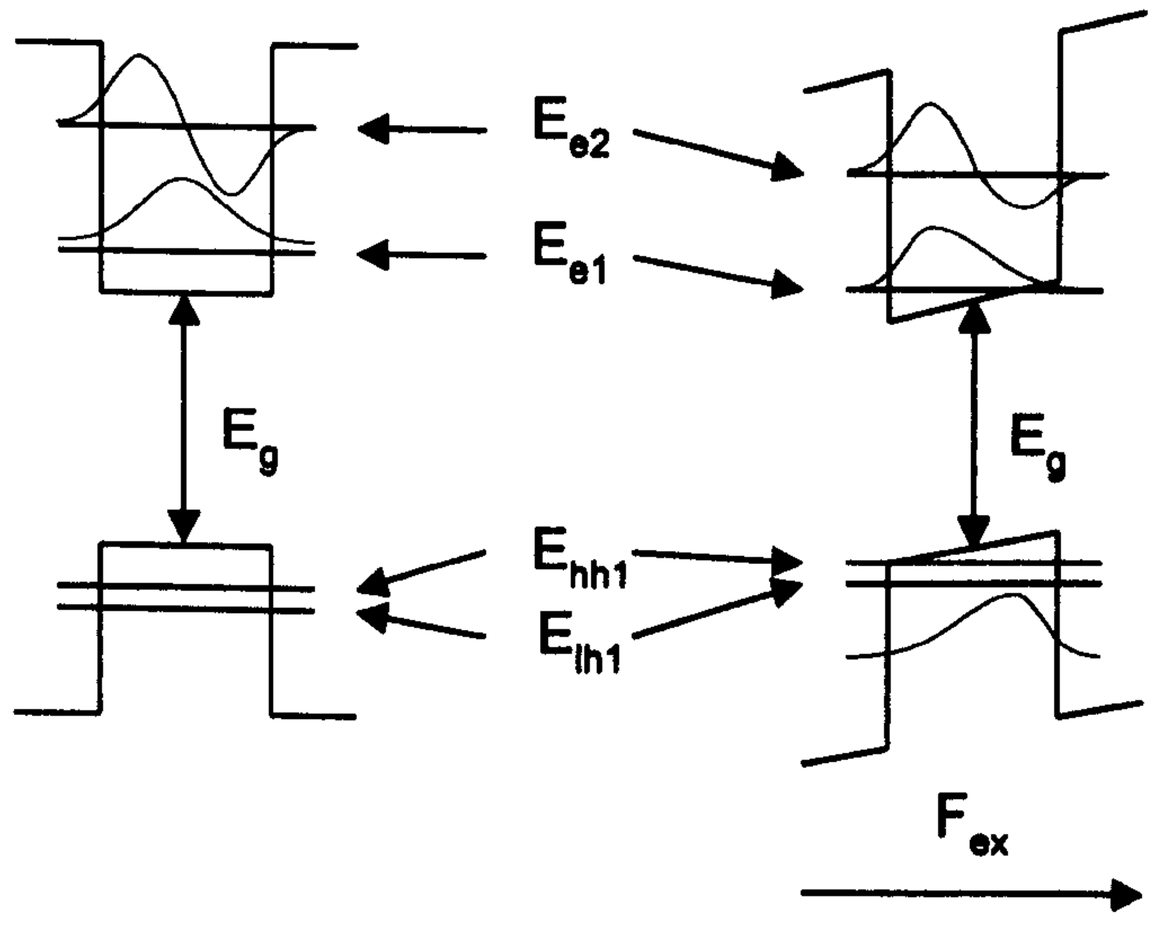

Fig. 6-1 Quantum-well system (a)without external electric field, and (b)with external electric field F_{ex}.

---

[1] Weisbuch, C. and Vinter, B., 'Quantum semiconductor structures:fundamentals and Applications', San Diago: Academic Press, c1991

[2] Zory, P. Jr., edit, 'Quantum-well laser', London : Academic Press, c1993.

[3] Schmitt-Rink, S., Chemla, D. S., and Miller D. A. B.,'Linear and non-linear optical properties of semiconductor quantum wells', Advances in Physics, 1989, VOL.12, No.2, pp.89-188.

There are two kinds of holes in the semiconductor, the light hole and the heavy hole. Each has different effective mass and also different E_n.

An incident photon may be absorbed if its energy is sufficient to excite a electron from the valence band to the conduction band, creating a electron-hole pair. The lowest energy absorption occurs when the electron-hole pair are bound together to form an exciton [1]

$$E_p=E_{hh1}+E_{e1}+E_g-E_{ex} \qquad \textbf{Eq. 6-1}$$

where E_{hh1} is the first heavy hole state energy, E_{e1} is the first electron state energy, E_g is the bandgap of the well material, E_{ex} is the exciton binding energy. E_p is known as the effective absorption edge. For photons of lower energy the QW is rather transparent.

When a semiconductor quantum-well (QW) structure is placed in a electric field F_{ex} perpendicular to the QW layer, the potential well is tilted by the electric field. Solving such a system results in lower energy of the bounded states and changed shape of the wave function. The effect is well-known as "quantum-confined Stark effect (QCSE)" [2].

The decrease of the lowest energies of electrons and hole results in the shift of effective absorption edge towards the low energy or long wavelength direction. As a result the absorption at those energies below the original effective band edge E_p is increased. In QW structures, the lifetime of excitons is greatly increased over that in the bulk material due to quantum confinement, the resonance peak caused by exciton absorption at energy E_p thus becomes quite sharp, which enhances the absorption changes caused by QCSE. These effects can be used to modulate the intensity of the light propagating through the QW system and is the basis of QW electroabsorption (EA) modulators.

EA modulators in various III-V semiconductor material systems[3,4] have been under intensive research in recent years. Wood et al studied the basic principles of device design and performance limiting factors[1]. Except for the junction capacitance, an important effect in EA modulators is the field screening effect of the photogenerated carriers under high incident light power[5,6] . This effect reduces the saturation power and high frequency response under high optical power. Various measures have been employed to reduce

---

[1] Wood, T. H., 'Multiple quantum well waveguide modulators', Journal of Lightwave Technology, VOL. 6, No.6, 1988, pp.742-757.

[2] Schmitt-Rink, S., *et al*, 'Linear and non-linear optical properties of semiconductor quantum wells', Advances in Physics, 1989, VOL.12, No.2, pp.89-188.

[3] Macbean, M. D. A., 'Multiple Quantum Well Structures as Optical Waveguides', Ph.D Thesis, University of Glasgow. 1986.

[4] Devaux, F., et al, 'InGaAsP/InGaAsP multiple-quantum-well modulator with improved saturation intensity and bandwidth over 20GHz', IEEE Photonics Technology Letters, VOL.4, NO.7, 1992, pp.720-723.

[5] Suzuki, M., Tanaka, H., and Akiba, S., 'Effect of hole pile-up at heterointerface on modulation voltage in InGaAsP electroabsorption modulators', Electronics Letters, VOL.25, NO.2, 1989, pp.88-89.

[6] Wood, T. H., et al, 'Electric field screening by photogenerated holes in multiquantum wells: a new mechanism for absorption saturation', Applied Physics Letters, VOL.57, NO.11, 1990, pp.1081-1083.

this effect. These included the introduction of strain in the QW[1] to reduce valence band offset, the use of shallow quaternary/quaternary QWs[2], etc.

EA modulator have been applied in many uses such as the generation of transform-limited short optical pulses[3]. Monolithic integration with DFB lasers[4] and laser amplifiers[5] has been realised. Bandgap shifted MQW EA modulators have also been fabricated in the department[6].

6-2 Design and Fabrication of the device

Practical modulators are required to have wide bandwidth or fast response time, high saturation energy, low insertion loss and high modulation index. Some of these requirements are contradictory to others, which causes difficulties in wafer design. For a modulator to be integrated on the same wafer as a laser, the problem is further complicated by the trade-off between the two devices. For example, a high modulation index would require a large number of QWs in the wafer design, whereas this could increase the threshold current of the laser. A modulator with fast response should have small device capacitance, which can be achieved with a thicker intrinsic barrier layer, but in the mean time the modulation index is jeopardised because thicker intrinsic layer means smaller electric field for the same modulation voltage. While the capacitance of the material itself is important, equally important are the distributed parameters (capacitance or inductance) introduced by the electrodes, bonding wires, etc. These often result in serious set back in device performance.

In this section it is sought to discuss the above mentioned problems exposed by the experiment data obtained from different devices. Approaches of improvement is presented as a result.

6-2-1 Materials

The modulator investigated were based on DQW laser materials used for the ring lasers. Two materials were investigated. As described in Chapter 2, MBE material B429 has a SCH structure with doped quantum wells and cladding layers but un-doped barrier layers. MBE material B500 also has a SCH structure but with un-doped wells, un-doped $Al_{0..2}Ga_{0.8}As$ barrier layer and two un-doped $Al_{0..4}Ga_{0.6}As$ buffer layers between the

---

[1] Czajkowski, I. K., et al, 'Strain-compensated MQW electroabsorption modulator for increased optical power handling', Electronics Letters, VOL.30, NO.11, 1994, pp.900-901.

[2] Devaux, F., et al, 'InGaAsP/InGaAsP multiple-quantum-well modulator with improved saturation intensity and bandwidth over 20GHz', IEEE Photonics Technology Letters, VOL.4, NO.7, 1992, pp.720-723.

[3] Yamada, E., Wakita, K., and Nakazawa, M., '30GHz pulse train generation from a multiquantum well electroabsorption intensity modulator', Electronics Letters, VOL.29, NO.10, 1993, pp.845-847.

[4] Tanaka, H., Suzuki, M., and Matsushima, Y., 'Optical short pulse generation by a DFB laser/EA modulator integrated light source', IEEE J. of Quantum Electronics, VOL.29, NO.6, 1993, pp.1708-1713.

[5] Koyama, F, et al, 'GaInAs/GaInAsP strained quantum well monolithic electroabsorption modulator/amplifier by lateral bandgap control with nonplanar substrates', Electronics Letters, VOL.29, NO.24, 1993, pp2104-2105.

[6] Lullo, G., McKee, A., McLean, C. J., Bryce, A. C., Button, C. and Marsh, J., 'Fabrication of electroabsorption optical modulators using laser disordered GaInAs/GaInAsP multiple quantum well structures', Electronics Letters, 1994, VOL.30, NO.19, pp.1623-1625

barrier and the doped $Al_{0..4}Ga_{0.6}As$ cladding layers. So optically they had the same waveguide structure. But electrically material B500 has a thicker un-doped layer which will reduce the device capacitance.

6-2-2 Device Structure

The device structure of the modulators is illustrated in Fig. 6-2.

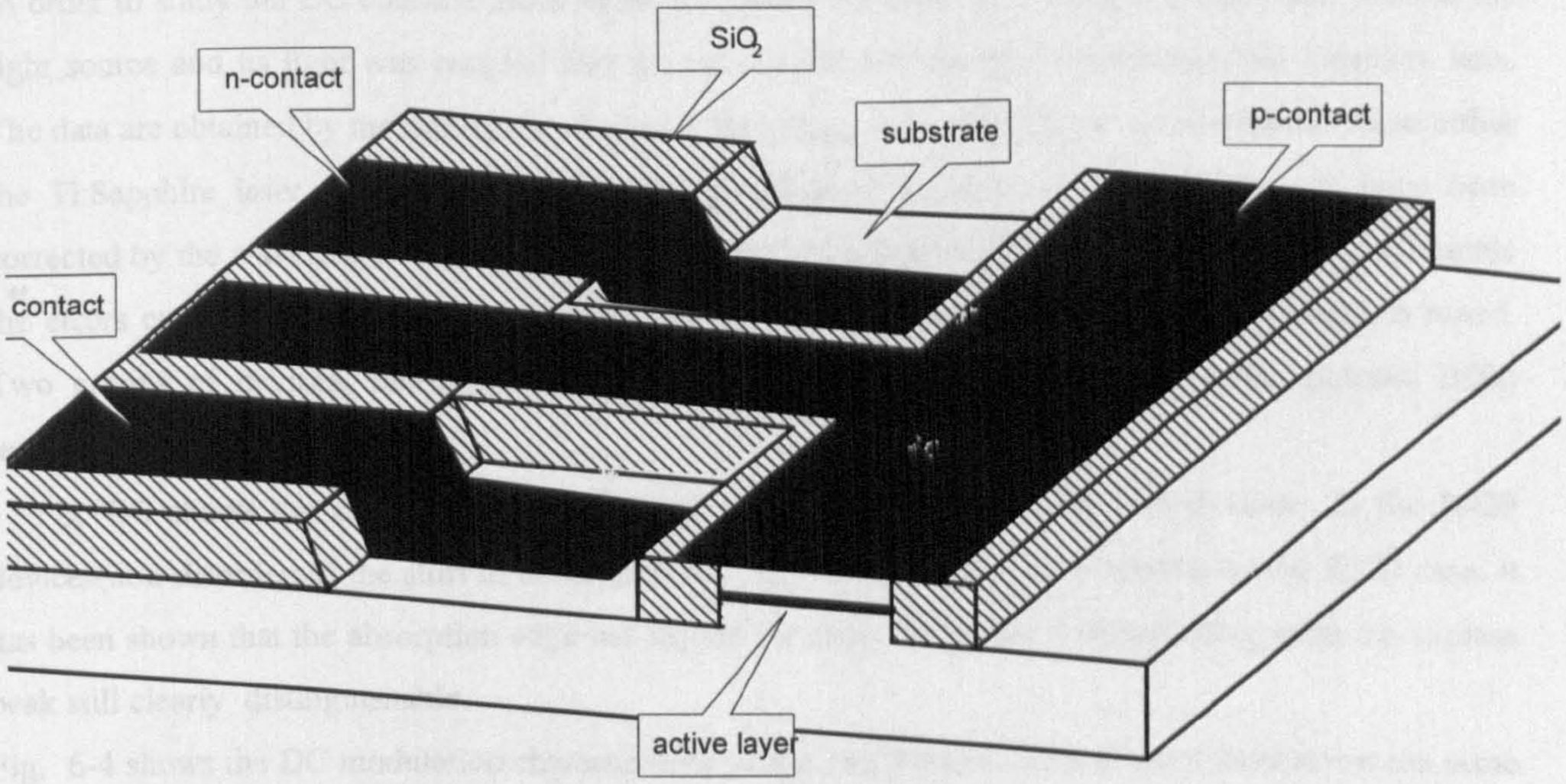

Fig. 6-2 Electroabsorption Modulator with high frequency electrode design.

The modulator waveguide is a deeply etched ridge waveguide. The waveguide width is 5μm. The reason for the deep etch is two fold. Firstly, this will enable a thick insulator layer to be deposited between the p-contact metallisation and the n substrate, thus reduce the capacitance of the contact pad. Secondly, the deep etch through the lower cladding down to the substrate makes it possible to make n-contact on the same side of the p-contact, as shown in Fig. 6-2. The p-contact and the n-contact pads along its two sides form a microwave waveguide. This is intended for matching the contact pad geometry with that of the microwave probe of the Hewlett-Packard network analyser. But careful design of the waveguide should also benefit the impedance matching between the device and the microwave source and future mounting on micro strip line plates.

6-2-3 Fabrication

The waveguide is defined by photolithography and dry etching. A 2μm thick SiO_2 layer is then deposited and the windows for n-contact are opened by photolithography and dry-etching in C_2F_6 plasma. Because the exposed semiconductor surface for n-contact was formed by dry-etching and may have subjected to dry-etch damage, a wet-etch step is employed to remove about 0.1μm of the semiconductor to improve n-contact quality. Windows for p-contact were opened by the self-aligned process described in Chapter 2.

The two types of contacts on the same side of the wafer were deposited separately. Both are proved to be good ohmic contacts.

6-3 Characterisation Results

6-3-1 DC Modulation Characteristics

In order to study the DC characteristics of the modulators, a tuneable Ti:Sapphire laser was used as the light source and its light was coupled into the waveguide modulators by a microscopic objective lens. The data are obtained by measuring the change of the output light power from the waveguide when either the Ti:Sapphire laser wavelength or the applied voltage is changed. The measured data have been corrected by the wavelength response of the laser/detector without the modulator waveguide to eliminate the errors caused by the variation of detector responsivity and laser power when wavelength is tuned. Two groups of devices, fabricated on non-disordered material B429 and disordered material B500 respectively, are measured.

Fig. 6-3 shows the absorption coefficient vs. wavelength curves of the two devices.. In the B429 devices(non-disordered) the shift of absorption edge due to QCSE is clearly shown. In the B500 case, it has been shown that the absorption edge has shifted for about 40nm due to disordering, with the exciton peak still clearly distinguishable.

Fig. 6-4 shows the DC modulation characteristics of the two devices. Both devices have about the same length of 600μm. For the data to be comparable, the wavelength of the incident light is set at the band edge of the device to be measured (870nm for the non-disordered and 825nm for the disordered devices, respectively). The device made on B429 has a maximum modulation index of 8.8dB/V when applied voltage varies from 2.0 to 4.0V, compared with the smaller value of 6.6dB/V of the B500 device, which can be attributed to the higher electric field in the B429 devices due to thinner un-doped layer in its wafer structure. For the B429 device a total modulation depth of about 23dB is obtained when the voltage varies from 0 to 6V.

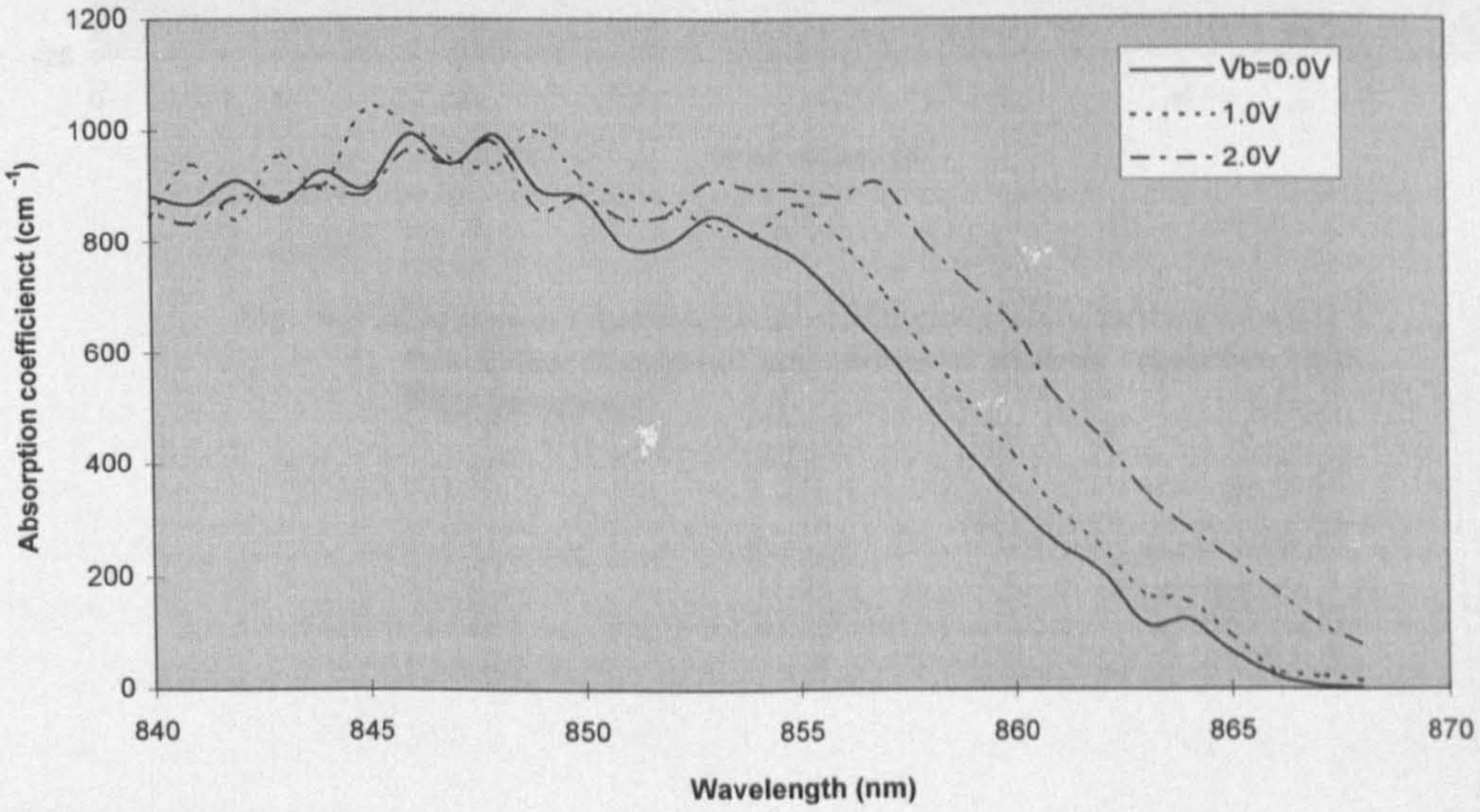

(a)

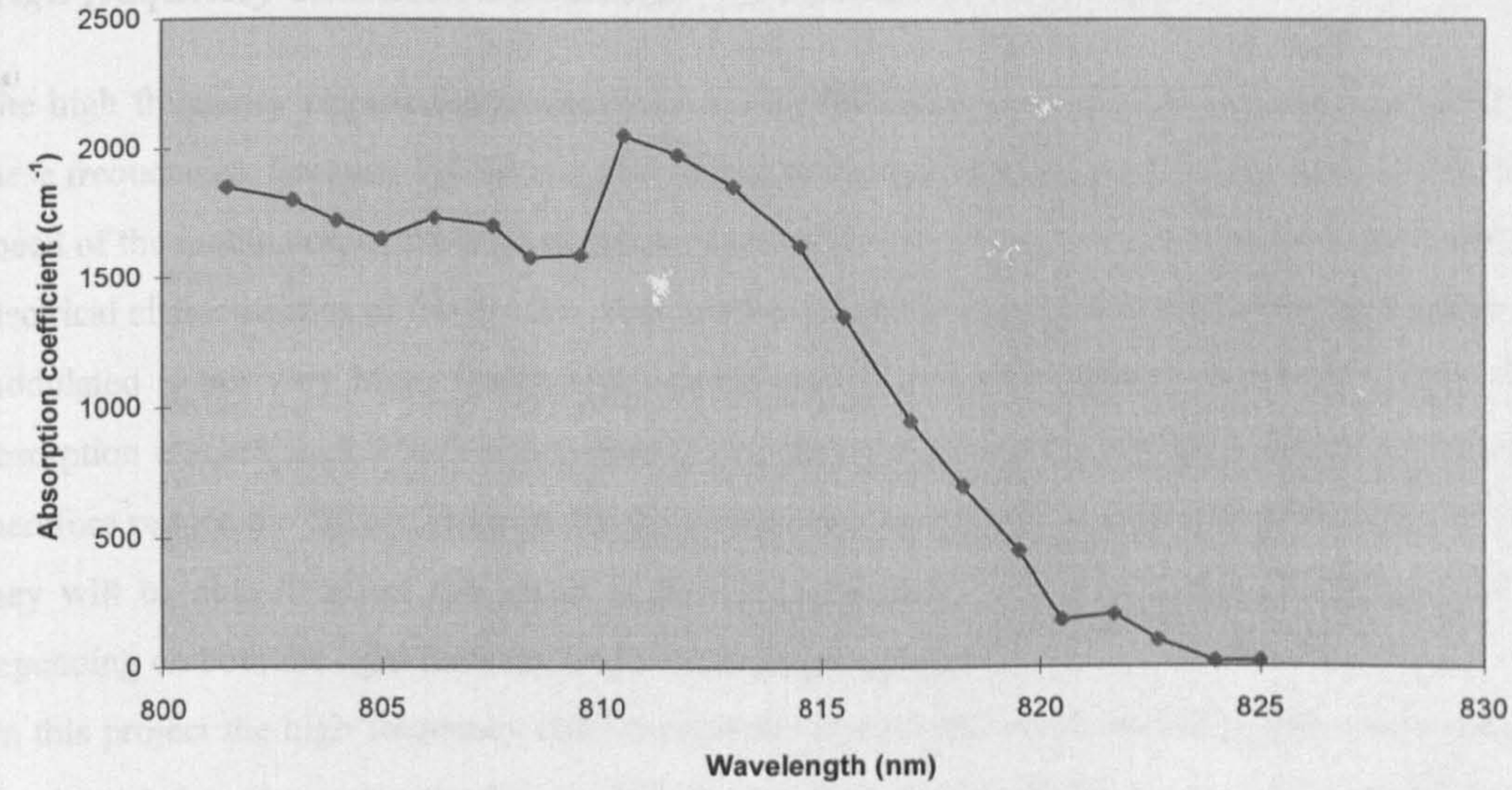

(b)

Fig. 6-3 Absorption spectrum of the modulator waveguides fabricated on (a) material B429 and (b)disordered material B500.

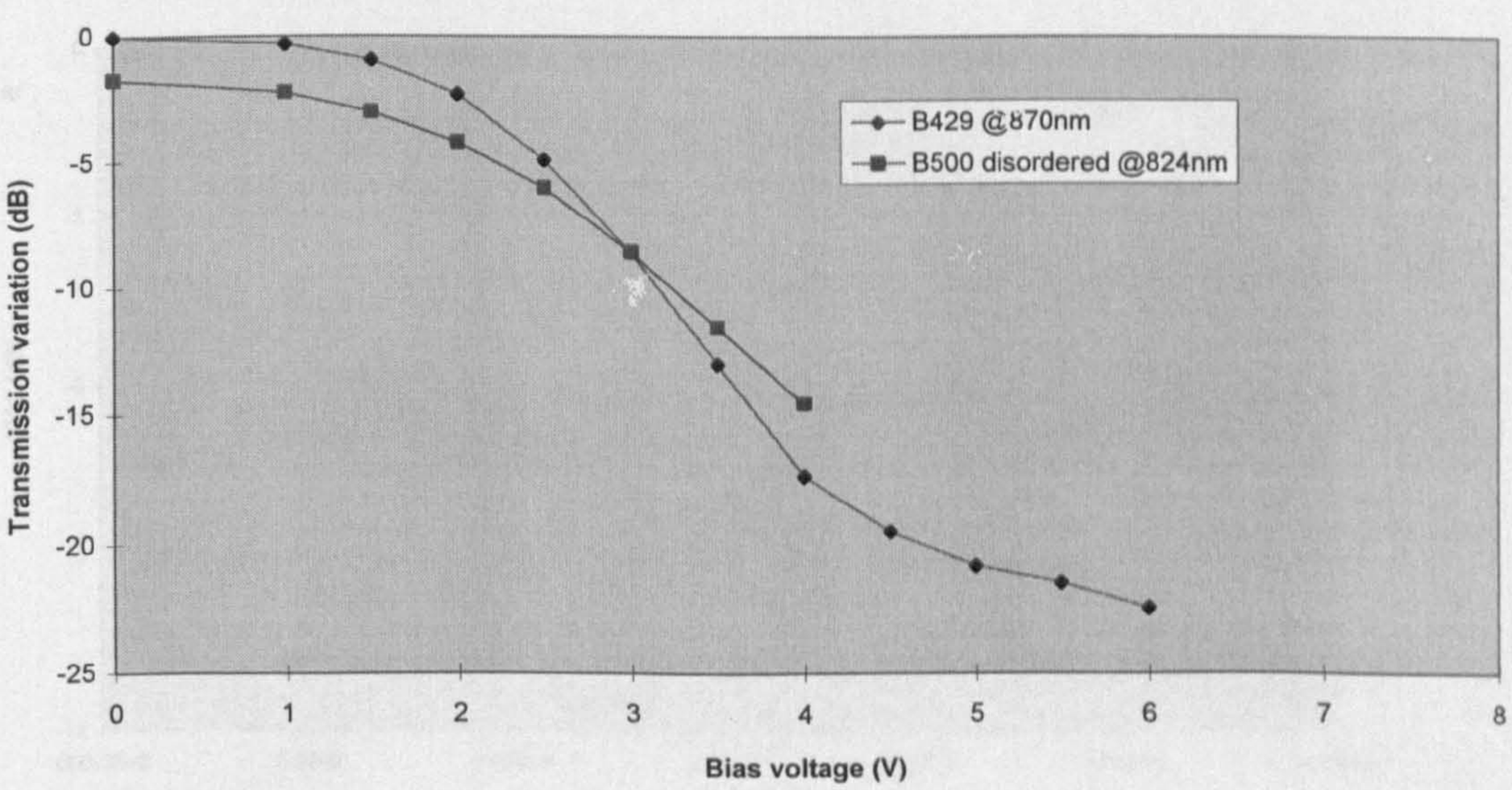

Fig. 6-4 Modulation Characteristics of the modulators fabricated on the two different material and measured at their respective band edge wavelength.

6-3-2 Capacitance and High Frequency Characteristics

High frequency characterisation and equivalent circuit model

The high frequency electrical characteristics of the modulators is important in order to operate them at these frequencies. Because QCSE is a very fast phenomenon with a time constant in the order of 1ps, the speed of the modulator, or the highest frequency at which it can be used, is essentially determined by the electrical characteristics of the device. This applies generally in situations where the light intensity being modulated is not very high. Under high optical power, the photocarriers generated by the inter-band absorption reaches such a high concentration that they can screen the applied external electric field and therefore reduce the QCSE. Because these carriers have escape time constants in the range of 10-100ps, they will be able to affect the speed of the EA modulator [1,2] in the frequency range of 10-30GHz, depending on both the light intensity and the carrier escape time.

In this project the high frequency (HF) measurement was carried out on HP8100B network analyser. It was intended to determine the HF equivalent circuit of QW modulators as a one terminal microwave network so that an understanding of the device's HF characteristics can be achieved and better devices can be designed in the future.

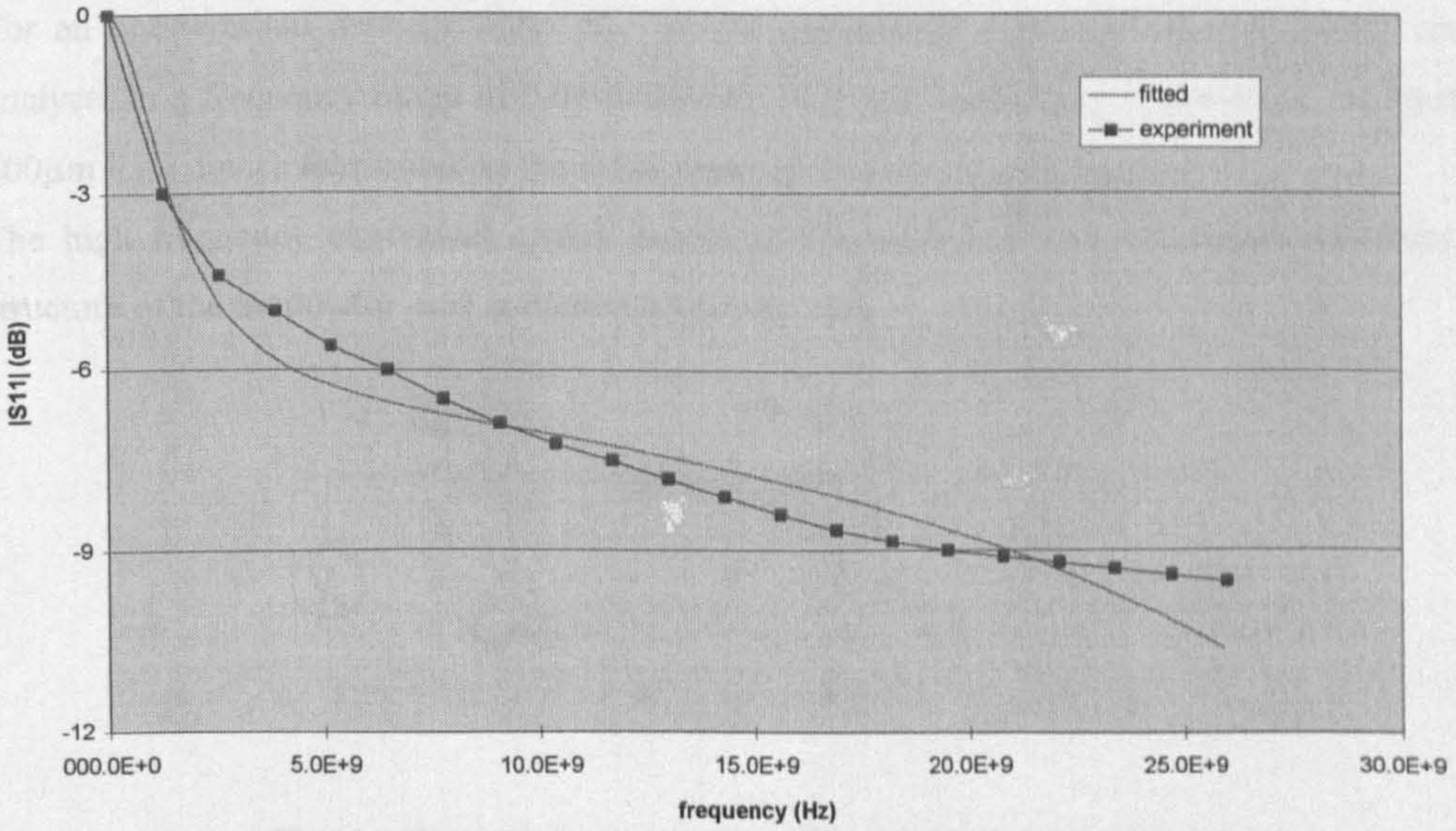

(a)

[1] Suzuki, M., *et al*, 'Effect of hole pile-up at heterointerface on modulation voltage in GaInAsP electroabsoption modulators', Electronic Letters, VOL.25, pp.88-89, 1989.

[2] Wood, T. H., 'Electric field screening by photogenerated holes in multiple quantum well s: A new mechnism for absorption saturation', Appl. Phys. Lett., VOL.57, pp.1081-1083.

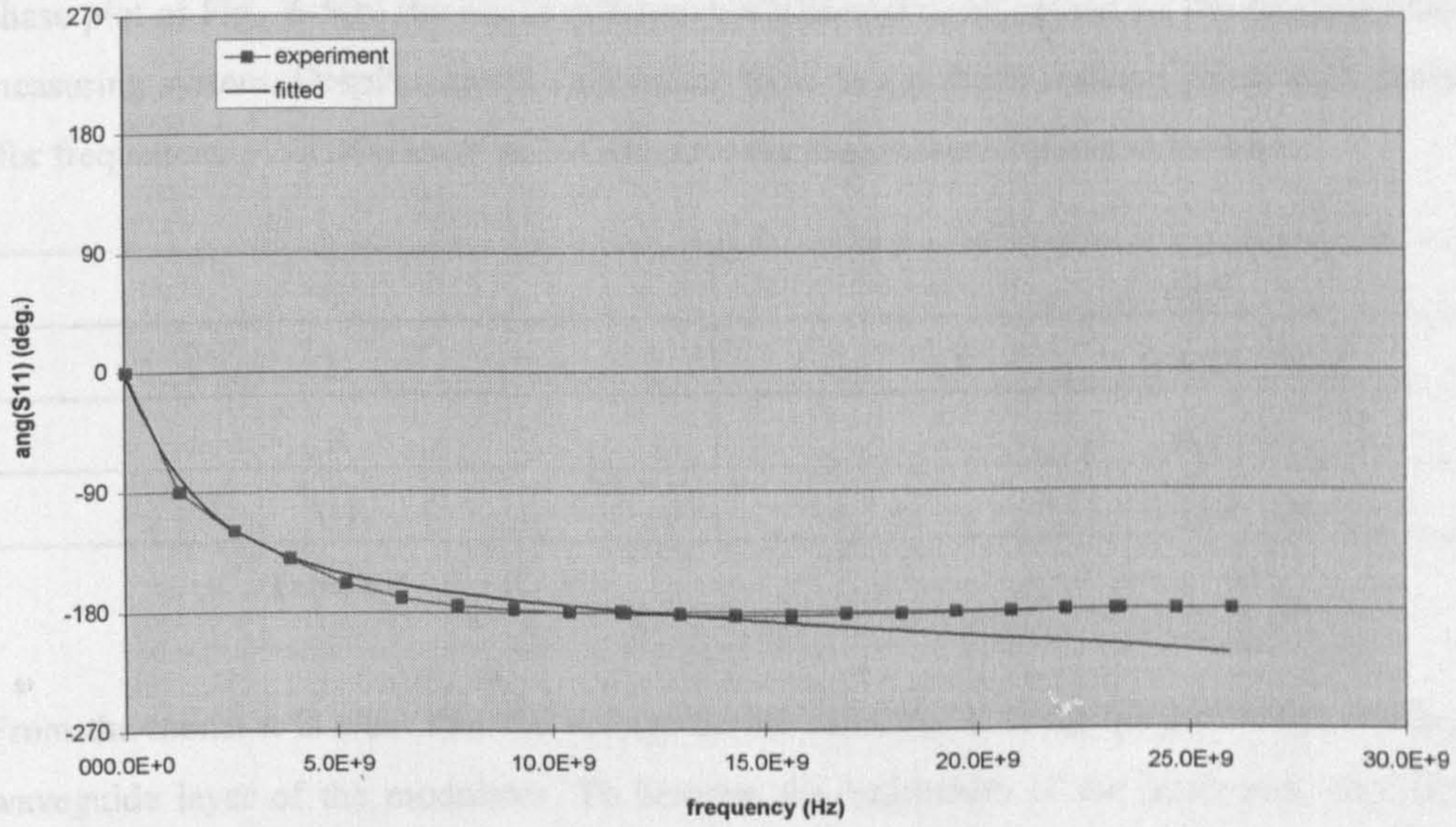

(b)

Fig. 6-5 Measured frequency response of S11, (a)amplitude and (b)phase. Device material: B429.

For an one-terminal network only S_{11} of the s-parameter matrix exists and is read on the network analyser in a frequency range of 0.04 to 26GHz. A typical frequency response of S_{11} measured from a 500μm long device fabricated on the B429 material is illustrated in Fig. 6-5.

The high frequency equivalent circuit model of the modulator can be determined from the physical structure of the modulator and is illustrated in Fig. 6-6.

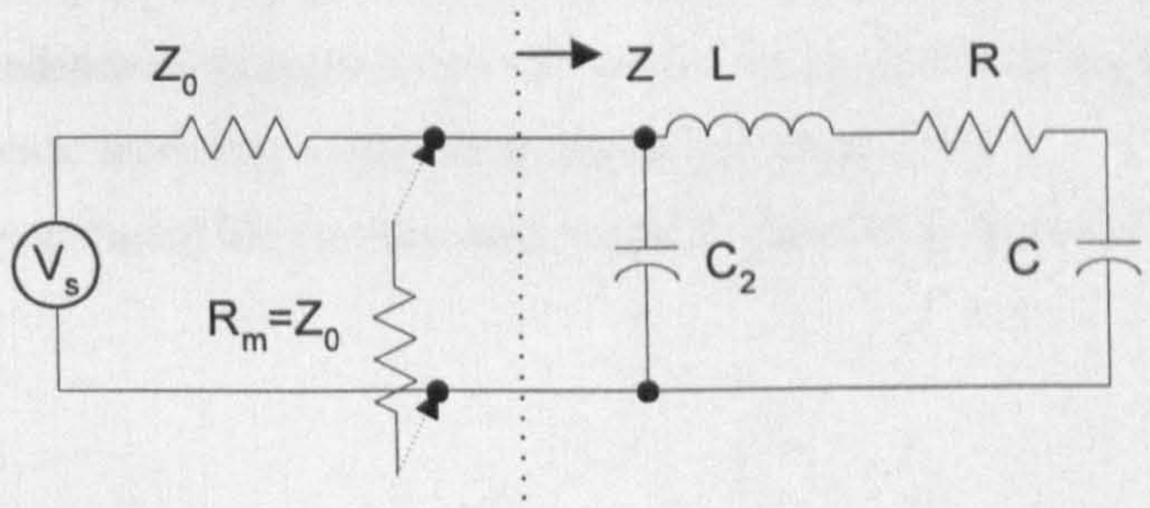

Fig. 6-6 The high frequency circuit model of the EA modulator.

In Fig. 6-6 the capacitor C stands for the junction capacitance of the modulator. The resistor R is the combination of ohmic contact resistance and the semiconductor's body resistance. L is the inductance of the input contact metal stripe. C_2 is the capacitance between the contact pad and the ground (n^+-substrate).

The S_{11} parameter of such a circuit can be easily calculated and the element values are adjusted to fit the experimental curve. The solid lines in Fig. 6-5(a) and (b) are the fitted S_{11} response which correspond to the parameter values listed in Table 6-1. The error between fitted and the measured amplitude values of

S_{11} is less than 1dB. The phase difference is less than 10 degrees in frequencies up to ~23GHz. In the phase plot of Fig. 6-5(b) the phase difference is believed to be caused by the residual phase error of the measuring system. Despite careful calibration, there is a positive residual phase shift increasing from 0° (for frequencies <20GHz) to10° at 23GHz, causing the measured phase to increase.

C	1.9pF
L	0.1nH
R	9Ω
C1	0.1pF

Table 6-1

From the model it is clear that the voltage across capacitor C is the actual voltage across the un-doped waveguide layer of the modulator. To broaden the bandwidth of the modulator, the following efforts should be made to maximise this voltage at high frequencies.

1)Reducing the serial resistance R. The value of R mainly depends on the quality of the ohmic contacts, especially that of the p^+-contact because the n^+-contact (with substrate) is much larger in area. Because the bulk resistance of semiconductor material, mainly that of the cladding layers which have moderate dopant concentrations, also contributes to R, it is appropriate to use relatively heavier doped cladding layers than that may be used in a laser structure and the cladding layers should be kept reasonably thin. The resistance of device should be able to be reduced to several ohms. In order to reduce the skin effect the metal contact layers should be made thicker, probably by plating.

2)Reducing the contact capacitance C_2 by using thick insulator layer. Here the value of C_2 has been kept small by the thick SiO_2 insulating layer comparing to the value of C=2pF of the junction.

3)Maintaining impedance matching between the source and the device by shunting a R_m=50Ω resistor to the input of the device, preferably a integrated resistor free of parasitics.

4)Most importantly, reducing the junction capacitance C. This will be discussed below.

The junction capacitance

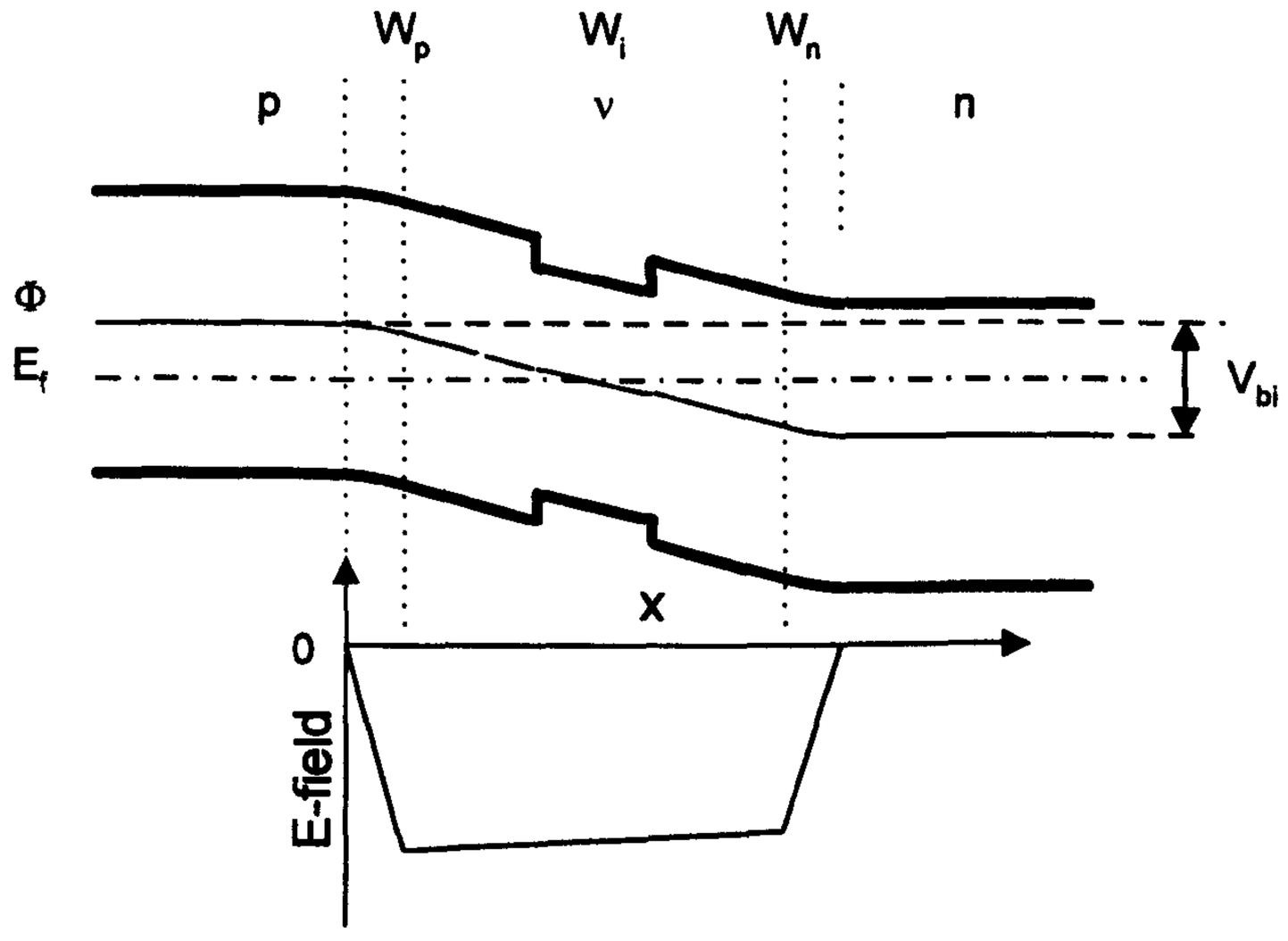

Fig. 6-7 The band diagram and electric field in the p-ν-n junction in material B500.

Because of n-type background doping when growing the 'intrinsic' layer, the MBE material B500 used in the project has p-ν-n junction structure shown in Fig. 6-7 The band diagram and electric field in the p-n-n junction in material B500. Assuming the doping concentration in the ν layer is small so that it is totally depleted, the characteristic capacitance (i.e., capacitance per unit area) of such a structure can be calculated by the following formula, [1]

$$C = \frac{1}{\frac{W_p}{\varepsilon_{sp}} + \frac{W_i}{\varepsilon_{si}} + \frac{W_n}{\varepsilon_{sn}}} \qquad \textbf{Eq. 6-2}$$

where W_p and W_n are the width of the space-charge region in the p and n region respectively, and W_i is the ν layer thickness. ε_{sp}, ε_{si} *and* ε_{sn} are the dielectric constants of the respective regions. Values of W_p and W_n can be found by integrating Poisson's equation

$$\frac{d^2\Phi}{dx^2} = -\frac{\rho}{\varepsilon_s} \qquad \textbf{Eq. 6-3}$$

where ρ is the space charge density. Under room temperature and in the depletion region, ρ equals electron charge *e* times the doping concentrations, i.e., acceptor concentration N_a in p region and minus donor concentrations $-N_\nu$ and $-N_d$ in ν and n regions. Boundary condition of

---

[1] Sze, S. M., 'Physics of semiconductor devices', 2nd ed. New York : Wiley, c1981.

$$\Phi(W_p + W_i + W_n) - \Phi(0) = V_{bi} \qquad \textbf{Eq. 6-4}$$

and charge-neutrality condition

$$N_a W_p = N_v W_i + W_n N_d \qquad \textbf{Eq. 6-5}$$

should be satisfied by the final solution. V_{bi} is the built-in potential of the junction and is determined by the difference of electrostatic potential between the two ends of the junction which in turn is determined by the doping concentrations

$$V_{bi} = \frac{e}{kT} \ln\left(\frac{N_d N_a}{n_{ip} n_{in}}\right) \qquad \textbf{Eq. 6-6}$$

where n_{ip} and n_{in} are the intrinsic carrier concentrations of the p and n region materials at temperature T. k is the Boltzmann constant. When an external reverse bias voltage V_b is applied, V_{bi} should be replaced by $V_{bi}+V_b$ in the calculations.

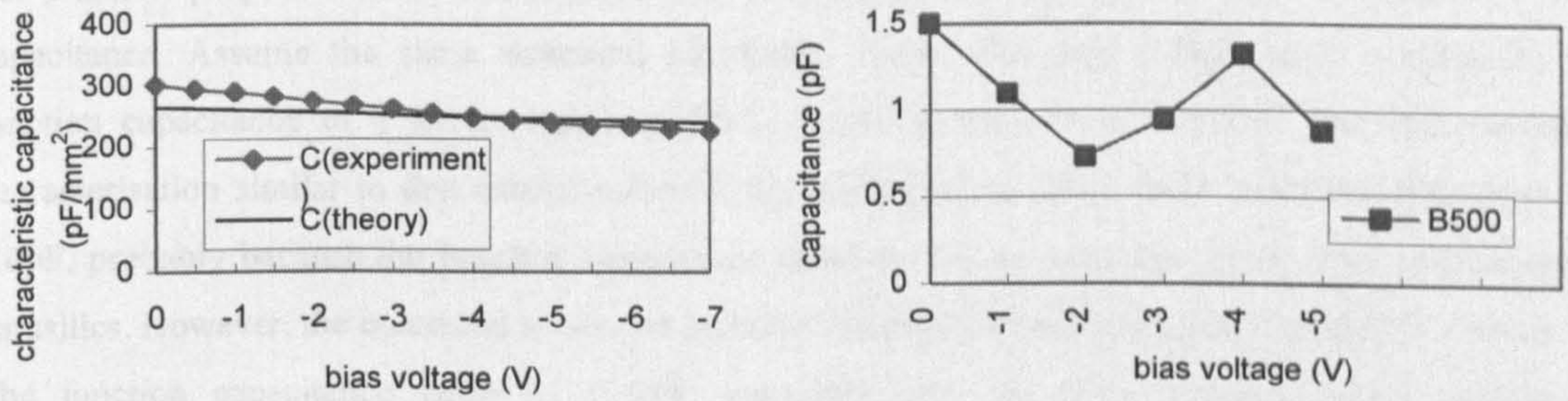

(a) (b)

Fig. 6-8 (a)The characteristic capacitance of material B500, (b)The junction capacitance of device fabricated on B500 as functions of reverse bias.

The material B500 has a 0.23μm thick ν-$Al_{0.2}G_{0.8}As$ waveguide layer and two 0.1mm thick ν- $Al_{0.4}G_{0.6}As$ spacer layer to each side of the waveguide layer. The p and n doping concentrations in the cladding layers are $5X10^{17}cm^{-3}$. The characteristic capacitance is calculated using the dielectric constant of GaAs and ignoring the small difference between the dielectric constants of layers with different Al composition. The parameters are listed in Table 6-2. The result is plotted in Fig. 6-8 along with experimental data as a function of reverse bias voltage.

The theoretical curve in Fig. 6-8(a), as expected for a p-i-n structure, indicates very robust capacitance against external bias. The experimental data (measured at 1MHz), however, shows larger zero bias capacitance and more variability with bias voltage. This indicates that the background doping in the ν-layers could be as high as $5X10^{16}cm^{-3}$, much higher than the value quoted in Tab.6-2, which was obtained from an bulk intrinsic material grown on the MBE machine earlier. The high background

doping concentration in the supposedly intrinsic layer prevents the depletion region from punching through the whole thickness of the layer, resulting in higher capacitance than predicted by the p-i-n model.

parameter	value
doping concentration in p-cladding	$5X10^{17}cm^{-3}$
doping concentration in n-cladding	$5X10^{17}cm^{-3}$
background doping concentration in ν-layers	$1X10^{14}cm^{-3}$
ν-layers thickness	0.43μm
dielectric constant	

Tab. 6-1 Material structure parameters of B500.

For practical purpose it is now possible to predict with the experimental data the modulator's junction capacitance. Assume the same structural parameters (5μm wide and 500μm long waveguide), the junction capacitance of a device made on B500 would be about only 0.85pF. The high frequency characterisation similar to that carried out with the B429 devices gives rather scattered data from 0.8-1.6pF, probably because the junction capacitance value is now so small that it has been submerged by parasitics. However, the measured values are certainly smaller than those measured on B429 samples.

The junction capacitance value of C~2pF measured from the B429 devices, which indicates a characteristic capacitance of ~800pF/mm^2, is larger than the calculated value of about 600pF/mm^2 for this material, which has about half the un-doped layer thickness as that of B500. There explanation to this phenomenon would be that the background doping in the waveguide layer is high (>$1x10^{16}cm^{-3}$) so that the total depletion region width is reduced.

According to the circuit model of Fig. 6-6, the bandwidth of the modulator when shunted by a 50Ω impedence matching resistor will be (ignoring L and C_2)

$$f_{3dB} = \frac{1}{2\pi(\frac{1}{2}Z_0 + R)C} \qquad \text{Eq. 6-7}$$

Using the R and C value obtained from the curve fitting (Table 6-1), the bandwidth of the modulator made on B429 will be about 2.46GHz. For B500 device with C~1.6pF the bandwith would about 3GHz assuming the same R value.

Waveguide profile

In addition to the wafer design, the waveguide profile would be important to maintaining small junction capacitance. As shown in Fig. 6-9, if a strip-loaded waveguide profile were used, the p-i-n junction area

would extend far wider than the waveguide width. Because the doped layers, as indicated by hatched areas, are quite conductive, under reverse bias the voltage would be applied to such a large junction area, resulting in enormous capacitance. To ensure the junction capacitance is kept as small as possible, the etch depth of the waveguide should be sufficient for the first doped layer below the un-doped waveguide layer to be reach.

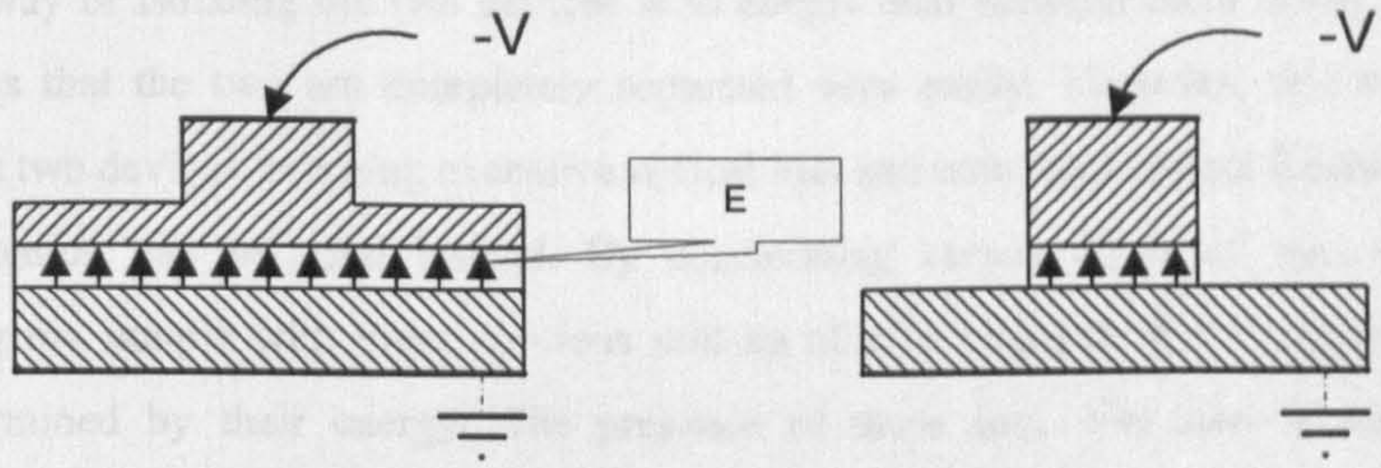

Fig. 6-9 Modulators with different waveguide profile, (a)strip-loaded and (b)deep ridge.

6-4 Integration Considerations

Except for these considerations in wafer structure, there are other factors that must be take into consideration in terms of integration.

Bandgap difference

As already discussed in Chapter 2, for integration to be possible, the bandgap of the modulator must be tuned towards the higher energy in a proper amount. If this shift of bandgap is not sufficient, the insertion loss would too high and the overall contrast ratio available would be reduced. On the other hand, if the bandgap shift is too large then a high reverse bias voltage would be needed. This is not desirable because under high electric field, exciton lifetime significantly shortens, so the related resonance absorption peak tends to smear out, which reduces the contrast ratio available. From the spectrum measured from the as-grown material B429 and the disordered material B500, it is indicated that the appropriate amount of absorption edge wavelength difference between the light source would be about 10nm. Such a wavelength difference would put the light source wavelength at the foot of the modulator's absorption edge so that a small on-state insertion loss could be achieved and a moderate voltage (<5V) would be enough to induce adequate absorption.

Electrical isolation

In an semiconductor laser-modulator integration, the modulation signal could cause the injection current of the laser to fluctuate if they are not electrically isolated to an appropriate extent. This fluctuation can

than undermine the laser's spectrum quality and output power stability. It has been shown that the isolation resistance needed between the two devices can be as high as more than 1MΩ [1].

Such high isolation resistance cannot be achieved by the shallow etching method used in mode-locked lasers to isolated the saturable absorber and the gain sections, where the isolation resistance is in the order of 5-10kΩ.

A simple way of isolating the two devices is to deeply etch between them down to the substrate. The advantage is that the two are completely separated very easily. However, this will leave an air gap between the two devices, bringing excessive optical loss and unwanted optical feedback into the laser.

Ion implantation can be used instead. By accelerating certain kinds of ions to high energy and bombarding the sample with them, the ions will be able to penetrate the semiconductor and stop at a depth determined by their energy. The presence of these ions will then dramatically increase the semiconductor's resistivity. By successive implantation at a series of different energies, the ions can be made to distribute continuously from the surface to a designated depth, forming a high resistance 'wall' between the devices which are protected by stop masks. By choosing the appropriate ion species and dose, optical loss in the isolation gap can be made very small.

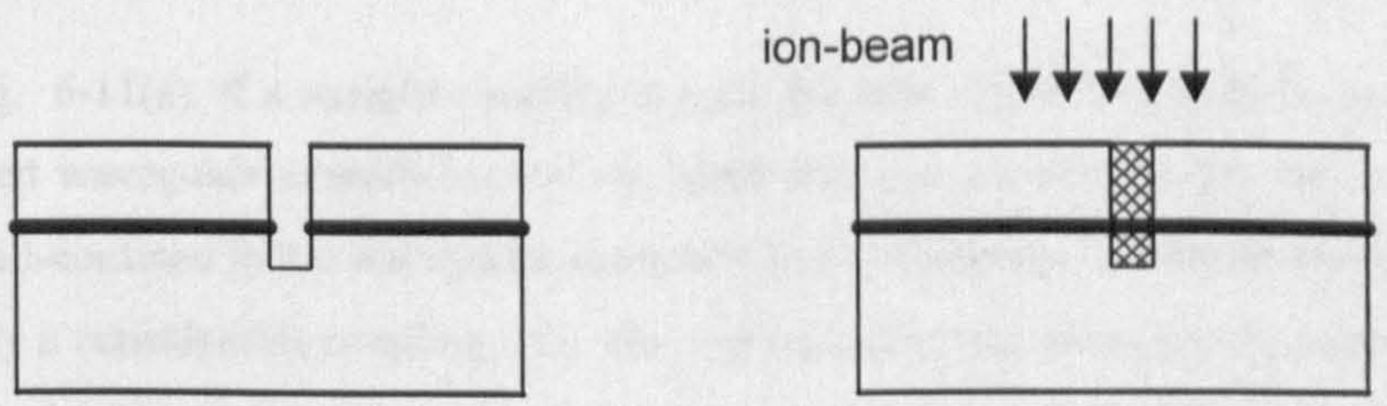

Fig. 6-10 Schemes for isolating the laser and the modulator, (a)deep etching and (b)ion implantation.

Optical coupling

From the fabrication point of view, having two different waveguide depths on the same sample requires one more photolithography and etching step, which may not be very difficult. However, because the modulator and the laser may have different waveguide profiles, optical coupling loss may arise at the interface.

---

[1] Tanaka, H., *et al*, 'Optical short pulse generation by a DFB laser/modulator integrated light source', IEEE Journal of Quantum Electronics, VOL.29, No.6, pp.1708-1713.

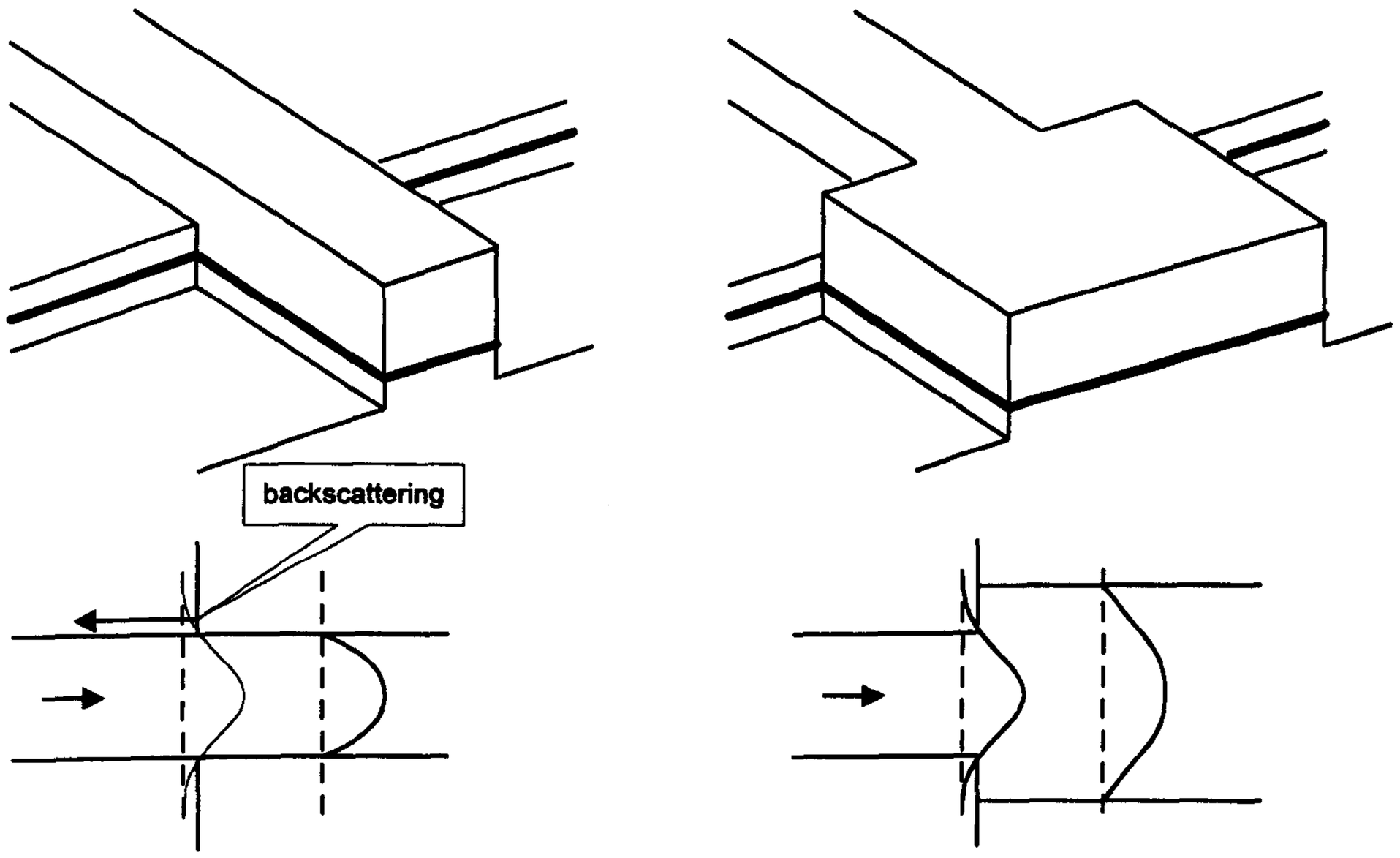

Fig. 6-11. Butt-joint coupling between the two waveguides, (a)of the same width, and (b)of mode-matched widths.

As shown in Fig. 6-11(a), if a straight coupling is used, because of the facts that the optical field in the weak strip-loaded waveguide extends beyond its width and that the field in the strongly guided ridge waveguide is well-confined in the waveguide, there will be a considerable mode mismatch at the interface and consequently a considerable coupling loss. The semiconductor-air boundary encountered by the light will also cause significant back-scattering. To improve the match between the modes in the two waveguides, the ridge waveguide should be made wider. The optimal size of the waveguide can be found by maximising the overlap integral (Chapter 3, Eq. 3-8) between the modes of the two waveguides. The ridge waveguide can then be tapered into the desired width.

6-5 Summary

In this chapter electroabsorption (EA) modulators employing the QCSE, made on the same quantum well material used for the semiconductor ring lasers (SRLs), have been studied. It has been demonstrated that, despite the material containing only two quantum-wells, effective modulator can be fabricated. The typical device can provide a modulation index up to 8.8dB/V with a maximum available modulation depth of about 23dB. The voltage needed to reach this modulation depth, which is 6 volts, are still quite high for applications in the gigahertz frequency range, for on a matched 50Ω source this would mean about 25dBmW modulation signal power if non-return-to-zero (NRZ) random data were to be applied. An effective way to improve the performance, as already discussed in Chapter 2 (2-1-2), is to increase the number of quantum-wells n_{qw}. In the early stages, one of the main concerns in material design is to reduce the threshold current of the long cavity SRLs. That consideration justifies fewer quantum-wells. However, when the SRLs are in the extended cavity form, which is inevitable if mode-locked at 10GHz,

the gain section are expected to produce higher gain per unit length than that in a non-extended cavity SRL simply because the rest of the cavity is lossy. According to the theory laid out in Chapter 2, this would also favour an increased number of quantum-wells. So in future design, n_{qw}=3 or 4 may be a better choice for both modulators and extended-cavity SRLs.

The high frequency characteristics of the modulators have been analysed and the equivalent circuit model has been derived from the data. A device capacitance of 1.6pF (bandwidth 4GHz) has been achieved. Although this is not yet enough to operated at 10Gb/s which requires a minimum bandwidth of 5GHz, it has been made clear that the device capacitance can be made as small as ~0.85pF with the current material and device parameter. Further reduction is possible if the material is grown to have sufficiently low background doping in the un-doped layer and the width of the waveguide may also be reduced from 5μm to 2-3μm. Matters concerning the integration of the modulator with the SRL, such as electrical isolation, optical coupling, etc, have also been discussed.

7 Conclusion and Future Work

7-1 Summary of the project

The work described in this thesis is aimed at exploring the possibility of optically integrating an OTDM transmitter system operating at a high bit-rate on an appropriate substrate. It has been shown that such an OTDM transmitter system could be integrated on III-V semiconductor quantum well (QW) substrates if the design of the substrate, the choice of fabrication techniques and the design of the devices are carefully considered. Suitable device structures for the three main kinds of devices involved in OTDM transmitters, namely light source, optical multiplexers (couplers) and optical modulators, have been discussed. Significant progress, both theoretical and experimental, has been achieved in all these aspects, which are summarised in the following.

7-1-1 Light source

To produce a suitable light source for such a integration, semiconductor ring lasers (SRLs) have been studied because of its potential of forming an integrated short light pulse source without employing either facet mirrors or precision gratings, and therefore is simple in fabrication. The following results have been achieved:

1) Large SRLs with cavity circumferences up to several millimetres have been successfully operated in both pulse pumped and CW mode. Such large SRLs are needed for producing mode-locked pulse trains with frequencies in the order of tens of gigahertz.

2) The low external efficiency associated with SRLs, due to both its long cavity length and large feedback ratio, has been dealt with. The external efficiency of semiconductor ring lasers has been improved over the value of ~16% of previous devices employing a single 0.5/0.5 2x2 MMI coupler. By using the asymmetric 2x2 MMI coupler, 3x3 MMI coupler and dual 2x2 MMI coupler as the SRLs' output coupler, its external efficiency has been increased by factors of 1.2, 1.4 and 1.7, respectively. The dual 2x2 device was AR coated to get η_{ex} values as high as 33%. This value is reasonably good for a device in a PIC where the consecutive devices are connected by low loss waveguides. The performance of the dual MMI coupler SRL has been improved significantly in terms of external efficiency.

3) Multiple (up to 4) outputs have been produced from these devices, which enables them to be used in an OTDM system as the light source without incorporating additional power splitters.

4) The mechanisms causing non-linearity in SRLs L-I characteristics have been studied and the linearity shown to be improved by several means including AR coating, deeper waveguide profile and passive output coupler.

5) Passive waveguides and extended cavity SRLs with very long cavity length (up to 7.5mm) have been fabricated by employing the IFVD technique and successfully operated. The linearity of the L-I characteristics of the extended cavity SRLs is as good as F-P lasers.

6) The mode-locking properties of semiconductor ring lasers has been studied theoretically. By means of computer simulations based on both the lumped element model and the travelling wave model, an in-depth understanding of the passive mode-locking process in SRLs has been achieved. The mode-locking properties of several cavity configurations, namely the symmetric configuration, the asymmetric configuration and the dual absorber configuration, have been compared. It is shown that in terms of wider mode-locked region and shorter pulse width, the dual absorber configuration is superior to the others. Moreover, the dual MMI, dual absorber configuration is more suitable for OTDM application not only because it generates four outputs and therefore eliminates the need to use addition power splitters, but also because the pulse timing from these outputs is such that only T/4 delay lines are needed to produce the correct timing difference between the 4 channels.

The theoretical study enables the prediction of operational modes of an SRL with intra-cavity saturable absorber under certain gain section injection and absorber reverse bias voltage, provided sufficient information concerning the semiconductor QW material.

7) Experimentally, mode-locked SRLs with both asymmetric and dual absorber, dual MMI coupler configurations have been successfully fabricated and operated.

The asymmetric configuration shows operation properties very similar to that predicted by the computer simulation. A mode-locked spectrum as wide as 200GHz (HMFW) with very small chirp has observed, corresponding to a pulse width of about 2.4ps.

The pulse width of the dual absorber configuration has been measured to be about 9ps with a time-band width product of 0.45. The wider pulse width can be attributed to the band-width limiting effect caused by facet feedback. Mode-locking mixed with self-pulsation and pure self-pulsation have also been observed in injection and reverse bias conditions agree with that predicted by simulation. The designing, fabrication, and CW and mode-locked operation of large ridge waveguide SRLs are reported here for the first time.

As a result of the continued research on semiconductor ring lasers at Glasgow, it can now be firmly established that this kind of device is a very suitable and *practical* light source for PIC applications that require either CW or short pulse outputs.

Waveguide Coupler

Multi-mode interference (MMI) couplers have been studied in this project. They were chosen is because of both their good tolerance to errors in fabrication and their outstanding feature of allowing multiple access, a major requirement for multiplexers and demultiplexers. It is intended that MMI couplers play two roles in the proposed integrated OTDM transmitter. They will be used as the output couplers of the

semiconductor ring lasers (which actually take the place of the power splitter if the dual 2x2 MMI coupler device or 3x3 MMI coupler device is used) as well as the multiplexer.

1) MMI couplers have been modelled using a effective index (EI) slab waveguide approximation. The parameters of the MMI couplers have been calculated and optimised by charting the mode excitation, propagation and interference processes in the system consisting of input, multi-mode and output waveguides. The tolerance to various waveguide geometric parameters are calculated.

2) Experimentally, besides 2x2 MMI couplers used in SRLs, 3x3 and 4x4 MMI couplers with strip-loaded waveguide profile are also fabricated and tested. The 3x3 MMI couplers shows a homogeneity of 1.3 dB among the outputs while for 4x4 MMI couplers the best homogeneity achieved is about 3dB.

7-1-2 Electroabsorption (EA) modulators

For semiconductor QW substrates, electroabsorption (EA) is certainly the most attractive modulation mechanism to explore. EA modulators have been experimentally studied in this project from several aspects.

1) The junction capacitance of the QW materials has been measured and compared to the theoretically calculated value by solving the Poisson equation across the p-i-n junction.

2) A modulator structure intended to reduce the parasitic capacitance between the p- and n-contacts by using deep etched waveguide and thick insulation layer (<2μm) has been designed and fabricated on two different double QW materials.

3) Their DC modulation characteristic has been studied. Despite the substrate material having only two QWs because of threshold considerations of the light source, a modulation index of 8.8dB/V has been achieved with a maximum available modulation depth of 23dB.

4) The high frequency characteristics of the modulators have been analysed experimentally. S parameter measurements up to 26GHz have been carried out. An equivalent circuit model has been derived from the measured data. The model allows the bandwidth of the modulator to be determined. It also highlights the need to reduce both the junction capacitance and device series resistance in order to increase the bandwidth of the modulator.

7-1-3 Integration

In this work, it was intended to investigate all the devices from the integration point of view. This has been reflected in many aspects in the device design and fabrication process. Integration has always been a very important factor to consider in the determination of substrate material structure, device configuration, waveguide structure and fabrication techniques. As a result, the devices developed in this project are suitable for the proposed purpose of an integrated OTDM transmitter system.

Investigation into integration techniques has also been carried out. The most important was to introduce bandgap difference on a semiconductor QW material. IFVD technique is studied and produced some

encouraging results such as the extended cavity SRL, which integrates an active section with a passive MMI coupler. Vertically coupled waveguide structures have also been investigated in an attempt to produce extended cavity lasers.

7-2 Future work

The emphasis of this work has been placed on developing devices that will be needed to realise the proposed integrated OTDM system, particularly large mode-locked semiconductor ring lasers as the light source. To finally realise the integrated system, the following work should be done.

7-2-1 Light source

In this project, large SRLs have been improved significantly in terms of configuration and external efficiency. Passive mode-locked operation of these SRLs has also been realised. The main remaining task concerning the light source therefore is to improve the performance of the extended cavity SRL and to realise its mode-locked operation. This is necessary if devices producing 10GHz pulse trains are to be realised and the problem of linearity is to be finally solved. The realisation of such a device largely relies on a reliable method to fabricate low loss passive waveguides. Techniques employing semiconductor disordering have been shown to produce such waveguides. But serious problems such as controllability, reproducibility and surface quality remain largely unsolved.

As discussed in Chapter 4, the vertically coupled waveguide structure have a number of attractive advantages including controllability, capability of producing very low loss passive waveguides and negligible material damage. Design considerations using this scheme has already been discussed in that chapter. It is believed that extended SRLs employing such a structure should be easier to fabricate and should have better performance than those fabricated by disordering techniques.

Mode-locked operation of extended cavity SRLs can also be simulated by the methods used in chapter 5. Because the passive sections change the spatial light intensity distribution in the cavity as well as introduce additional loss, the mode-locking injection-bias voltage range will be different. Nevertheless, the principles discussed in chapter 5 should apply.

Another problem worth considering is active or hybrid mode-locking. Passive mode-locking has the obvious advantage of not requiring a external oscillator. However, the timing jitter of a passive mode-locked laser pulse train may be too large to meet the requirement of a communication system. Active or hybrid mode-locking lasers, on the other hand, are synchronised by a external electronic or optical signal and can therefore be very stable. They may also have wider stable operation region because they do not only rely on the delicate interplay between the absorber and the gain section. Mode-locking operation can be forced by external signal where passive mode-locking will not appear.

7-2-2 MMI couplers

The main problem concerning the MMI coupler is the adverse effect of strip-loaded waveguide profile employed. Because MMI couplers are passive devices, there is no reason why deeply etched ridge waveguide cannot be used. Because deep etching is also necessary for modulators, it is worth considering using a deep ridge waveguide profile for all the waveguides except for the light source. This requires only one more level of photolithography and etching. The coupling between two different waveguide profiles, as discussed in chapter 6, can readily be achieved by tapered waveguide adapters. Side-wall scattering loss may be higher than in a strip-loaded waveguide, but should not be excessive because modern dry-etch techniques can produce very smooth side-walls. PECVD silica optical buffer layers can also be applied on the side-walls to reduce scattering loss.

7-2-3 Modulators

The main concern about modulators is bandwidth. Reducing the device capacitance is therefore a priority. As calculated in chapter 6, the characteristic capacitance of a p-i-n structure with over 0.4μm intrinsic layer thickness is about 270pF/mm^2. For a device to have bandwidth of 10GHz its capacitance should be less than 0.64pF. The waveguide width can be reduced to, e.g., 2μm. In such a case the length should not be longer than 1.18mm. But parasitic capacitance between contacts can be of the same order, as is shown in the equivalent circuit model in chapter 6. Therefore it may be necessary to design the p-contact as a 50Ω transmission line and terminate this transmission line with an on-chip 50Ω thin film resistor, as illustrated in Fig. 7-1.

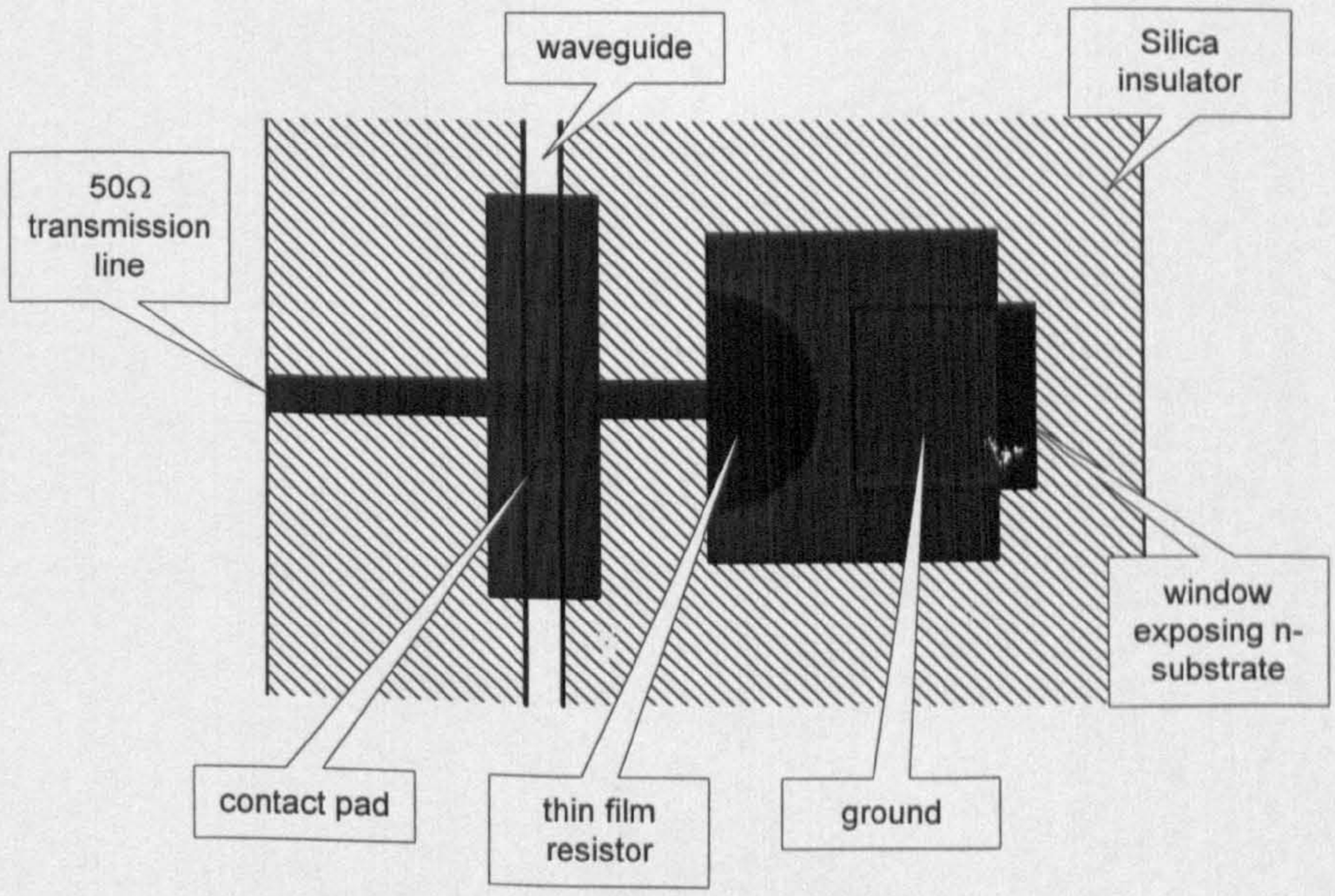

Fig. 7-1 Suggested modulator electrode.

7-2-4 QW Material and Integration

An increased number of QWs in the active layer may be necessary in future work. Firstly this will enhance the modulation index of the modulator at a certain device length, which is often limited by the capacitance consideration. Secondly, as discussed in chapters 2 and 4, extended cavity SRLs may also need more QWs to optimise their threshold current, particularly when a vertically coupled waveguide structure is used. A material with 4 QWs may be the optimum structure for this particular application.

The integration of a modulator with the light source and the passive waveguides still poses problems. A vertically coupled waveguide structure enables passive waveguides to be made. But the suitable bandgap of modulators, which lies between those of the other two devices, still needs to be created. A proper solution has to be found if disordering techniques are not to be used.

Despite the above mentioned difficulties in the way to a fully integrated OTDM transmitter system or any photonic integrated circuit (PIC) containing different kinds of optoelectronic devices, it is nevertheless worth pointing out that these difficulties are bound to be overcome as a result of continued effort. The success of these efforts, as part of a whole range of on-going research activities, will contribute significantly to the development of the next generation of high-speed optical communication and information processing systems.